Optimisation of a Low-Cost Production Automotive Engine for Range Extender Application in an Electric Vehicle

Agarwal, Ashwini

Award date:
2020

Awarding institution:
University of Bath

Optimisation of a Low-Cost Production Automotive Engine for Ranger Extender Application in an Electric Vehicle

Ashwini Agarwal

A thesis submitted for the degree of Doctor of Philosophy

University of Bath

Department of Mechanical Engineering

March 2020

Abstract

Electrification of vehicles is the direction the automotive industry has embarked on to address the well documented problems of air quality and climate change. Advantages of electric vehicles include zero tail pipe emissions, low energy cost and city-friendly driveability. However, a fundamental drawback is their limited range and high recharge time required.

The range extended electric vehicle (REEV) is a solution that enables the driver to be range anxiety free, seeks to achieve a practical compromise between the onboard battery size and the single charge driving range. The range extender or auxiliary power unit (APU) consists of an onboard fuel convertor, usually an internal combustion engine (ICE) that converts fuel such as gasoline into electrical power while the vehicle is in operation. This enables the traction battery storage capacity to be reduced whilst still maintaining an acceptable driving range. The ICE can be optimised for a limited number of steady state points which offer significant improvement in fuel economy as well as emissions.

Thermal management, a critical part in a vehicle is governed by two constraints – packaging and cooling performance. The packaging space in the vehicle limits the cooling system size. It becomes even more challenging in a hybrid system since extra components are in operation compared to a conventional car. Further, to mimimise fuel consumption of the APU, it is important that the engine and generator are operated at their maximum efficiency in addition to optimising the complete system to reduce any parasitic losses in the auxiliary systems. However, they have conflicting temperature requirements to achieve their own optimal efficiency.

Cost is one of the most significant factors for such a powertrain as the range extender is an additional system to a vehicle that already includes an expensive fully

capable electric system. Therefore, the APU must maximise its cost advantage over the proportion of the battery pack that it is effectively replacing.

With the above as the background, this research work elaborates on the considerable experimental work undertaken to optimise a very low-cost 624cc production automotive engine of c. 25kW for running as an APU in critical speed/load ranges. The engine optimisation process only included changes that were possible in the normal volume-production process. This included introduction of a new engine management system and electronic throttle, bespoke engine inlet and exhaust manifold development, engine calibration for improved fuel economy and well as introduction of an electric water pump. The optimisation achieved a best engine BSFC of 245g/kWh at 2500rpm with 92% reduction in engine inlet manifold volume.

On commissioning of the APU, the total dry weight of the APU was measured to be 81.5kg as against an initial target of 80kg. Experimental analysis showed the ESFC was below the target best ESFC of <270g/kWh under optimal temperature conditions of the engine, M/G and inverter unit in separate coolant circuits for the engine and generator. The APU produced a peak power of 22.78kW at 5100rpm. Best ESFC of 260g/kWh was measured at 2500rpm, and the ESFC remained below 270g/kWh across 2000 to 3500rpm at full load. The specific performance of the APU at peak power was 270W/kg which was within the target of 250 to 313W/kg.

The experimental analysis also demonstrated that it is possible to operate the APU in a combined engine-generator coolant loop, with marginal drop of 4% in power and 2% increase in ESFC. However, the combined loop provides greater flexibility of package installation and simplifies vehicle integration, with reduction in parasitic losses. It also reduces the overall package cost.

This research contributes in the area of optimising an industry first low-cost production, low-cylinder count engine for range extender application as well as

thermal management of an APU by providing an insight on the performance of the engine and generator in a single coolant loop with changing coolant and oil temperatures. This is considered to be the novelty of this research since literature review revealed that though researchers had written about potential cost savings on combining of coolant circuits, there was no evidence that it had actually been implemented.

Acknowledgement

I would like to express my most sincere gratitude to my lead supervisor Professor Chris Brace for giving me the opportunity to work in PVRC and simultaneously pursue my PhD. Despite my limited background in automotive research, his continuous support and guidance helped me to find my feet and I was able to embark on this journey. His infectious enthusiasm, broad outlook and encouragement kept me motivated to keep going even after leaving the University. I would also like to express my appreciation to my second supervisor Professor Sam Akehurst. Your immense practical knowledge on test facilities helped me a lot.

I would also like to express my gratitude to Dr Andrew Lewis, my third supervisor and now also a dear friend. I learnt and benefitted immensely from you. Your experience in commissioning, operation of test equipment / test cells and data analysis was of tremendous help. You have been an incredible mentor for which I shall always be grateful.

I would like to thank the project partners, Tata Motors European Technical Centre and Ashwoods for giving me the chance to work collaboratively on this project which was conducted with the financial support of Innovate UK and their support is acknowledged. My thanks especially to Gary Kirkpatrick, Johnathan Breddy, Peter Strange, Marco Cecotti, Christopher Mudd, Yash Gandhi from TMETC, Lloyds Ash and Calum Roke from Ashwoods. Thanks for your help and advice throughout the project.

My sincere thanks to Bob Gusthart, senior technician and his team including Jim Cansell, Martin Fullick, James Burge and Tom Holley for the assistance given during the project. Despite work pressure on various projects pulling in different directions, they always prioritised the LowCAP test cell for which I am grateful. The smooth progress made during the research was largely due to their willing and timely support.

I would also like to thank Dr Richard Burke for providing me the opportunity to work with the research group from University of Bristol. Thank you, Jing Na, Anthony Siming Chen, Yingbo Huang and Professor Guido Herrmann. It was great to interact with you all.

I would like to thank my colleagues at PVRC especially Deepak Hari, Leon Rodrigues, Dian Liu, Calo Avola, Ed Chappell, Simon Pickering, Karl Giles and Nic Zhang. It was a pleasure to work with you in different capacities as the project progressed. Thanks to most of you adding PhDs against your names post my joining PVRC, this mountainous journey seemed surmountable.

I would like to thank my parents for their words of encouragement. Wish you were here mom to share this achievement.

Finally, I would like to thank my wife. Your constant poking and reminding me to always look at the glass being half full kept me going!

Contents

List of Figures

List of Tables

List of Abbreviations

AAA	Automobile Association of America
ABDC	After Bottom Dead Centre
AFR	Air-Fuel Ratio
APC	Air/Cylinder/Cycle
APU	Auxiliary Power Unit
ASC	APU Supervisory Controller
BEV	Battery Electric Vehicle
BMEP	Brake Mean Effective Pressure
BSFC	Brake Specific Fuel Consumption
BTDC	Before Top Dead Centre
CAN	Controller Area Network
CAS	Combustion Analysis System
COV	Coefficient of Variance
DOE	Design of Experiment
ECU	Electronic Control Unit
ESFC	Electric Specific Fuel Consumption
ETC	Electronic Throttle Control
EMS	Engine Management System
EOI	End of Injection
EPW	Electrical Pulse Width
EV	Electric Vehicle
EWP	Electric Water Pump
GCU	Generator Control Unit
GDI	Gasoline Direct Injection
GMEP	Gross Mean Effective Pressure
GSA	Geometric Surface Area
HWP	Hardware Protection
HV	High Voltage
HYZEM	Hybrid Technology approaching efficient Zero Emission Mobility
IAT	Inlet Air Temperature
IAP	Inlet Air Pressure
ICE	Internal Combustion Engine
IMEP	Indicated Mean Effective Pressure
IPM	Interior Permanent magnet Motor

KLSA	Knock Limited Spark Advance
LCA	Life Cycle Analysis
LEZ	Low Emission Zone
LPM	Litres/minute
LV	Low Voltage
MAF	Mass Air Flow
MAP	Manifold Absolute Pressure
MBT	Maximum Brake Torque
MEP	Mean Effective Pressure
MIL	Malfunctioning Indicating Lamp
MITRE	Micro Turbine Range Extender
MIMS	Mineral Insulated Metal Sheathed
MPW	Mechanical Pulse Width
NEDC	New European Drive Cycle
NRPC	Number of Combustion Events per Revolution
NVH	Noise Vibration and Harshness
OFA	Open Frontal Area
PEM	Proton Exchange Membrane
PEV	Plug-in Electric Vehicle
PFI	Port Fuel Injection
PHEV	Plug in Hybrid Electric Vehicle
PMEP	Pumping Mean Effective Pressure
PRT	Platinum Resistance Thermometer
RE	Range Extender
RESS	Renewable Energy Storage System
REEV	Range Extender Electric Vehicle
RON	Research Octane Number
SOC	State of Charge
SOI	Start of Injection
TREV	Turbine Recharged Range Extender
TTW	Tank to Wheel
TWC	Three Way Catalyst
UHEGO	Universal Heated Exhaust Gas Oxygen
ULEZ	Ultra-Low Emission Zone
VSC	Vehicle Supervisory Controller
VE	Volumetric Efficiency
WOT	Wide Open Throttle

List of Symbols

a	Speed of sound, feet/sec
A	Cross sectional area of tuned pipe, in^2
K	Constant, ratio of Helmholtz frequency to engine speed
L	Length of tuned pipe, in
$\dot{m}$	Mass air flow, g/s
n	Number of results
N_{cyl}	Number of cylinders
N_{eng}	Engine speed, rpm
P	Manifold air pressure, kPa
R	Universal gas constant, 287 J/kgK
r_c	Compression ratio
T	Ambient temperature in °K
V_{cyl}	Volume of cylinder
V_d	Displaced cylinder volume
υ_e	Volumetric efficiency
V_{eff}	Effective volume, in^3
σ	Standard deviation
y	Individual experimental results
ηv	Volumetric efficiency

CHAPTER - 1
Introduction

This chapter presents the background for the electrification of the modern automotive powertrain and the features of range extended electric vehicles. The second part introduces the aims and objectives of this research work. The thesis structure is given at the end of this chapter.

1.1 The Modern Electric Hybridised Powertrain

The desire to reduce man made CO_2 emissions to combat global warming and to improve the energy security of individual nations is driving a move towards increasing electrification of the vehicle.

Advantages of electric vehicles include zero tail pipe emissions, low energy cost and city-friendly driveability. However, a fundamental drawback is the limited range and high recharge time required when compared to their combustion engine counterparts. Range Extended Electric Vehicles (REEVs) operate as normal electric vehicles for most of their operating time, until the battery state of charge falls below a certain point. This switches on the Auxiliary Power Unit (APU) such as an internal combustion engine (ICE) which is connected to a generator that maintains battery state of charge [1].

The APU acts to extend the range of an otherwise fully electric vehicle (EV) and the vehicle driveline architecture reflects that of a series only hybrid electric vehicle (HEV) where the energy is transferred electrically between the ICE and the vehicle as shown in Figure 1-1.

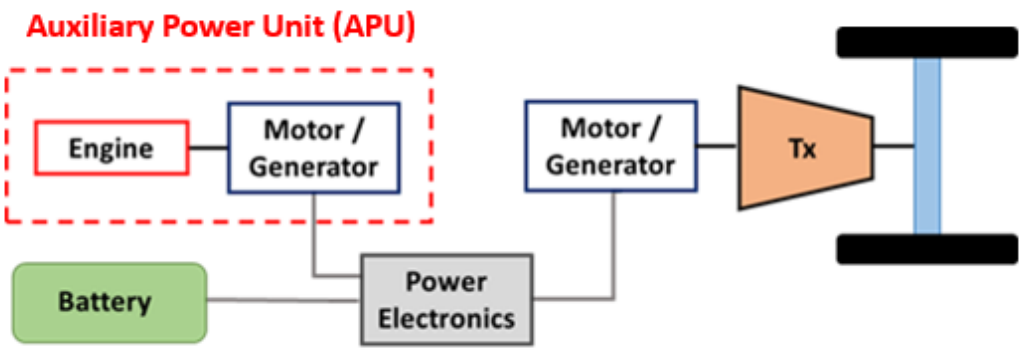

Figure 1-1 Range extended electric vehicle architecture [2]

According to Kay et al [1], REEVs can exhibit a 43% greenhouse gas (GHG) reduction compared with conventional ICEs which will increase to 47% by 2020 with the decarbonisation of electricity. Emissions of CO_2 can also potentially be further reduced with sustainable biofuels.

1.2 Characteristics of an Engine for Range Extender Application

The basic requirements of an engine for range extended application include compactness and being lightweight, good fuel efficiency, low emissions levels to meet prevailing regulations, excellent noise vibrations and harshness (NVH) behaviour, and meeting all these at a low cost [3-5]. These can be met either by developing a bespoke engine or by taking a production engine and then making the necessary changes for range extender application. The merits/demerits of both approaches are covered in greater depth in Section 2.12.

1.3 Aims and Objectives

For this research a pragmatic approach was taken which included selecting a very low-cost highly optimised production automotive engine and then enhancing it for running as an APU in critical speed/load ranges for range extender application. The engine modifications to be considered would only include changes which were possible in the normal volume-production process. Finally, during the integration process, it was aimed to combine the ICE, generator and power electronics in a single coolant circuit to reduce parasitic losses as well as reduce overall package volume and weight without significant drop in overall system efficiency. Since the RE was replacing a portion of the high voltage battery, it was important to accrue the maximum benefit by keeping the overall package weight of the RE to the minimum possible.

This research formed part of a collaborative project between Tata Motors European Technical Centre (TMETC), Ashwoods Automotive Ltd and University of Bath. The scope of the project was to design, model and evaluate an industry first low-cost auxiliary power unit intended primarily for use in a REEV. Figure 1-2 shows the main project responsibilities/deliverables of the partners for this Innovate UK funded research project. The research project began in July 2013 and concluded in July 2016.

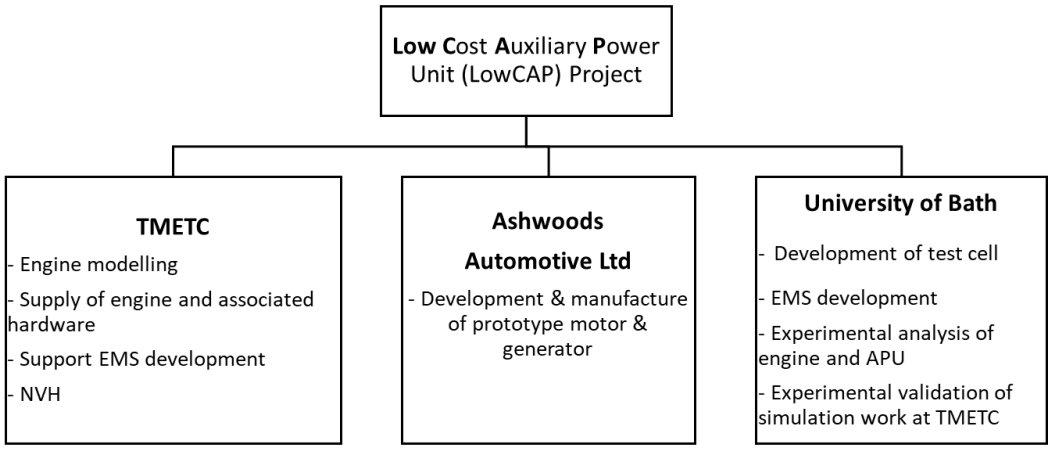

Figure 1-2 Roles and responsibilities - LowCAP project, funded by Innovate UK

The role of the University of Bath was to perform experimental analysis to support the progress of the project. This involved:

- Commissioning of the bespoke test cell at University of Bath.
- Benchmarking the performance of the base engine supplied by TMETC.
- Thermal survey of the base engine.
- Experimental analysis and calibration for introduction of bespoke engine management system and electronic throttle.
- Experimental analysis to validate intake and exhaust manifold simulation results undertaken at TMETC.

- Engine calibration as modifications were carried out on the engine including intake and exhaust manifolds, spark timing optimisation and introduction of electric water pump.
- Upgrade the test cell as it progressed from the conventional engine test cell to a high voltage APU testing facility.
- Experimental analysis of the performance of the APU in order to operate the motor/generator and the engine in a single coolant loop.
- Measure performance of the APU over the New European Drive Cycle (NEDC).
- Experimental analysis of the three-way catalyst of the APU.

Accordingly, this dissertation discusses the development of a low cost APU c. 20-25kWe for a range extender application utilising a low-cost, well optimised production automotive two-cylinder gasoline engine, which was in use in the Indian market.

An electric specific fuel consumption (ESFC) of less than 270g/kWh for the APU was aimed for. This target had been set based on the production engine performance and considering efficiencies of commercially available generators and inverters of similar topology [6]. This translated to a best BSFC in the region of 245g/kWh. This compared favourably with the bespoke Mahle RE of similar 10bar BMEP, having a target minimum BSFC of 240g/kWh [7].

A target (dry) weight for the complete APU of less than 80kg was aimed for, which along with 20-25kWe target power, the specific performance of the APU would be 250 to 313W/kg [6].

The package volume was to be minimised as far as possible by using a highly integrated approach that included examining the possibility of a combined cooling circuit for the engine and generator. Whilst the base engine envelope, see Figure 1-3,

could not be changed significantly, the intake, exhaust, after-treatment and generator package volumes were to be developed to minimise any increase in overall dimensions as far as possible, see Figure 1-4 and Figure 1-5 respectively.

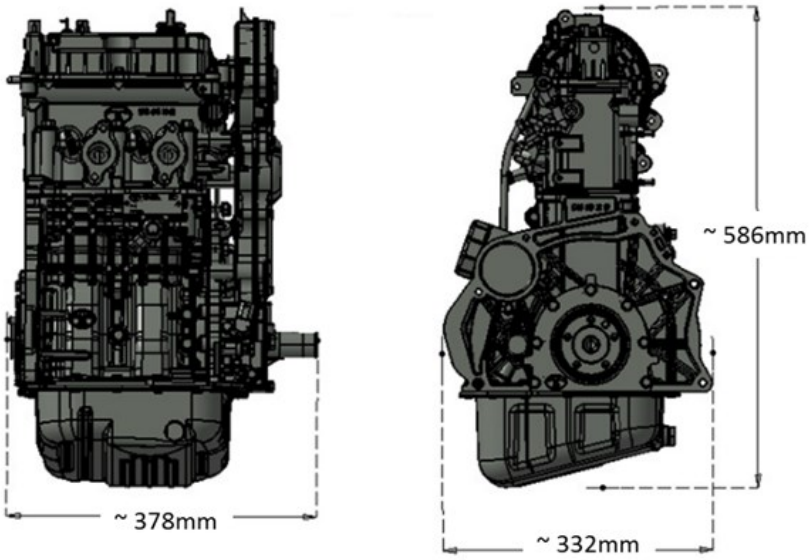

Figure 1-3 Base engine major dimensions without intake, exhaust and after-treatment [6]

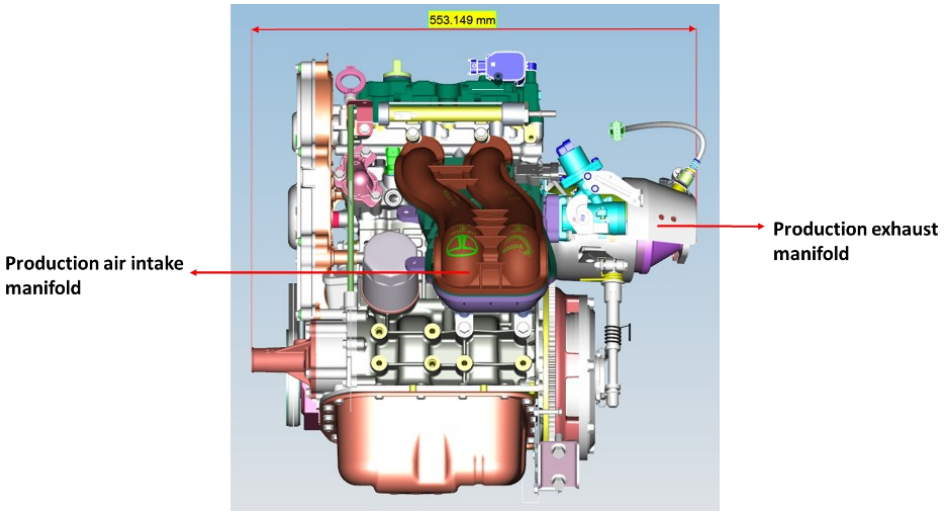

Figure 1-4 Engine overall dimensions with intake, exhaust and after-treatment, viewed from inlet manifold side [6]

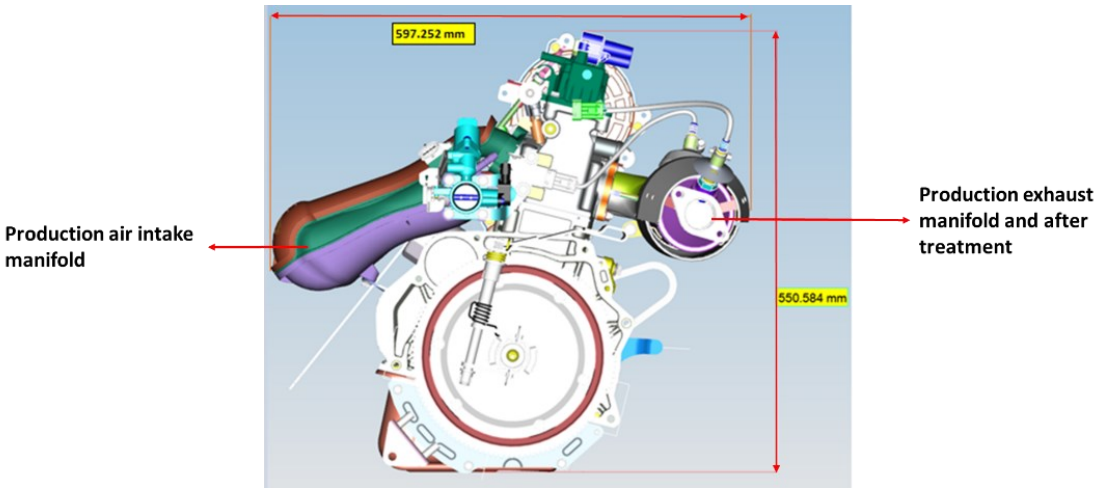

Figure 1-5 Engine overall dimensions with intake, exhaust and after-treatment, viewed from flywheel end [6]

Given the research constraints of packaging and low cost, opportunity was envisioned to be in the following areas at some additional cost for better integration for range extender application: -

- **Introduction of a bespoke EMS and electronic throttle**. This would enable development of the control strategy to suit the production engine for RE application as well as integration with the generator controller unit (GCU) and the overall vehicle supervisory controller (VSC). Introduction of the electronic throttle would facilitate the incorporation of the engine torque control strategy without any driver input, considered essential for range extender application.

- **Intake and exhaust manifold design**. The criteria for bespoke intake and exhaust manifold development was to minimise the APU package volume in order to improve vehicle package whilst targeting improved performance between 2000 – 4500rpm. This was because low-speed high torque and high-speed high power points were not expected to be used in RE application from fuel efficiency and NVH aspects.

- **Operation at lambda 1 across a wider portion of the engine operating range**. Since the APU was being developed for European markets where RON 95 gasoline is standard, there was an opportunity to optimise ignition timing and reduce exhaust enrichment to achieve an improvement in fuel economy and the potential for effective catalyst operation.

- **Reduction in overall package and parasitic drive losses by using a single coolant system for engine and generator**. Development of a thermal management system using a single coolant loop for the APU unit reducing parasitic loads and simplifying vehicle integration as well as reducing overall package volume.

- **Bespoke catalyst to meet EU6 emission norms**. Development of the close coupled catalyst to achieve EU6 emission requirement.

1.4 Thesis Structure

As per the objectives of this research work, the detailed contents are presented in the following chapters of this thesis.

Chapter 2 is review of the previous work in the related areas of REEV. It covers the benefits and shortcomings of electric vehicles, how an APU overcomes the shortcomings of a BEV, RE operating strategies, requirements of a RE engine, engine concepts, REs in the market, thermal management of a RE and finally pros and cons of a bespoke engine versus a production engine for RE application.

Chapter 3 details the base engine provided by TMETC, the bespoke test cell development at University of Bath, commissioning of the test cell and benchmarking the performance of the base engine.

Chapter 4 discusses introduction of the new engine management strategy including the commercially off the shelf electronic control unit (ECU) and electronic throttle unit.

Chapter 5 details the development and introduction of the bespoke intake and exhaust manifolds on the engine. Detailed experimental analysis was carried out to validate the simulation undertaken at TMETC.

Chapter 6 describes calibration efforts to improve the engine performance and BSFC by reduction in exhaust enrichment, spark timing optimisation and introduction of an electric water pump.

Chapter 7 details the thermal survey of the base production engine to quantify the effect of changes in oil and coolant temperature on engine BSFC.

Chapter 8 describes the commissioning and performance of the APU. It details the changes to the test cell to support testing of a high voltage APU and other modifications to the engine and motor/generator cooling circuit. ESFC testing of the APU was carried out under optimal thermal conditions for the engine and electrical machine with separate coolant circuits. Subsequently the performance of the APU was compared under varying thermal conditions and combining the engine and generator coolant circuit.

Chapter 9 covers the performance of the APU in charge sustain mode over the NEDC. It demonstrates that the APU was successfully able to produce the necessary power based on a representative vehicle model developed by TMETC.

Chapter 10 covers the emissions performance of the APU over the NEDC including cold start emissions performance. Based on the performance, strategies to improve catalyst light-off and steady state emissions were explored.

Chapter 11 summarises the results and key findings from this research work. The research limitations and future work that could be undertaken in the field introduction of APUs in BEVs are discussed.

CHAPTER - 2
Literature Review

This chapter presents benefits and shortcomings of pure electric vehicles and the role that a range extender plays in addressing some of the shortcomings. A literature review has been carried out on the requirements of a range extender engine, possible engine concepts and current range extenders in the market. Research gaps/opportunities have been highlighted which this research project aimed to address.

2.1 Introduction

In this chapter a review of published work will be presented, highlighting the benefits and shortcomings of electric vehicles. The next section covers the role a range extender plays in overcoming the primary shortcoming of an electric vehicle i.e. driving range. Then the pros and cons of different high-level APU operation control strategies are investigated based on the results of previous researches. The next part of the review highlights the requirements of a range extender, pros and cons of various engine concepts and the various range extenders currently in the market. Then the cooling arrangements for hybrid powertrains are discussed. Lastly, the advantages of selection of the production engine vis-à-vis development of a bespoke engine for range extender application are covered.

2.2 Definition of EV, APU and REs

In accordance with SAE nomenclature [8, 9], a hybrid electric vehicle (HEV) is defined as a vehicle that can draw propulsive energy from both of the following sources of energy: a consumable fuel and a rechargeable energy storage system (RESS) that is recharged by an electric motor-generator system, an external electrical energy source or both. An electric vehicle (EV) is a vehicle powered solely by energy stored in an electrochemical device. This implies that the EV's propulsion is achieved entirely by electric motors, regardless of the means of obtaining that electric energy. Further, a battery electric vehicle (BEV) is a vehicle that receives its on-board propulsion power solely from batteries, unlike a hybrid vehicle that may receive a portion of its power from a separately fuelled power source such as an internal combustion engine. An auxiliary power unit (APU) is a device that converts consumable fuel energy into mechanical or electrical energy. The APU is a secondary energy or propulsion source. Some examples of APUs are ICEs, gas turbines or fuel cells. A range extender (RE) is a small engine-powered generator or APU added to a

battery EV. This generator sustains vehicle operation beyond the range provided by the batteries alone [8].

For this research, a range extended electric vehicle (REEV) is considered as a battery electric vehicle which is additionally equipped with a RE to provide electrical energy to extend the range of the vehicle when the battery state of charge (SOC) drops below a pre-defined level.

2.3 Benefits of Electric Vehicles

Apart from the obvious benefit of zero tailpipe emissions, BEVs have other benefits as well. On a tank-to-wheel (TTW) basis, EVs are more energy efficient than comparable combustion engines [10]. Table 2-1 below summarises the efficiency indicators of BEVs and PHEVs vis-à-vis their ICE counterparts.

Table 2-1 Illustrative energy efficiency indicators of BEVs & PHEVs versus IC engine counterparts [10]

Vehicle type	Renault Zoe	Renault Clio	Volvo V60	
	BEV	gasoline	diesel-PHEV	diesel
Fuel consumption [l/100km NEDC]		4.3		6.4
Fuel consumption [kWh/100km NEDC]		~39		~64
Electricity consumption [kWh/100km]	14.6*		~22†	

* According to NEDC procedure.
† For the Volvo V60 PHEV, estimates for driving only electrically and driving only in combustion engine mode were derived from car magazine tests (AMS, 2014) and weighted equally (50:50) for all further fuel cost savings calculations.

BEVs cost much less to maintain as there is no oil or oil filter, no exhaust system, no fuel pump, no alternator, and no transmission. The electric motor has few moving parts while the IC engine has hundreds of moving parts. The BEVs servicing schedule is much easier with considerably less downtime for regular maintenance and repair. As per Professor Tony Seba, Stanford University economist, Tesla's S model car has

18 moving parts, one hundred times fewer than a combustion engine car, making maintenance virtually zero [11].

The BEV batteries are sealed so they don't need any maintenance, though may need periodic replacement. Most BEV batteries are covered by an eight-year warranty, this includes all Tesla models as well as the recently launched Jaguar I-Pace [12].

Many governments provide incentives to encourage the increased sales of EVs. The ultimate purpose is to meet their greenhouse gas emissions target to put more EVs on the roads. These incentives can include subsidies for the purchase price [13, 14], see Figure 2-1, assistance with charging stations, preferential traffic lanes [15] and other inducements. Also, there are incentives for home and workplace charging equipment, public installation of charging equipment, preferential parking for EVs, preferential access to restricted highway occupancy vehicle lanes, and utility policies that promote EVs. Other important incentives are those directed more towards vehicle manufacturers, such as research and development funding, vehicle efficiency and CO_2 standards, super-credits as well as direct EV mandates such as the California Zero Emission Vehicle program.

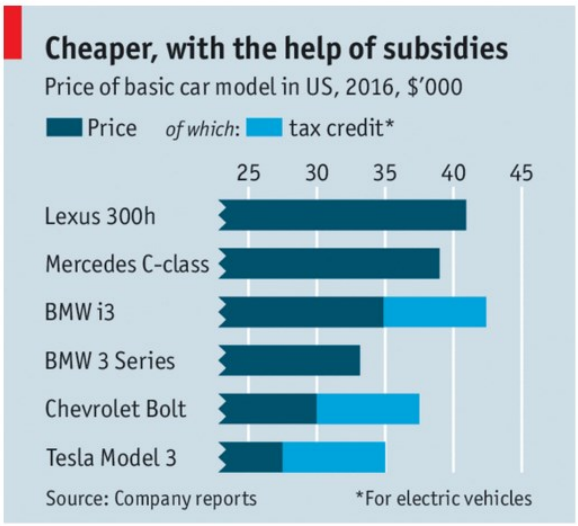

Figure 2-1 Government subsidies on electric vehicles purchase price to encourage uptake [14]

From May 2016 Germany commenced to subsidise electric car purchase to accelerate the sluggish growth in the EV sector to help Germany approach its goal of putting one million electric cars on the road by 2020, up from around 50,000 out of Germany's 45 million cars. Car buyers receive €4000 on purchase of the purely electric vehicle and €3000 for a plug-in hybrid, with the cost shared 50-50 between the public purse and the car makers. German auto giants Volkswagen, Daimler and BMW signed up for this programme [13].

Sales of electric cars in China saw a dramatic increase because of government incentives, see Figure 2-2. It is expected that the market to grow by nearly 50% a year for the rest of this decade in China [16]. Likewise in UK, between April and June 2014 there were 2738 electric vehicles registered compared with 9657 in the same period during 2015, a rise of 250% [15]. In 2018 the UK government scrapped the £2500 subsidy on Plug-in hybrid vehicles and the sales of hybrid vehicles dropped by 50.4% in June 2019 as compared to June 2018 [17]. Even the subsidy on electric vehicles was reduced from £4500 to £3500. This just goes to demonstrate that government subsidy is a major contributing factor towards growth of sales of electric vehicles and continued support would be required if the alternatively fuelled vehicle sector is to grow.

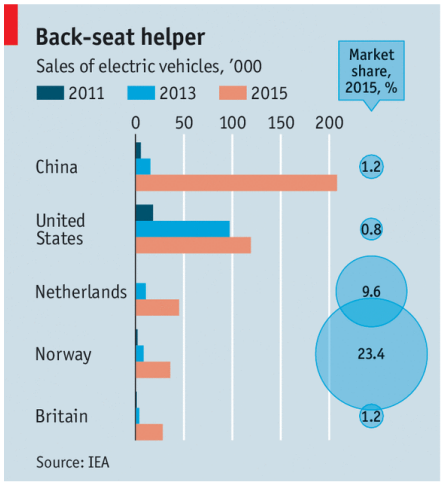

Figure 2-2 Rise in electric cars sales including plug-in hybrids in China due to government support [16]

Another concept, particularly popular in Europe and China are Low Emission Zones (LEZ). These are designated areas, usually in cities, that place a restriction on vehicle with high emissions. The restrictions can range from an outright ban, restrictions for certain times of the day, or a financial penalty for emissions. A BEV can eliminate the costly inconvenience of being restricted from a LEZ. An Ultra-Low Emission Zone (ULEZ) has been introduced within the same area of Central London as the congestion charge that operates 24 hours a day, 7 days a week, every day of the year [18].

Thus, while the retail prices of BEVs are still considerably higher than their fossil-fuelled counterparts, the savings on fuel and maintenance over the BEV's lifetime plus government incentives can produce a price that is competitive with gasoline.

Because electric vehicles have limited range on a single charge as compared to their ICE counterparts, there is a need to develop a substantial charging infrastructure. While governments are investing in building up the EV charging infrastructure, to expedite its process auto manufacturers have also come together in investing in its development. In the United Kingdom BMW, Daimler, Ford and Volkswagen group including Audi and Porsche decided in 2016 to build 400 ultra-fast charging sites with the capability to charge at a speed to 350kW [19, 20]. Such initiatives are expected to attract more people to buy electric cars. The UK government as recently as August 2019 announced an investment of 40 million pounds to improve the UK charging infrastructure [17].

Another technology which is being investigated is charging while driving, both contact and contact-less charging. Honda carried out considerable research on their contact-type, high power charge-while-driving system that can simultaneously supply power and charge during vehicle operation. They demonstrated a charging power of 100kW, with a maximum voltage of DC 375V and a maximum current of 300A, with

the vehicle speed at the time of charging varying from 7kph to 70kph [21]. They also carried out a lucid discussion on the merits of contact-type EV charging over wireless charging, which as per them is several years away.

Further, as per Kay et al [1] EVs stand to benefit the maximum from technology development in the area of weight, drag and rolling resistance reduction. Electric powertrains being highly efficient and thus weight, drag and rolling resistance account for a much larger proportion of the total efficiency losses. Reducing these losses may also allow the battery size to be reduced for a given range, in turn further reducing the vehicle weight and cost.

EV sales have swelled by 11 times in four years and crossed 2 million vehicles across the world in 2018 [22], see Figure 2-3. As per Frost & Sullivan more than 2.8 million electric vehicles are likely to be sold globally in 2019 [23].

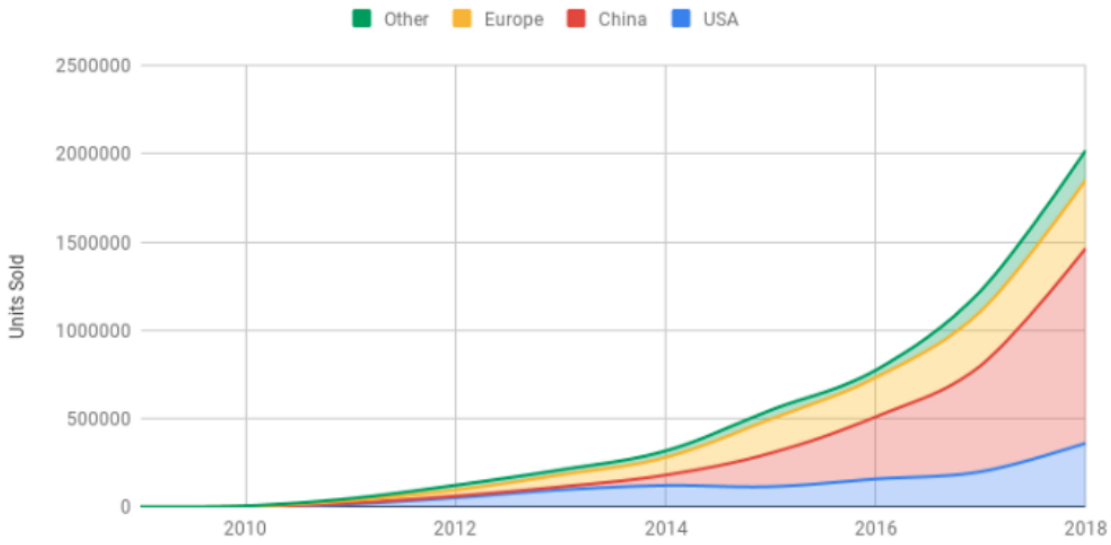

Figure 2-3 Global sales of electric vehicles in 2018 crossed the 2 million mark [22]

While today the proportion of EVs on the world's road is still well below 1%, most forecasters had reckoned that by 2025 that would rise to around 4%. This figure is seeing an overhaul as carmakers announce huge expansions in their production of EVs. Exane BNP Paribas bank predicts that EV penetration could form around 11% of the vehicles on the road worldwide by 2025, see Figure 2-4 or even higher.

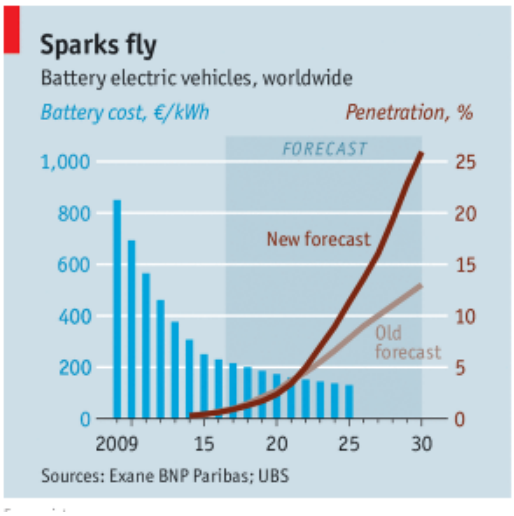

Figure 2-4 Electric vehicle penetration expected to be 11% of total vehicles worldwide by 2025 [24]

This surge in numbers has two explanations; the rising cost of complying with emission regulations and the dropping cost of electric vehicle batteries. EVs are a way of meeting the ever-increasing stricter emission targets, albeit an expensive one. But the gains expected from less dear methods such as turbocharging small capacity engines, start-stop technology and weight reductions are unlikely to be enough to meet the future emission targets.

2.4 Shortcomings of Pure Electric Vehicles

While EVs are viewed as desirable as they do not generate pollutants while passing through inhabited areas and can potentially rely on its energy being provided by a selection of renewable sources, they however have relied on batteries as the source

of energy since the end of the 19th century. Despite the innovative nano-materials applied to lithium based NiMH and Li-ion type batteries, it has inherent disadvantages like low energy density, high cost, heavy, and consequently additional drawbacks like mass compounding.

Turner et al [3] compared the gravimetric and volumetric energy density of various fuels and their storage systems. Figure 2-5 clearly illustrates the significantly higher energy density of traditional fossil fuels over batteries.

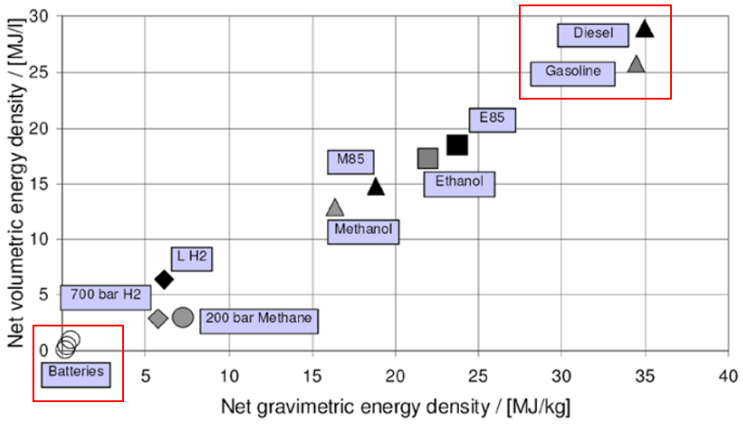

Figure 2-5 Gravimetric and volumetric energy density of fuels and their storage systems [3]. The gap between batteries versus diesel and gasoline is highlighted

Ribau et al [25] in a survey on electric/hybrid vehicles concluded that, on average BEVs have a consumption of around 0.12Wh/km for each kg of vehicle mass as shown in Figure 2-6. For a 1500kg vehicle (approximately the curb weight of the Nissan Leaf and Opel Ampera) this yields consumptions around 180Wh/km, which would require a Lithium-ion battery pack of volume 117 litres and weight of around 180kg for each 100km range (with a volume around 1.17l/km and a weight around 1.8kg/km). Considering an ICE based vehicle with consumption of around 7l/100 km, assuming density of 95 RON fuel of around 0.75kg/ltr [26], this implies that for 100 km range, the weight of the fuel would be 5 kg. In comparison, the BEV energy storage would be around 17 times bigger and 35 times heavier than that of conventional vehicles for the same available range.

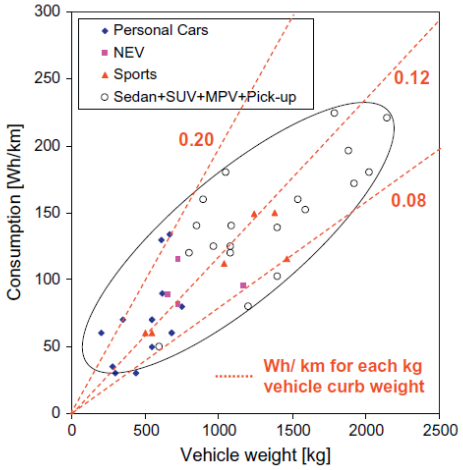

Figure 2-6 Battery consumption per km as a function of vehicle curb weight [25]

Thomas [27] highlighted that lithium–ion batteries used in BEVs are too heavy and occupy too much volume. In principle, more batteries can be added to any BEV to extend range, however the mass and volume occupied by these batteries grows non-linearly with additional range due to a process called mass compounding. Because of adding more batteries, extra structure must be added to support these batteries. This extra mass will in turn require larger motors to provide the desired vehicle acceleration, and the brake system must be slightly larger to safely stop the vehicle. The vehicle frame and suspension systems must be augmented to carry this additional mass, further increasing total vehicle mass. Thus, additional batteries will be required to propel this heavier vehicle the required distance in an iterative, non-linear feedback process. Adding a load such as 100 kg of batteries will require an additional 59.8kg for 12 vehicle subsystems such as structure, brakes and suspension systems.

Further, electrical power storage is considerably more expensive than liquid energy storage. With lithium being a vital component of current batteries, because of its higher specific power and energy compared to other battery technologies, see Figure 2-7, there is a global scramble to secure supply of lithium by the world's largest battery producers and by the end-users such as car makers. Kay et al [1] have

highlighted that there are potential resource risks for the rare earth metals that are required for the electric motors and materials for batteries.

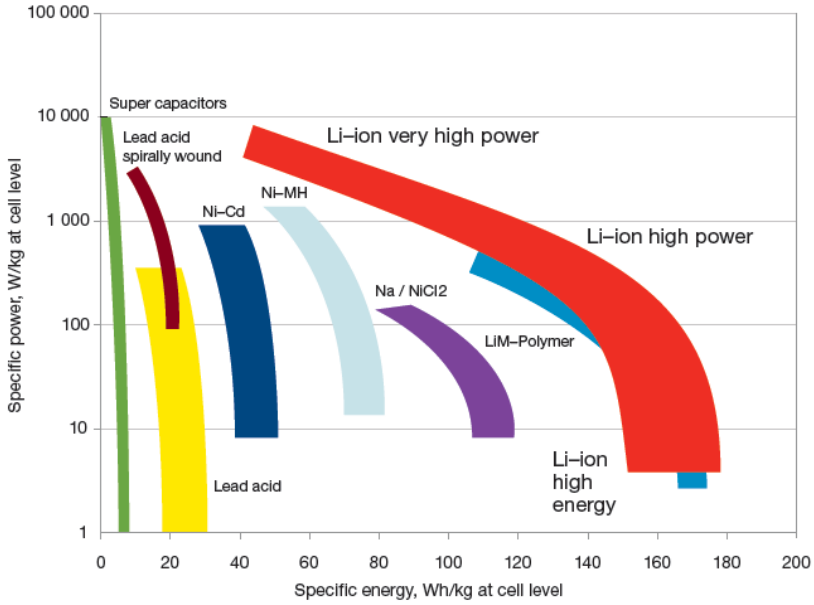

Figure 2-7 Specific power versus specific energy of various battery technologies. Lithium-ion has higher specific power and energy compared to other battery technologies [1]

The Economist [28, 29] highlighted that the price of 99%-pure lithium carbonate imported to China more than doubled in the two months to the end of December 2015, to USD13,000 a tonne as shown in Figure 2-8.

Figure 2-8 Price of lithium carbonate imported to China [29]

In addition, current lithium-ion batteries often use extremely rare elements in their chemistries such as cobalt. The materials most used for cathodes in EV batteries are a combination of nickel, manganese and cobalt known as NMC. The demand for these elements is also soaring [30-32]. When chemistry prevents the removal of a truly rare element, the economics of mass production will ensure that instead of getting cheaper, these batteries will become more expensive [3], see Figure 2-9.

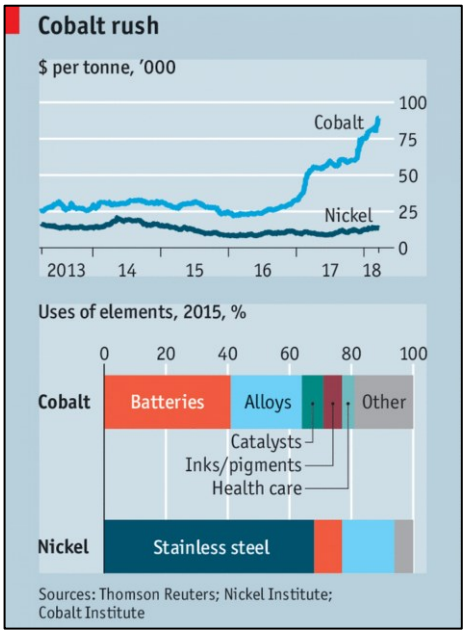

Figure 2-9 Rise in cost of rare metals [32]

Improvement in battery technology has reduced the cost of batteries while increasing range, it is still presently in the range of USD 300/kWh. With Nissan [33] launching the 30kWh battery model in Europe while maintaining the battery pack size of its earlier 24 kWh battery with marginal increase of 21kg in weight and an increased driving range of 155 miles between charges, the cost of the battery is still around USD 5500. This increased driving range is substantially less than what a driver of a traditional car is used to, in addition to the issue of long recharging times.

Thus, customers must pay a great deal more vis-à-vis a conventional car for their personal mobility or they must adjust to a significantly reduced vehicle range and

increased stress due to range anxiety i.e. the fear of getting stranded in an EV without the possibility of recharging. However, General Motors declared that the cost of the battery in their Chevrolet Bolt electric vehicle, which would be an industry leading USD145/kWh [34, 35]. GM goes on to state that by 2022 the cost is estimated to be USD 100/kWh, see Figure 2-10. This is reported to be quite competitive with Tesla, which is seen to be ahead of other manufacturers, with a price of USD 100/kWh by 2020 [34].

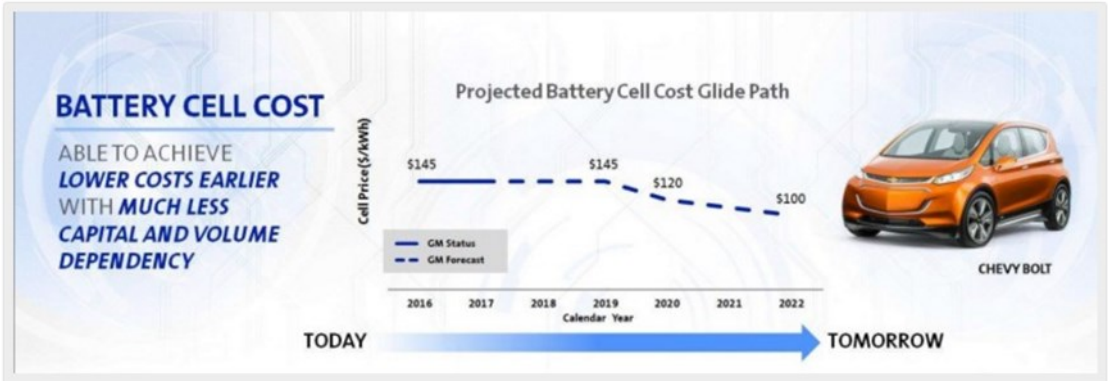

Figure 2-10 General Motors Chevrolet Bolt battery cost glide path [34]

Further, despite the huge historical spread in battery costs amongst vehicle manufacturers, these are beginning to converge and falling [36], see Figure 2-11.

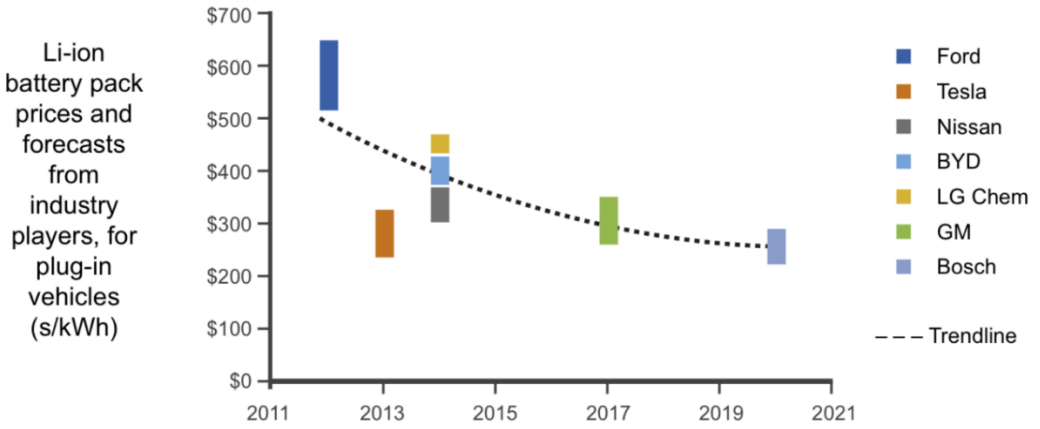

Figure 2-11 Despite an initial large historical spread, the price of Lithium-ion batteries is converging and falling [36]

A widely promoted solution called battery switching [37] was expected to alleviate range anxiety. At battery switch stations, vehicles position themselves over a pit with a servo-controlled lift. The battery is dropped down to below-road level, replaced by another fully charged battery, and conveyed to a warehouse for recharging. With battery switching, refuelling an EV would take minutes and therefore achieve the convenience of conventional cars. In addition, battery switching enables the decoupling of the battery and the vehicle, eliminating the higher upfront capital costs that EVs incur over traditional cars. Vehicle owners simply enter a leasing contract with EV service supplier provider, buying a fixed number of miles over a defined period.

However, this phenomenon failed to gain traction because of the substantial technical and economic challenges. First, battery switch stations must be able to handle different battery sizes and shapes as well as different vehicle chassis, adding considerable engineering complexity. This problem is prohibitive if there is an absence of industry standards. Second, compatibility needs to be established across countries, especially in Europe to ensure cross-border mobility. Third, batteries are high-tech expensive devices, easy to damage and degrade over time. This raises important issues for commercial arrangement for ownership and safety assurance of the batteries. Fourth, battery switching systems require large amounts of capital for excess battery capacity and switch stations. Failure of Better Place [38] a battery service provider in Israel underlined some the challenges above. Without battery-switching, pure EVs have a limited range and they take a long time to recharge.

Emergence of rapid chargers have addressed the issue of long charging times [39]. Although expensive to install, rapid chargers allow for either 80% charging in 30 minutes or effective topping up for partly charged vehicles in 10 to 15 minutes. Ultimately this means that a vehicle can be topped up whilst the driver takes a short break.

This would require a large network of public charging infrastructure to ensure that drivers can charge their vehicles away from home. The pace of charging infrastructure growth is also an issue as San Diego's leading car sharing company car2Go came to realise over its 5 year operations despite electrification being identified as top priority in the US as highlighted in Section 2.3. When Daimler's car2Go launched its car-sharing service in San Diego in 2011, its entire fleet of 400 vehicles was composed of electric cars. However, in March 2016 car2Go declared that they were withdrawing their fleet of Smart Fortwo electric drive city cars and replacing them with gasoline models because of lack of charging infrastructure in the area. Car2Go blamed the Department of Energy, which had a plan to install 1000 charging stations in San Diego by the end of 2011, however only 400 were installed around the city till March 2016, which made it very difficult for car2Go to maintain an EV fleet [40]. Tajima et al [21] also highlight the congestion at rapid chargers in Japan.

Another factor affecting BEV range is ambient temperature. It is well known that cold and hot weather shorten EV range [41], below 20°C battery life decreases linearly with temperature [42, 43]. With lower temperatures, the internal resistance of the battery increases, chemical reactions in the electrolyte of the battery slow down causing a limitation of power output as well as recharging capability [44]. A study conducted by Automobile Association of America (AAA) Automotive Research Centre showed that EV driving range can be nearly 60% lower in extreme cold and 33% lower in extreme heat [42]. Data from FleetCarma [45], a company that tracks data from fleet managers and private owners indicated that the optimum ambient temperature for maximum EV range seems to be between 15.5°C to 24°C, see Figure 2-12.

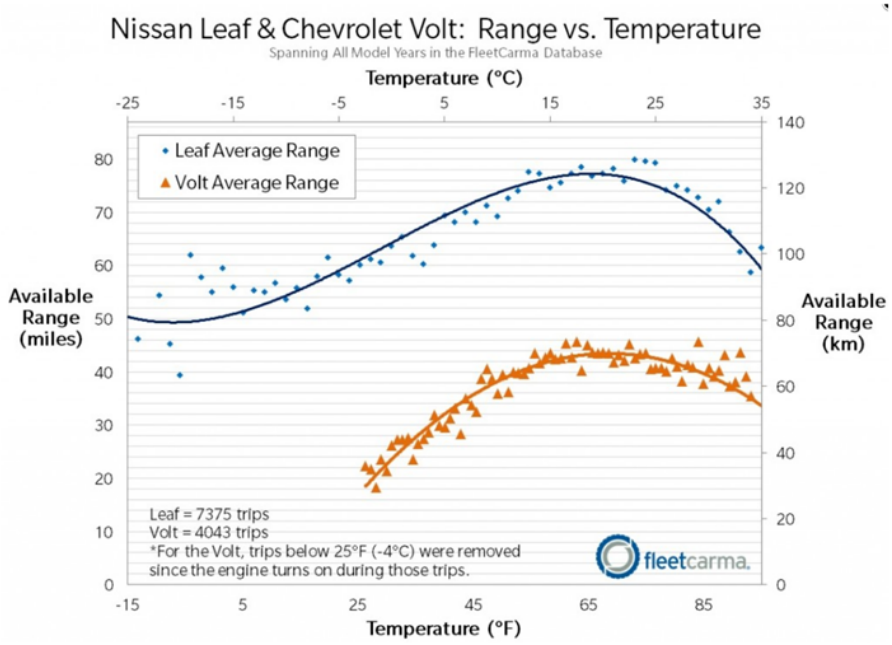

Figure 2-12 Data from FleetCarma on Nissan Leaf and Chevrolet Volt depicts battery range variation with temperature [45]

OEMs like Nissan recognised this factor and introduced a battery blanket to keep the battery pack warmer [46].

High temperatures increase the chemical degradation of the battery and therefore reduce battery life [44]. Nissan is testing a revised lithium-ion cell chemistry that appears to be as durable in sustained extreme heat as its current battery is under normal conditions [47].

Thorn [48] and Guenter et al [49] highlight that under extreme driving conditions i.e. slow traffic and demanding requirements for cabin heating or cooling – the electrical range might become less of a question of distance but more of total operation time. Guenter et al [49] analysed the power requirement for cabin conditioning for both hot and cold conditions, see Figure 2-13, and under these conditions the driver may even be faced with the dilemma of driving or air conditioning.

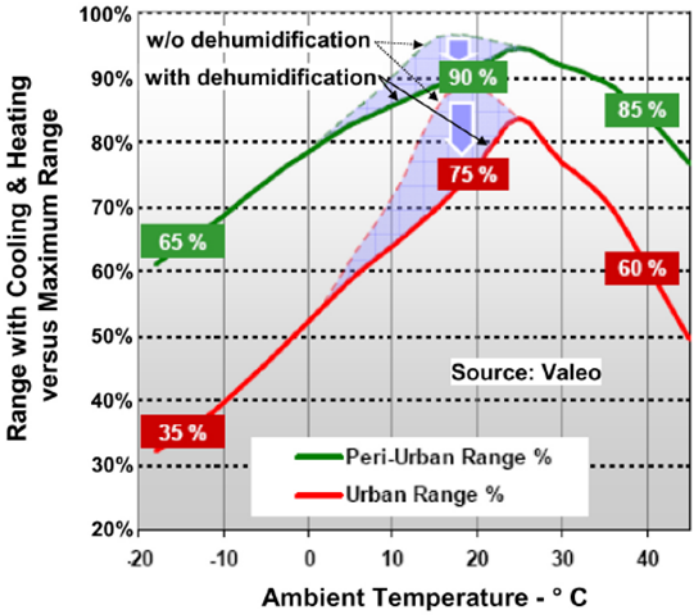

Figure 2-13 Impact of air conditioning on electric range of BEVs. As air conditioning power demand increases, the EV range sees a rapid drop [49]

2.5 Range Extender – The Solution for a BEV

In comparison to a battery, the gasoline fuel tank is a phenomenal energy storage device. Because of this property, an APU fitted on a BEV solves the paramount problem from the customer point of view – range anxiety. The RE represents a highly integrated auxiliary power source with a much superior level of energy density and lower production costs compared to battery systems for an equivalent driving range. The APU converts liquid fuel such as gasoline into electrical energy whilst the vehicle is driving. In addition, it also enables the traction battery storage capacity to be reduced, though still maintaining an acceptable driving range. For majority of the duty cycle the driving range provided by the battery should be sufficient, especially for urban driving. For the occasional long journeys when the battery and fuel are both depleted, the driver can simply refuel the gasoline tank as in a traditional vehicle. Bassett [4], Figure 2-14, illustrated the RE power and battery size trade off to reach an optimum compromise.

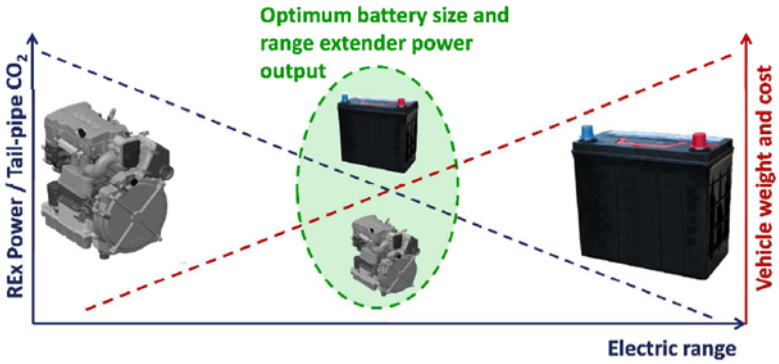

Figure 2-14 Range extender power and battery size trade off. There is a region where the right balance exists between battery size (EV range) and range extender power. Daily commutes are done in EV mode, and the occasional long journey is supported by the APU in charge sustain mode [4]

Thus, an APU in a REEV provides the functionality to complete longer journeys, at lower total vehicle cost than a pure EV with a large battery [50] as illustrated in Figure 2-15.

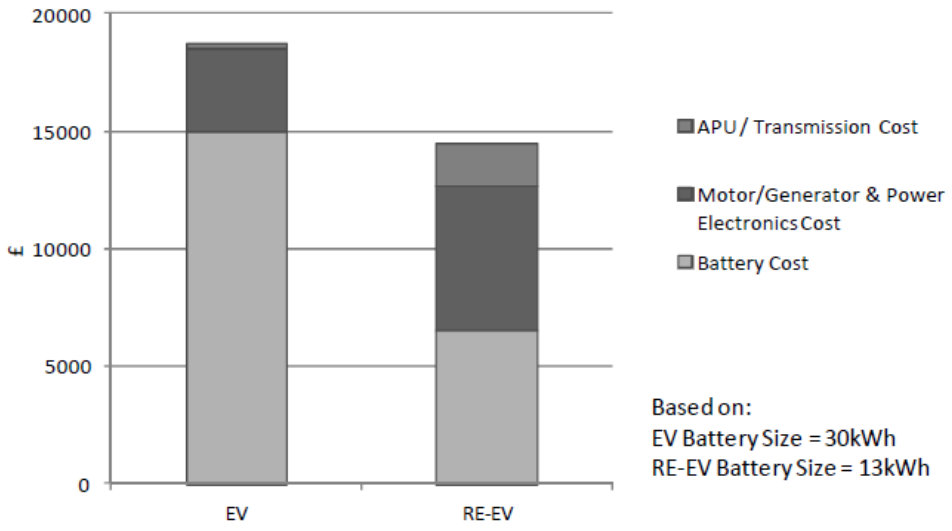

Figure 2-15 Powertrain cost advantage of a REEV in comparison to an EV [50]

Current EVs usually have a higher nominal driving range compared to the real-life average driving distance which is usually much lower. Studies show that typical daily driving range in Germany is below 50 km (80-90% of journeys) [49, 51]. Further for pure city vehicles this percentage is shifted to even lower distances [52], see Figure 2-16.

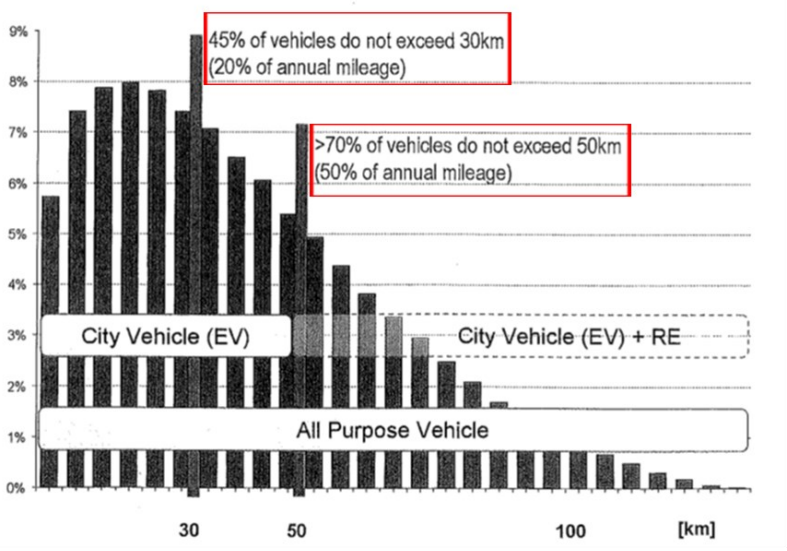

Figure 2-16 Statistics of all daily driving requirements in Germany. More than 70% of the vehicles do not exceed 50km which is well within the capability of an EV on a single charge [52]

A similar analysis carried out by Aimee et al [41] on the first generation Chevrolet Volt E-REV, with an all-electric range of 35–38 miles (56–61 kms), showed that drivers were able to travel 74% of their total miles in charge depleting mode without requiring ICE support. They also showed that drivers could attain even higher EV ranges utilising the benefit of daytime charging and efficient driving behaviours in moderate climates.

As per Kay et al [1] typically up to 60% of an average UK drivers' mileage can be in fully electric mode. Thus, for daily use additional battery weight is carried around in the vehicle without being used. Beside battery cost, the portion of the battery capacity not being utilised is reducing the efficiency of the complete vehicle. Therefore, the battery capacity could be designed for the typical daily driving range and an ICE powered RE covering larger energy requirements (higher power demand or longer driving distance).

The integration of a combustion engine thermal management concept into the thermal architecture of an EV is challenging, however the RE provides the key solution to keep the EV alive under severe ambient conditions. It supports bringing the battery

into the required temperature window as well as ensures adequate cabin climate control under hot and cold ambient conditions. Providing reasonable cabin climate conditions by pure electrical means would result in a dramatically reduced EV range [53].

2.6 Power Output Consideration for a Range Extender

In a REEV the battery pack delivers the peak demands of power to the traction motor. Since the battery is not discharged towards the minimum SOC defined by durability aspects, but a certain reserve is always kept to cover short term peak power requirements exceeding the RE power, therefore the RE can be sized such that it only needs to meet the mean power demand [4, 49]. The capacity of the battery enables it to average out the peaks and troughs in power requirement. Basset [4] in Figure 2-17 showed the logged data from the Mahle RE wherein despite the highly variant nature in traction motor power, the battery SOC remained fairly constant with the RE operating strategy that roughly follows the mean traction motor power demand.

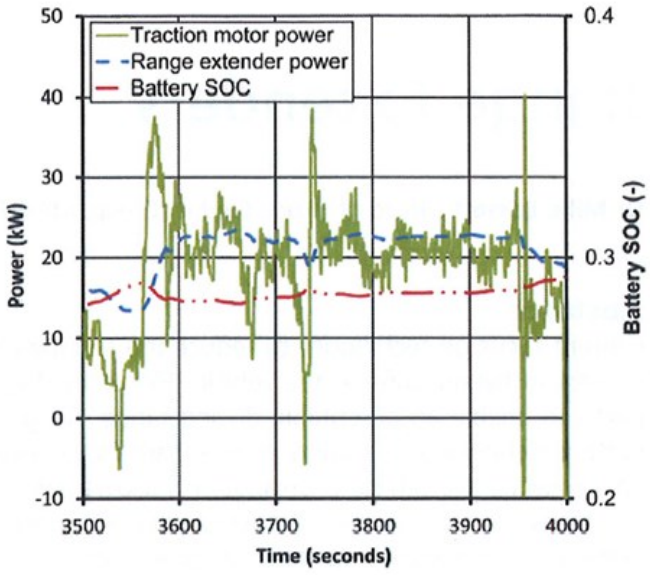

Figure 2-17 REEV battery SOC variation during a portion of a trip, based on data logged from the MAHLE RE demonstrator vehicle [4]

The amount of power a vehicle requires to complete a drive cycle is a function of several factors, including vehicle mass, drag and friction. The REEV can theoretically provide an ideal solution since it can use its energy storage system to smooth out the vehicle loads and therefore the engine could operate at limited conditions which can be made very efficient.

Based on the Artemis cycle, detailed in Chapter 9, Bassett et al [54] worked out the requirements for a hypothetical range extended electric vehicle for a typical European C-class vehicle. The RE mechanical output was strongly dependent upon desired cruise speed capability with sustained battery state of charge (SOC) as illustrated in Figure 2-18.

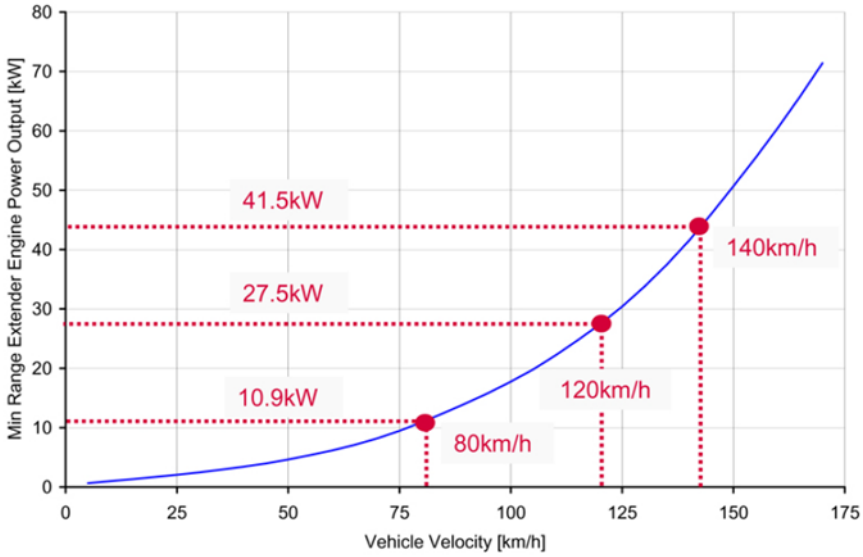

Figure 2-18 E-REV range extender fuel converter mechanical power requirement variation to maintain constant battery SOC (charge sustain) with varying cruising speed (1500 kg vehicle mass) [54]

Turner et al [3] carried out a similar analysis to establish the necessary power output of a practical series hybrid vehicle, dependent on maximum vehicle speed and gradeability for conditions of extended climbing with a depleted battery. This was assessed for a vehicle mass of 1650kg and typical drag coefficient and rolling friction for a conventional vehicle. They opted for a weight more than that of a typical C or D-

segment car, because of the unknown mass of the battery pack. They fixed a reasonable target maximum vehicle speed in charge-sustaining mode (akin to cruise performance with fully depleted batteries) of 70mph (120km/h). This would represent the minimum change to the motorist's driving habits on a long journey when the battery is fully depleted. Coupled with realistic electrical system efficiencies of 90% for the generator/motor, they concluded that peak engine power of 35kW would be needed to achieve 70mph (120km/h) vehicle cruise speed. Additionally, in the real-world scenario, ancillary loads (heating/cooling and infotainment) need to be considered and were anticipated to be up to 3kW for a luxury vehicle.

They also concluded that based on a vehicle operating on RON 95 gasoline, with thermal efficiency of 20% on the NEDC drive cycle, the useful continuous power requirement from the engine averaged would be just 3kW over the completed drive cycle. Catering for the ancillary loads, they concluded that 15kW could therefore be expected to cover most driving conditions up to an average speed of 30mph (48km/h), i.e. typical urban and extra urban conditions.

Hubmann et al [51] to meet an electrical power requirement of 25kW, selected 30kW as the power output of the ICE to cover losses in the overall system and other influencers like differing ambient conditions and ageing of parts. Pischinger et al [53] for a performance target of 62mph (100km/h) for an uphill gradient of 3% in order to enable vehicle operation at a speed 10km/h faster than the truck speed on German highways arrived at a power demand of approximately 25.8 kW at the wheels. Taking into consideration the component efficiencies, the power demand of the combustion engine was calculated to be 30kW.

For this study, the Artemis Urban and Artemis Motorway drive cycles were considered by TMETC while selecting the power requirement for the APU, covered in more detail in Chapter 3 [6].

2.7 Operating Strategies of an APU in a REEV

Since the battery acts as a buffer, the range extender can be operated independently of the driver demand, and it is not necessary that the generated power is always equal to the required traction power. The general operating strategy normally has two phases, a charge depleting phase and the charge sustaining phase [55], see Figure 2-19.

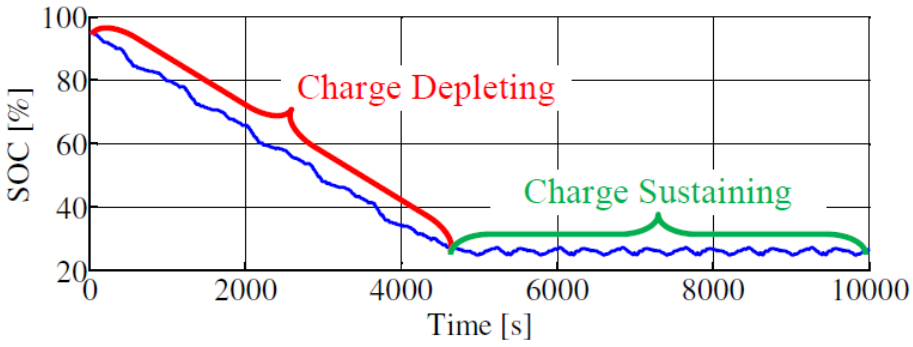

Figure 2-19 General operating strategy of a range extender in a BEV. The two phases of charge deplete (EV mode, APU off) and charge sustain (with APU in operation) are highlighted [55]

During the charge depleting phase, the APU is not operating and all the traction power is being provided by the battery, which gives vehicle zero tailpipe emissions. This phase is when the battery state of charge (SOC) is high. When the battery SOC drops below a predefined threshold, the APU switches on to maintain a certain level of SOC. As mentioned in Section 2.6, the battery SOC is never allowed to go below this SOC level due to battery durability aspects [55, 56]. Also a certain reserve is kept to cover short term peak power requirements exceeding the RE power [4].

APU operation impacts the system's fuel economy and efficiency. Hence the time to switch the APU on, its load and speed set points are critical to APU performance. Since there is an extra stage between the fuel's chemical energy to the vehicle's kinetic energy process, the energy conversion in a REEV is comparatively inefficient. Electricity from the grid is comparatively cheaper. Consequently, the APU

usually does not intend to charge the battery over the manufacturer's pre-defined SOC. When there is a short term transient peak power demand such as accelerating, the residual battery SOC can cover such requirements.

Rogge et al [55] compared the performance of three APU operating strategies in simulation, which were single operating point, three operating points, and a characteristic curve. The simulation was based on a vehicle similar to the Mitsubishi i-MiEV and the APU was based on the Lotus APU which was a 1200cc 3-cylinder engine and a permanent magnet synchronous generator [3]. The single point strategy operates the engine at its maximum efficiency (36kW) load condition. However, if the generated power is greater than the traction power demand, the battery is used as a buffer to absorb the extra power. This results in a high number of charge /discharge cycles that have a detrimental effect on battery life [55]. The 3 point operating strategy (16kW, 26kW and 36kW) allows the engine to adopt the most appropriate power rating based on vehicle power demand and protect the battery by reducing the charge/discharge cycles [55]. The characteristic curve strategy is based on the engine's minimum fuel consumption curve. With this strategy, the engine output can match the exact power requirement as long as it is above 4.7kW. Operating points below 4.7kW are excluded as the engine offers very poor efficiency. The simulation was conducted using the Hybrid Technology Approaching Efficient Zero Emission Mobility (HYZEM) driving cycles, developed for evaluating hybrid vehicles [57] and the New European Driving Cycle (NEDC), these cycles are discussed in Section 9.4 and 9.5 respectively. For comparison of the three strategies, the vehicle started with the same amount of fuel and 100% SOC for each run. The results showed that the single operating point strategy gives the best range and thus has the least fuel consumption of the three strategies in all drive cycles. The characteristic strategy is not efficient in urban cycles because the range extender is operated for long durations at low power rates and at a low efficiency. However, when only the highway driving is considered, very little difference was observed between the strategies due to the long duration of high-power demand.

Tupule et al [58] stated a similar result as above. A series hybrid system equipped with a small sized battery was used to cater for the daily commuting range. For long range driving the APU switched on for considerable periods. In this case, the single operating point strategy was the worst among the three as regards battery ageing effect. This is because the battery acts as an energy buffer to absorb the excess engine power that led to higher charging/discharging cycles.

Tupule et al [58] also discussed a blended mode control wherein the engine is used consistently with the electric motor during the entire trip. Power sharing between the engine and the battery is optimised such that the SOC continues to decrease during the trip and reaches the pre-defined minimum value only at the end of the trip. Such a strategy requires a prior knowledge of the driving pattern as well as sophisticated control algorithms as well as GPS information and historical traffic data to characterise the driving pattern.

2.8 Requirements of a Range Extender Engine

The basic requirements of a RE [3-5, 59, 60] can be tabulated as follows: -

- Compactness and lightness of the complete package as the RE engine is always carried by the vehicle, and even though it is operated infrequently it contributes to electric energy consumption even when switched off.

- Good fuel efficiency in order to maximise the benefits on CO_2 reduction of the EV.

- Low emissions levels to meet stringent regulations.

- Excellent noise vibration and harshness (NVH) behaviour, preferably the driver should not be able to distinguish when the engine is running. In EV mode,

the vehicle is virtually silent, and ideally the operation of the RE should be undetectable by the passengers i.e. should not impact the electric driving experience.

- Low cost as the RE system is essentially an additional cost to a re-specified BEV and therefore it must maximise its cost advantage over the proportion of the battery pack that it is effectively replacing.

As per Guenter et al [49] NVH, package and weight are the most important criteria whereas the efficiency of the ICE is less important due to the low share of ICE operation. Bassett et al [61] provide a similar argument because as the electric-only range of the vehicle increases, the weighing factors affecting the tailpipe emissions reduce the declared mass of emissions, see Figure 2-20.

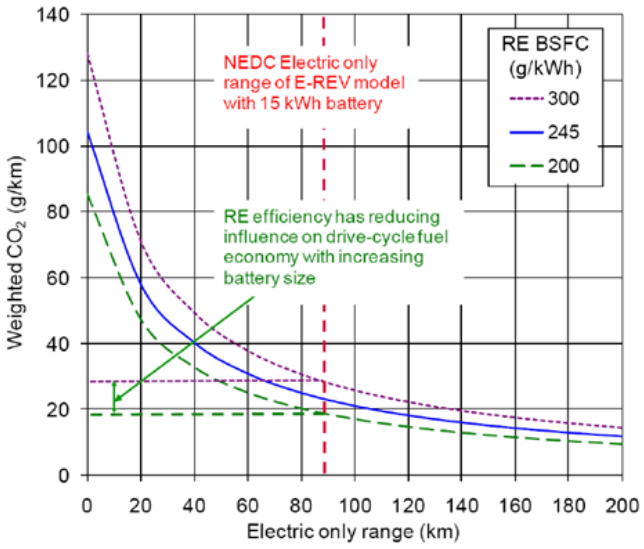

Figure 2-20 NEDC weighed CO_2 variation with varying electric only range and range extender fuel consumption [61]

Daimler-Benz AG while shortlisting options for their RE considered availability of the selected technology also as one of the key criteria [59], see Figure 2-21.

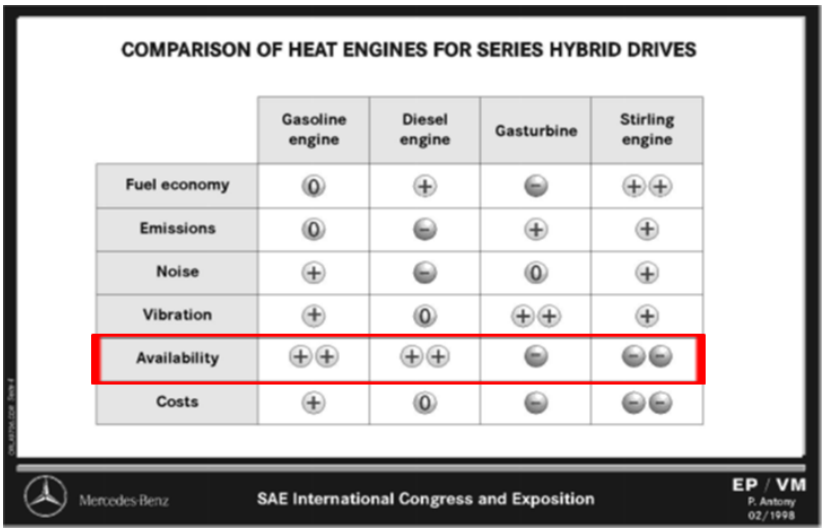

Figure 2-21 Comparison of heat engines for series hybrids. Daimler-Benz AG consider availability of engine technology as one of the key selection criteria [59].

As per Bassett [4], cost is the most significant factor for such a powertrain as the range extender is an additional system to a vehicle that already includes an expensive fully capable electric system. However, addition of a RE may make it possible to make the REEV cheaper or cost neutral as it enables reduction in the capacity of the expensive battery pack.

Fischer et al [52] in the AVL RE development, covered at Section 2.10 advocated that acoustics, comfort and dependability were the highest development priorities since the ICE operation should not or only indirectly be noticeable by the customer and that it should operate even after a long standstill. Pischinger et al [53] in the FEV RE development, covered at Section 2.10, regarded low noise operation as key for usage in an EV as it should have the least impact on electric driving experience.

2.9 Engine Concepts for Range Extender Applications

Internal combustion engines as range extenders for EVs are developed to operate at a limited range of load and speed. Thus, these engines are much more efficient than the usual accelerating engines found in conventional cars, as they always run at

specified conditions and are designed / optimised only for running at these conditions. Potentially critical operations for emissions, reliability or fuel consumption may be simply discarded from the set of working points [3, 5, 9, 49]. Removal of the mechanical link between the engine and the wheels permits consideration of various concepts which would have otherwise not been feasible. As per Hubmann et al [62] the available space and required power output are the biggest drivers for the engine concept selection.

As per Pischinger et al [53] a reciprocating gasoline engine offers a mature and proven technology for a RE application and can fulfil all future emission legislations as well as encompass the benefits of the use of existing fuelling infrastructure.

Turner et al [3], Bassett [4], Mattarelli et al [5] and Boretti [63] carried out a lucid discussion on engine concepts for RE applications which include gasoline engines (2-stroke versus 4-stroke), diesel engines, rotary engines, gas turbines and fuel cells. Merits and demerits of these various technologies are discussed in the succeeding paragraphs.

2.9.1 Gasoline Engines (2-stroke engines and 4-stroke engines)

The 2-stroke gasoline benefits from the double cycle frequency, allowing the designer the flexibility to either draw a very compact and light unit for a given power target, or limit the maximum rotational speed with ensuing advantages in terms of mechanical efficiency and NVH [60]. It also does not suffer from throttling losses at part load, but loses some of its charge air to the exhaust under some conditions leading to direct carry over in the case of external fuel mixture [3].

This can be eliminated by direct injection, but this leads to excess air operation. At low load and speed, 2-stroke GDI engine can work with lean/stratified mixture because of high turbulence levels, the compactness of the chamber and the injector

capability to generate a proper stratification of the charge. The adoption of a conventional 3-way catalyst should allow the complete reduction of CO and HC, while NOx is anyway low [5].

This stratified operation strategy will not be able to comply with emission regulations at high loads and speeds. The engine can be made to operate with a stoichiometric mixture within the cylinder, however a worsening of NOx emissions is envisaged due to peaks of oxygen concentration in the exhaust flow occurring at the end of the scavenging process. This would result in the freezing of the reduction of NOx. Thus, a 2-stroke engine would probably require a NOx trap. These are expensive and require regeneration strategies [3].

As compared to a 2-stroke, the 4-stroke has significant advantages which include ease of manufacture, simplicity of after-treatment and the minimisation of throttling loss if the engine is made to operate at full load. As the RE is expected to operate only at a few steady state points, therefore optimisation is much easier and potentially critical operations for emissions, fuel consumption and reliability may be simply discarded from the set of working points [3].

2.9.2 Diesel Engine

Diesel exhaust after-treatment systems have increased in complexity, size and weight in recent years because of stringent exhaust particulate and NOx regulations [3-5]. Further as brought out earlier in section 2.8, the RE will essentially operate at full load and hence un-throttled, the magnitude of efficiency benefit enjoyed by the diesel engine over an equivalent gasoline engine is significantly reduced. The diesel engine has additional NVH disadvantages compared to gasoline engines [4]. Compression ignition engines, without turbocharging, are not attractive, because of the low power density, but turbocharging is immediately discarded because of cost implications [5].

2.9.3 Wankel Rotary Engine

The Wankel rotary engine has some advantages as regards RE application which include being extremely compact, light and has excellent NVH characteristics [3, 4, 51]. It operates on the 4-stroke cycle and its emissions, especially HC, require a comprehensive optimisation of the mixture formation and combustion, can be controlled by a simple 3-way catalyst. Guenter et al [49] also highlighted that by utilising the Atkinson cycle, the late exhaust opening and resulting extended expansion not only improved the efficiency and HC emissions but also reduced the pressure pulse with exhaust opening and consequently the gas exchange noise. Further, the rotary engines provided advantages both in terms of run-in behaviour as well as friction level with non-warmed up engine over a conventional ICE. Also, the catalyst light off profits from the high exhaust temperature of the rotary engine.

The main drawback of the Wankel engine is the non-availability of large-scale manufacturing devices for specific rotary engine components and therefore the industry is demanding solutions based on conventional piston engines [3, 51]. Further once the intake and exhaust systems are considered, the overall package is comparable to its reciprocating counterpart. Also, the sealing of the rotor tips is a persistent challenge for such engines as is the compromised shape of the combustion chamber. There is renewed interest in this technology with Mazda announcing that it will introduce one of its BEVs in 2020 with a Wankel engine range extender engine [64].

2.9.4 Gas Turbine Range Extender

Several proposals and examples of REEVs fitted with gas turbine REs exist [65-68]. To achieve high efficiency, a recuperator is needed to transfer heat from the exhaust to the combustor inlet, which increases the size, weight and cost of the unit [4]. To avoid the use of the recuperator the pressure ratios must be increased along with the turbine entry temperature. Current turbine entry temperatures of turbochargers

are around 1050°C, however still below what is required to achieve a reasonable specific fuel consumption (SFC) at maximum power in a gas turbine. Increasing this value would have detrimental effect on NOx emissions, and would require considerable effort, though not impossible, to control NOx [3].

Gas turbines offer low vibration and good noise characteristics coupled with a reasonable package volume. However, they have higher production costs and long development times in comparison to both the reciprocating piston and the rotary engine [3, 4].

Jaguar introduced its C-X75 gas micro-turbine extended range EV concept at the Paris motor show 2010 [69]. There appears to be a renewed interest in this technology with Delta Motorsport [70] working on the development of a 17kW micro turbine range extender (MITRE) for EVs and Wrightspeed Inc, a developer of range extended EV powertrains for medium and heavy duty vehicles unveiling a 80 kW radial inflow, axial turbine, intercooled and recuperated [71].

Techrules, a new automotive research and development company based in Beijing introduced their concept 1030bhp turbine-recharged electric vehicle (TREV) with six electric motors and a theoretical top speed of 217mph at the 2016 Geneva motor show. It uses a very small micro turbine to directly drive the generator that produces electricity that powers the electric motors that turn the wheels. The turbine produces 36kW to drive the generator and power the ancillaries. The micro turbine uses an air bearing in place of the conventional oil lubricant film and is claimed to be so low maintenance that it would potentially be sealed for life with only the air filters needing renewal [72].

2.9.5 Fuel Cell

The New Automotive Innovation and Growth Team (NAIGT), formed in April 2008, published a 20-year vision for the UK automotive industry and made recommendations on how this should be realised. The report presents mass-market EVs and hydrogen fuel cell powered vehicles as desirable end games in terms of low fleet averaged CO_2 emissions [4, 73], see Figure 2-22.

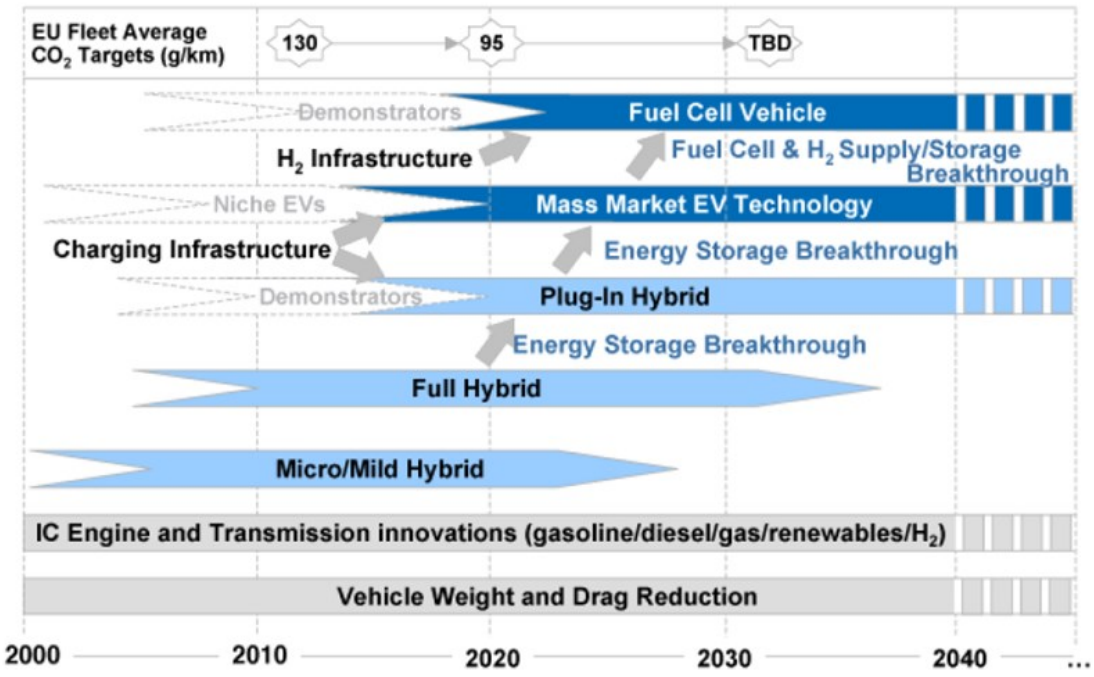

Figure 2-22 Product development roadmap by NAIGT with fuel cell powered vehicles being the desired endgame [73]

As per Bassett [4], the fuel cell is in many ways the ideal RE unit as it enables direct conversion of fuel into electricity without the intermediate step of producing mechanical power, see Figure 2-23. This has the added benefit of zero mechanical vibrations or noise other than those generated by coolant pumps and air blowers. The energy conversion of fuel cells is usually very high. Warburton et al [74] reported an overall efficiency of almost 54% from their London taxi demonstrator using the proton exchange membrane (PEM) fuel cell that are evaporatively cooled.

The attributes of a fuel cell of being silent, vibration free and zero emissions at point of use allow greater flexibility in the vehicle power management strategy as compared to an ICE. The strategy can exploit the favourable attributes of the fuel cell to reduce the inefficiencies inherent in charging and discharging the main battery by up to 40% and operating at non-ideal power points [75].

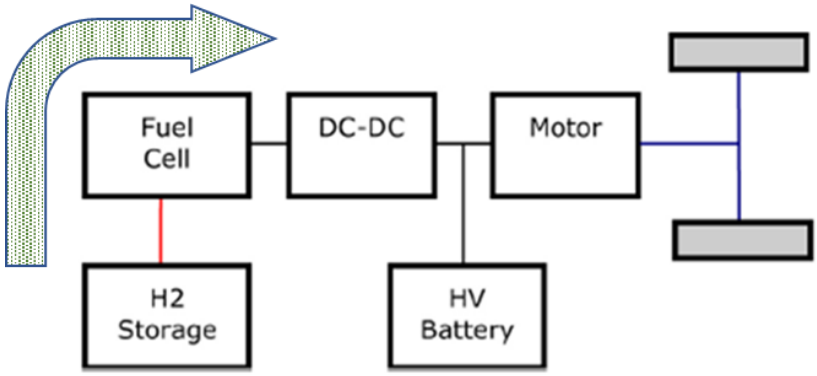

Figure 2-23 Fuel cell RE powertrain configuration. Direct conversion of fuel into electricity without intermediate step of producing mechanical power [74]

The most significant barriers to the introduction of fuel cell technology are cost (maximising power density and reducing cell quantities and area), fuel supply infrastructure and elements of durability under dynamic and climatic conditions [74]. The motivation for a RE is to be able to refill quickly with a highly energy dense fuel, using an existing and readily available refuelling infrastructure, diesel and gasoline in contrast to hydrogen, are ideal in this regard. Further hydrogen must be stored at high pressures, involving cumbersome tanks and limiting the on-board storage capacity [4].

2.10 REs Currently in the Market

Mahle developed a bespoke 900cc, inline 2-cylinder, 4-stroke petrol engine for their range extender vehicle concept to meet the requirement of minimum package volume, low cost and good NVH. The engine consisted of a single overhead cam and ran a compression ratio of 10:1, alongside a flexible Mahle ECU. The generator unit

was a 38kW water-cooled permanent magnetic axial flux motor. The entire unit weighed 70kg. The unit was coupled to an EVO AF130 axial flux generator, which had a maximum efficiency region around 4000rpm. The demonstrator vehicle used by Mahle was an Audi A1 1.2. The Mahle Rex unit was shorter than the 1.2 litre turbocharged 4-cylinder engine that it replaced. The vehicle was then tested on the NEDC drive cycle under two separate conditions specified in the hybrid vehicle test procedure regulations – one with battery SOC 20% and one with a fully charged battery. The vehicle had considerably lower exhaust CO2 emissions at 42g/km compared to the baseline vehicle which had 119g/km [7]. The APU had a peak system efficiency of 283g/kWh(e) and rated system efficiency of 292g/kWh(e) [6].

Lotus developed a compact range extender vehicle for the Limo Green project, which involved Jaguar Land Rover and funding from the UK government. The bespoke engine was a 3-cylinder, 1200cc, four stroke gasoline with a heavily constrained area of operation. The main criteria considered before finalising the 4-stroke gasoline engine were weight, cost and efficiency. It was decided that NVH could be dealt with during the development and installation process. The engine speed was constrained to 3500rpm with an option to run at 4000rpm for higher power requirements in the future. The general specification of the engine was 36.8kW with 10.7bar BMEP [3].

BMW launched its i3 EV with the range extender as an additional option costing around £3150 extra. The vehicle consists of a 22kWh battery pack which provides an all-electric range of 80-120 miles. The range extender option comprises of a 650cc Kymco engine (W20) from the BMW C650 GT scooter rated to 25kW, which is connected to an AC machine [76]. The range extender is mainly used to maintain a battery state of charge to keep the electrical system going until the next recharging station. For this purpose, the package has a 9-litre fuel tank and in total weighed 150kg.

The new Metrocab from makers Frazer-Nash research Ltd and Ecotive Ltd has been operating on a pilot fleet basis in London since November 2014. The vehicle is driven by two 50kW brushless motors, powered by a 12.2kWh Lithium ion battery pack. The vehicle claims to produce less than 50g/km CO_2 in the range extender mode and has a fuel consumption of 98 mpg when tested on the Public Carriage Office (PCO) drive cycle. The range extender engine consists of a 3-cylinder, 1000cc gasoline engine which provides 3kW on-board charging of the batteries [77], further details whether the engine is a bespoke or production engine could not be found.

FEV's compact range extender prototype consisted of a V-2 engine with a vertical oriented crankshaft [53]. The engine was 800cc petrol powered producing an output of 40kW at 4500rpm. The engine was closely connected to two generators via gears to increase the speed of operation of the PM machines and to make use of the full engine vibration compensation technology [78]. The PM machines have a power output of 15kW each. The main bearings of crankshaft and generator shaft were machined together in one part to make handling of gear tolerances easier. The FEV range extender cooling solution used the same coolant as in the engine to cool the generator unit and the inverter. The RE was installed underneath the rear seats and the luggage compartment, which facilitated easy assembly/disassembly and the exhaust system did not have to be routed past the battery. Specific fuel consumption at best point was 245g/kWh at 2500 rpm, Euro 6 compliant. The permanent electric motor output was 3kW at 4500rpm. The module weight was 62kg without the exhaust system.

EP Tender is another manufacturer who attempted a compact retrofit range extender for automotive applications. The company developed a trailer mounted range extender comprising a 600cc engine with a generator of 22kW capacity [79]. The entire unit was enclosed and on wheels, which could be attached to the rear of an EV. The trailer had a 35-litre gasoline tank and had an average consumption from 6–7 l/100 km

when batteries were discharged. Practicality and aesthetic appeal of this technology makes it a less preferred solution among consumers.

AVLs direct drive range extender was developed as a low cost and best fuel economy range extender. This prototype used a unique 2-cylinder piston engine based on a cost and friction optimized design originating from 2-wheelers. The engine was a 570cc with a maximum power output of 25kW at 6000rpm and operated within 1000rpm and 6000rpm. This engine was coupled to a 15kW PM generator unit. The system was tried in an Audi A1 with a 60kW PM machine as the traction motor [49].

The benefits of the Wankel rotary engine have been covered earlier at Section 2.9.3. Using their experience in the development of rotary engines, AVL developed their pure range extender. The single piston rotary engine with 254cc displacement was limited to 5000rpm for full power (18kW) operation, producing 15kW electrical output. To reduce the vibrations from the RE unit to the car body, it was installed in a suspension frame system which was mounted on the rear part of the chassis with a few elastic bearings and rubber mounts. Apart from that, a box was used to accommodate the RE unit in an acoustic enclosure. The air inlet and outlet were designed as acoustic labyrinths with high sound attenuation. These designs allowed the sound level to be less than 65dbA at 1m away and 58dbA in the cabin [52].

Despite the very small packaging, excellent NVH characteristics and acceptable fuel efficiency even under stringent emission challenges, the main drawback seen by AVL was the non-availability of large-scale manufacturing for specific rotary engine components. Therefore AVL developed a single cylinder ICE to replace the Wankel engine, packaged in the same RE box arrangement except the exhaust muffler for thermal considerations [51]. The single cylinder engine had a stroke/bore ratio of 0.67 and produced 30kW at 5800rpm. The corresponding electric power output was 25kW. The package space constraint meant the engine was tilted to an angle of 70° and the crankshaft was not coaxial with generator shaft anymore. A gear stage was introduced

thus. Two separate cooling circuits for the engine and the generator were used allowing them to operate in the optimum thermal state respectively. 1st order mass forces are most severe NVH source for one-cylinder engine. AVL used 2 balancer shafts which were in plane with the crankshaft reducing the forces by up to 2.4 times. With further optimised crankshaft counterweight inertia, the vibration level was brought down to nearly the same as the rotary engine.

Mazda's range extender prototype was based on the Mazda 2 small hatchback. Initially the electric car developed based on this hatchback had a 350V 20kWh battery under the floor of the vehicle, powering a 75kW electric traction motor. The range extender consisted of a 330cc Wankel engine optimised to run at 4500rpm producing a power of 22kW. The generator produces a continuous output of 20kW [80]. The Wankel engine being highly compact was placed horizontally along with the generator and the fuel tank under the rear boot floor of the vehicle, with the engine, electric generator, nine-litre fuel tank and ancillaries weigh just 100kg. The estimated CO_2 emissions of the range extender vehicle over the NEDC drive cycle is 13g/km. Mazda had announced that one of the electric vehicles that they shall introduce in 2020 shall have a small, lightweight and exceptionally quiet rotary engine [64].

The Chevrolet Volt consists of a 4-cylinder 1400cc IC engine producing 63kW connected to a generator rated to 55kW. The vehicle has a 16kWh battery pack that weighs 197kg. The vehicle operates as an EV most of the time, till the battery state of charge drops to a low level, after which the IC engine starts charging the battery. The vehicle has a fully electric range of 80km and around 600km of extended range using the IC engine. At high speeds, the internal combustion engine can be mechanically connected to the driveline using a clutch [81].

Polaris developed a range extender package in the view of the industry moving towards engine downsizing and powertrain electrification. Their design was proved on an EV based on the VW Polo, which then had a range of 50km in full EV mode and

500km when the engine was used to charge the battery pack [82]. The engine consisted of a 325cc single cylinder which in conjunction with an electric motor produced an electrical output of 22kW and weighed 38kg.

Volvo developed a range extender vehicle based on the C30 compact car with the aim of reducing exhaust CO2 emissions to under 50g/km on the NEDC. The system consisted of a 3-cylinder ICE producing 45kW that would run in series with an electrical generator rated to 40kW. The vehicle had a range of 100km in full EV mode and up to 1000km with the ICE range extender. The battery pack was a smaller sized 12kWh unit, while the fully electric version of the C30 had a 24kWh battery pack [48].

GETRAG developed a range extended EV with plug in capability to travel up to 50km in all electric mode. The vehicle consisted of a 2-speed planetary gear set that mechanically linked the engine and the electric motor together with the output drive. This system allowed for the either series or parallel operation of the EV. The major portion of the driving dynamics was covered using the battery pack and all electric mode, while the engine is used in a small part of the overall vehicle performance map. The electric motor provided continuous output of 30-45kW, depending upon vehicle platform, with maximum output of 45-80kW. The GETRAG range extender demonstration vehicle was a Ford Fiesta and produced 35g/km of CO_2 on the NEDC. It also had a 14kWh capacity battery pack rated to 400V [83].

Intelligent energy introduced their evaporatively cooled fuel cell stacks for RE application in a fleet of five conventional London taxi black cabs in 2012 since its first exposure to the public in 2010. The standard black taxi chassis was modified to accept an electric drive, electrical battery storage, 35MPa hydrogen gas storage and a PEM fuel cell system with no change to rear passenger space or function and minimal impact on the luggage and driver area [74]. The taxi had a 14kWh battery and the fuel cell rated at 30kW, with a reported overall efficiency of almost 54%.

A summary of the various range extenders discussed in the preceding paragraphs is tabulated at Table 2-2 below.

Table 2-2 Summary of REEVs in the market

Manfacturer	Engine Size / Specification	Generator Specification	Battery Size	Weight	Range	Reference
Mahle	Bespoke 2-cylinder 900cc, 30kW, 72Nm @2000-4000rpm	38kW, water-cooled PM axial flux	350V, 14kWh	50kg engine (70 kg with generator)	70km EV mode	[3, 73]
Lotus	Bespoke 3-cylinder, 1200cc, 36.8kW @3500rpm	-	-	56 kg engine	48 km EV mode	[3]
BMW	Retrofit 2-cylinder, 650cc, 25kW, 55Nm	-	22kWh		200km EV mode	[76]
Frazer-Nash & Ecotive Ltd	1000cc	-	12.2kWh	-	-	[77]
FEV	Bespoke V-2, 800cc, 40kW@4500rpm	2*15kW PM machines	-	-	-	[53, 78]
AVL	Bespoke 2-cylinder, 570cc, 25kW@6000rpm	15kW	-	40kg engine	-	[49]
AVL	Bespoke Single-cylinder, rotary, 18kW@5000rpm	15kW	-	-	-	[52]
AVL	Bespoke Single-cylinder, 30kW@5800rpm	25kW	-	-	-	[51]
Mazda	Bespoke Rotary, 330cc, 22.37kW@4500rpm	Continuous output of 20kW	346V, 20kWh	-	-	[80]
Chevrolet	4-cylinder, 1400cc, 63kW	53kW	16kWh		80km EV mode	[81]
Polaris	Bespoke Single cylinder, 325cc	22kW		38kg engine	48km EV mode	[82]
Volvo	3-cylinder, 45kW	40kW	12kWh	-	110km EV mode	[48]
GETRAG	3-cylinder, 1000cc, 57kW@3500rpm	40kW	400V, 14kWh	100kg	50km EV mode	[83]
Intelligent Energy	30kW PEM fuel cell	-	14kWh	-	-	[74]

2.11 Thermal Management in an APU

Thermal management is a critical part in a vehicle. It is governed by two constraints – cooling performance and packaging. The packaging space in the vehicle limits the cooling system size. It becomes even more challenging in a hybrid system since extra components are in operation compared to a conventional IC engine. One of the key requirements of an APU is to provide its maximum electrical power most efficiently i.e. with minimum fuel consumption. To do so, it is important that the engine and the generator are operated at their maximum efficiency in addition to optimising the complete system to reduce any parasitic losses in the auxiliary systems.

The system efficiency is one of the key parameters for an APU since it decides the maximum possible electric power that can be delivered with a given amount of fuel, i.e. the fuel economy. The operating temperature of the APU thus plays an important role on both engine and motor/generator efficiency. However, they have conflicting requirements to achieve their own optimal efficiency.

The positive effect of higher coolant operating temperatures on an engine's fuel economy and emissions is well documented [84-86]. With the conventional engine cooling system, with an engine driven passive water pump designed to cope with the peak-heat rejection rate at WOT conditions, based on a coolant temperature set point, the engine and its cooling systems operate at less than ideal conditions at part-load, such as city driving or slow cruising, leading to higher fuel consumption and emissions output. This is discussed in greater detail in Chapter 7.

On the other hand, the performance of the motor/generator and the power electronics is limited by their peak working temperatures, mainly restricted by the insulation. As for the motor windings which is mainly copper, the resistance will rise with temperature. This will result in more copper losses. Hence lower operating temperatures are preferred for better efficiency as opposed to the ICE [51, 52].

Hence thermal management of an APU merits considerable attention. However, despite extensive literature search, details on this subject as regards current range extenders in the market were not available except for the BMW-i3 RE and Chevrolet Volt. There was a brief mention in regards the FEV compact range extender cooling solution that indicated that the coolant used to cool the engine is also used to cool the generator unit and inverter [53, 78]. Likewise, for AVL's single cylinder range extender, the cooling system is split into two different cooling jackets for generator and engine cooling without internal connection, and the cooling system is driven by an electric water pump [51].

As a pure electric vehicle without a range extender, the BMW-i3 has cooling circuit for the high voltage components. If a range extender is installed, then the necessary cooling of the combustion engine is done by a second cooling circuit [87], see Figure 2-24. The coolant is recirculated in the engine using a conventional engine-driven mechanical coolant pump and control is achieved using a wax element thermostat.

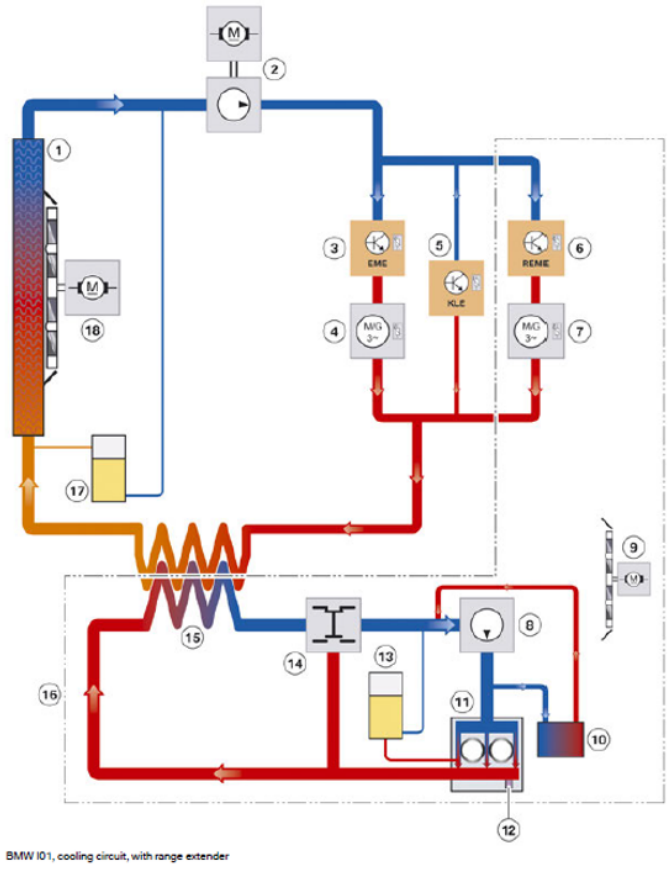

Index	Description
1	Radiator
2	Electric coolant pump 80W
3	Electric machine electronics (EME)
4	Electrical machine
5	Charger electronics (KLE)
6	Range extender electrical machine electronics (REME)
7	Electrical machine for REX
8	Mechanical coolant pump
9	Additional electric fan
10	Engine oil-to-coolant heat exchanger
11	Combustion engine W20
12	Coolant temperature sensor
13	Expansion tank
14	Thermostat
15	Coolant-to-coolant heat exchanger
16	Equipment only with range extender
17	Expansion tank
18	Electric fan

Figure 2-24 BMW-i3 REX cooling circuit. Engine and motor/generator coolant circuits are independent of each other [86]

The Chevrolet Volt uses four independent cooling loops to achieve the thermal requirements of each subsystem [88]. The power electronics and the onboard charger are cooled in one circuit that uses the upper section of the front radiator. The lower section of the radiator is for the battery. The engine and the two motor/generators have their own cooling circuit with radiator for different temperature levels, see Figure 2-25.

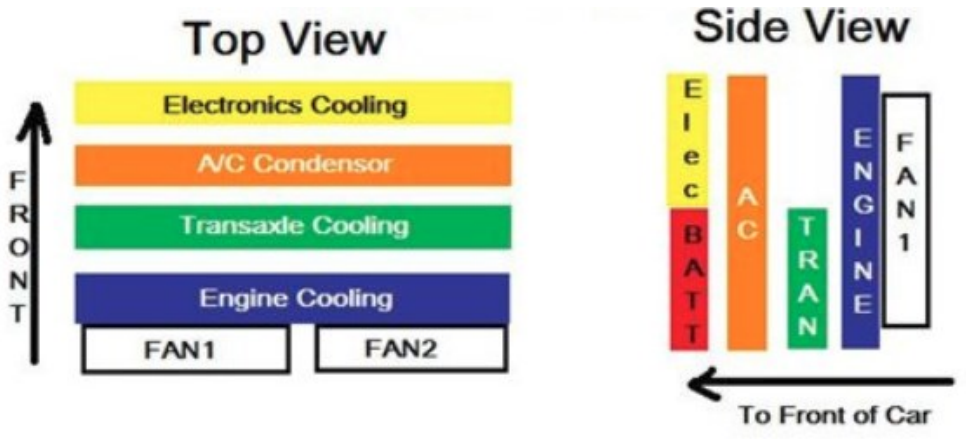

Figure 2-25 Chevrolet Volt Radiator layout for cooling the 4 independent cooling circuits [88]

All the four circuits use electric water pumps (EWP) instead of the engine driven mechanical water pump. Conventional mechanical coolant pumps are engine driven (belt/gear) and hence their rpm is governed by the engine rpm. Coolant pumps need to ensure sufficient cooling even at low engine rpm with high engine loads and at elevated ambient temperatures, and so for normal operation such as city driving or slow cruising, they are inevitably oversized.

The use of an electric coolant pump with appropriate thermal management of the combustion engine has measurable advantages. Demand driven cooling, which is independent of engine speed, particularly in the cold-start phase reduces impeller energy consumption and leads to corresponding improvement in fuel economy. The Lotus bespoke RE engine also employed a EWP for similar reasons [3].

Another major benefit of an electric coolant pump is its ability to keep running after the engine has shut down to prevent the heat soak problems to which some engines are prone. Further the lack of dependence on a mechanical drive also results in considerable flexibility in component packaging within the engine compartment [89].

Multiple cooling circuit design is effective, but the system complexity, installation/packaging requirements and associated costs are significant. Combining cooling loops of some subsystems can accrue cost benefits. The Toyota Prius consists of a cooling loop for the ICE at around 105°C and the Power electronics/electric machine loop at 65°C. Staunton et al [90] estimated that by combining the two loops approximately $188 per vehicle could be saved.

In a range extender the engine operation is intermittent. This results in an increased number of cold starts. Hence a quick warm up is very helpful to reduce engine cold start emissions and friction loss during this phase. More is discussed about this aspect in Chapter 10.

2.12 Selection of a Production Engine vis-à-vis a Bespoke Engine

There has been considerable debate on whether to select a production engine or develop a bespoke engine for RE application. As brought out earlier in the report, most car manufacturers have developed bespoke engines for RE application [3, 53, 91]. Benefits of bespoke engines are that they are highly optimised to purpose, have potential for better integration with e-machine, often capable of flexible installation keeping package optimisation in mind and higher operating speed can drive better e-machine performance. The drawbacks of bespoke engines include that it may need unusual manufacturing process, setting up of a new/adapted manufacturing plant and no other demand outside the RE application. Setting up of a new manufacturing facility involves high cost and developing a new engine will also require unique engineering and validation programme.

On the other hand, production engines benefit from their manufacturing highly optimised for high volume production, are usually certified for emission performance, proven for vehicle use, have existing service network and cost less because of higher volumes [50], an approach followed by BMW for their BMWi3 RE [76] and EP

Tender [79]. Mattarelli et al [5] tend to disagree with this approach. As per them the engineering cost for converting an existing engine for other applications (motorcycles, small gen-sets etc.) into REs would be not much lower than the development from scratch. However, they do not qualify their statement with more details. Further production engines may have their challenges in terms of limited options for installation and more difficult to integrate with an e-machine. Considering the anticipated production volumes of REEVs is likely to be relatively small, to achieve an acceptable cost modification of an existing volume production engine would be a preferable route over a bespoke engine.

The pros and cons of using a production engine vis-à-vis a bespoke engine are tabulated in Table 2-3.

Table 2-3 Comparison of production engine versus bespoke engine for APU application

Parameter	Production Engine	Bespoke Engine
Highly optimised for high volume manufacture	✓	×
Certified for emission performance	✓	×
Proven for vehicle use	✓	×
Existing service network	✓	×
Selling price benefits from total derivative volumes	✓	×
Options for installation and orientation	Limited	Developed based on requirement
Integration of e-machine	More challenging	Easier
Performance optimisation allowable for APU application	Limited	Developed based on requirement

2.13 Research Gaps / Opportunities

Based on the high voltage battery costs and the daily urban driving commute of an average driver, introducing a range extender in a BEV made economic sense. The RE represents a highly integrated auxiliary power source with a much superior level of energy density and significantly lower production costs compared to battery systems

for an equivalent driving range. For most of the time the driving range provided by the battery should be enough, especially for urban driving. For the occasional long journeys when the battery and fuel are both depleted, the driver can simply refuel the gasoline tank as in a traditional vehicle.

Opportunity was hence seen to select a very low-cost highly optimised production automotive engine and then enhance it for more fuel-efficient running in critical speed/load ranges for the REEV duty cycle. Engine operation would be optimised for low dynamic use with restricted engine map. Operating points such as low speed and high-speed torque would be avoided, with the battery being used to smooth out the vehicle loads.

The engine modifications to be considered would only include changes which were possible in the normal volume-production process.

As mentioned in Section 2.11 not much information was available regarding thermal management of a range extender. Whatever information was available indicated that the engine and generator (including power electronics) were thermally managed in independent circuits. Combining the high temperature ICE cooling circuit with the low temperature power electronic/electric machine low temperature cooling circuit would accrue cost and packaging benefits. Opportunity was seen to fill this research gap by combining the two coolant circuits and demonstrate by experimental analysis that satisfactory performance could be achieved without significant loss in efficiency. This would also reduce parasitic losses as well as reduce overall package volume and weight. Since the RE was replacing the high voltage battery, it was important to accrue the maximum benefit by keeping the overall package weight of the RE to the minimum possible.

Based on the opportunities above, a collaborative research project was conceived in partnership between TMETC, Ashwoods Automotive Ltd and the University of

Bath. The scope of the project was to design, model and evaluate an industry first low-cost Auxiliary Power Unit (APU) intended primarily for use in a REEV. The project was part funded by Innovate UK. The research project began in 2013 and concluded in July 2016.

2.14 Conclusion

This chapter presents a literature review on the benefits and shortcomings of electric vehicles. Since the range extender benefits from the advantages of a conventional ICE, it provides a means of overcoming the primary range anxiety issue of electric vehicles. Further it also facilitates battery downsizing which has other benefits as well.

Since the APU in a REEV is not directly connected to the drive shaft, the ICE does not have to output high torque other than turning an electric generator, especially at low revolution speed. Therefore, a low-cylinder-count is commonly used for this application which facilitates reduction of cost, weight, package size etc. Also, the engine operation as a RE is more flexible. This is because low speed-high torque and high speed-high power load points were not expected to be used in RE application from fuel efficiency and NVH aspects.

The low-cylinder-count engine inherently exposes more vibration and speed fluctuations due to the less frequent firing events. The literature review of the current REEVs brought out the efforts by manufacturers to minimise the vibrations both actively or passively. In the EV mode, the vehicle is virtually silent, and ideally the operation of the RE should be undetectable by the passengers i.e. should not impact the electric driving experience. Manufacturers and researchers have either developed from scratch or heavily modified IC engines to attain their required IC engine performance. This approach increases both R&D and manufacturing costs of the engine and its components.

Lastly the advantages of selection of a production engine vis-à-vis development of a bespoke engine for range extender application were covered. It is opined that based on the literature review wherein over 70% of the journeys do not exceed 50km and the RE would not be used, the development of a bespoke engine for RE application is not warranted. At the same time, there is need to keep sight of the rapidly dropping battery prices, weight, improved range as well as doubling of production as it is likely to influence the economic model for a range extender.

CHAPTER - 3
Base Engine Selection and Benchmarking

This chapter presents the criteria for the RE power requirement and the base engine selection. It then discusses the bespoke engine test cell at the University of Bath and test data repeatability. At the end, the base engine performance is discussed.

3.1 Introduction

In this chapter, the criteria for selecting the RE power requirement for this research is discussed. The next section presents the selection of the base engine based on the RE power requirement and using an in-production engine.

Subsequently, the development of the bespoke engine test cell at the University of Bath is covered. This includes a discussion on repeatability of test data and the importance of using a reference fuel for consistency in test results.

Lastly the performance of the production engine is mapped across its entire operating regime, both at part load and full load. A BSFC map is generated which then became a yardstick to compare the effect of subsequent optimisation of the engine for range extender application.

3.2 RE Power Requirement, 20–25kW

An APU may be sized from an emergency limp home device of relatively low power, to a device that provides the full functionality of the EV once the battery has been depleted. For the purpose of this study, the APU considered was that would provide the latter capability.

The electrical power output of the RE for this study was defined by considering the average electrical load drawn from the high voltage (HV) bus during extended range (or charge sustaining operation) for 3 vehicle applications. This load is the sum of tractive power (suitably corrected for drive system losses) together with ancillary load requirements.

The three vehicles considered by TMETC to develop the appropriate RE power requirements were [6]:-

- Tata Motors Manza REEV
- Tata Motors X451 REEV
- JLR Evoque-E (REEV)

The Tata Motors Manza REEV was the outcome of Tata Motors Horizonext campaign with sustainability and EV technology among the key focus areas. TMETC developed the Manza REEV demonstrator vehicle. Some of its technical specifications are at Table 3-1 below.

Table 3-1 Tata Motors Manza REEV specification [6]

Vehicle	Unit	Target (Status)	Remarks
Vehicle category	-	C-segment sedan	
Kerb weight	kg	1375	
Performance test weight	kg	1525	
GVW	kg	1705	
Maximum vehicle speed	kmph	132 (82 mph)	
R101 (A) NEDC range (EV)	km	88	
R101 (B) NEDC CO_2	g/km		
R101 NEDC CO_2	g/km	<40	
EV range (real world)	km	56	Artemis combined
Total range (real world)	km	350	Artemis combined
Fuel economy @ charge sustaining 70 mph	mpg	46	

The second vehicle chosen was the REEV variant of the Tata Motors MEGAPIXEL, a B-segment vehicle being developed for European and global markets. Concept specifications of MEGAPIXEL REEV are at Table 3-2 below.

Table 3-2 Tata Motors B-segment REEV concept specification [6]

Vehicle	Unit	Target (Status)	Remarks
Vehicle category	-	B-segment hatch	
Kerb weight	kg	Not disclosed.	Industry confidentiality
GVW	kg	Not disclosed.	Industry confidentiality
Maximum vehicle speed	kmph	Not disclosed.	Industry confidentiality
R101 (A) NEDC range (EV)	km	62	

Vehicle	Unit	Target (Status)	Remarks
R101 (B) NEDC CO_2	g/km	Not disclosed.	Industry confidentiality
R101 NEDC CO_2	g/km	<30	

The third vehicle was JLR's electric Evoque (Evoque-E) which was meant to be a BEV. Specifications are at Table 3-3 below.

Table 3-3 JLR Evoque-E specification [6]

Vehicle	Unit	Target (Status)	Remarks
Vehicle category	-	BEV/SUV	
Kerb weight	kg	1914	
GVW	kg	2440	
Maximum vehicle speed	kmph	210	
R101 (A) NEDC range (EV)	km	325	
R101 (B) NEDC CO2	g/km	0	BEV
R101 NEDC CO2	g/km	0	BEV
Total range (real world)	km	na	

As discussed earlier in Section 2.6, the RE power output is strongly dependent upon desired cruise speed capability with sustained battery state of charge (SOC) as illustrated in Figure 2-18. A similar exercise based on electrical power versus speed was carried out by TMETC for the 3 selected vehicles and it was found that the electrical power required falls within a range from 15kWe to greater than 30kWe for motorway cruising speed [6], see Figure 3-1

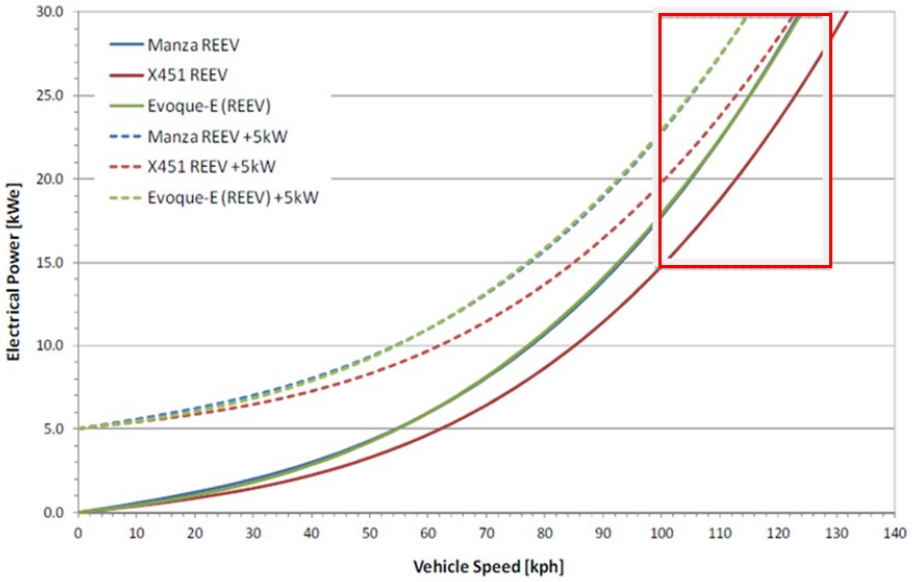

Figure 3-1 Vehicle electrical power requirement of 15-30kW versus speed for the three vehicles considered. Power calculation based on vehicle weight including kerb weight plus 250kg, highway speed 60-70mph, flat road (0% gradient), 5kW ancillary loads and charge sustaining APU operation [6]

Based on this electric power range and the base engine performance capability coupled with the primary requirement of this study to optimise the ICE using low cost changes well within the normal volume-production process, a maximum electrical power output of 20–25kW was aimed at. This would result in a small compromise in maximum charge sustaining speed and/or ancillary performance for the Manza REEV and Evoque-E (REEV) but was accepted for this research.

3.3 Base Engine Specification

The base engine selected for this research was a Bharat Stage 4 (BS4) emission version of Tata Motors Limited 273 2-cylinder 624cc naturally aspirated gasoline engine for Indian market application [2, 6]. Being a production engine, it accrued the benefit of low cost as compared to the development of a bespoke engine, as has been discussed in Section 2.12.

The main specifications of the engine are given in Table 3-4 below.

Table 3-4 Specifications of the TATA 273MPFI engine [2]

Displaced volume	624cc
Bore / Stroke	73.5mm * 73.5mm
Compression ratio	10.3:1
Maximum power	37bhp @ 5500rpm
Maximum torque	51Nm @ 4000rpm
Firing order	1-2 (360° firing)
Number of valves	2 per cylinder, single fixed overhead camshaft
Fuel system	Sequential port fuel injection with closed loop A/F control
Emission compliance	Bharat stage (BS) III or IV
Coolant specification	50:50 (water:Ethylene glycol)
Engine management system	Bosch Motronics EMS
Weight	54.7kg with AC

The base engine including the production manifolds is shown in Figure 3-2.

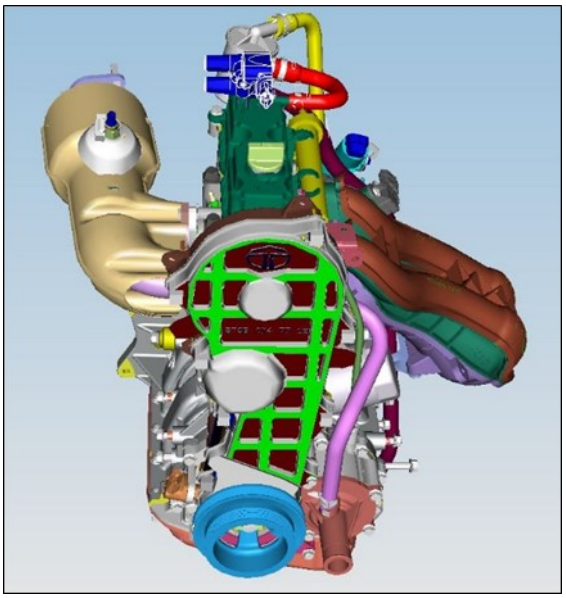

Figure 3-2 Production 273MPFI engine including intake and exhaust manifold [2]

The base engine, which was first introduced during the Tata Motors Nano car launch in 2008, already had some of the low-cost features that have subsequently been incorporated by other engine manufacturers during their bespoke RE engine development programmes quoting the Nano engine. Some of these are covered in the succeeding paragraphs.

The Nano 273MPFI base engine has a 2-cyclinder, in-line engine layout as it has the lowest package volume, lowest projected production cost and least weight for an engine of this size. It also has an open-deck structure since it is the lowest cost option for high volume series production. MAHLE during their assessment for calculating total production cost as well as total mass of the complete RE bespoke engine development likewise arrived at a 2-cylinder, in-line engine layout [61]. Further while deciding on their bespoke engine block design, MAHLE, quoting the Tata Nano engine chose an open-deck structure since it is the lowest cost option for high volume series production.

The 273MPFI base engine has fixed valve timing. MAHLE also opted for fixed valve timing. Trends in the last twenty years show a wide range of complex systems in the valve trains of passenger cars primarily to improve performance and simultaneously meet the increasingly stringent emission requirements. As mentioned earlier in the report, unlike a traditional passenger car engine, the RE engine is required to operate at a few discrete steady-state speed and load points which obviates much of the benefits accrued through variable valve timing [61]. At the same time, it reduces the cost of the overall package.

Like the 273MPFI base engine, the MAHLE RE engine also has a directly mounted oil pump (no chain) and metal spin–on type oil filter to reduce cost.

MAHLE have also opted to bolt the generator rotor directly to the crankshaft palm, which apart from reducing the assembly size, has cost benefits as well. A similar approach had been planned for this project as well.

3.4 Engine Test Cell

The experimental work was performed in a bespoke engine test cell at University of Bath.

The test cell control system used was CADET V-14 from Sierra CP Engineering enabling monitoring in real time and logging a range of relevant engine parameters. A dedicated host computer running the CADET V14 software was used to create a virtual instrument for data scaling, processing and logging. Post processing of data was carried out using MS Excel and/or Matlab software.

3.4.1 Dynamometer

The test cell included a 50kW AC dynamometer and drive system suitable for motoring and absorption. Key parameters of the dynamometer are in Table 3-5.

Table 3-5 AC dynamometer key parameters

Speed (rpm)	0 / 3000 / 5100 / 8500
Absorbing power (kW)	0 / 50 / 50 / 35
Absorbing torque (Nm)	164 / 164 / 95 / 40

Calibration of the dynamometer was undertaken at regular intervals using calibration arms and weight pans to ensure accuracy of test data.

3.4.2 Engine Torque

Engine torque was measured using a HBM T40B torque flange. Its measuring range was 0–500Nm with an accuracy of ± 0.25Nm, class 0.05. The torque flange was located at the dynamometer end.

3.4.3 Lambda Value and Air/Fuel Ratio (AFR)

Exhaust gas lambda for both exhaust ports was measured using an ECM wideband lambda sensor with CAN interface. These sensors were programmable for all fuel types (H:C, O:C, N:C ratios). These were calibrated in atmosphere prior to testing. The sensors output lambda (λ) and AFR with an accuracy of ±0.6% (at

stoichiometric), ±0.9% (average, elsewhere) and $\%O_2$ with an accuracy of ±0.1% (absolute).

3.4.4 Fuel, Coolant and Oil Flow Measurement

The fuel consumption was measured using a micro motion Coriolis flow meter with a range of 0 to 93.5kg/hr and accuracy ±0.10% of actual measured flow rate. Oil flow was measured using a Krohne OPTIMASS 6400 C Coriolis mass flowmeter. Its flow range was 0 to 30LPM. The system consisted of the measuring sensor and a converter which provided a corresponding voltage signal. Its accuracy was ±0.1% of the actual measured flow rate. Coolant flow was measured using a Krohne electromagnetic flowmeter with a flow range of 0 to 35LPM.

3.4.5 Temperature Measurements

Temperature parameters were monitored using Chromel-Alumel (type-K) mineral insulated metal sheathed (MIMS) thermocouples. The shielded thermocouples had a response time of approximately 1 second with an accuracy of 0.0075*T, where T is the temperature measured. Platinum resistance thermometers (PRT) were also used to measure temperature which had an accuracy of 0.3 ± 0.005*T, where T is the temperature measured.

The ambient temperature in the test cell was controlled at 25±2ºC. It is highlighted that the cell temperature was not automatically controlled but required manual intervention by the operator to switch on the set of exhaust fans when the test cell temperature reached 27°C. Likewise the operator had to switch off the exhaust fans when the cell temperature dropped to 23°C. This was one of the main drawbacks of the test cell set up and there were instances when the test cell temperature exceeded the limits during testing. These excursions would have affected the results to a certain extent by affecting the air density entering the engine inlet manifold. This would have

affected the amount of fuel injected and as a result the BSFC. The oil and coolant flows were measured, and their temperature set points maintained within ±2ºC tolerance band.

3.4.6 Pressure Measurement

Various pressure parameters like oil pressure, coolant pressure and fuel pressure etc were monitored using Druck UNIK 5000 series pressure sensors with an accuracy of ±0.25% full scale.

3.4.7 Combustion Parameters

The engine combustion parameters were measured and logged by an AVL Combustion Analysis System (CAS). Parameters recorded were spark timing, start of injection (SOI), end of injection (EOI), in-cylinder pressure, inlet and exhaust manifold pressures with respect to crank angle.

To measure in-cylinder pressure, Kistler piezoelectric pressure transducer type 6052C31 were installed in the cylinder head coupled to a signal conditioning unit which fed into the AVL CAS. The linearity of the sensor was ±0.25% full scale.

Proper crank angle phasing was achieved by installation of a Kistler crank angle optical encoder type 2614CK, having a speed range of 0-12000rpm.

The SOI, EOI and spark timing was measured using Kistler miniaturised electrical impulse sensors type 2105A30 with linearity error of 0.3%. The miniaturised sensors were required because of the paucity of installation space and the regular sensors, because of their weight were breaking the electrical harness wiring.

Based on the Hall effect measurement principle, the sensors provide an output voltage proportional to the current. This is amplified using amplifier type 2105A20 which is then connected to the AVL CAS.

3.4.8 Emissions Measurement

Undiluted emissions concentrations were measured continuously for catalyst gas samples wherever appropriate using Horiba MEXA 7000 analysers. Heated transfer line, at a temperature of 191°C was located at the exit of the exhaust ports. The Mexa instrument was calibrated before every experiment using span gases of known concentration and zeroed with nitrogen gas.

Schematic of the experimental setup is shown in Figure 3-3. The engine mounted in the test cell coupled to the dynamometer is shown in Figure 3-4. Engine ancillaries such as AC compressor and alternator were removed during engine testing.

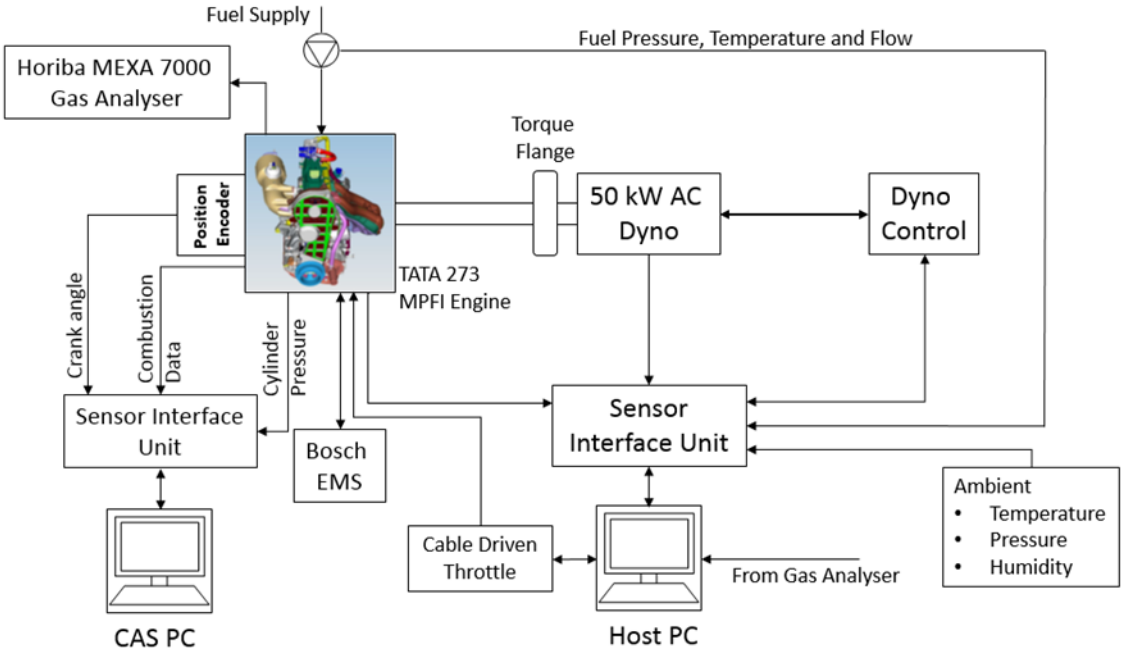

Figure 3-3 Schematic of the bespoke test cell experimental set up at University of Bath.

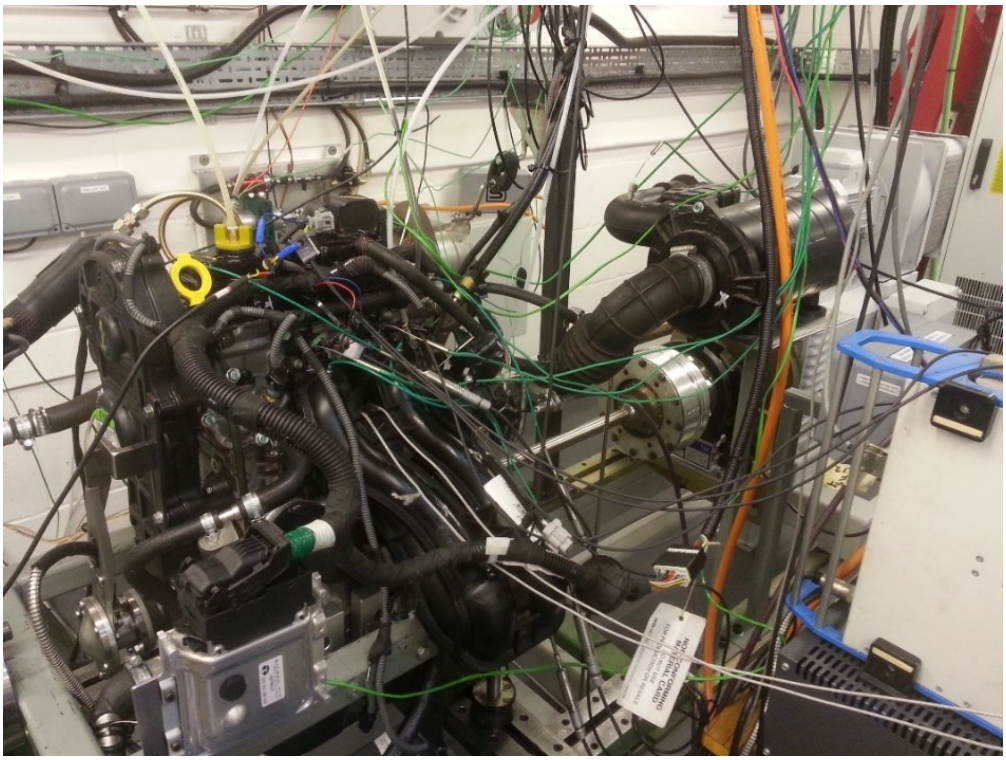

Figure 3-4 Engine mounted in the test cell. The 50kW AC dynamometer is on the right [2]

3.5 Reference Fuel

Test procedures designed to evaluate engine performance require fuels which have the least possible variations of their chemo-physical data. To ensure consistency of experimental data all engine testing at University of Bath was conducted with reference gasoline, Carcal RF02-08 E5 (48337) whose properties are at Table 3-6. This ensured reproducibility of test results with respect to fuel quality.

Table 3-6 Carcal RF02-08 E5 (48337) gasoline fuel properties. Reference fuel was used to ensure reproducibility of test results with respect to fuel quality

Method	Description	Min	Max	Results	Unit
ASTM D4052	Density at 15°C	0.7430	0.7560	0.7518	g/mL
Distillation					
ASTM D86	I.B.Pt.			37.9	°C
ASTM D86	Evaporated at 70°C	24.0	44.0	29.2	%
ASTM D86	Evaporated at 100°C	48.0	60.0	52.6	%
ASTM D86	Evaporated at 150°C	82.0	90.0	88.5	%
ASTM D86	F.B.Pt.	190.0	210.0	192.1	°C
ASTM D86	Residue		2.0	1.0	% vol
Engine Tests					
ASTM D2699	R.O.N.	95.0		98.8	Units
ASTM D2700	M.O.N.	85.0		87.4	Units
FIA					
ASTM D1319	Aromatics	29.0	35.0	31.7	% vol
ASTM D1319	Olefins	3.0	13.0	7.7	% vol
ASTM D1319	Saturates			55.6	% vol
General Properties					
EN 13016-1	Vapour pressure (DVPE) 37.8°C	56.0	60.0	56.5	kPa
EN 238	Benzene content		1.0	0.4	% v/v
ASTM D525	Oxidation Stability	480		>480	minutes
ASTM D381	Gum, - washed		4	<0.5	mg/100mL
ASTM D130	Copper Corrosion, 3hrs at 50°C			1A	
EN 237	Lead content		5	<2.5	mg/L
ASTM D3231	Phosphorous content		1.3	<0.2	mg/L
IP 490	Sulphur Content		10.0	5.1	mg/kg
IP 466	Ethanol	4.7	5.3	5.0	% v/v
IP 438	Water Content		0.015	0.008	% v/v
CALCULATION	Oxygen Content			1.87	% m/m
To Be Recorded					
ASTM D5291	Carbon Content			85.39	% mass
ASTM D5291	Hydrogen Content			12.74	% mass
IP 12	Gross Heat of Combustion			45.36	MJ/kg
IP 12	Net Calorific Value			42.66	MJ/kg
CALCULATION	C/H Mass Ratio			6.70	Ratio
CALCULATION	C/O Mass Ratio			45.66	Ratio
CALCULATION	Atomic H/C Ratio			1.7784	Ratio

3.6 Repeatability of Test Data

To validate experimental results, results are usually recorded more than once. If the recorded results are the same, there is arbitrarily more confidence in the measured result. However, if there is variation in the results, the experimenter will either repeat the experiment or change the test set up based on the assumption that there are other factors affecting the result. If many measurements are made, one would obtain a distribution/spread of results. The corresponding curve is known as the normal or Gaussian distribution. The shape of the Gaussian curve is such that the frequency of small deviations from the mean value is much greater than the frequency of large deviations. The sample mean is an important measure of the location of the data,

however it gives no information about the scatter, for which standard deviation, σ, is commonly used, see equation (1), where σ is the standard deviation, y is the individual experimental results, y bar is the mean of the experimental results and n is the number of results. It is important to note that the above definition of standard deviation is arrived at after applying the Bessel correction factor since in an experimental set up there are finite set of measurements [92].

$$\sigma = \sqrt{\frac{\sum(y - \overline{y})^2}{n - 1}} \tag{1}$$

The standard deviation is given in the units of the experimental measurement. Therefore, it is not possible to use the standard deviation to make valid comparisons of experimental variability between experiments unless the results of the experiment are measured in the same units. Therefore, it is more common to express the standard deviation as a percentage of the mean as it allows for direct comparison of experimental variability [93]. This is known as coefficient of variation (CoV) or variance, see equation (2).

$$CoV = \frac{Standard\ deviation}{mean} * 100 \tag{2}$$

For well-designed engines, the variance of the indicated mean pressure is less than 1% [94]. For certification testing, guidelines are provided in accordance with ISO1585 which is ±2% on net power [95]. As per BS5514 the permissible deviation in engine torque as measured repeatedly during a single test run on a single test bed is 2% [96]. Traditional limits of repeatability are around 1% coefficient of variation (CoV) at 95% confidence level [97]. For this research a similar target of CoV was

aimed for. To ensure that the test data recorded was repeatable and reproducible, testing was carried out under following conditions: -

- 2000rpm, 2bar BMEP.
- 2000rpm wide open throttle (WOT).
- 3000rpm, 5bar BMEP.
- 30000rpm WOT.

Data was logged after the oil and coolant temperature and engine torque had stabilised at 90°±2°C. Each test log was a 10 second average and 20 logs were taken at each test condition. Engine torque and BSFC at 3000rpm, WOT recorded are shown in Figure 3-5 and Figure 3-6 respectively.

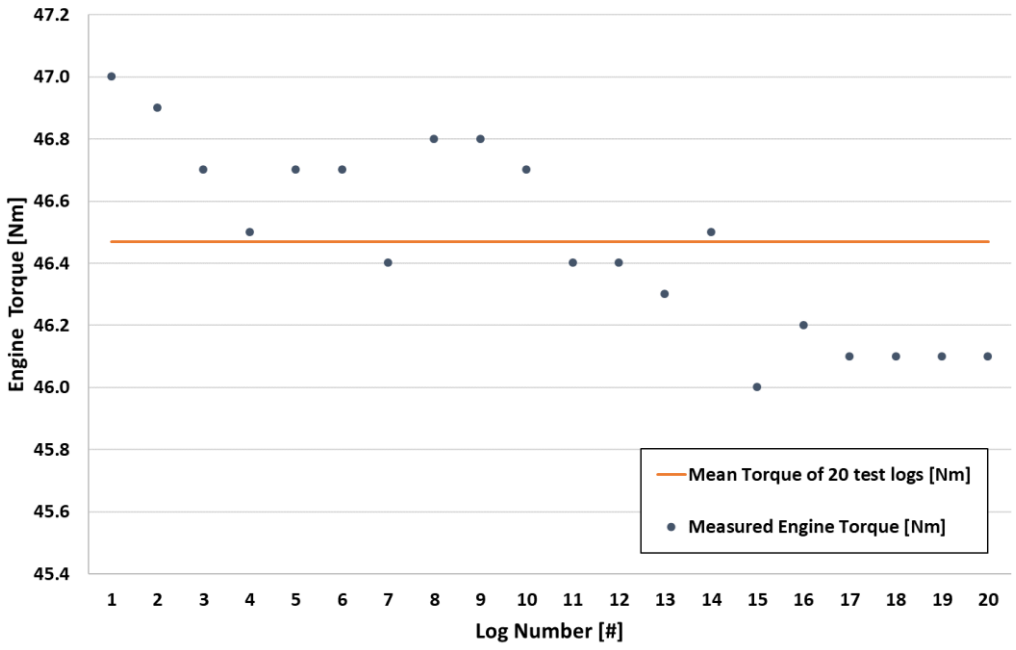

Figure 3-5 Repeatability of measured engine torque at 3000rpm, WOT. Statistical parameters like minimum, maximum, mean, standard deviation and coefficient of variance are detailed in Table 3-7

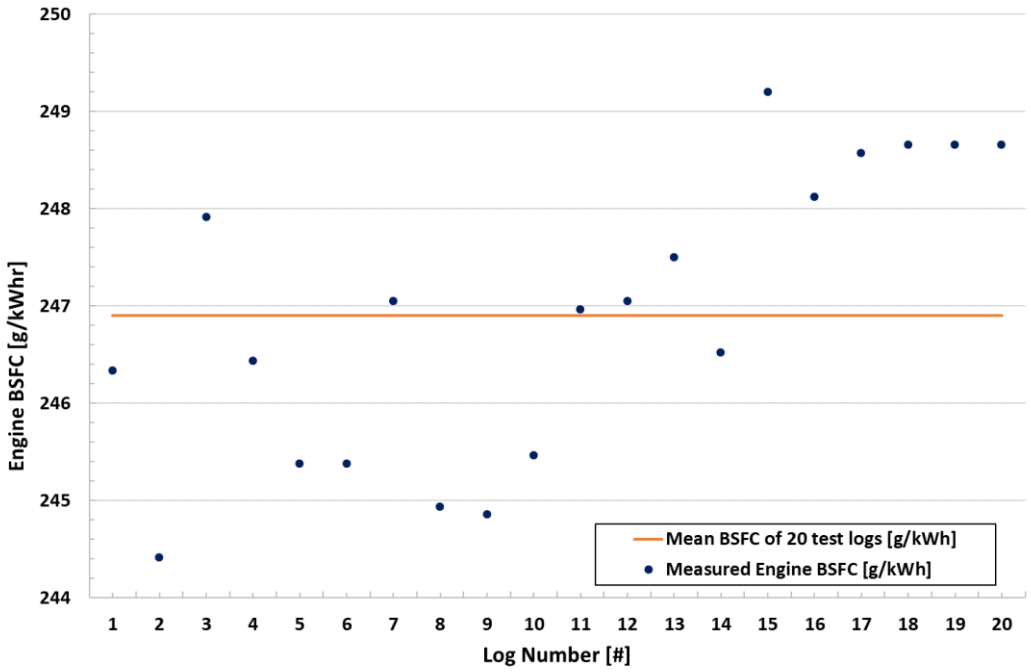

Figure 3-6 Repeatability of measured engine BSFC at 3000rpm, WOT. Statistical parameters like minimum, maximum, mean, standard deviation and coefficient of variance are detailed in Table 3-7

As per the test results, the mean, standard deviation and coefficient of variance of the engine torque, power, BSFC and fuel flow at 3000rpm at WOT are shown in Table 3-7 below.

Table 3-7 Minimum, maximum, mean, standard deviation and coefficient of variance of engine torque, power, fuel flow and BSFC during repeatability testing – 3000rpm, WOT

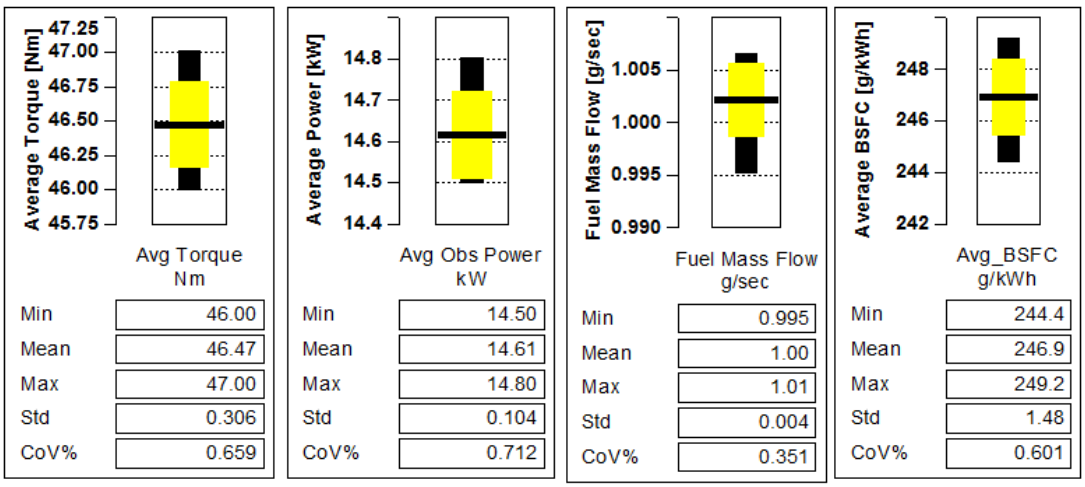

The results indicate that the deviation in engine torque during a single test run on a single test bed is within 2% in accordance with BS5514. Based on the results obtained above, the repeatability of the test cell set-up was considered satisfactory to progress to the next stage of experimental work. Reproducibility checks were not carried out.

3.7 Base Engine Performance Characterisation

The performance of the engine was characterised at both part load and WOT across 1500rpm to 5500rpm. Engine ancillaries such as AC compressor and alternator were removed during engine characterisation since they would not be required in an electric vehicle. The engine would be started by the motor/generator and the AC compressor was expected to be an electric HV compressor. Engine throttle was varied in steps of 10% and engine speed varied from 1500 to 5500rpm and data logged. Figure 3-7 shows the engine airflow versus engine speed for varying throttle positions.

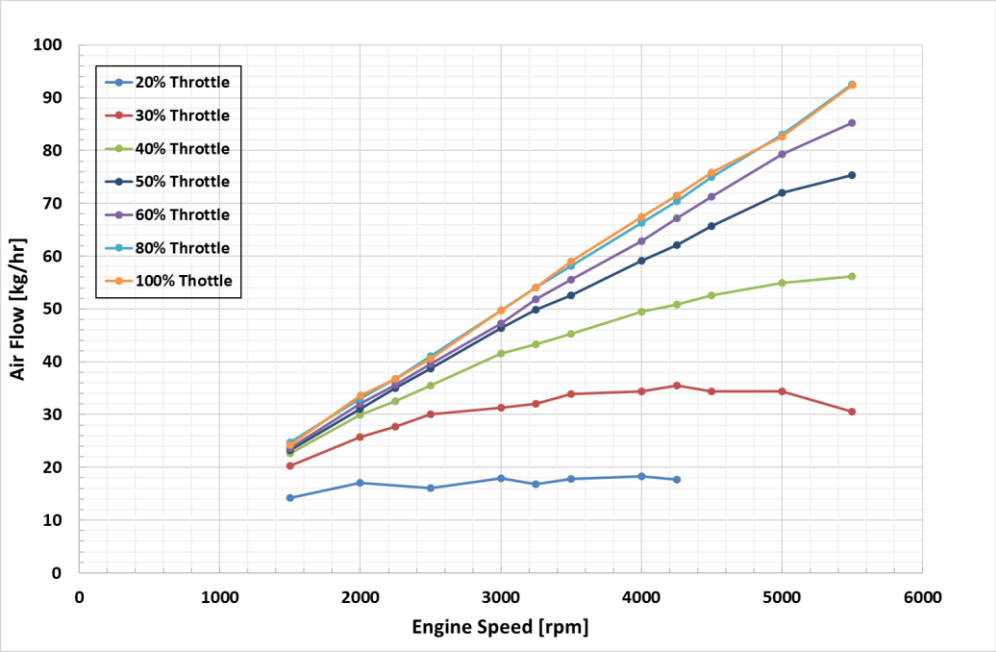

Figure 3-7 Engine airflow versus engine speed for varying throttle positions during benchmarking of base engine performance

When logging, the CAS recorded data for 300 engine cycles and the average value recorded. An example is shown in Figure 3-8. It illustrates the combustion parameters at engine speed of 3000rpm, WOT. Blue and red lines indicate cylinder 1 and cylinder 2 parameters respectively. The zero crank angle is the top dead centre firing (TDCF). Since the engine is even fired, the cylinder 1 and 2 data should be 360°C apart. In order to compare the cylinder to cylinder variation, the two traces were shifted to be co-located.

It was seen that the cylinder 2 developed higher peak pressure compared to cylinder 1. This difference was consistently seen in all tests. Subsequent investigation confirmed that this was not due to sensor calibration.

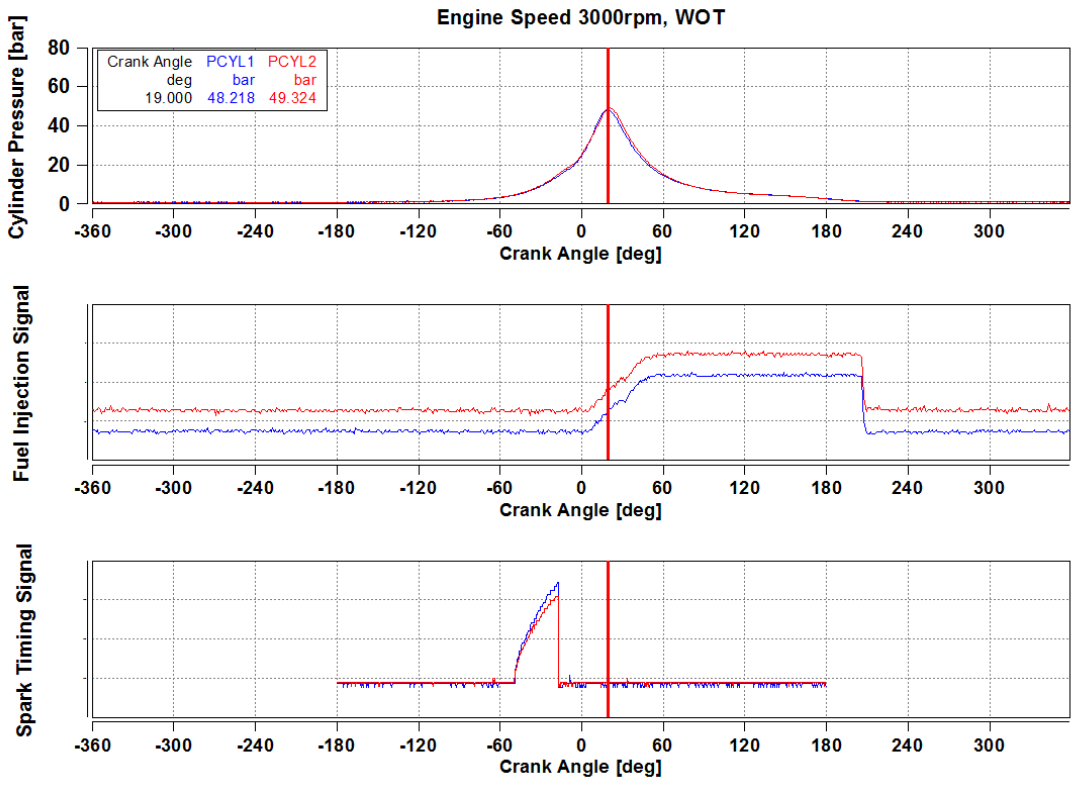

Figure 3-8 Engine combustion paraments at engine speed of 3000rpm, WOT. The plots show cylinder pressure, start of fuel injection (SOI), end of fuel injection (EOI) and spark timing with respect to crank angle.

Figure 3-9 shows the engine average exhaust temperature versus engine speed for varying throttle positions. Peak exhaust temperatures of around 750°C were measured. Subsequently during the spark timing optimisation process, this was the target exhaust temperature which was considered as the limit.

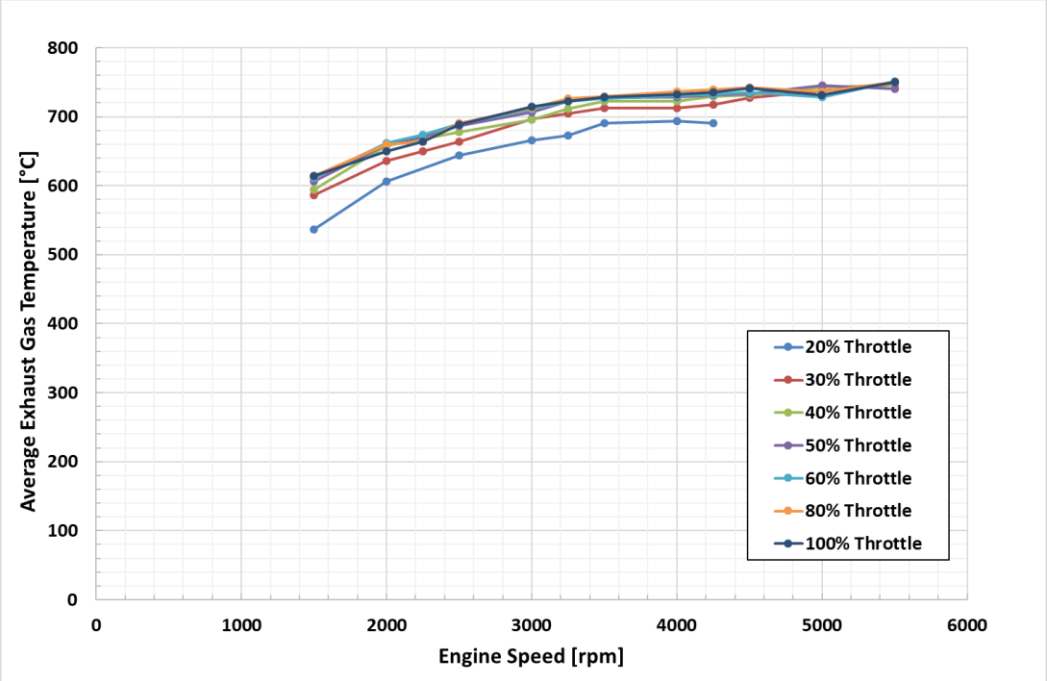

Figure 3-9 Engine average exhaust gas temperature versus engine speed for varying throttle positions during benchmarking of base engine. Peak exhaust temperatures of 750°C were measured.

Figure 3-10 shows the engine lambda values versus engine speed for varying throttle positions with full load torque curve superimposed. At WOT, the engine was running lambda 1 for up to 3500rpm, after which it began enriching the air fuel mixture to control exhaust gas temperatures.

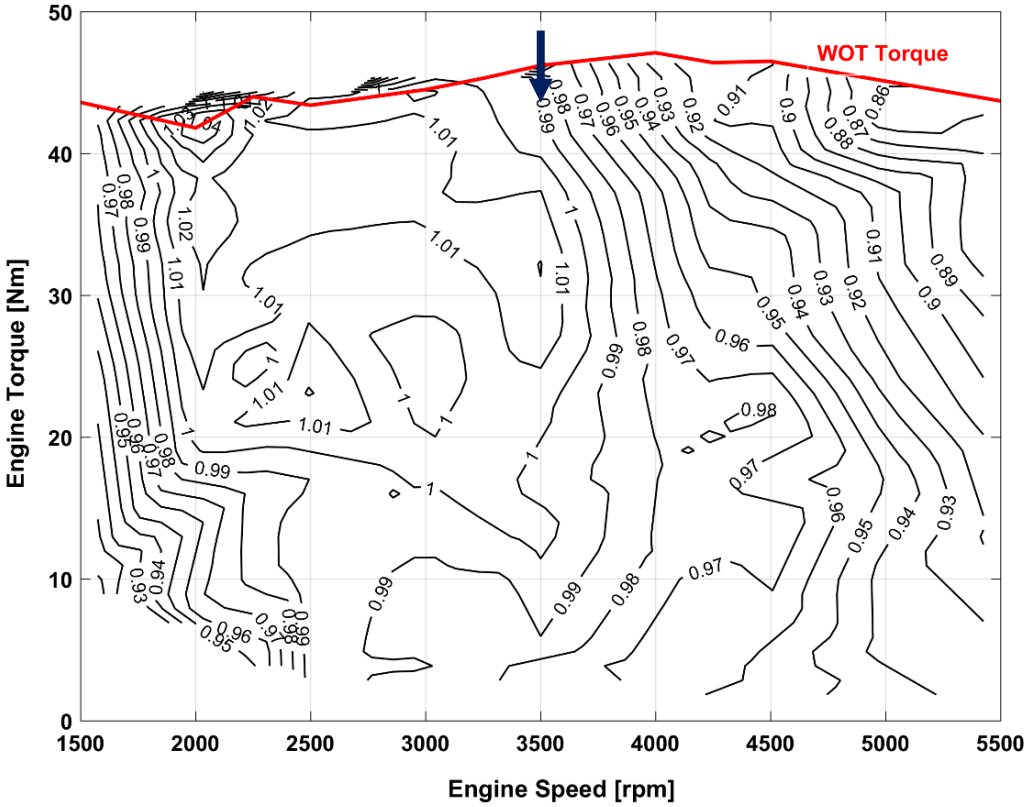

Figure 3-10 Measured lambda values with varying engine speed and torque during benchmarking of base engine performance. The WOT torque curve has been superimposed on the lambda map. At WOT, the engine was running lambda 1 for up to 3500rpm (see arrow), after which it began enriching the air fuel mixture to control exhaust gas temperatures.

The BSFC map is shown in Figure 3-11 along with the full load torque curve superimposed. It was against this BSFC benchmark that the effectiveness of the proposed modifications was to be compared, the aim being: -

- To improve the torque/power across the engine operating range from 2000-4500rpm, the proposed operating points of the RE.
- To maintain/improve the BSFC while reducing the overall engine package.

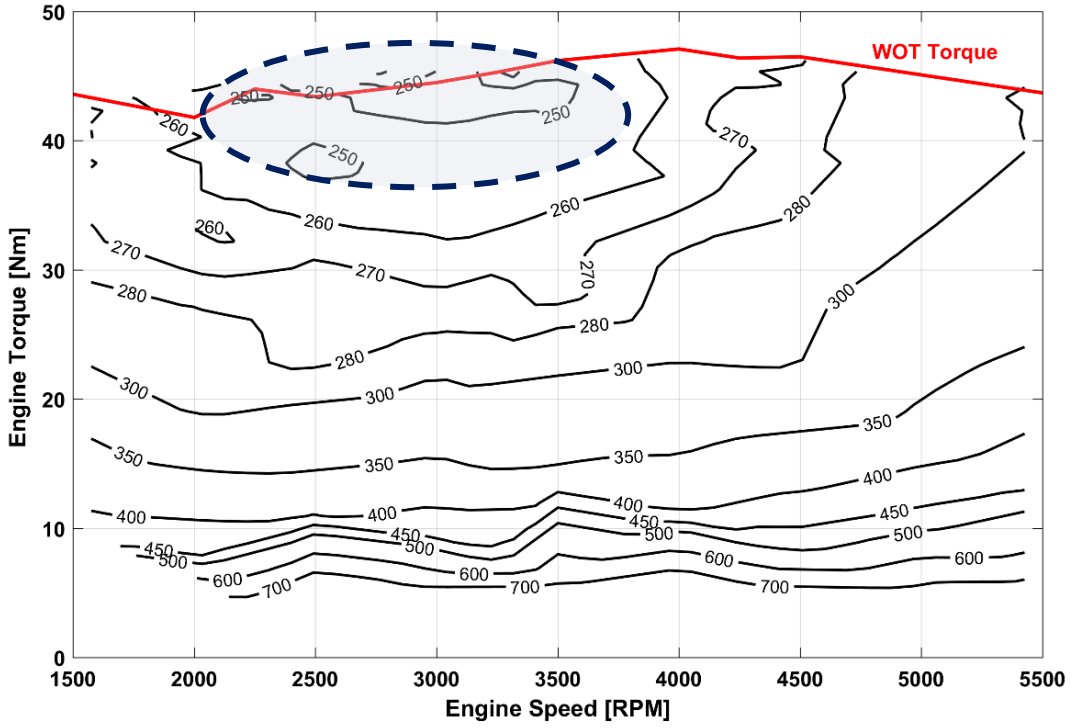

Figure 3-11 Measured BSFC values with varying engine speed and torque during benchmarking of base engine. The wide open throttle torque curve has been superimposed on the BSFC map. Region of 250g/kWh BSFC is highlighted.

A best BSFC of 245g/kWh was measured at 2250rpm, WOT. BSFC of the order of 250g/kWh was measured from 2000 to 3500rpm at WOT.

3.8 Conclusion

In this chapter the electrical power output of a RE for essentially a C-segment vehicle were worked out by TMETC to be of the order of 20 to 25kW during extended range (or charge sustaining mode). This output is the sum of the tractive power and ancillary load requirements.

The next section presented the selection of the base engine based on the RE power requirement using low-cost, in-production engine. Based on the base engine performance capability coupled with the primary requirement of this experimental

study to optimise the ICE using low cost changes well within the normal volume-production process, a maximum electrical power output of 20–25kW was aimed at.

Subsequently, the development of the bespoke engine test cell at University of Bath was covered. This included a discussion on repeatability of test data and the importance of using a reference fuel to have consistency in test results. The repeatability of the test data was found to be well within the permissible deviation of 2% as measured repeatedly during a single test run on a single test bed.

The performance of the production engine was mapped across its entire operating regime, both at part load and full load. A BSFC map was generated and a best BSFC of 245g/kWh was measured at 2250rpm, WOT. BSFC of the order of 250g/kWh was measured from 2000 to 3500rpm at WOT. This became a yardstick to compare the effect of subsequent optimisation of the engine for RE application.

The work presented in this chapter formed part of the technical paper titled ‘Development of a Low-Cost Production Automotive Engine for Range Extender Application for Electric Vehicles’ that was presented at the SAE World Congress, Detroit in April 2016. Paper reference is 10.4271/2016-01-1055.

CHAPTER - 4
New Engine Management Strategy

This chapter presents the need and development of the bespoke APU engine management strategy. The second part discusses the EMS calibration methodology and introduction of the electronic throttle. At the end, the performance of the engine with the bespoke EMS is compared with the production EMS.

4.1 Introduction

An auxiliary power unit is a complex system of bespoke parts which can be separated into two independently functional units. The electric generator with its control unit being one and the other being the engine with its control unit. These independently functional units are mechanically linked, and they are actively coordinated by an additional control unit, the APU supervisory controller.

The first section of this chapter presents the development of the bespoke engine controller or engine management system (EMS) for integration of the engine with a generator for range extender application.

The next section explains the introduction of the electronic throttle which facilitates the incorporation of the torque control strategy since the throttle needs to be driver independent for an APU application.

Subsequently the engine performance, post modifications is compared with the base engine to confirm its performance is satisfactory.

4.2 New Engine Management Strategy

4.2.1 Overall Control Strategy

The APU control structure comprises essentially of three components. The APU Supervisory Controller (ASC) which controls the other two components namely the Engine Management System (EMS) and the Generator Control Unit (GCU). The ASC is subordinate to the overall Vehicle Supervisory Controller (VSC).

The VSC is responsible to command the APU Supervisory Controller (ASC) to start or stop the APU based on the requirements from the battery state of charge and

the driver power demand. It provides the ASC with the target speed and power. The ASC in turn communicates the target speed request to the GCU and the target torque request to the EMS. The desired engine operating condition is achieved through the actuation of the throttle whilst maintaining target air fuel ratio and optimum ignition timing [2]. The schematic of the overall control architecture is shown in Figure 4-1.

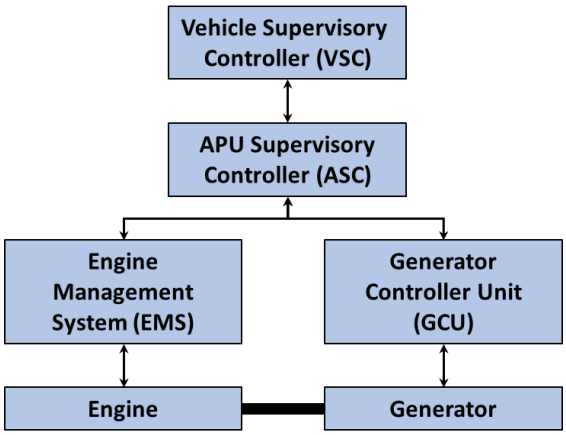

Figure 4-1 Overall control architecture. The EMS and GCU are under the APU supervisory controller (ASC) which is controlled by the VSC

The VSC, ASC and GCU are out of the scope of this research and are therefore not discussed further. The EMS control development was undertaken by my co-supervisor Dr A.J. Lewis and the engine calibration work was undertaken by me.

The production engine utilised a Bosch Motronic EMS to which calibration level access was not available. For integration of the engine with a generator for a range extender application, which would entail torque management and engine operation over a limited number of points, there was a need to replace the production EMS with a bespoke EMS.

The bespoke EMS would allow the necessary access to the control and calibration variables. Accordingly, a new Motohawk EMS control strategy was developed which involved adapting the control strategy from an off the shelf 6-

cylinder engine control strategy to suit the production engine and integrate it with the GCU and the ASC.

4.2.2 Overview of EMS Requirements and Calibration

The role of the EMS is to control the engine to the desired operating condition. The control is performed through the actuation of the throttle, the fuel injectors and ignition. During the first phase of development, the throttle was cable driven and not controlled by the EMS but would result in a manifold air pressure (MAP) value, which was read by the EMS.

Figure 4-2 describes the overall EMS control architecture that was to be employed within the APU control architecture. Sensor inputs are shown in blue, the actuator commands in red and the ASC requests in black.

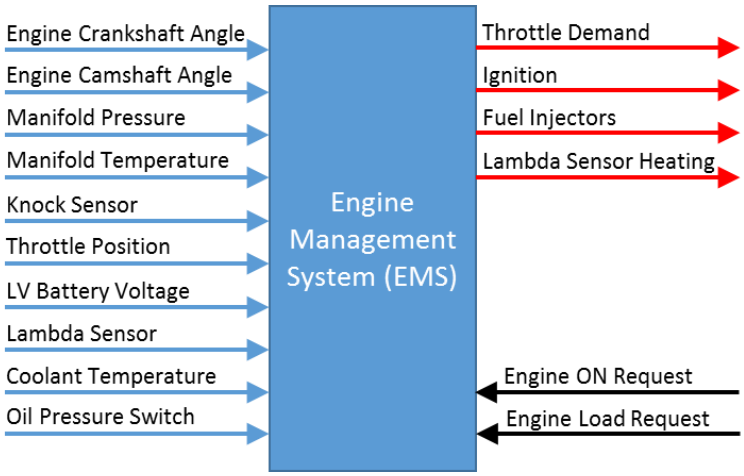

Figure 4-2 EMS control architecture. Sensor inputs are shown in blue, the actuator commands in red and the ASC requests in black [2]

The bespoke EMS should be able to translate a torque command into a throttle position independent of driver input, based on look-up tables characterised on the test bench during the benchmarking process, as well as return a value of maximum torque available. The maximum torque is based on the estimated air flow with open throttle.

The EMS should be able to respond to an engine off command, when the Engine ON request is false by removing the fuel and ignition to the engine, to stop the APU. This is necessary to avoid overcurrent in the battery when the APU is pushing current to the battery close to the current limit and a regeneration (braking) event is imposed by the driver.

The EMS should guarantee safe and robust operation of the engine under any operating conditions i.e. temperature, humidity, loading, speed etc.

In order to deliver the functions above, the following control features were present: -

(a) Engine torque control.

(b) Closed loop fuel control.

(c) Lambda sensor temperature control.

(d) Ignition control.

(e) Component protection.

The main inputs / demands to the EMS were: -

(a) Torque Demand. Initially the torque demand was via an analog signal from the dynamometer to the cable throttle actuator. The pedal demand from the dynamometer host system was fed to the cable throttle actuator. The resultant manifold pressure was read by the EMS. Subsequently it was an internal signal from the ASC once the electronic throttle was incorporated. This is covered in greater detail subsequently in Section 4.3.

(b) Engine coolant temperature.

(c) Inlet manifold pressure and temperature (combined sensor).

(d) Lambda sensor.

(e) Engine speed / position sensor. This was an additional induction sensor from a 36-2 pattern encoder disc. At the later stage of the research, once the generator was coupled to the engine, the speed input would be received from the GCU.

(f) Camshaft sensor. The production engine was not provided with a camshaft sensor, this was additionally installed.

(g) Knock sensor.

(h) Throttle sensor.

The main outputs from the EMS were: -

(a) Spark timing. A spark manager block controlled the required spark advance, see Figure 4-3. A 2-D lookup table (17x17) with engine speed and indicated load as the axis were populated from the data captured during the baseline of the engine with the Bosch EMS. The spark manager included a spark limiter (rate limiter and engine coolant temperature limiter), temperature compensation offset and desired equivalency ratio offset. The spark start angle was calculated based on the desired spark advance and the coil characterisation.

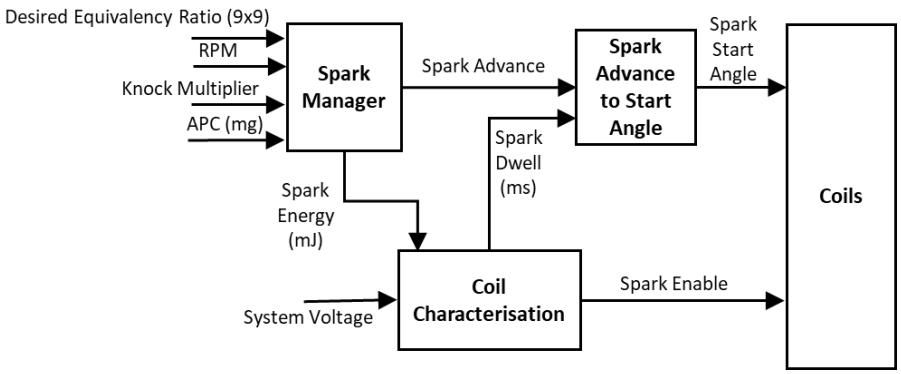

Figure 4-3 Spark timing control strategy to calculate spark start angle based on desired spark advance and coil characterisation

(b) Injector timing and duration. Figure 4-4 shows an overview of the injector timing and duration control strategy.

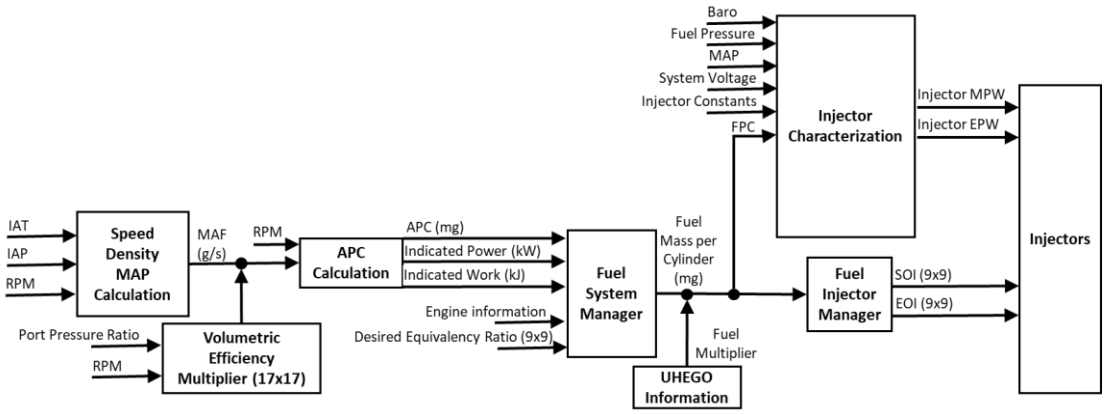

Figure 4-4 Injector timing and fuel injection duration control strategy

(c) Lambda sensor heating.

Initially the calibration tables in the control strategy were populated using the baseline data captured while running the engine with the production EMS. This enabled the new EMS to control the engine satisfactorily. The major tables that needed to be populated were volumetric efficiency (VE), desired equivalency ratio, spark timing, start of injection (SOI) and end of injection (EOI). These tables essentially display speed on the y-axis and engine load [air per cylinder per cycle (APC) (mg/cyl/cycle)] on the x-axis.

To illustrate with an example, the VE of the engine is fixed for a given inlet and exhaust manifold geometry. The 2-dimensional look-up table (17*17) axis were port pressure ratio (manifold air pressure/barometric pressure) and engine speed. For validation, the mass air flow calculated with the EMS was compared to test bed data measured during the benchmarking, and required changes made to the VE table.

4.3 Introduction of Electronic Throttle Control (ETC)

As mentioned above, during the first phase of the EMS development the throttle was cable driven as in the production engine. Once the engine was running satisfactorily on the new EMS, the electronic throttle was incorporated. The electronic throttle facilitates the incorporation of the torque control strategy since the throttle can be moved without any driver input [2]. The torque request from the ASC is interpreted in a feed forward throttle position demand based on look up tables populated from the previous mapping experimental work based on equation (3) below.

$$\dot{m} = \left(\frac{P}{RT}\right)\left(\upsilon_e V_{cyl}\right)\left(\frac{N_{eng}N_{cyl}}{60 * NRPC}\right) \tag{3}$$

Where,

$\dot{m}$ is the mass air flow, g/s

P is the manifold air pressure, kPa

R is the Universal gas constant, 287J/kgK

T is the ambient temperature, °K

υ_e is the volumetric efficiency, %

V_{cyl} is the volume of cylinder

N_{eng} is the engine speed, rpm

N_{cyl} is the number of cylinders

NRPC is the number of combustion events per revolution, 1

Closed loop throttle position control exists within the EMS. Target throttle position is determined from the indicated load and engine speed look-up table. Internal position feedback was used within a PID controller in the EMS model to hold throttle position. A schematic of the engine torque strategy is shown at Figure 4-5.

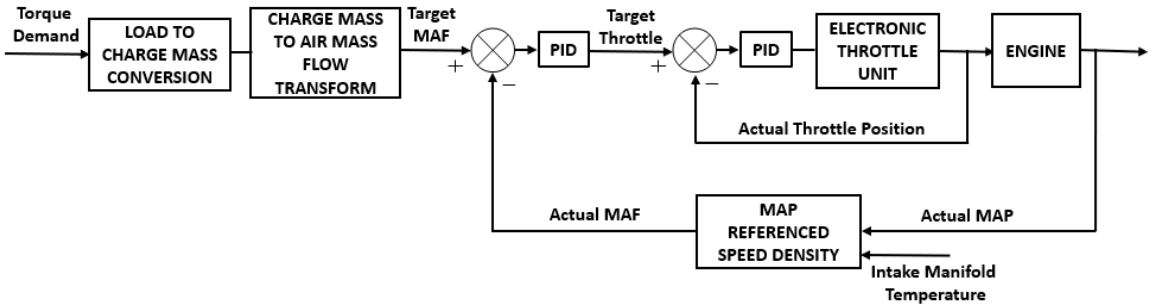

Figure 4-5 Engine torque control strategy facilitates conversion of torque demand to the required electronic throttle opening position independent of driver input

4.4 Engine Performance

Figure 4-6 compares the performance of the engine with the Bosch EMS versus the Mototune EMS at WOT.

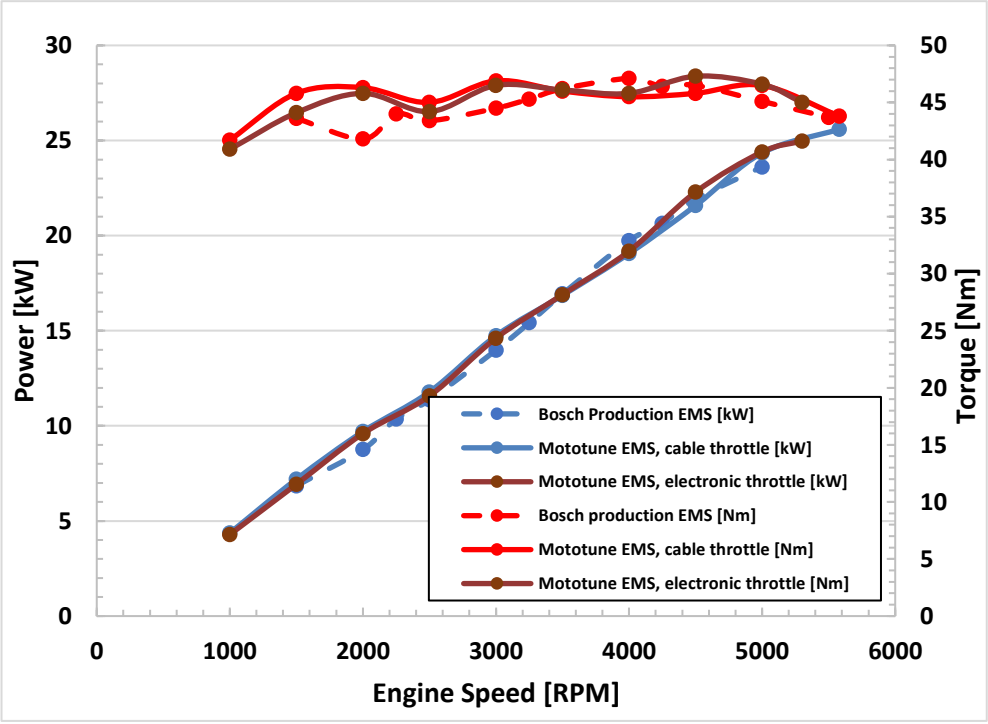

Figure 4-6 Comparison of engine power and torque for Bosch production EMS and Mototune EMS with cable driven and electronic throttle

The power curve of the engine had a good match under all three conditions. This was considered more critical than torque as when the engine would be coupled to the generator the ASC would control the APU based on a power.

4.5 Conclusion

Since calibration level access was not available for the production Bosch ECU, it was necessary to develop a bespoke engine controller for use in an APU application. This chapter dwelled on the APU control architecture wherein the power demand is split into a torque demand and a speed demand. The torque demand was translated into a throttle position whereas the speed is controlled by the GCU. Since the generator had still not been integrated with the engine, the speed was controlled by the dynamometer.

The bespoke EMS was calibrated based on the engine data captured during the benchmarking process as described in Chapter 2. Once the engine was running satisfactorily, the cable driven throttle was replaced with the electronic throttle.

The performance of the engine with the bespoke controller and electronic throttle was found to have a good match with the production EMS. This laid the foundation for progressing to the next stage of the experimental research which involved development of bespoke engine manifolds.

The work presented in this chapter formed part of the technical paper titled ‘Development of a Low-Cost Production Automotive Engine for Range Extender Application for Electric Vehicles’ which was presented at the SAE World Congress, Detroit in April 2016. Paper reference is 10.4271/2016-01-1055.

CHAPTER - 5
Bespoke Manifold Development

This chapter presents the development of bespoke inlet and exhaust manifolds to generate power circa 20–25kW at 4500rpm. Experimental techniques were employed to validate simulation results undertaken at TMETC. The results achieved 92% reduction in manifold size while achieving greater engine torque up to 4500rpm.

5.1 Introduction

To allow the APU to generate power circa 20-25kW, it requires the engine to operate at a relatively high engine speed of around 4500rpm. To achieve power output circa 20-25kW, the production engine's power needed to increase. Due to limited speed range in which the engine shall operate in when used as an APU and due to increase in the engine's minimum operating speed to 2000rpm, driveability was no longer the target, and power outside of the target speed range could be sacrificed to reach the target power output [6].

One of the means of achieving this was development of bespoke inlet and exhaust manifolds, which are well within the normal volume-production process. The criteria for bespoke intake and exhaust manifolds development was to minimise their volumes to improve vehicle package whilst targeting improved performance between 2000–4500 rpm. Tuning of the intake and exhaust manifolds can be used to increase engine performance across a limited engine speed range. However, due to the target packaging size the tuned solution needs to be of a compact design.

The volumetric efficiency of an engine has a direct impact on its performance, and an improvement in an engine's VE can provide improved power output [98, 99]. Reducing the level of airflow restriction and pressure drop on the engine will increase the amount of air the engine can induct, which will increase the volumetric efficiency. This parameter was selected as the measure of engine performance as it is easily comparable between simulations/experimental analysis and would show how effective the bespoke intake and exhaust manifolds had been in improving the airflow and cylinder filling, which would in turn lead to an increase in power output.

In this chapter development of bespoke intake and exhaust manifolds has been covered. A combination of simulation in a 1-D environment (GT-Power) and experimental testing was applied to optimize these attributes. Simulation work was

undertaken by TMETC. Experimental work was undertaken at University of Bath to corroborate the simulation results.

Subsequently the effect of the bespoke manifolds on engine performance was quantified and compared with the production manifolds.

5.2 Bespoke Intake Manifold Development

An engine manifold is the part between the cylinder(s) and throttle body. In a multi-cylinder engine, its role is to evenly distribute air flow between each cylinder and to create the air-fuel mixture for port fuel injection (PFI) engines. The inlet manifold determines how much air can be drawn through both during transients and in steady state, how fast the air is moving and how well it can be mixed with the fuel.

An intake manifold is composed of two parts, in conjunction with the throttle body, which include the plenum and the runner(s). The plenum is the chamber which collects the air before it is diverted down to each cylinder via the runner. The runner is also where the fuel is mixed prior to the engine (with the noted exception of direct injection).

The intake system restricts the amount of air which an engine of a given displacement can induct. Volumetric efficiency is the parameter used to measure the effectiveness of the engine's induction process. Volumetric efficiency is only used with 4-stroke engines which have a distinct induction process. It is defined as the volume flow rate of air into the intake system divided by the rate at which the volume is displaced by the piston. Typical maximum values of η_v for naturally aspirated engines are in the range 80 to 90% [99]

A well-designed intake manifold will deliver a uniform air/fuel charge to the cylinder as far as possible with appropriate velocity to sufficiently maintain η_v at low

and high engine speeds. Intake manifolds can come in various configurations from simple to complex. There can be multiple plenums and/or multiple runners feeding a given cylinder. There are pros and cons to each of these configurations, where the balance of performance is measured for a given engine and design goal [98].

The methods of intake tuning can be separated into two categories, inertial ram cylinder charging and wave tuning. Both look at the intake manifold dimensions to increase the air entering the combustion chamber, with inertial cylinder charging working to provide good airflow and minimal pressure drop, and wave tuning working to use the dimensions of the intake to utilise pressure waves made by the engine to force more air into the combustion chamber [98].

5.2.1 Inertial Ram Cylinder Charging

In this phenomenon, the momentum acquired by the air-fuel charge entering the cylinder during the induction period is utilised.

At the end of the exhaust stroke and the beginning of the induction stroke the inlet valve opens and the piston commences to move away from TDC. The outward accelerating piston quickly expands the space between the cylinder-head and piston crown. The depression created in this rapidly enlarging space is transmitted to the inlet port. The drop in pressure immediately causes the column of air-fuel charge in the induction tract to move as whole towards the open inlet valve. The large cross-sectional area of the piston relative to that of the much smaller intake tract cross-sectional area, plus the acceleration of the piston, forces the column of air-charge in the tract to acquire a high flow velocity.

The inlet valve remains open for the complete outward movement of the piston on its induction stroke and for some of the return compression stroke. This crank-angle lag ABDC before the inlet valve closes utilises the inertia of the air-fuel charge moving

through the induction manifold tract to valve port to ram itself into the cylinder, thereby raising the density of the cylinder air-charge [98], see Figure 5-1.

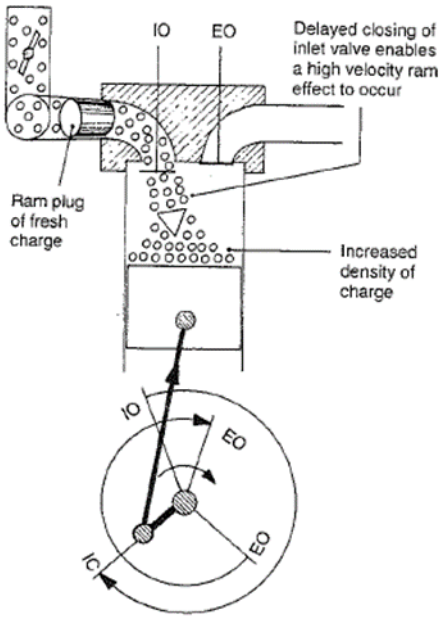

Figure 5-1 Inertial ram cylinder charging. Increased density of air-charge as the piston starts to move towards TDC [98]

The momentum built up by the fast-moving column of air-charge in the intake tract is brought rapidly to a halt when the inlet valve closes against the flow. At this point the kinetic energy of the fast-moving column of air-charge is converted into pressure energy in the blanked-off inlet port. Consequently, the density of the trapped charge rises. It is this rise in pressure at the port which enables the induction period to have an early start due to the pressurised charge momentarily stored behind the inlet valve head when it opens next.

The greater the momentum produced, the greater the rise of pressure, and if energy losses are very low in accelerating the flow, the inertia ram effect can increase the VE by cramming extra mixture into the cylinder [98].

5.2.2 Wave Tuning (Helmholtz Resonator)

Engelmann [100] presents an lucid description of the Helmholtz resonator theory. The Helmholtz resonator originally consisted of a spherical chamber with a pipe projecting from it, see Figure 5-2 (a), the chamber being the equivalent of the manifold gallery and the branch pipes in addition to the inlet valve ports and cylinder, whereas the pipe projecting from the chamber becomes the tuned induction tract [100-102].

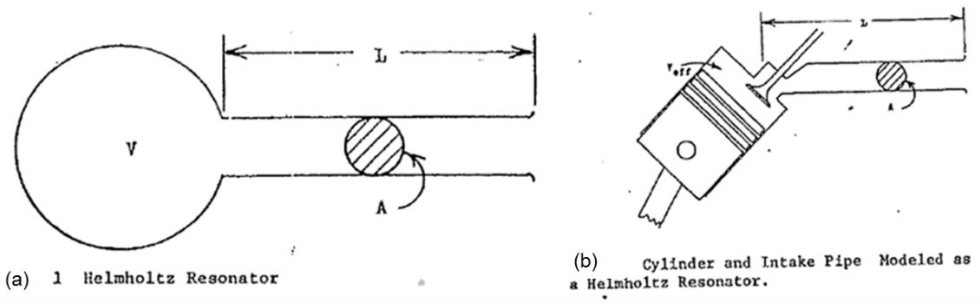

Figure 5-2 Simple Helmholtz resonator (a) and equivalent model for a single cylinder (b) [101]

To understand the Helmholtz resonator theory, it is useful to think of the pipe being acted on by forcing function produced by the piston. As the piston moves downward during the intake stroke, a reduced pressure occurs at the inlet valve relative to the pressure at the open end of the pipe. At mid stroke the piston is near its maximum velocity and the maximum pressure drop occurs across the valve which results in the maximum negative pressure (rarefaction wave) at the inlet valve. The rarefaction wave travels down the pipe to the open end and is reflected as a compression wave. A tuning effect occurs when the compression wave arrives at the time of valve closure when the piston is moving inwards towards TDC. The pressure wave will force the air, which would otherwise reverse under piston pressure, into the combustion chamber.

This theory can only predict the resonant frequencies of an intake system and cannot give a magnitude for the volumetric efficiency at the resonant frequencies

[101]. A single cylinder engine modelled as a Helmholtz resonator is shown in Figure 5-2 (b). The effective resonator volume V_{eff} is chosen to be one-half of the displaced volume plus the clearance volume. At this point the piston velocity is close to its maximum and the pressure in the inlet system close to its minimum. The tuning peak occurs when the natural frequency of the cylinder volume coupled to the pipe is about twice the piston frequency [99, 101].

For a single cylinder engine, the equation for the resonant tuning rpm is given by: -

$$RPM = \frac{162}{K} a \sqrt{\frac{A}{LV_{eff}}} \tag{4}$$

Where,

RPM is the rpm at tuning frequency,

162 is a constant for FPS units

a is the speed of sound (feet/sec),

A is the cross-sectional area of tuned pipe (in^2),

L is the length of tuned pipe (in),

K is the constant, ratio of Helmholtz frequency to engine speed, 2.0 – 2.5 range for most conventional engines,

V_{eff} is the effective volume (in^3), which is given by: -

$$V_{eff} = V_d(r_c + 1)/[(r_c - 1)] \quad in^3 \tag{5}$$

Where,

V_d is the displaced cylinder volume,

r_c is the compression ratio.

Engelman [100] discusses the Helmholtz theory for multi-cylinder engines. For these configurations, the intake pipes of the cylinder not undergoing induction are treated as additional volumes. In Figure 5-3 the two pipes, (L_1, A_1) and (L_2, A_2), and the two volumes, V_1 and V_2 form a vibrating system with two degrees of freedom and two resonant frequencies.

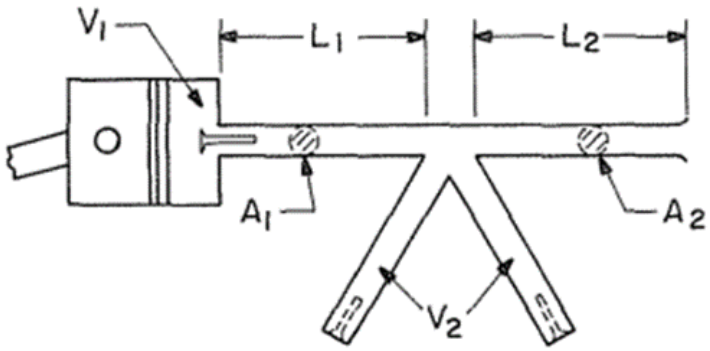

Figure 5-3 Multi cylinder Helmholtz resonator [101]

An advantage of using this approach on the production parallel twin engine under consideration is that the induction strokes do not overlap as the engine has a 360° firing interval, and this allows for the entire volume of the intake manifold to supply only one cylinder at a time. This means that the volume of both runners and the shared volume of the air box can be combined when using this method, rather than needing separate volumes, which would allow for a smaller overall package.

The Helmholtz resonator method and derivatives from it, see Figure 5-4, have been substantially used over the years.

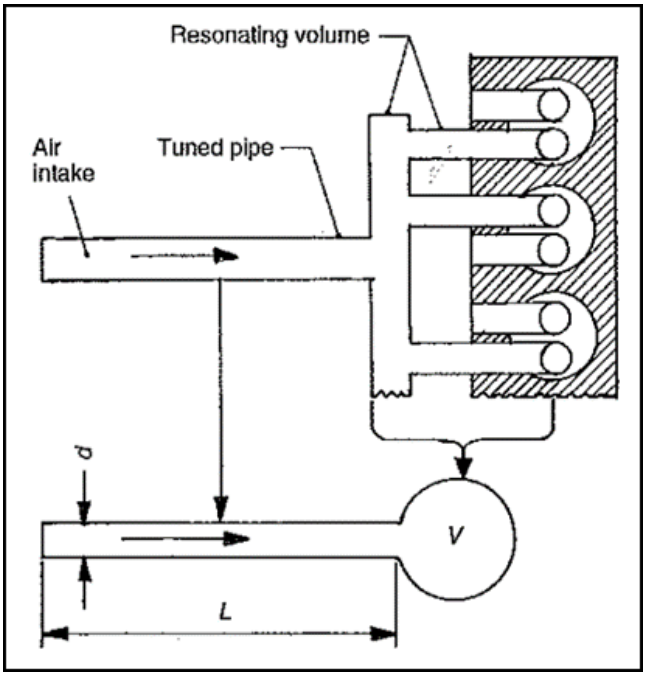

Figure 5-4 Comparison of the Helmholtz resonator with a tuned manifold system for multi-cylinder engines [98]

The resonator volume needs to be carefully chosen such that it resonates at an engine speed at which the boost torque is required, usually the peak torque of the engine, as well as to experiment with the tuned pipe length to obtain best results. Either side of the engine speed chosen, the pressure-wave ram effect quickly deteriorates [98].

Heisler [98] also provided a lucid discussion on effect of runner dimensions on VE characteristics. He showed that for a given runner length, both small and large runner diameters produce approximately the same peak VE in the cylinder. However, the VE with the small diameter runner peaks much earlier than the larger diameter runner, see Figure 5-5.

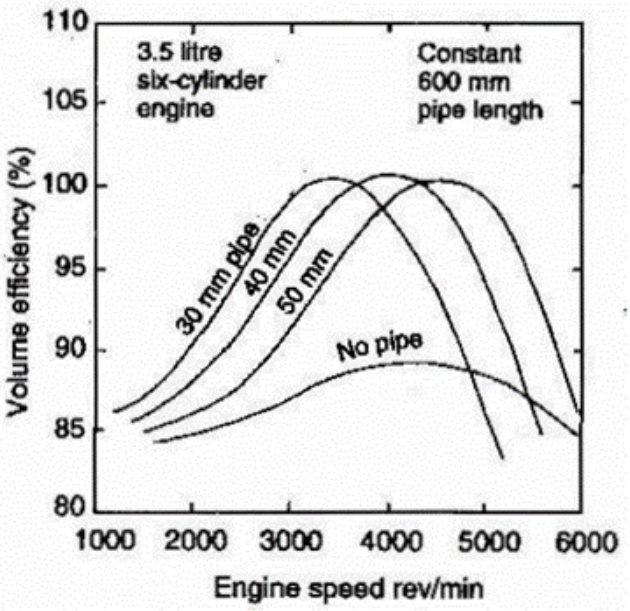

Figure 5-5 Effect of varying runner diameter with constant runner length. As the runner diameter decreases, the VE peaks much earlier. However the magnitude of the peak is independent of runner diameter [98]

For a given runner diameter, as the runner length increases, the peak efficiency shifts lower in engine speed [98]. This is due to several reasons. First, as the length increases, so does the surface area of the flow stream which results in additional resistance. As the air velocity increases with engine speed, the effect of this frictional resistance increases causing VE to shift lower in engine speed. Conversely, as the length gets longer, the charge column of air will get greater as it builds up over the greater length resulting in peak VE rising. This means as length increases, VE magnitude increases while shifting earlier in engine speed, and trails off quicker after peak VE is reached, see Figure 5-6.

While the preceding sections covered the theoretical aspects of inlet manifold tuning, nowadays the same is carried out using the 1-D simulation package GT Power as was done by TMETC.

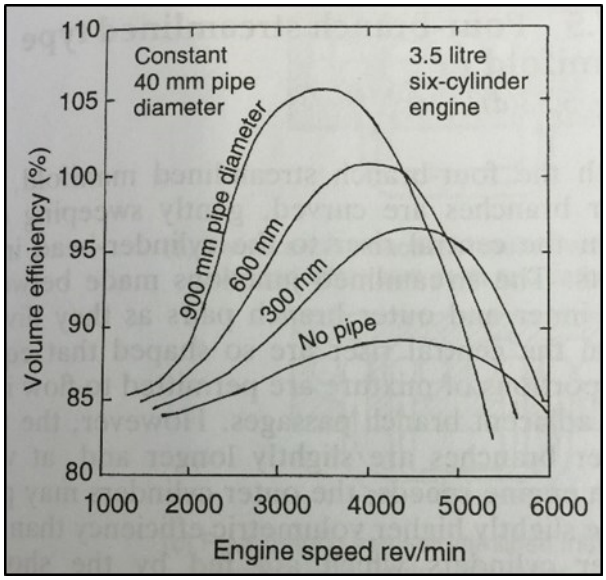

Figure 5-6 Effect of varying runner length with constant runner diameter. As the runner length increases, the VE magnitude increases while shifting earlier in engine speed [98]

5.3 Intake & Exhaust Manifold Simulation at TMETC

Simulation studies were carried out at TMETC using a detailed 1-D engine model, see Figure 5-7.

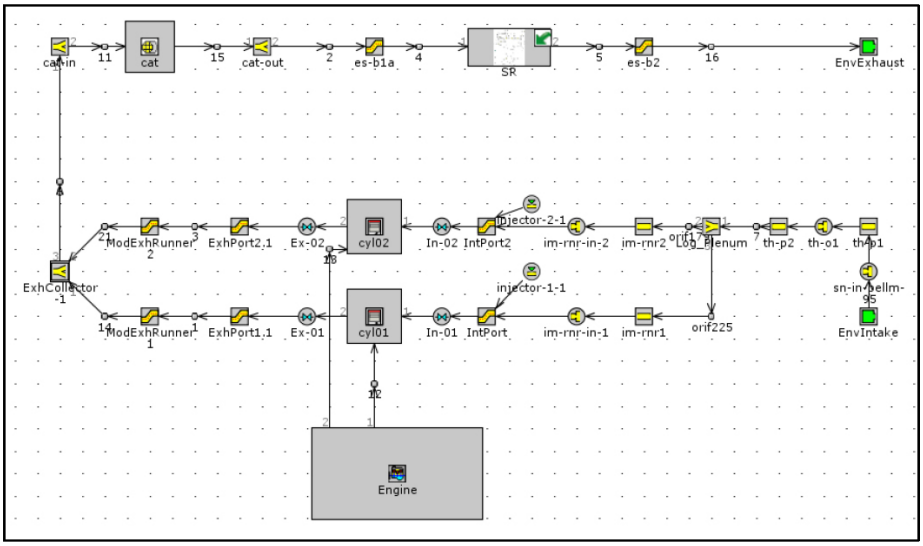

Figure 5-7 GT Power engine simulation model developed at TMETC [2, 103]

This included the use of individual cylinder feeds to allow for a common volume reducing the overall size of the manifolds. The volumetric efficiency of the engine was selected as the measure of engine performance as it was easily comparable between simulations and showed how effective the intake and exhaust manifolds were in improving the airflow and cylinder filling, which in turn would lead to an increased power output [103].

5.3.1 Runner Length Sweep

The intake length was varied from 0mm to 1500mm across an RPM range of 0-5500rpm to produce a contour map to display volumetric efficiency and torque against rpm and runner length. The diameter was fixed as that of the original intake at 32mm. The length sweep ranged from 50mm up to 1500mm in intervals of 10mm between 50 and 500mm and intervals of 50mm between 500 and 1500mm. In line with the theory covered in Section 5.2 above, the longer runners produced the highest volumetric efficiency at lower engine speeds, and as the target engine speed for peak power was increased the runner length was required to be reduced to maintain high volumetric efficiency values. Simulation results showed that for peak power at 4500rpm the runner length for 32mm diameter was 460mm [103].

The relation between runner length and runner diameter closely follows Equation (4) and is shown in Figure 5-8. According to the Helmholtz resonator equation, for a runner diameter of 32mm, at a resonant frequency of 4500rpm, the runner length should be 456mm which is very close to the simulation runner length of 460mm in the preceding paragraph. As mentioned earlier in Section 5.2.2, Equation (4) can only predict the resonant frequencies of an intake system and cannot give a magnitude for the volumetric efficiency at the resonant frequencies.

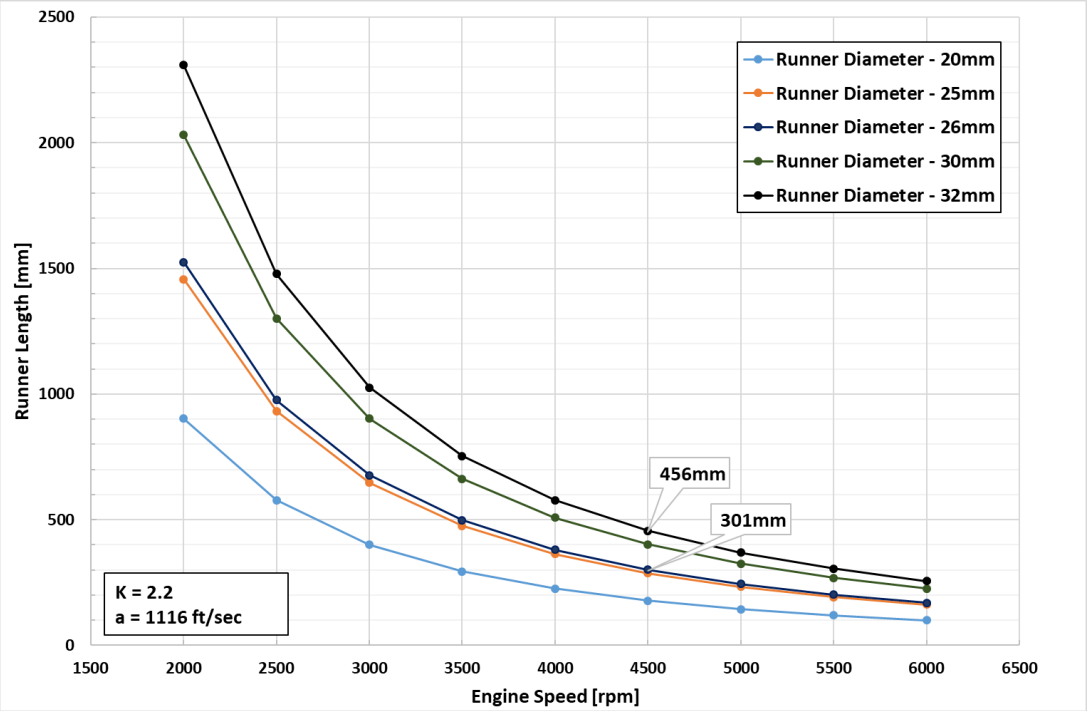

Figure 5-8 Relation between runner length and runner diameter based on Helmholtz Resonator Equation (4) for varying resonant frequencies. At a resonant frequency of 4500rpm, for a runner diameter of 32mm the runner length is 456mm and for a runner diameter of 26mm the runner length is 301mm

5.3.2 Runner Diameter Sweep

Keeping the original runner length of 320mm, the runner diameter was varied from 20mm to 100mm in 5mm increments. Results showed that there were only a small range of runner diameters that could produce an acceptable volumetric efficiency. For the target engine speed of 4500rpm the simulated runner diameter was 26mm [103]. This matches closely with the runner length of 301mm calculated based on the Helmholtz resonator Equation (4) and shown in Figure 5-8 above.

5.3.3 Diameter and Length Sweep

To investigate the relationship between length and diameter, they were changed together to provide a sweep across a large set of dimension combinations that were tested across the engine speed range. The diameter was varied from 20 to 30mm and

the length 400 to 500mm. Each combination was tested at 500rpm increments between 500 and 5500rpm. Simulation showed that at 4500rpm the optimum runner diameter was 26.5mm and length of 460mm [103].

5.3.4 Runner Bend Angle Simulation

To allow for a compact packaging solution, it was evident that straight runners would not be a viable option, and bent runners would be required. Accordingly, the impact of including a bend was tested by carrying out a simulation sweep with a fixed length as the radius of the pipes was increased in increments of 10° between 0° and 260° and a runner length of 400mm was used. It was seen that a small variation in volumetric efficiency was present, but at 4000rpm where the 400mm runner would deliver its highest volumetric efficiency, the peak value changed very little as the radius changed from its minimum and maximum values [103].

5.3.5 Resonator Simulation

In order to examine the effect of wave tuning as outlined in Section 5.2.2 above, a simple resonator was modelled based on Figure 5-4. Although the simulations carried out did not provide a clear set of dimensions that could be applied to the resonator, they did provide a range of values that could be useful, such as the effective range of diameters in which a high volumetric efficiency value could be achieved [103].

Two examples of the models tested are shown in Figure 5-9. Once a model was entered in GT Power, it was possible for the software to change the dimensions and update the model, and the power delivery from the resonator simulated. Results showed that 0.24 litre resonator could deliver a 100% volumetric efficiency with 100mm runners and 100mm feed pipe.

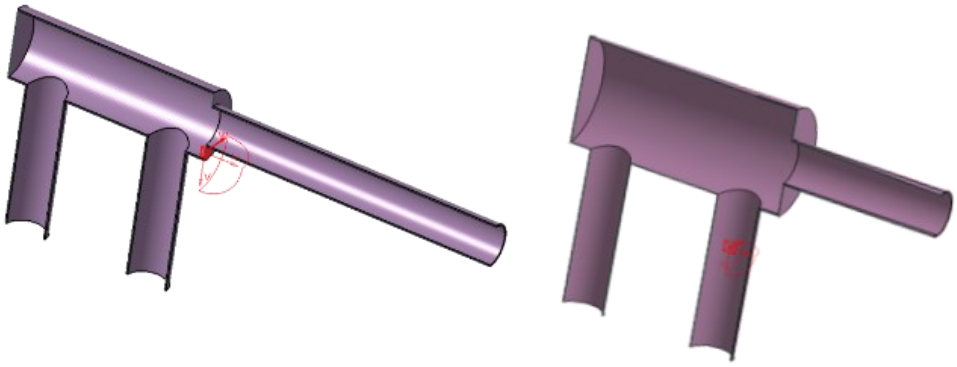

Figure 5-9 Examples of resonators simulated at TMETC [103]

Based on the results, it was possible to achieve the desired power improvement at the target engine speed of 4500rpm, however two routes to achieving could be adopted. Either the optimum dimension 460mm open ended runners could be used, but these were quite long and would pose a packaging problem, or a resonator which was a compact solution, which while still delivering an increase, did not match the performance of the long runners.

The results above showed that intake runner length and diameter were critical to achieve high volumetric efficiency. However, the optimized runner length of 460mm was considered too long from a packaging perspective and a resonator system selected for its compact size with only a small reduction in volumetric efficiency.

5.4 Experimental Evaluation of Inlet Manifold Variation

In order to maintain a modular approach which was more amicable from packaging perspective as well as giving an improved performance over the base inlet manifold, the intake runner length was kept variable, a resonator was included and accordingly a Design of Experiment (DOE) was prepared by TMETC [2] and provided to University of Bath to evaluate and is shown in Table 5-1 below.

Table 5-1 DOE for inlet manifold tuning by varying intake runner lengths, pre-plenum chambers and side plenum chambers. Runner diameter was kept constant at 26mm

Test	Runner length, mm	Plenum chamber	Pre-plenum chamber feed pipe	Side plenum chamber	Throttle body position	Conical air filter
1	0	Yes	Yes (parallel to runner axis)	No	Parallel to runner axis	Yes
2	0	Yes	Yes (parallel to runner axis)	Yes	Parallel to runner axis	Yes
3	50	Yes	Yes (parallel to runner axis)	No	Parallel to runner axis	Yes
4	50	Yes	No	No	Parallel to runner axis	Yes
5	50	Yes	No	Yes	Parallel to runner axis	Yes
6	50	Yes	No	Yes (2 in number)	Parallel to runner axis	Yes
7	150	Yes	No	No	Parallel to runner axis	Yes
8	150	Yes	No	Yes	Parallel to runner axis	Yes
9	150	Yes	No	Yes (2 in number)	Parallel to runner axis	Yes

Figure 5-10 to Figure 5-18 show the test 1 to test 9 configurations as set up in the test cell during the inlet manifold tuning process. The diameter of the runners was fixed at 26mm which was the optimal diameter as per simulation in Section 5.3.2.

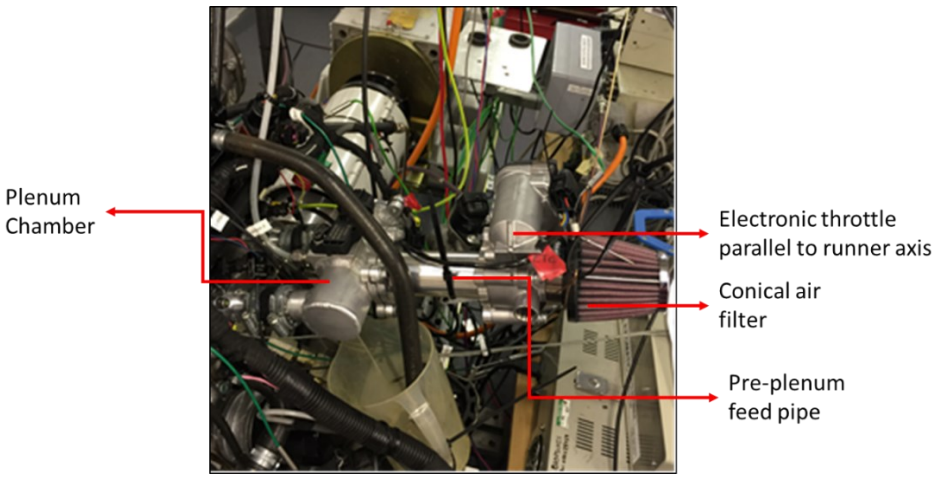

Figure 5-10 Test 1 configuration with inlet runner length of 0mm, single plenum chamber, pre-plenum feed pipe, throttle body parallel to the runner axis and conical air filter.

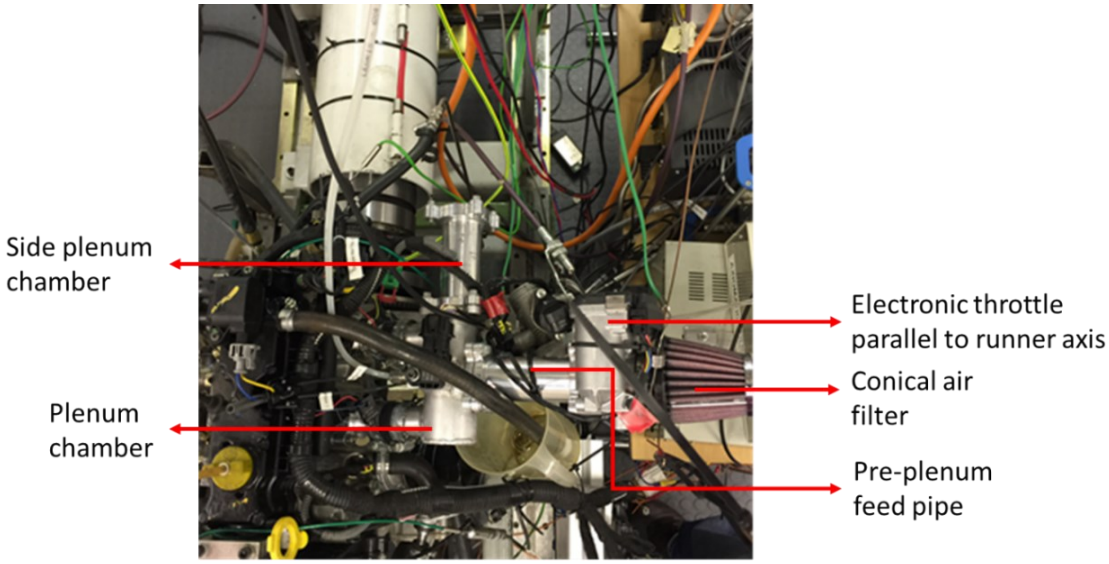

Figure 5-11 Test 2 configuration with inlet runner length of 0mm, double plenum chamber, pre-plenum feed pipe, throttle body parallel to the runner axis and conical air filter

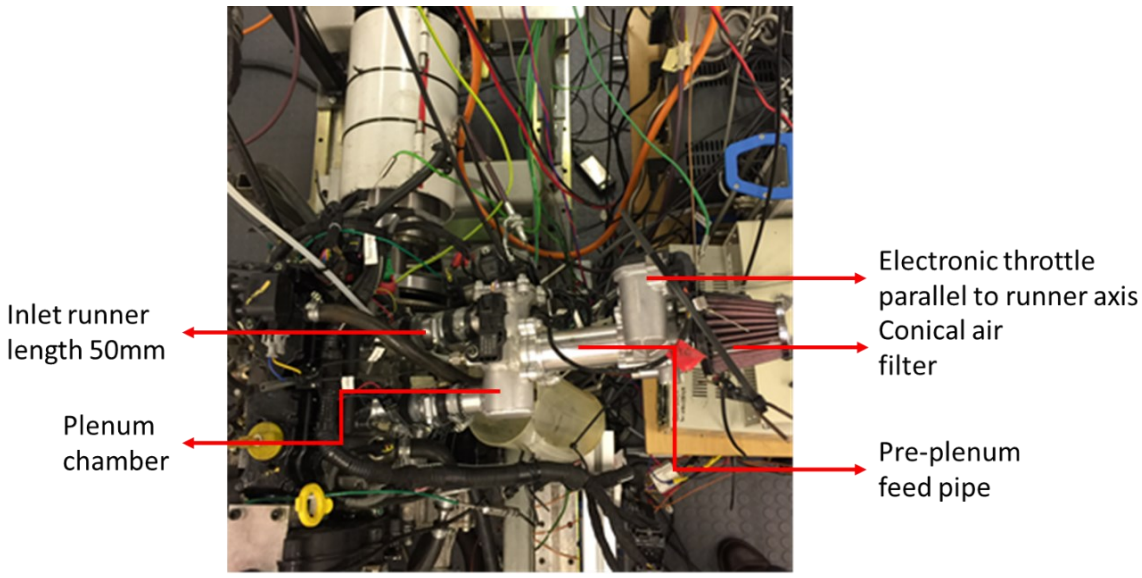

Figure 5-12 Test 3 configuration with inlet runner length of 50mm, single plenum chamber, pre-plenum feed pipe, throttle body parallel to the runner axis and conical air filter

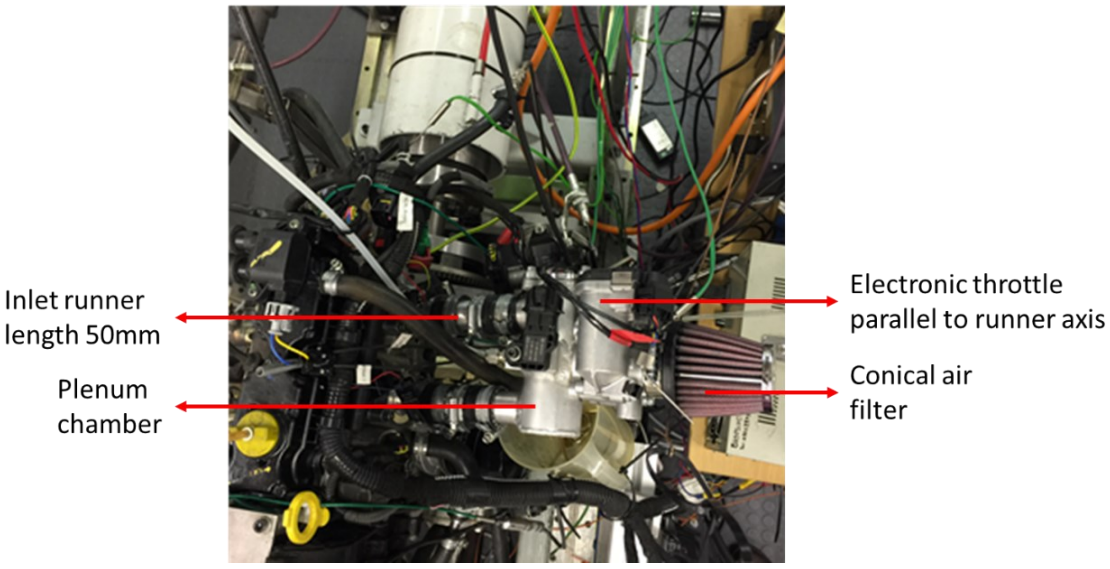

Figure 5-13 Test 4 configuration with inlet runner length of 50mm, single plenum chamber, throttle body parallel to the runner axis and conical air filter

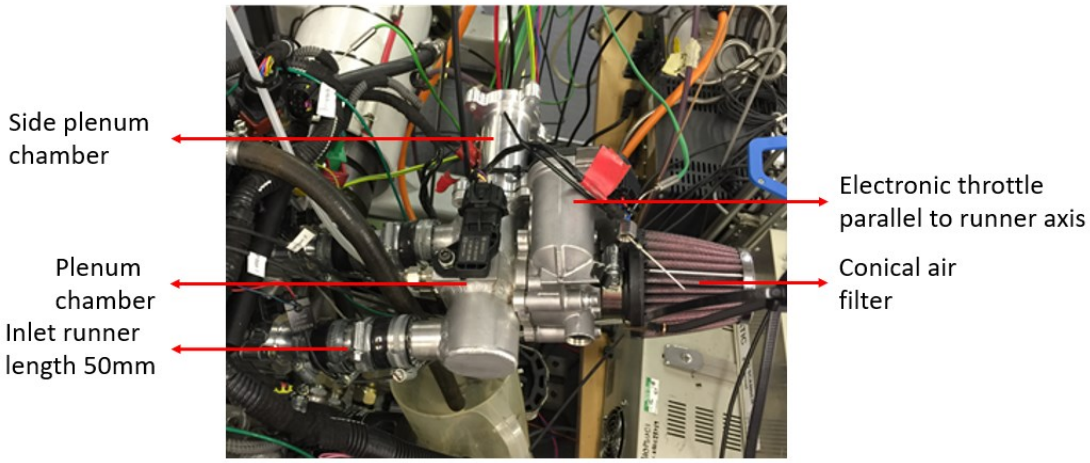

Figure 5-14 Test 5 configuration with inlet runner length of 50mm, double plenum chamber, throttle body parallel to the runner axis and conical air filter

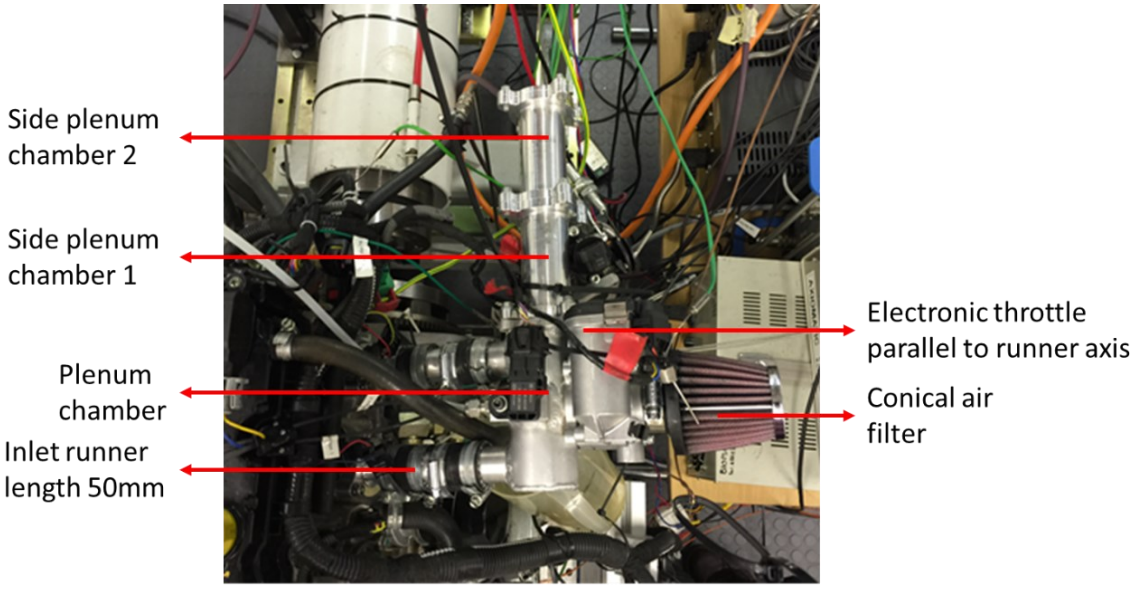

Figure 5-15 Test 6 configuration with inlet runner length of 50mm, triple plenum chamber, throttle body parallel to the runner axis and conical air filter

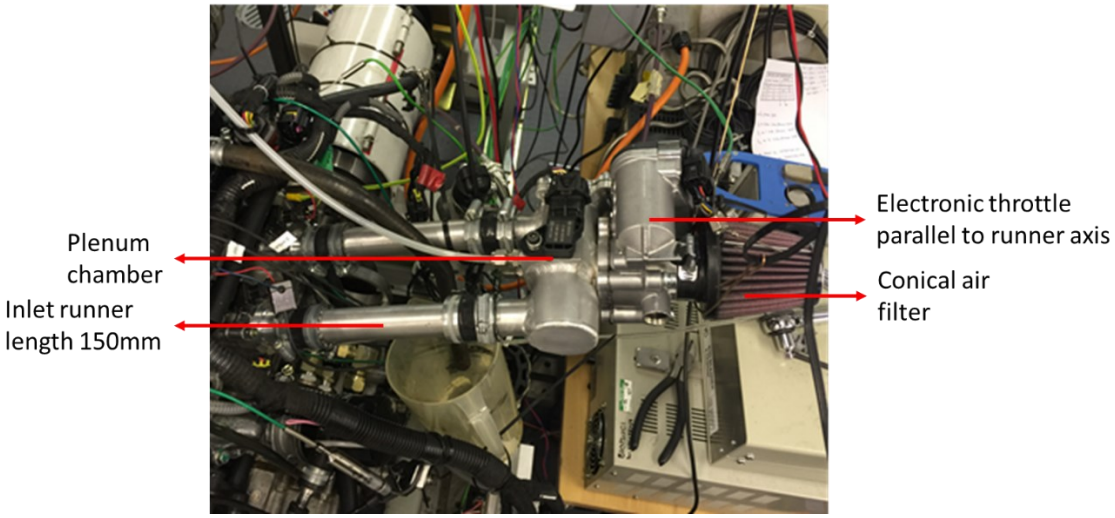

Figure 5-16 Test 7 configuration with inlet runner length 150mm, single plenum chamber, throttle body parallel to the runner axis and conical filter [2]

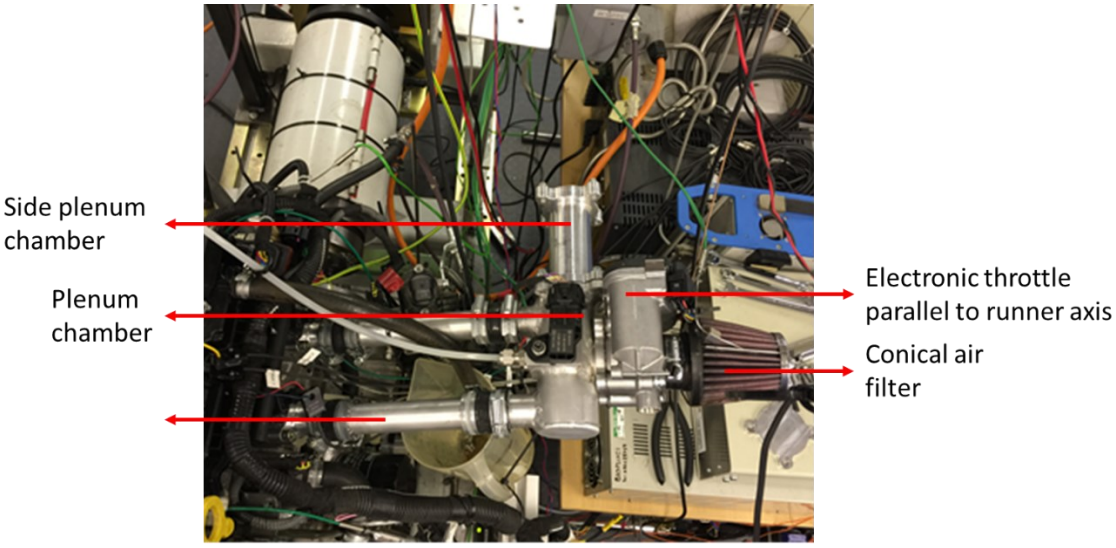

Figure 5-17 Test 8 configuration with inlet runner length 150mm, double plenum chamber, throttle body parallel to the runner axis and conical filter

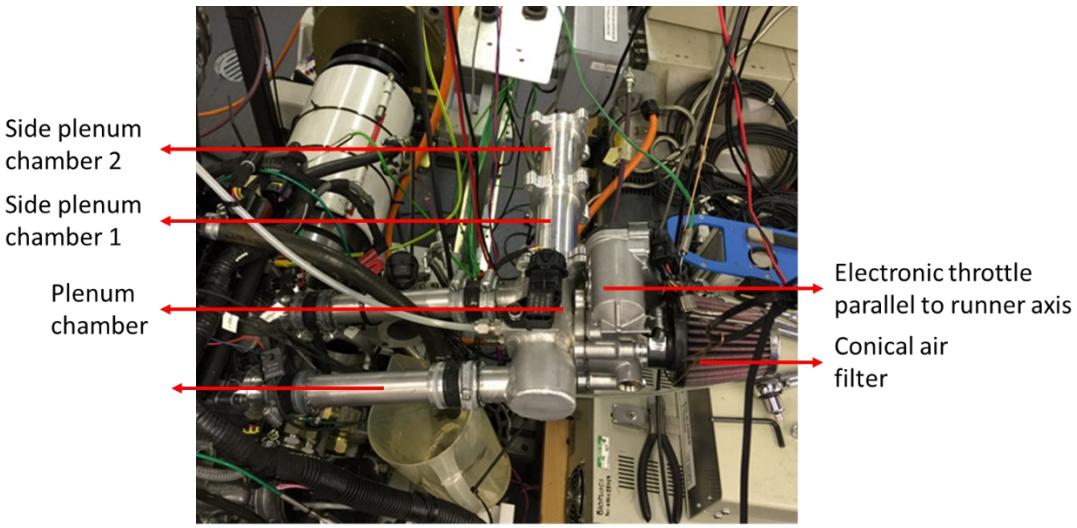

Figure 5-18 Test 9 configuration with inlet runner length 150mm, triple plenum chamber, throttle body parallel to the runner axis and conical filter

Figure 5-19 shows the effect of varying runner lengths and plenum volume as per the various test configurations on volumetric efficiency.

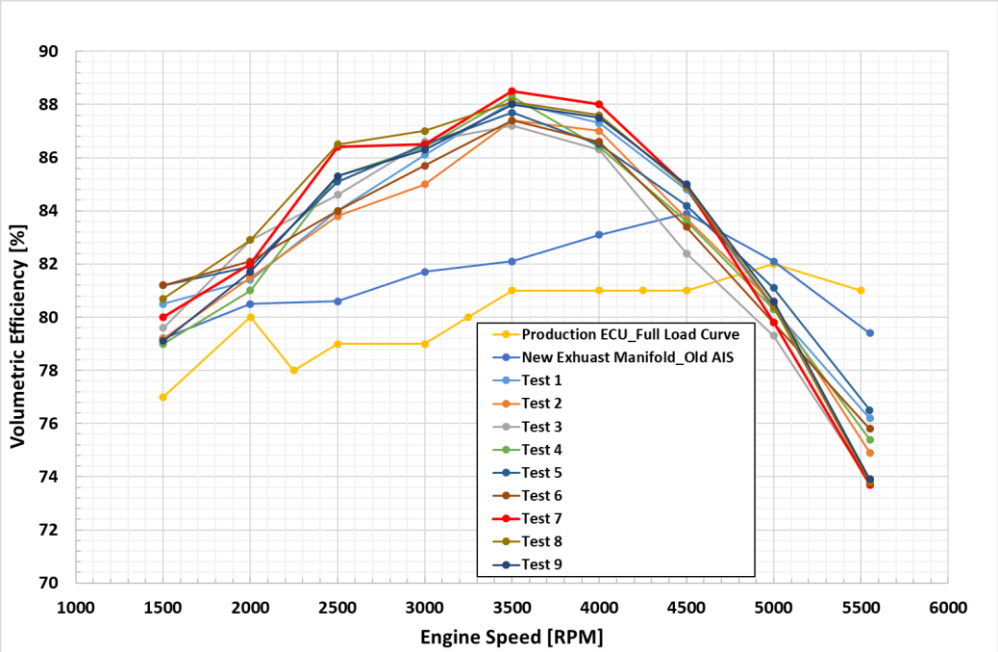

Figure 5-19 Experimental results of effect of varying runner length and plenum volumes on engine volumetric efficiency. Description of tests are in Table 5-1

Figure 5-20 shows the effect of varying runner lengths and plenum volume as per the various test configurations on engine torque.

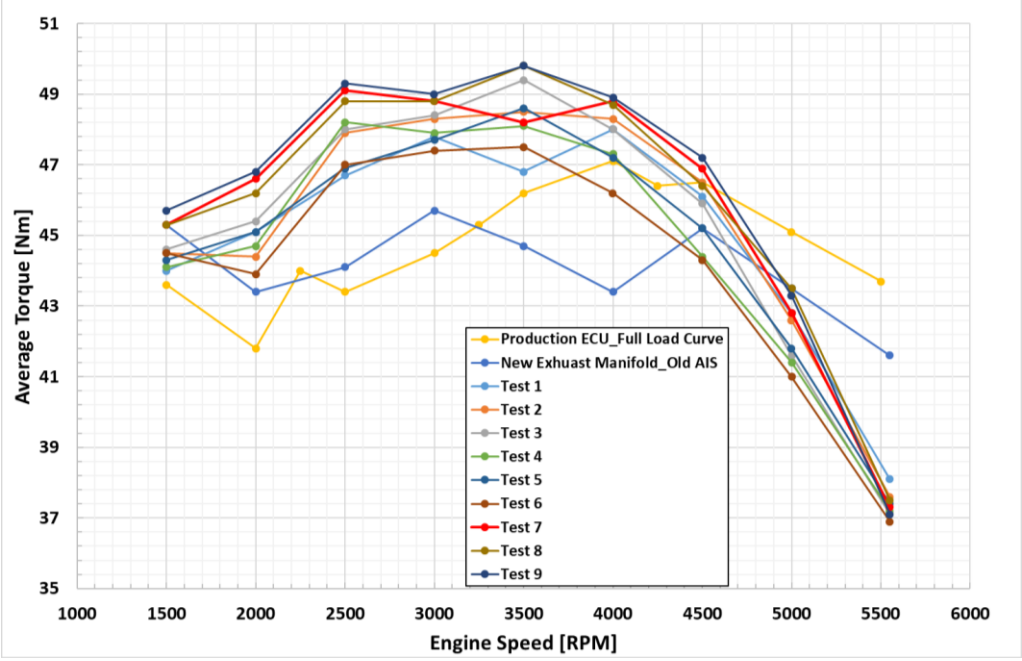

Figure 5-20 Experimental results of effect of varying runner length and plenum volumes on engine torque. Description of tests are in Table 5-1

Figure 5-21 below which is an extract of Figure 5-19 highlights how the experimental results are in line Heisler's theory [98] of effect of runner dimensions on volumetric efficiency as discussed in Section 5.2.2. The test 5 and test 8 intake manifold configurations are identical except for runner lengths. Test 5 has a runner length of 50mm while test 8 has a runner length of 150mm. In line with Heisler theory as the runner length increases, the magnitude of the VE increases, the VE peak shifts left, although not so apparent in this case, and quickly trails off after the VE peak is reached.

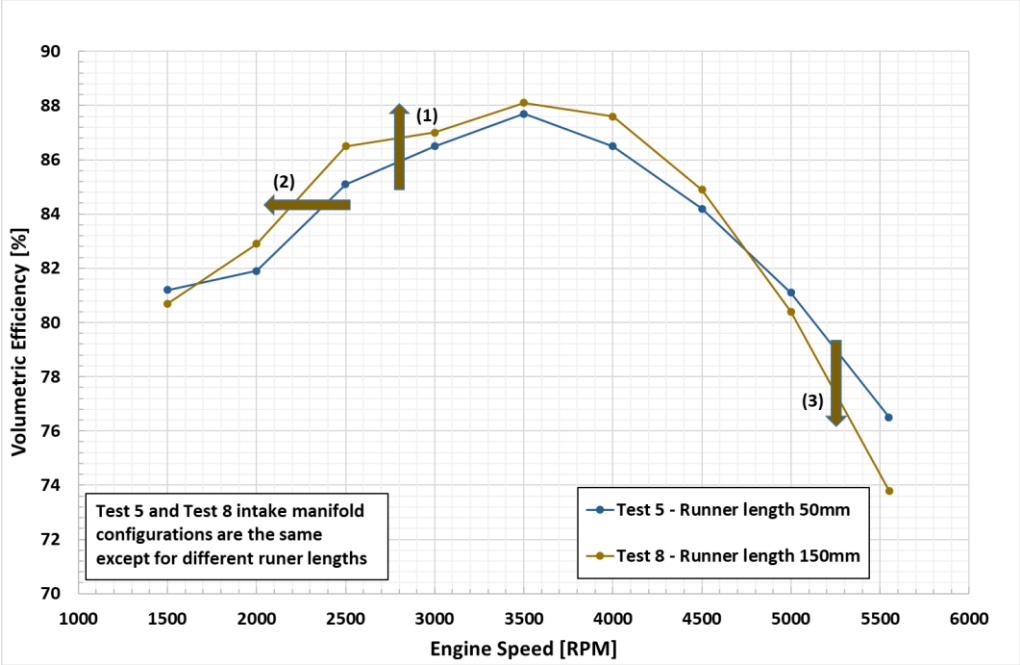

Figure 5-21 Change in η_v with change in runner length. As the runner length increases, the magnitude of the η_v increases (arrow 1), the η_v peak shifts left (arrow 2) although not so evident, and quickly trails off after the η_v peak is reached (arrow 3)

Based on the increased torque results as well as overall ease of packaging, it was decided to continue further development with the test 7 configuration. It is highlighted that while the exhaust manifold development has been covered in the subsequent section, at the time of inlet manifold development, the new exhaust manifold had already been installed on the engine.

5.5 Bespoke Exhaust Manifold Development

Heisler [98] provides a cogent explanation on the kinetic energy theory of cylinder scavenging. As per him the most important mechanism for extracting the residual exhaust gases from the combustion chamber at the end of the exhaust period is to utilise the kinetic energy of the outgoing exhaust gases to produce a compression wave followed by an expansion wave in which the gas pressure is reduced to a depression in the exhaust port region of the exhaust system. This depression created during the valve overlap period considerably helps to draw residual exhaust gases out of the combustion chamber and into the exhaust port and at the same time pulls in the fresh charge from the induction port to fill this evacuated space, see Figure 5-22 and Figure 5-23.

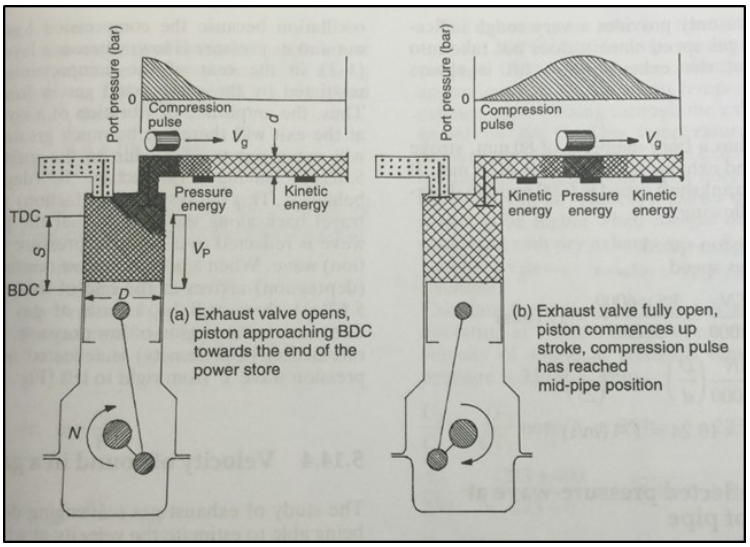

Figure 5-22 Kinetic energy theory of scavenging (a) and (b) [98]

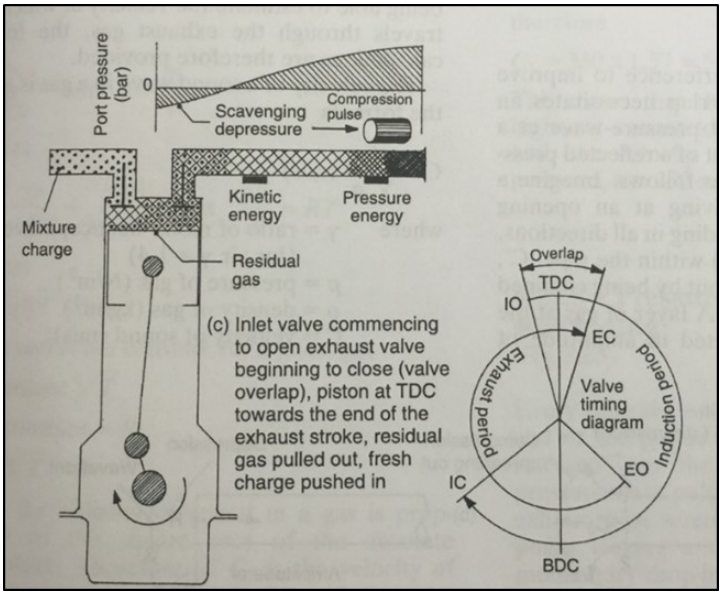

Figure 5-23 Kinetic energy theory of scavenging (c) [98]

If the exhaust manifold only has short branch pipes there will be insufficient time for the compression wave to leave behind it a depression capable of pulling out the stagnant gas so that the fresh charge arriving at the inlet port is prevented from entering the combustion chamber in the early part of the induction process. Conversely if the pipe length is very long the flow resistance may become excessive thereby creating its own back pressure, which will also slow down the scavenging and the filling process.

Another important factor with emission laws becoming more stringent and the requirement to reduce exhaust pollutants following a cold start is to reduce the thermal mass (or capacitance) of the exhaust manifold. This facilitates bringing the catalytic converter to the light off temperature more quickly using the heat in the exhaust [94].

5.6 Experimental Evaluation of Exhaust Manifold

Simulation results at TMETC showed that exhaust system had negligible impact on performance and the requirement was only to minimise back pressure within a

favourable package [2]. Figure 5-24 shows the bespoke exhaust manifold on the engine with instrumentation to monitor manifold pressures, temperatures and lambda values.

Testing was subsequently undertaken without a catalyst downstream, and instead a back-pressure valve was installed, and its position suitably calibrated to match the back pressure like that of the production catalyst.

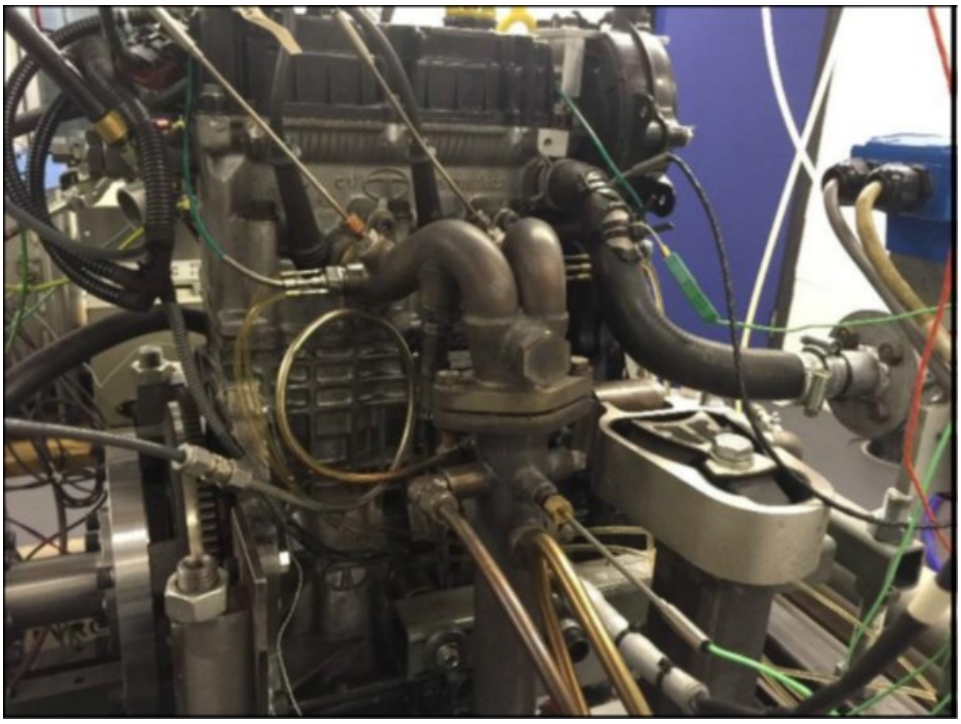

Figure 5-24 Bespoke exhaust manifold on engine in test cell. Thermocouples for measuring exhaust gas temperature, exhaust gas pressure transducers, lambda sensor and connection to the emissions analyser heated line can be seen [2]

5.7 Engine Performance with Bespoke Manifolds

Based on the results obtained at Section 5.4 and 5.6 above, Figure 5-25 shows the difference in brake power between the proposed and original manifolds during testing.

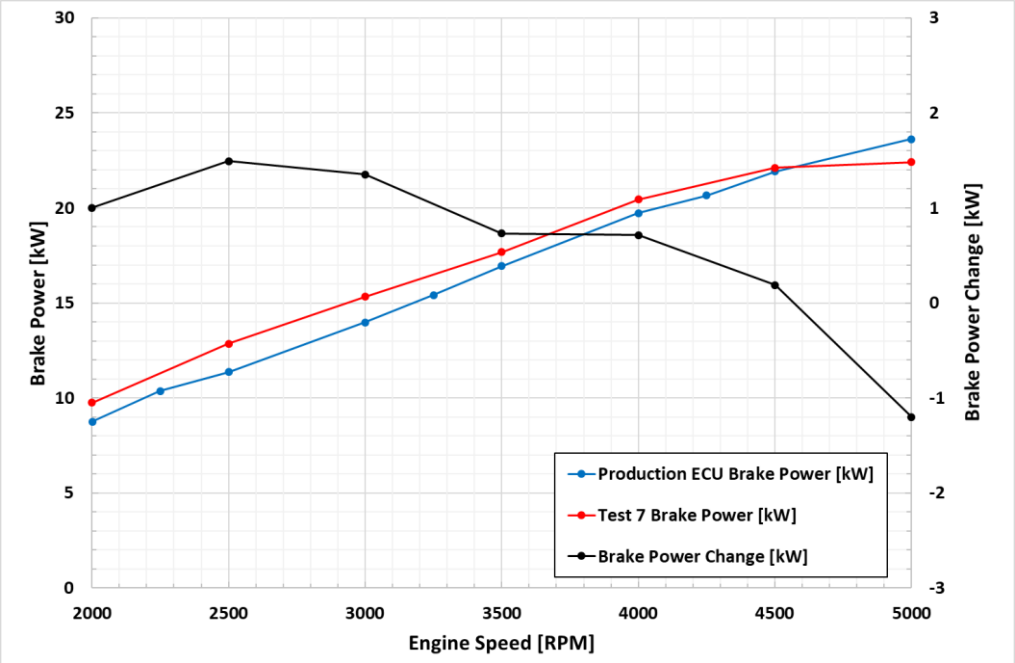

Figure 5-25 Experimentally measured brake power change – proposed versus original manifolds

The results show a gain in engine torque across the operating range of the engine, from 2000-4500rpm. After 4500rpm, there is a reduction in performance because the proposed manifold's compact size, which was considered to be an acceptable compromise for an APU application as the planned APU operating strategy follows WOT line across the engine speed range, with no requirement to run above 4500rpm. This strategy maximises the engine efficiency at any given power output by minimising throttling losses and friction. Part load running is avoided and therefore not considered a primary objective for the optimisation [2].

As mentioned in Section 5.4 above, further APU development work was continued with the Test 7 configuration. TMETC subsequently developed prototype inlet and exhaust manifolds, that were installed on the engine in the test cell during the latter stages of the project. The final configuration chosen maintained a 92% plenum volume reduction. The final configuration of the bespoke inlet and exhaust manifolds on the base engine are shown in Figure 5-26 and Figure 5-27.

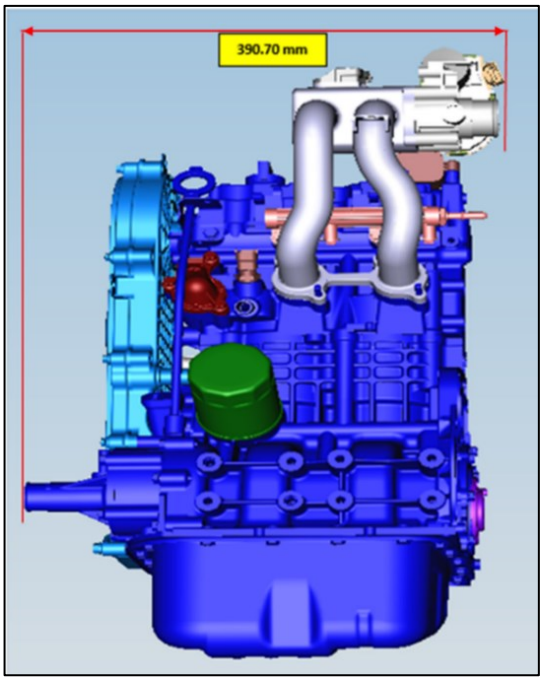

Figure 5-26 Base engine with bespoke inlet manifold, reduction in overall package width from 553.15mm to 390.70mm, courtesy TMETC

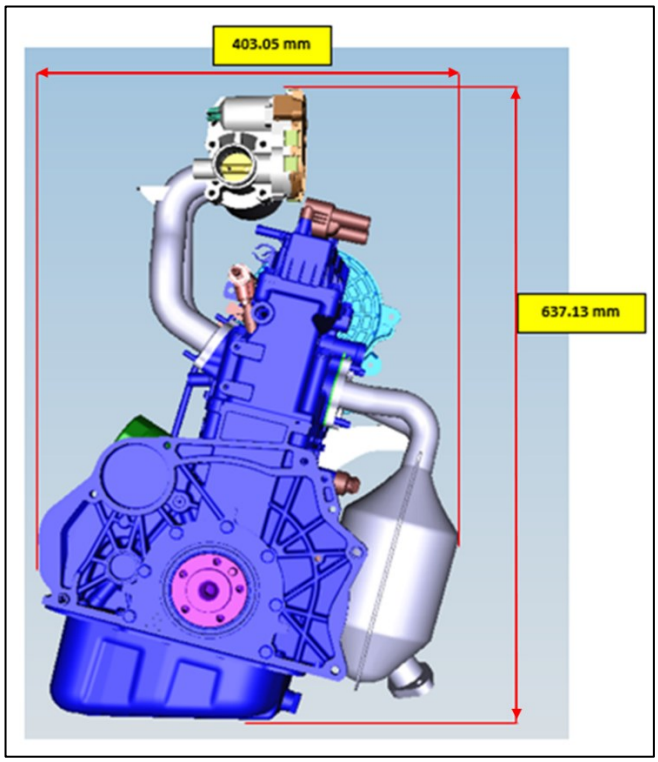

Figure 5-27 Base engine with bespoke inlet and exhaust manifold. Reduction in width from 597.25mm to 403.05mm. Overall height increased from 550.58mm to 637.13mm, courtesy TMETC

To facilitate packaging without significant compromise on performance, the final runner lengths chosen during rapid prototyping were; cylinder 1 – 246.9mm and cylinder 2 – 248.3mm. These were longer than what was experimentally tested in the test cell, however simulation studies had been carried out at TMETC.

5.8 Conclusion

One of the objectives of the research was to develop the APU to generate power circa 20-25kW. This required the engine performance to increase while introducing modifications within the normal volume production process.

Since the engine was being used for a range extender application where driveability was not an issue, it allowed the flexibility to optimise for a few operating points rather than the entire engine operating regime.

Development of bespoke inlet and exhaust manifolds was undertaken based on 1D-simulation at TMETC and experimental work at University of Bath.

Based on the results obtained, the final configuration chosen maintained a 92% plenum volume reduction while gaining in engine power across the proposed operating range of the APU from 2000 to 4500rpm. After 4500rpm, there was a reduction in performance because the proposed manifold's compact size. This was an acceptable compromise for the APU application as the planned APU operating strategy follows the WOT line across the engine speed range, with no requirement to run above 4500rpm. This strategy maximises the engine efficiency at any given power output by minimising throttling losses and friction.

However, future work could be planned to optimize the APU's performance at higher speeds for applications that require greater power.

The work presented in this chapter formed part of the technical paper titled ‘Development of a Low-Cost Production Automotive Engine for Range Extender Application for Electric Vehicles’ that was presented at the SAE World Congress, Detroit in April 2016. Paper reference is 10.4271/2016-01-1055.

CHAPTER - 6
Map Calibration and Introduction of EWP

This chapter presents the fine tuning engine calibration to run stoichiometric air fuel ratio as far as possible and achieve maximum best torque by optimising spark advance. The second part introduces the electric water pump and its control development. Lastly the engine performance, post modifications, is compared with the baseline production engine.

.

6.1 Introduction

After the development of bespoke manifolds in Chapter 5, this chapter discusses further engine calibration to improve the engine performance as well as gain improvements in engine BSFC.

Aspects which were looked at in detail were reduction in exhaust lambda enrichment and spark timing optimisation. Extensive experimental testing and calibration was undertaken to determine the limit of running the engine at stoichiometric air-fuel ratio as well as ensuring the maximum possible engine torque while staying within engine knock limits.

The next section discusses the introduction of the electric water pump (EWP) and its control development. Merits of the EWP and its role in an APU application are discussed.

Lastly the performance of the engine post calibration/modifications was compared with the baseline production engine.

6.2 Reduction in Exhaust Enrichment

The production engine was developed for operation in the Indian market and use of RON 91 gasoline. Since the APU was being developed for European conditions where RON 95 gasoline is standard, there was an opportunity to optimise ignition timing i.e. advance the spark timing and reduce exhaust enrichment to achieve an improvement in performance and fuel economy while preventing knock and maintaining exhaust temperatures within 750°C to 755°C as specified by TMETC. Having calibration level access in the Motohawk EMS, the baseline desired equivalency ratio calibration table was optimised to achieve lambda 1 operation at WOT up to 3750rpm as shown in Figure 6-1 while maintaining exhaust gas

temperatures within 750°C. This was achieved in conjunction with spark timing optimisation covered in Section 6.4.

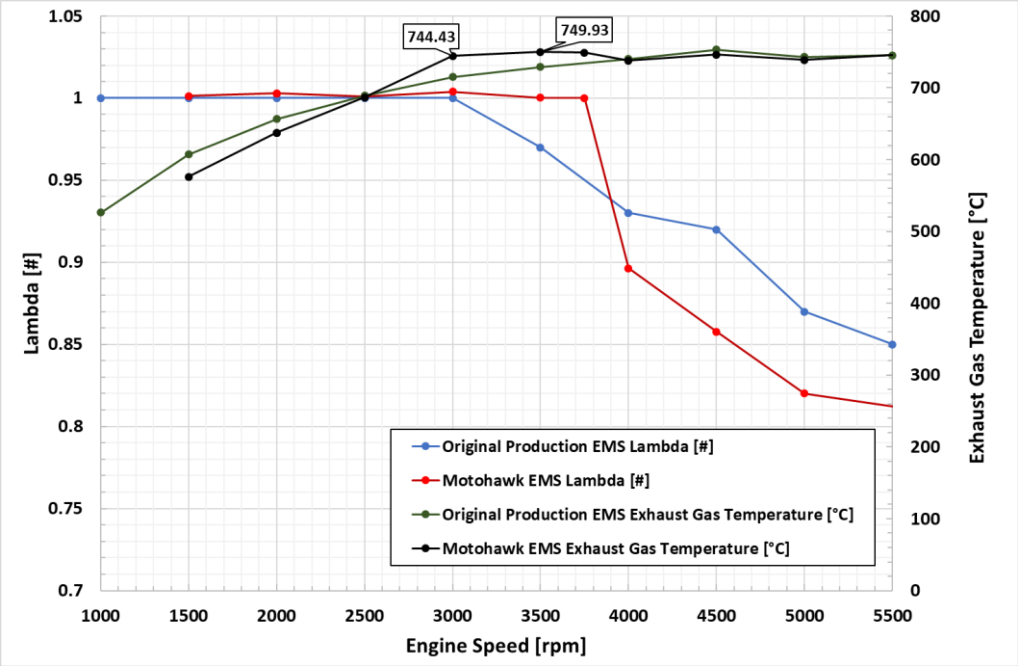

Figure 6-1 Comparison of lambda at WOT between production and Motohawk EMS. Lambda 1 operation at WOT extended to 3750rpm with bespoke EMS [2]

6.3 RON 91 versus RON 95 Gasoline

Octane number is a standard measure of the performance of an engine fuel. The higher the octane number, the higher compression it can withstand before detonating (igniting). In gasoline spark-ignition (SI) engines, the air-fuel mixture is heated due to being compressed and is then ignited by the spark plug to burn rapidly. If the mixture is heated or compressed too much, it may self-ignite before the ignition system sparks. This results in engine knock. The most common type of octane rating is the Research Octane Number (RON). As per Stone [104] unity increase in RON will increase the knock limited spark advance (KLSA) by 1.5° to 2° crank angle.

6.4 Spark Timing Optimisation

Spark timing has a direct effect on power output. If ignition is too late (retarded spark timing) then although work done by the piston during the compression stroke is reduced, so is the work done on the piston during the expansion stroke since all pressures during the cycle will be reduced. There is also a risk that combustion will be incomplete before the exhaust valve opens at the end of the expansion stroke and could overheat the exhaust valve. On the other hand, if the ignition is too early (advanced spark timing) there will be too much pressure rise before the piston reaches TDC and the power will be reduced because the compression stroke work transfer which is from the piston to the cylinder gases increases. Also, with early ignition the peak pressure and temperature may be enough to cause knock. Ignition timing is therefore optimised to give maximum brake torque (MBT) and at this timing the magnitudes of the two opposing tends just offset each other. Timing which is advanced or retarded from this optimum gives lower torque [99, 104].

The spark optimisation was carried out from 1500rpm to 5000rpm in steps of 500rpm. At each rpm set point, the engine load [air per cylinder per cycle (APC) (mg/cyl/cycle)] was varied from 105mg (part load) to WOT in steps of 30 mg. At each step the existing spark timing was retarded / advanced in steps of 2°, 4°, 8° to have an overall sweep of 8° on either side of the existing timing. The data was logged using a 30sec averaging period to observe the small changes expected during the spark sweep. It was observed that at WOT the spark timing advance was limited by the onset of knock. Retarding the spark timing was limited by high exhaust temperatures. It was aimed not to exceed the temperature limit of 755°C [2].

In most cases, there was clear indication where the MBT occurs. Figure 6-2 shows that the MBT of 32.1Nm occurs at a spark timing of 30° BTDC at an engine load of 238 mg/cyl/cycle at an engine speed of 4000rpm and exhaust gas temperature of 748.1°C.

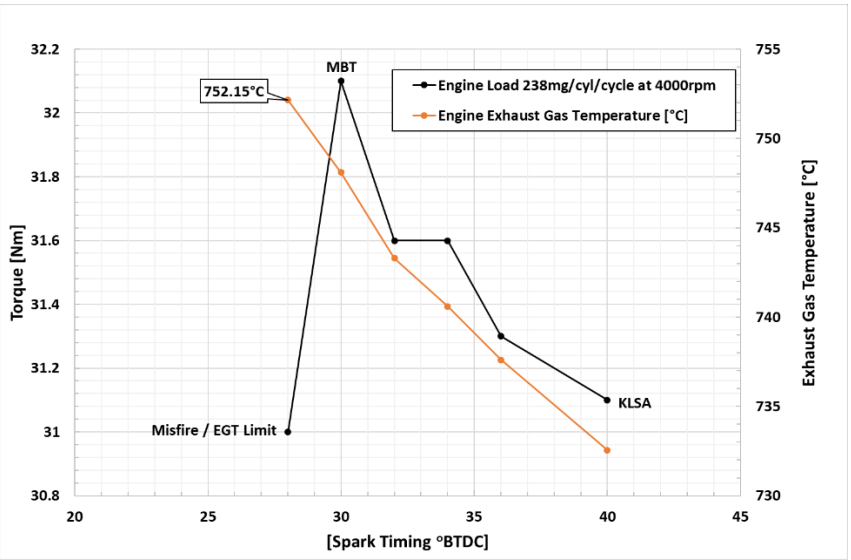

Figure 6-2 Spark timing sweep at 4000rpm, engine load of 238mg/cyl/cycle. MBT of 32.1Nm is at spark timing of 30°BTDC

However, because of the variation in measured torque observed, more so at part load, there were instances where such a peak was not clear. Figure 6-3 shows two peaks of 37.6Nm at spark timings of 26° and 32° BTDC at 3000rpm at an engine load of 245 mg/cyl/cycle. Nevertheless, a trend could be extracted.

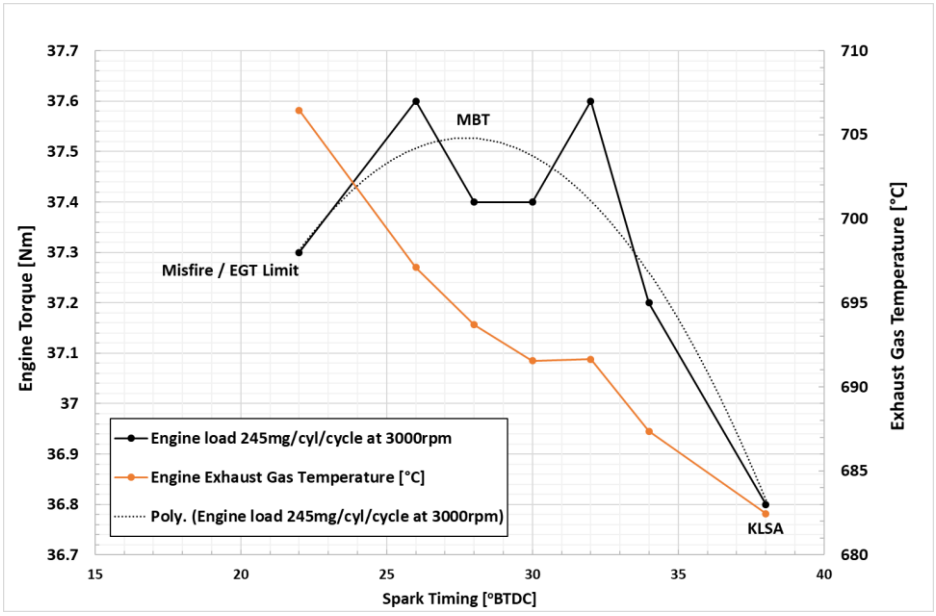

Figure 6-3 Spark timing sweep at 3000rpm, engine load of 245 mg/cyl/cycle. MBT peak not clear but the trend can be seen

At higher engine speeds and WOT, because of onset of knock or exhaust temperature limit (755°C) at times it was not possible to do the entire 16° spark timing sweep. At 5000rpm, WOT, the existing spark timing was of 29° BTDC. At this regime, the engine cylinder-2 exhaust temperature was 765°C. Therefore, the spark timing was not retarded and the performance was only checked for spark timing advance.

Based on the measurements, the optimised spark timing is shown in Figure 6-4. The optimised spark timing analysis resulted in a spark advance map with an undulating surface.

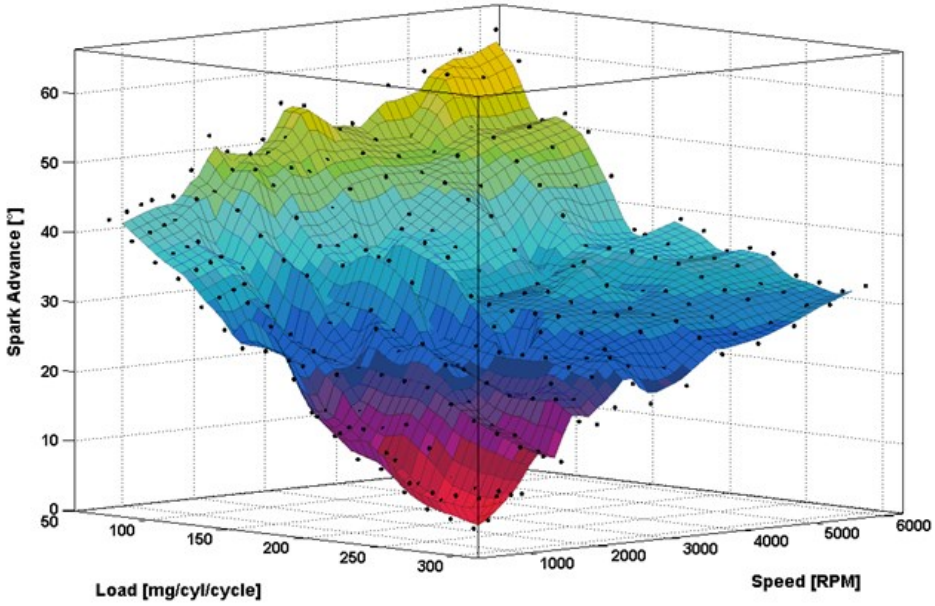

Figure 6-4 Optimised spark timing – undulated map [2]

It was decided to smooth the spark advance map to smooth out any irregularities in test data. This would minimise the excursions of engine speed and lambda from their corresponding set values during transiting from one load point to the other. The smoothed map shown in Figure 6-5 was generated using the Matlab curve fit toolbox (version 3.5.2, copyright 2001-2015 The MathWorks Inc.).

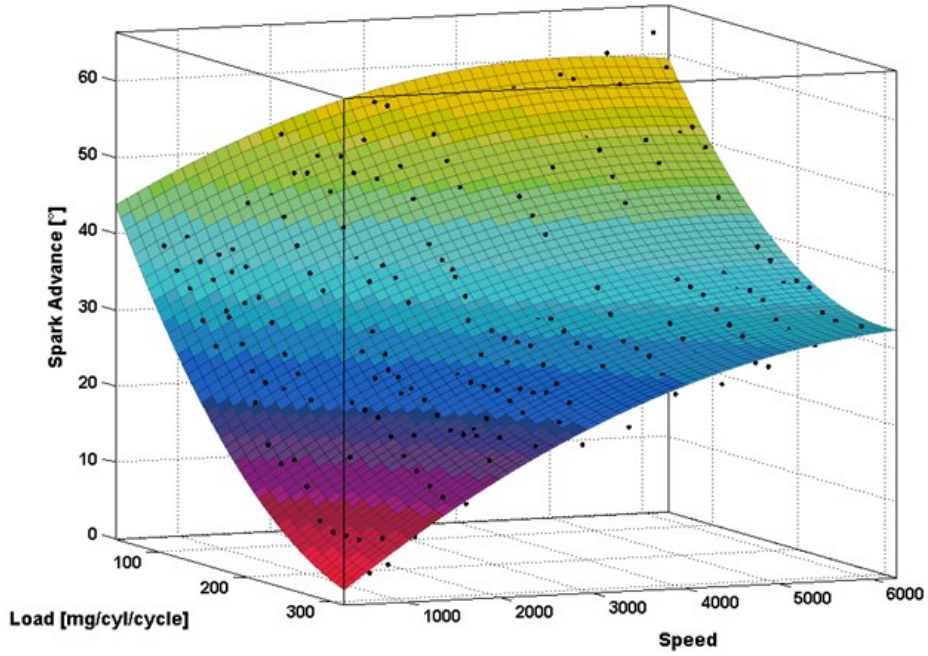

Figure 6-5 Optimised spark timing – smoothed map generated using Matlab curve fit toolbox [2]

During the smoothing procedure, in the spark advance calibration map there were instances where the spark timing has been advanced beyond the experimental optimised value.

Figure 6-6 shows the net change in spark timing after the smoothing process. Negative values indicate that after the smoothing process the spark timing had been retarded from its earlier value, while positive values indicate that spark timing had been advanced.

During testing it was found that the smoothing did not have any detrimental effect on the engine and it was concluded that the optimisation process was somewhat conservative, with some additional variation attributed to measurement imprecision [2]. However, there were a few points on the spark timing map where the spark timing required minor adjustment to avoid knock.

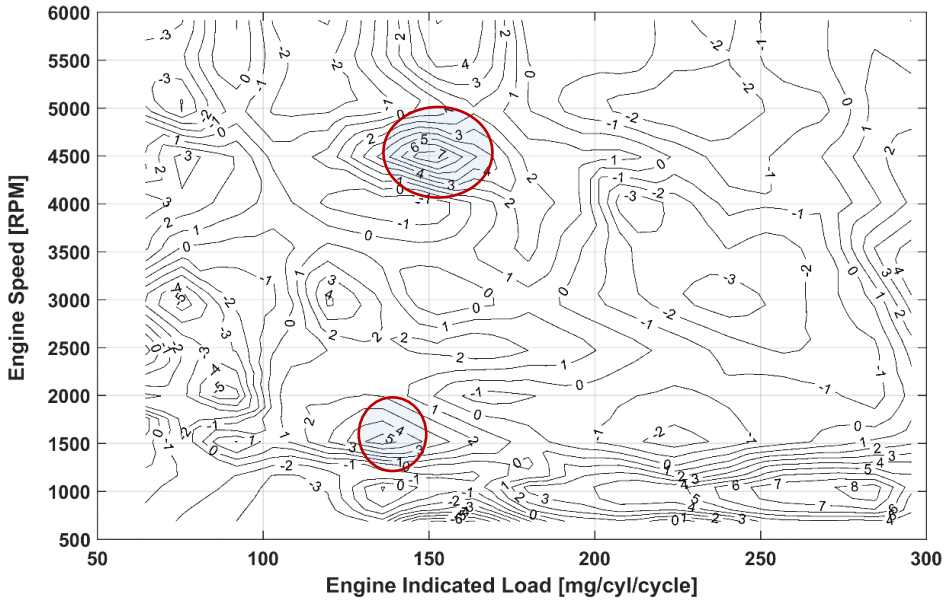

Figure 6-6 Net change in spark timing after the smoothing process. Negative values indicate that after the smoothing process the spark timing had been retarded from its earlier value, while positive values indicate that spark timing had been advanced from its earlier value. Circled areas indicate areas on the map where significant spark advance has occurred in the smoothing process, this however did not have any detrimental effect.

The BSFC comparison between the smoothed versus non-smoothed spark advance maps is shown in Figure 6-7. It was seen that the smoothed BSFC is mostly better up to 4500rpm after which the non-smoothed BSFC is better. From engine speed of 3000rpm to 4000rpm the improvement in BSFC of the smoothed spark advance map is of the order of 4% over the non-smoothed spark advance map.

Figure 6-8 shows the spark advance achieved in comparison to the production EMS at WOT across engine speed. An average of 5° spark advance was achieved at WOT across 1500 to 5500rpm. The results are in line with that predicted by Stone [104] at section 6.3.

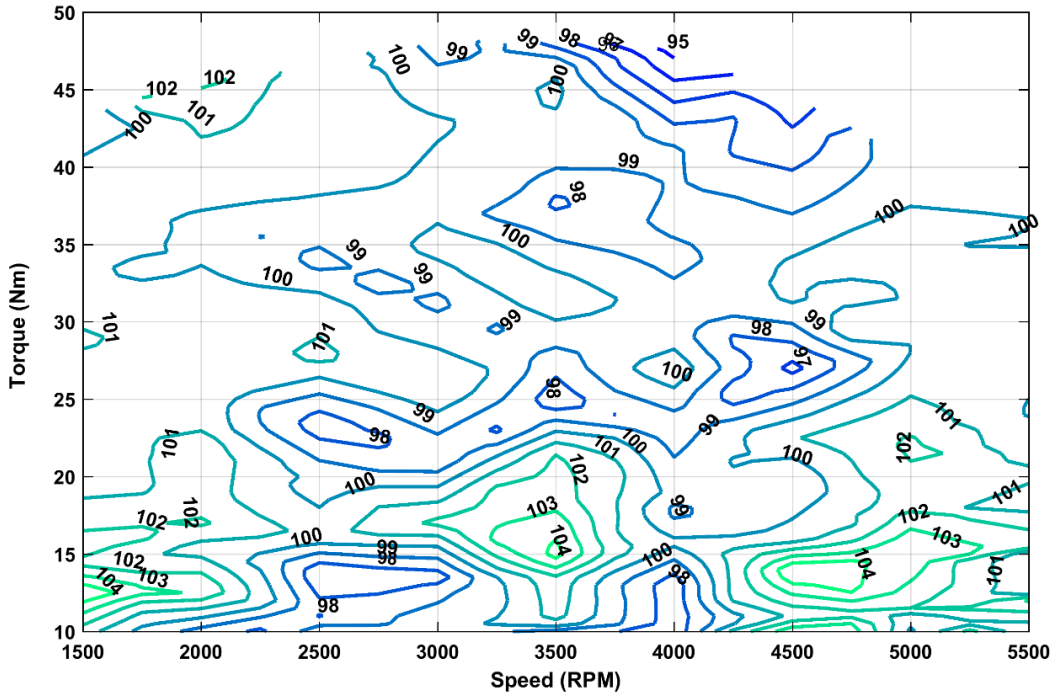

Figure 6-7 Smoothed spark timing map BSFC versus non-smoothed spark timing map BSFC. Numbers above 100 indicate smoothed spark timing BSFC is worse than non-smoothed spark timing map BSFC.

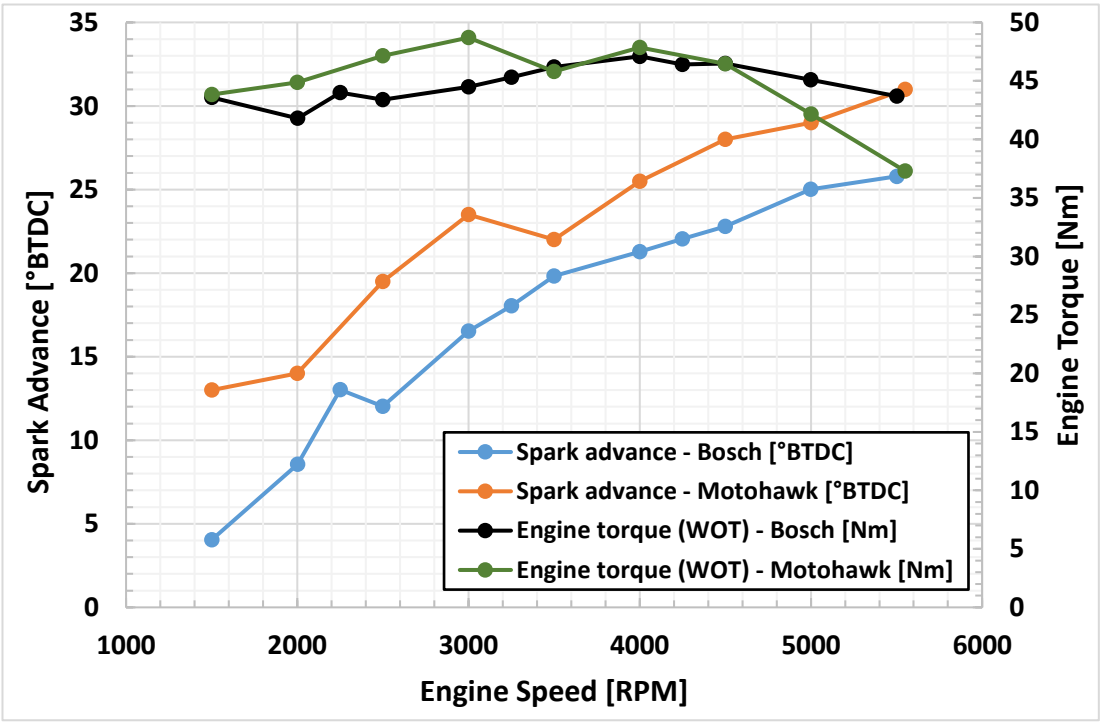

Figure 6-8 Calibration of spark advance using RON 95 reference fuel. An average of 5° spark advance was achieved at WOT across 1500 to 5500rpm

6.5 Introduction of Electric Water Pump

Conventional mechanical coolant pumps are engine driven (belt/gear) and hence their rpm is governed by the engine rpm. Coolant pumps need to ensure sufficient cooling even at low engine rpm with high engine loads and at elevated ambient temperatures, and so for normal operation such as city driving or slow cruising, they are inevitably oversized.

The use of an electric coolant pump with appropriate thermal management of the combustion engine has measurable advantages. Demand driven cooling, which is independent of engine speed, particularly in the cold-start phase reduces impeller energy consumption and leads to corresponding improvement in fuel economy. The Lotus bespoke RE engine also employed a EWP for similar reasons [3].

Another major benefit of an electric coolant pump is its ability to keep running after the engine has shut down to prevent the heat soak problems to which some engines are prone. Further the lack of dependence on a mechanical drive also results in considerable flexibility in component packaging within the engine compartment [89].

As one of the primary objectives of this research was to eventually run the APU in a combined engine–generator coolant loop to reduce parasitic losses and measure improvement in overall efficiency, the mechanical engine driven water pump had to be removed and replaced with an EWP.

The production engine had an integrated gear driven oil and water pump housing, so it was not possible to remove the mechanical coolant pump in its entirety. For the purpose of the experimental analysis, the impellor blades were removed leaving the shaft as it was common with the oil pump. Figure 6-9 shows the mechanical pump impeller before and after the blades were removed [2]

Figure 6-9 Mechanical coolant pump before and after removal of impeller blades [2]

The mechanical coolant pump was rated at 50litres/minute @ 0.8bar back pressure at engine speed of 5500rpm [105]. Based on the pump characteristics, the Pierberg CWA100-3 was selected to replace the mechanical pump by TMETC. The technical specifications of the selected Pierberg CWA100-3 EWP are given in Table 6-1 below.

Table 6-1 Pierberg CWA100-3 technical specifications

Nominal voltage	13.5V
Voltage range with full	12.5V to 16.5V
Ambient temperature	-40°C to 125°C
Coolant temperature	-40°C to 125°C
Speed range	84rpm to 7000rpm
Hydraulic duty point	30 l/min

Figure 6-10 shows the EWP cooling circuit and associated instrumentation. Four additional thermocouples were installed on the engine to measure the cylinder valve bridge and liner temperatures.

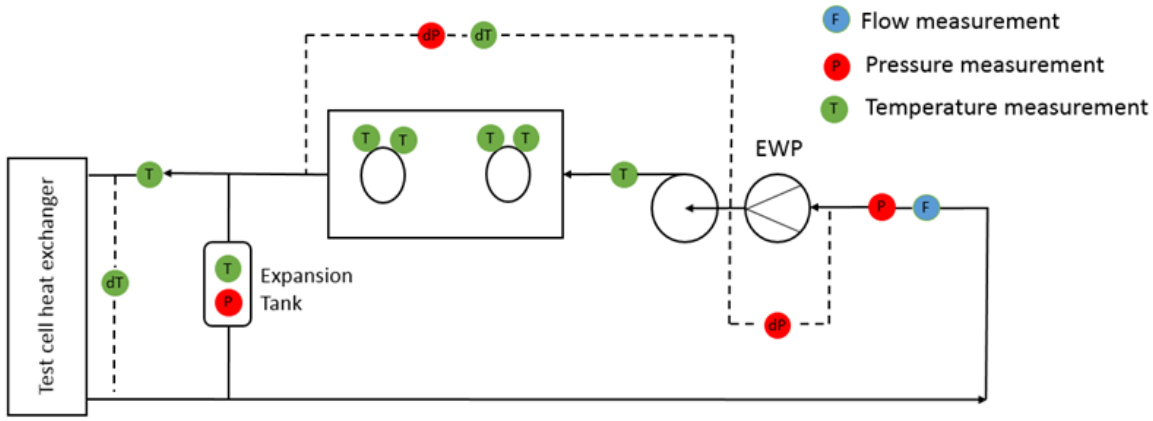

Figure 6-10 Engine cooling circuit with EWP and additional instrumentation. The outlet of the EWP is into the inlet of the non-functional mechanical water pump

6.6 Pump mapping and control development

The EWP was initially characterised alongside the functioning mechanical water pump in a separate coolant circuit, this allowed calibration of the EWP duty cycle without compromising or potentially damaging the engine, had the EWP been integrated in the engine cooling circuit from the beginning.

The initial plan was to mirror the output of the mechanical water pump, which had a linear relationship to engine speed. To achieve this, the engine was run and changes made to the pump duty map in Motohawk to match the coolant flow across the engine speed range. The calibration table was based on engine speed and engine load.

The mechanical and electrical pump flow rates are shown in Figure 6-11. The electric pump shows slightly higher flow rate at high engine speeds, this was due to the fidelity of the control map. Further calibration would improve this control.

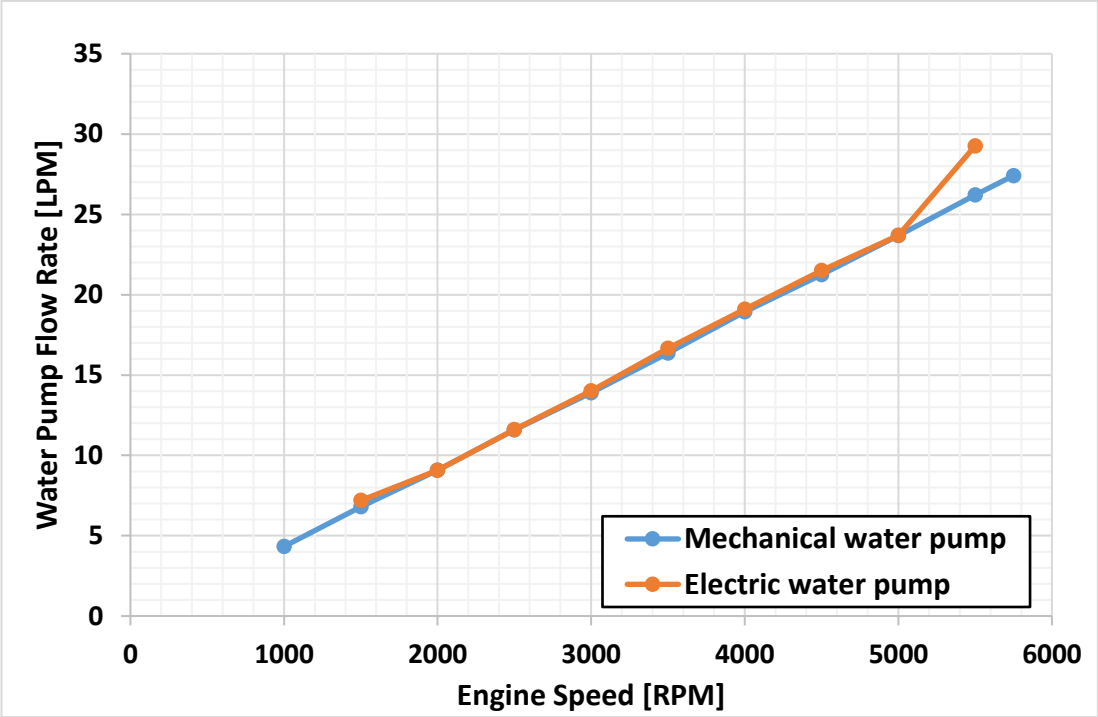

Figure 6-11 Comparison of Mechanical and EWP flow rate post calibration

6.7 Engine performance / BSFC Post Modifications

After the introduction of the new EMS, electronic throttle, bespoke manifolds, spark optimisation and EWP, the BSFC map of the engine was generated to quantify the effect of the changes on BSFC vis-à-vis the production engine. The BSFC map is at Figure 6-12. Best BSFC of 245g/kWh was achieved at 2500rpm at WOT.

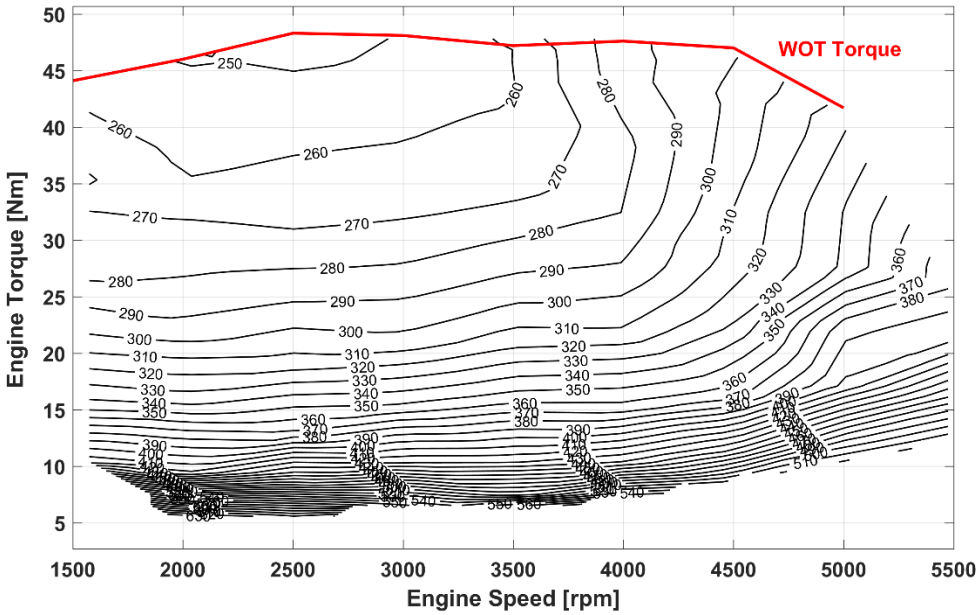

Figure 6-12 Engine BSFC map with bespoke ECU, electronic throttle, bespoke manifolds and EWP

The BSFC comparison between the baseline engine and optimised engine is shown at Figure 6-13. The BSFC improved or remained the same up to 4500rpm, after which it increases.

This is expected as because of the intake manifold tuning and reduction in manifold diameter which has resulted in decrease in engine torque as well as increase in enrichment of the air fuel mixture beyond 4500rpm to maintain exhaust gas temperature within limits.

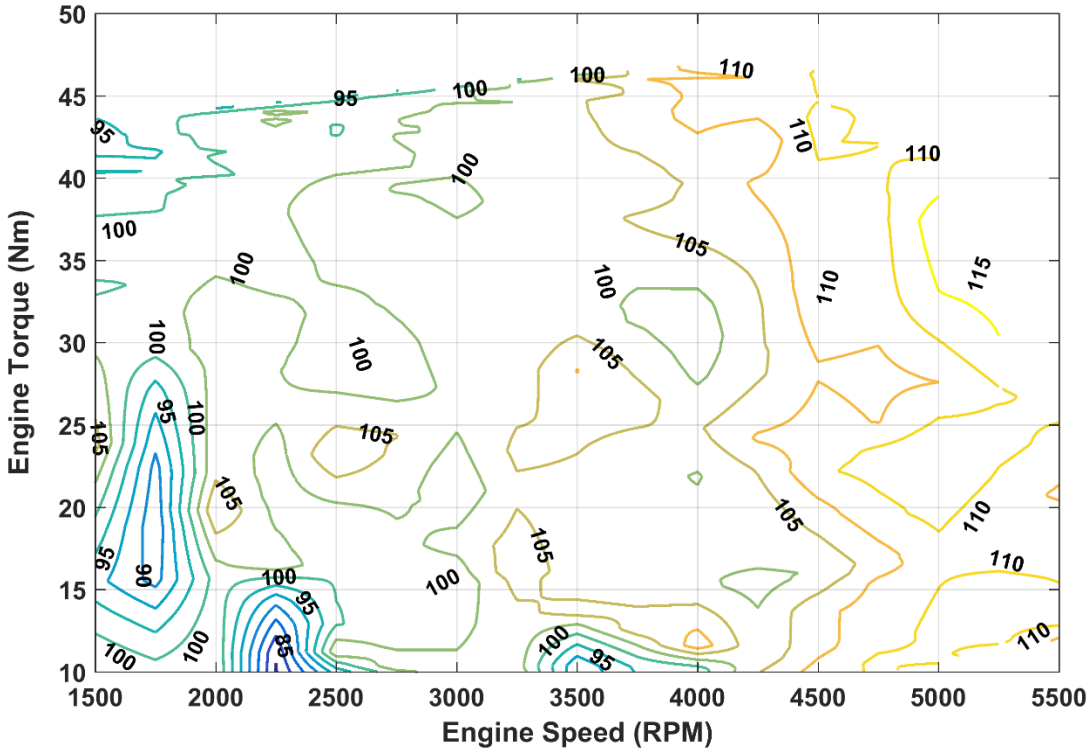

Figure 6-13 Comparison of BSFC maps of RE optimised engine and baseline engine. Numbers less than 100 indicate optimised engine BSFC is better than baseline engine BSFC. Increased BSFC post 4500rpm was expected because of the intake manifold tuning and reduction in manifold diameter which has resulted in decrease in engine torque as well as increase in enrichment of the air fuel mixture beyond 4500rpm to maintain exhaust gas temperature within limits

6.8 Conclusion

The chapter covered the further engine calibration to improve the engine performance as well as gain improvements in the engine BSFC.

Extensive testing was undertaken to reduce exhaust lambda enrichment and the engine could be run at lambda 1 up to 3750rpm at WOT, from the earlier 3000rpm while maintaining satisfactory exhaust temperatures.

Spark timing optimisation was carried out to achieve maximum best torque while staying within the knock limit. Based on the test results the spark timing map was smoothed to ensure smoother transition from one operating point to the other.

The next section discussed the introduction of the electric water pump and its control development. Merits of the electric water pump and its role in an APU application were discussed. The EWP would play a crucial role during subsequent integration of the engine and generator coolant loops.

Subsequent to the modifications/calibration, the engine BSFC map testing was undertaken and a best BSFC of 245g/kWh was achieved at 2500rpm at WOT.

Lastly the performance of the engine post calibration/modifications is compared with the baseline production engine. The BSFC improved or remained the same up to 4500rpm, after which it increased. This was expected as because of the intake/exhaust manifold tuning and reduction in manifold diameter resulted in decrease in engine torque as well as increase in enrichment of the air fuel mixture beyond 4500rpm to maintain exhaust gas temperature within limits.

The work presented in this chapter formed part of the technical paper titled ‘Development of a Low-Cost Production Automotive Engine for Range Extender Application for Electric Vehicles’ that was presented at the SAE World Congress, Detroit in April 2016. Paper reference is 10.4271/2016-01-1055.

CHAPTER - 7
Thermal Survey of Base Engine

This chapter presents the thermal survey carried out on the production engine to quantify the effect change in oil and coolant temperature had on engine BSFC. The engine BSFC increased by an average of less than 5% by reducing the oil and coolant temperature set point from 90°C to 60°C at full load across the operating regime.

7.1 Introduction

A key requirement of the APU is to generate maximum electrical power with minimum fuel consumption. Therefore, it is important that the engine and the generator are operated at the maximum efficiency in addition to optimising the complete system.

The operating temperature plays an important role on both engine and motor/generator efficiency. However, they do have conflicting requirements to achieve their own optimal efficiency.

This chapter covers the experimental work undertaken to determine the effect of change in engine coolant and oil temperature on engine performance. This thermal survey was carried out on the baseline production engine. Since the optimisation carried out in this research on the production engine did not make any design changes to the engine, the results of this survey could be extended to the engine with the modified manifolds, EWP and bespoke EMS.

7.2 Lubrication / Friction Considerations in an ICE

Lubrication regimes encountered in an engine range from high friction boundary lubricated contacts where the coefficient of friction may be as high as 0.2 to low friction hydrodynamic contacts where the coefficient of friction could be as low as 0.001. The Stribek diagram [106-108], see Figure 7-1, is used to relate the various regimes of lubrication to a duty parameter which is defined as the product of the absolute viscosity times the sliding speed divided by the unit load, see equation (6).

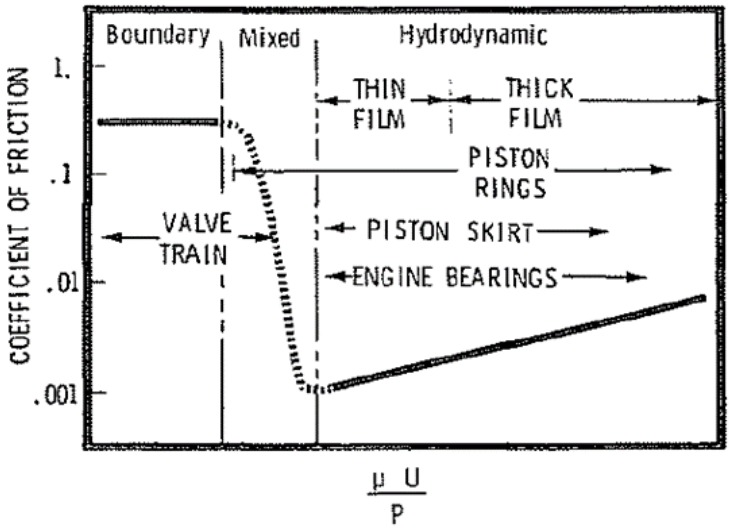

Figure 7-1 Stribek diagram showing various regimes of boundary, mixed and hydrodynamic lubrication versus duty parameter as defined in equation 6 below [107]

$$Duty\ parameter = \frac{\mu U}{P} \tag{6}$$

Where,

μ is the absolute viscosity,

U is the sliding speed,

P is the unit load.

Once the duty parameter for a component is computed, an estimate of the lubrication regime can be made. For high unit loads and low sliding speeds, boundary lubrication is indicated. In this regime, the coefficient of friction is independent of the duty parameter. For contacts operating at higher speeds, it is possible to separate the two surfaces with a complete hydrodynamic oil film and the coefficient of friction is then proportional to the duty parameter. This is referred to as hydrodynamic lubrication. As loads are increased on a hydrodynamic contact, film separating the two surfaces becomes thinner. Under this condition, it is possible for the asperities on one surface to contact asperities on the other surface. This situation is referred to as mixed lubrication. In this case the load is supported in part by the fluid film pressures and in

part by the interaction of the solid asperities. It also indicates that there is a lower limit to the reduction of the coefficient of friction possible by reducing the speed or the oil viscosity [106, 107].

7.2.1 Boundary Lubrication

In boundary lubrication regime the friction force is proportional to the normal load and this is frequently referred to as Coulomb friction [107], see equation (7)

$$F = fW \tag{7}$$

Where,

F is the friction force,

f is the coefficient of friction,

W is the normal load.

While the coefficient of friction is independent of the bulk lubricant viscosity, the sliding speed and the unit load, it can be influenced by the material combination and lubricant additives.

7.2.2 Hydrodynamic Lubrication

In hydrodynamic lubrication, relative motion between the two surfaces generates a fluid film pressure which separates the surfaces. Friction in hydrodynamically lubricated contacts, equation (8), depends on geometry, speed and lubricant viscosity.

$$F = \frac{\mu AU}{h} \tag{8}$$

Where,

μ is the absolute viscosity,

A is the area,

U is the velocity,

h is the film thickness.

From equation (8) it is evident that friction force is inversely proportional to the film thickness, decreasing film thickness for a given geometry increases the friction force. However thinner films develop higher fluid film pressures and thus carry higher loads. The net result is that as the applied load is increased, the coefficient of friction decreases as shown in Figure 7-1 in the hydrodynamic portion of the Stribek diagram. As per McGeehan [106], studies have shown that at zero gas pressure (low loads) the ring is easily twisted by the frictional forces to give an unfavourable hydrodynamic wedge. It is possible, therefore, that with increased gas pressure the onset of mixed lubrication is reduced due to the more favourable attitude of the ring in the groove. Engine journal bearings also fall under this category of lubrication.

7.2.3 Mixed Lubrication

As the hydrodynamic film thickness reduces, asperities on either surface begin to come in contact and the region of mixed lubrication is encountered. This regime is a combination of hydrodynamic and boundary lubrication. Unit loads on the contact can be large enough to cause localised elastic deformation which defines an elasto-hydrodynamic lubrication mode. Complex interactions between the surfaces and the lubricants makes analysis of this phenomenon very difficult, however it is known that surface texture controls the transition from the hydrodynamic to the mixed regime [107].

7.2.4 Operating Modes of Major Engine Components

The critical elements in the valve train including the cam-lifter interface and rocker-arm pivots, operate in the boundary to mixed regime because high loads are encountered at low sliding speed. Piston rings operate over the range of thick film hydrodynamic to mixed lubrication as the gas load and velocity of the piston ring vary extensively over one engine cycle. At top dead centre (TDC) where the gas forces are maximum the velocity of the piston ring is zero and contact occurs between the piston ring and the cylinder wall. Contact may be no more than local contact of asperities on the ring face while the bulk of the periphery of the ring is separated from the liner by the oil's squeeze film.

Hydrodynamic lubrication theory indicates that an oil film generated by the wedge action is dependent on the ring velocity and therefore the oil film thickness should be zero at both TDC and BDC. However, contact with the cylinder during the zero or low velocity periods near the ends of the stroke can occur only if the ring is able to penetrate the film generated by the wedge action during the high velocity part of the stroke. The oil film thickness at the ends of the stroke, therefore, depends upon the rate of diminution of the wedge-generated oil film under the influence of radial squeezing action of the ring [106]. This oil film is called squeeze film and its thickness is the smallest in the cycle. At mid-stroke, piston velocity is maximum, gas forces have reduced and a complete hydrodynamic oil film separates the piston ring from the cylinder wall.

The piston skirt because of its large contact area and low loading, is primarily a thin film hydrodynamic contact. Engine bearings operate in a hydrodynamic mode except for brief periods during starting and stopping.

7.3 Mean Effective Pressure (MEP)

Mean Effective Pressure (MEP) is commonly used to describe the engine output and is a parameter used for comparing performance of engines with different displacement [99, 104]. Figure 7-2 shows a plot of cylinder pressure versus cylinder volume (P-V diagram) of the base engine at WOT, 4000rpm.

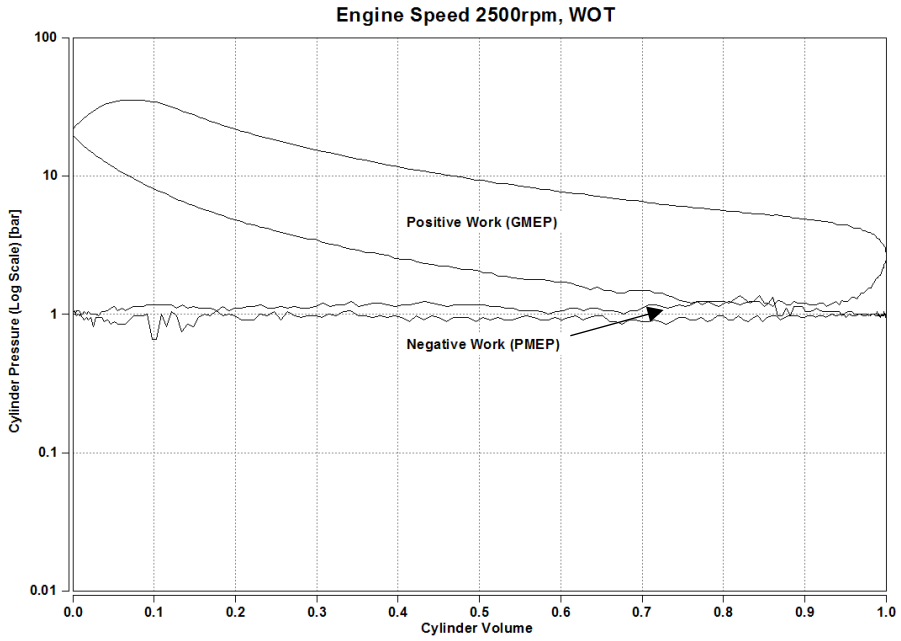

Figure 7-2 Actual time logged P-V diagram of base engine at engine speed 2500rpm, WOT from CAS

Gross Mean Effective Pressure (GMEP) is the positive work delivered to the piston during the compression and expansion stroke. The Pumping Mean Effective Pressure (PMEP) is the work required by the piston during the intake and exhaust strokes. PMEP is the negative work required by the piston to draw the air charge into the cylinder and push the exhaust from the engine. The Indicated Mean Effective Pressure (IMEP) is the net work extracted by the piston and is the difference between GMEP and PMEP.

Brake Mean Effective Pressure (BMEP) is the work available at the engine and can be calculated as:

$$BMEP = \frac{Tn_c}{V_d} 2\pi \quad (9)$$

Where,

T is the torque,

n_c is the number of revolutions per power cycle (i.e. for 4-stroke engine n_c =2),

V_d is the engine displacement.

Friction Mean Effective Pressure (FMEP) is the work lost due to mechanical friction and parasitic losses. Mechanical friction under hydrodynamic, boundary and mixed lubrication modes in the engine has been discussed above in Section 7.2.4. Parasitic losses are from driving engine ancillaries such as the oil pump water pump etc. The friction work or FMEP was expected to increase as the engine coolant and oil temperature set points were lowered as the viscosity of the oil increases with lower temperature, see Section 7.4. This would impact the BMEP of the engine and in turn the BSFC. Mechanical efficiency, η_m is a measure of how efficiently work available at the piston is transferred to the crankshaft, see equation (10).

$$Mechanical\ efficiency, \eta_m = \frac{BMEP}{IMEP} \quad (10)$$

7.4 Engine Oil 15W-40

The OEM recommended engine oil for the base engine for ambient temperature from -10°C and above was 15W – 40 API SJ [105]. The kinematic viscosity of the oil at 40°C is 105.10 mm^2/s and drops to 13.648 mm^2/s at 100°C [109], see Figure 7-3. Extrapolation at 110°C would give a kinematic viscosity of 5.59 mm^2/s.

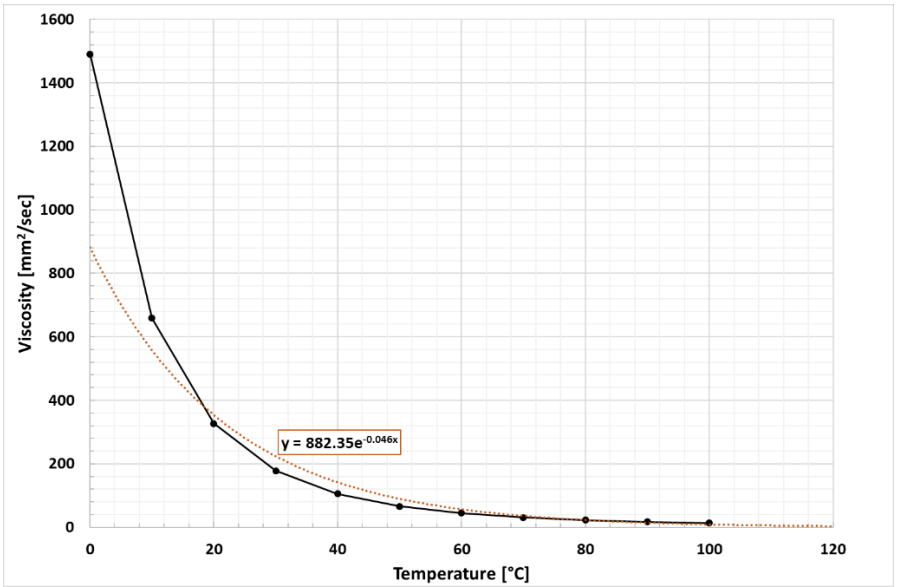

Figure 7-3 Variation of kinematic viscosity of 15W – 40 engine oil with temperature. An exponential trendline added to extrapolate viscosity at 110°C [109]

7.5 Thermal Survey of Baseline Production Engine

As it was planned to eventually run the APU in a combined engine – generator coolant loop to reduce parasitic losses and improve overall efficiency, this involved trying to meet the conflicting requirement of running the engine at a higher temperature and the generator as cool as possible.

The positive effect of higher coolant operating temperatures on fuel economy and emissions is well documented [84-86]. With the engine cooling system designed to cope with the peak-heat rejection rate at WOT conditions, based on a coolant temperature set point, the engine and its cooling systems operate at less than ideal conditions at part-load, such as city driving or slow cruising, leading to higher fuel consumption and emissions output. Increasing the operating temperature set point has been the most popular route to achieve improvement in fuel economy and emissions [86]. At higher coolant temperatures: -

(a) There is enhanced combustion process along the cylinder walls.

(b) A reduced heat flow to the cooling water.

(c) Optimised combustion chamber temperatures reducing piston /cylinder friction.

As per the production engine manual, the engine ran best when coolant was at 93°C [105]. At this temperature, the combustion chamber was hot enough to completely vapourise the fuel providing better combustion and reducing emissions. Secondly the oil used to lubricate the engine had the right viscosity, so the engine parts move more freely, and the engine wasted less power moving its own components around. As a result, there was reduction in wear and tear of engine parts.

The generator and the power electronics delivers better efficiency at lower temperature compared to the ICE [51, 52].

Therefore, preliminary experimental analysis was carried out to see the effect of variation of coolant and oil temperatures on the BSFC of the base engine. For this experimental work, the production baseline engine with the Bosch ECU (test bed version) was used.

The independent variables selected for the thermal survey comprised of: -

(a) Three engine outlet coolant temperature set points.

(b) Three engine oil gallery temperature set points.

(c) Four engine speeds.

(d) Three engine load settings.

The target speed/torque set points and target fluid set points specified are at Figure 7-4 and Figure 7-5 below respectively. The complete matrix of 81 test points is placed at Appendix A.

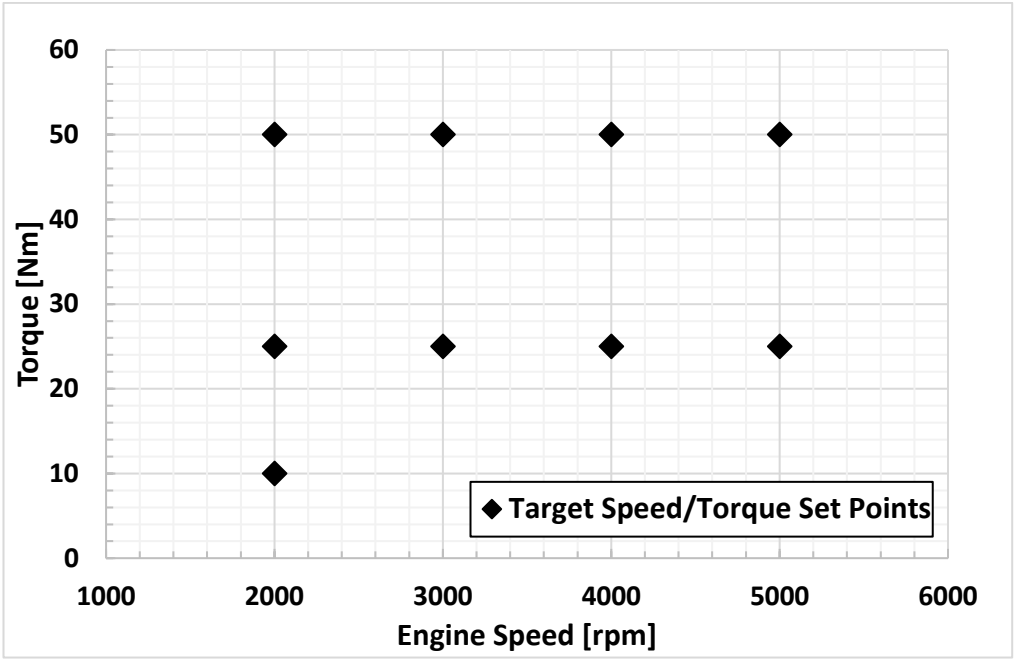

Figure 7-4 Target speed / torque set points for thermal survey of base engine

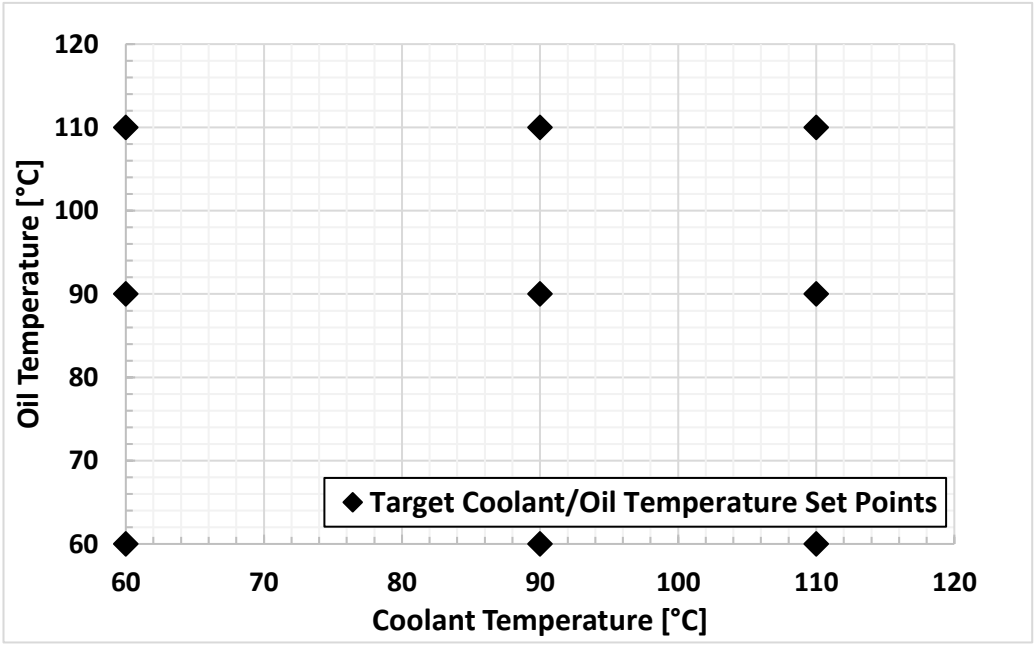

Figure 7-5 Target coolant / oil temperature set points for thermal survey of base engine

A fully open thermostat was installed on the engine to ensure that 100% coolant was flowing to the coolant heat exchanger. Schematic of the engine coolant and oil

circuits are below at Figure 7-6 and Figure 7-7 respectively. An adaptor was fitted on the oil circuit to allow connection to the test bed oil cooling system.

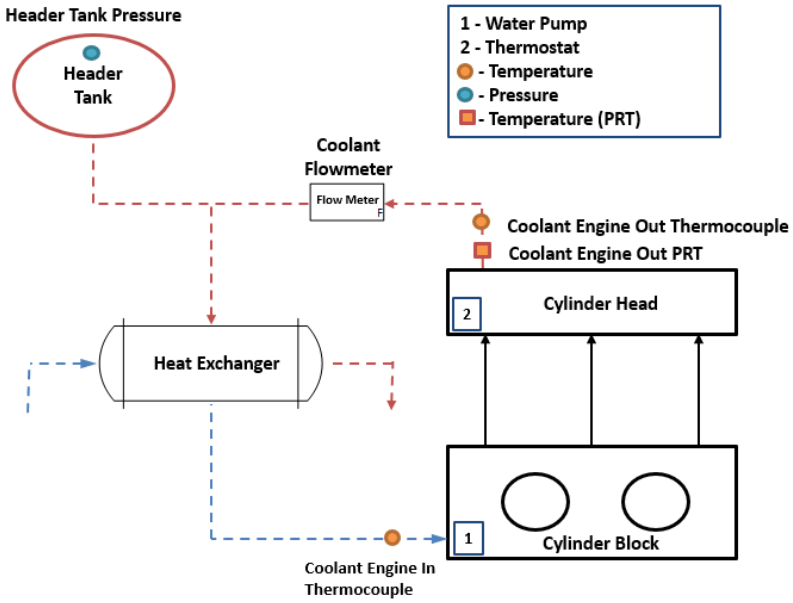

Figure 7-6 Engine coolant circuit in the test cell. Engine out temperature used as setpoint during thermal survey

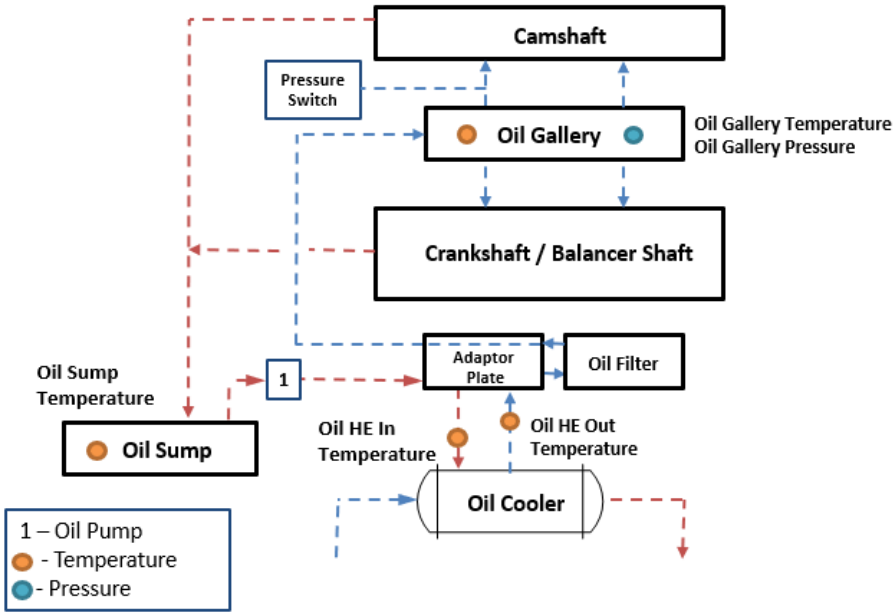

Figure 7-7 Engine oil circuit in the test cell. Oil gallery temperature used as setpoint during thermal survey

Thermal survey was successfully carried out for 54 out of the 81 test points. Engine testing could not be undertaken for the following target fluid set points:-

(a) Engine coolant outlet set point 110°C, oil gallery set point 110°C (09 test points).

(b) Engine coolant outlet set point 110°C, oil gallery set point 90°C (09 test points).

(c) Engine coolant outlet set point 110°C, oil gallery set point 60°C (09 test points).

This was because of the following reasons: -

(a) At coolant outlet temperature of 105°C, Hardware Protection (HWP) indicating high coolant temperature operated. This is a hardware protection in the Sierra CP Cadet software. To overcome this, the HWP settings were changed to 127°C.

(b) However, with the revised HWP setting, as the engine out coolant temperature rose to 112°C, the engine malfunction indicating lamp (MIL) came on. As a result, it was not possible to progress testing. The MIL setting is within the closed production Bosch ECU and since low level access was not available at this time, this setting on the ECU could not be altered.

The oil gallery and coolant engine out set points were varied as per the test schedule. Figure 7-8 and Figure 7-9 show the variation of oil gallery temperature and engine coolant out temperature at the various set points at WOT respectively. Some keys observations from the figures below were: -

(a) A coolant set point of 60°C maintains an oil gallery temperature below the set point of 110°C, below 5000rpm.

(b) Above 4000rpm the oil gallery temperature was found to exceed the set point of 60°C for coolant temperature set point conditions of 90°C despite 100 % cooling open for the oil heat exchanger.

(c) Coolant temperature control was very good throughout the test program and within ±2°C of the set point.

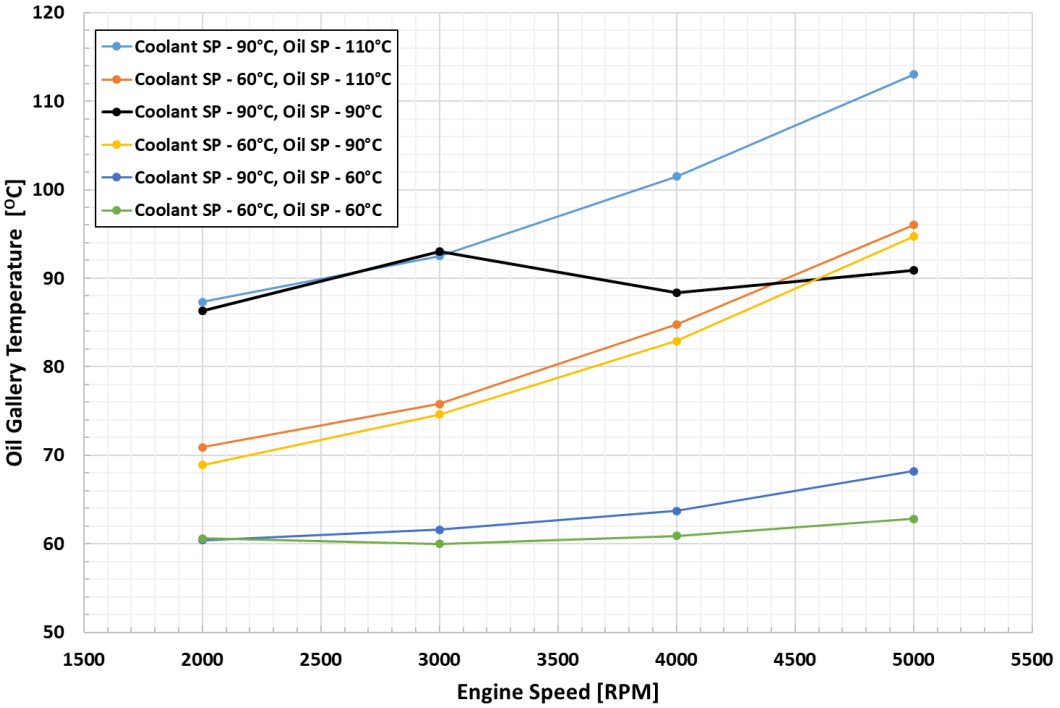

Figure 7-8 Oil gallery temperature variation at various setpoints versus engine speed, WOT

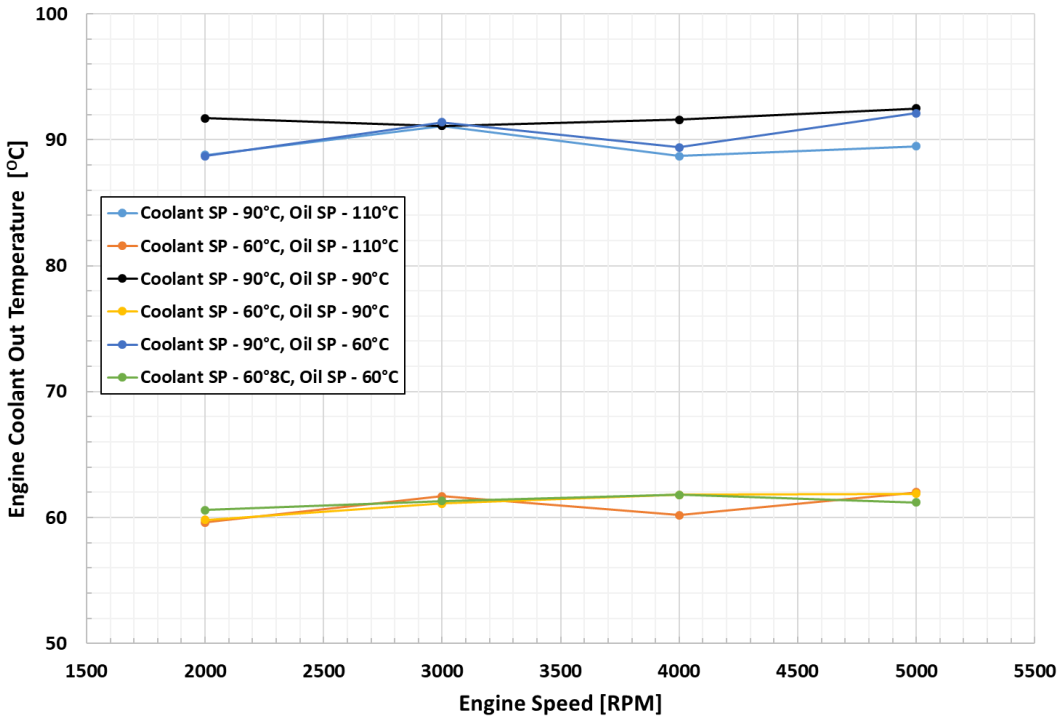

Figure 7-9 Engine coolant temperature variation at various setpoints versus engine speed, WOT

The results of the thermal survey on the BSFC are discussed in the succeeding paragraphs. As expected with decrease in oil and coolant set points, the friction work required showed an increase. Figure 7-10 shows the increase in FMEP when the oil and coolant set points are changed from 90°C to 60°C at full load condition at various engine rpm. Since there were no intermediate oil and coolant set points between 60° and 90°C, the increase in FMEP from 60°C to 90°C appear to be linear. However, it would not be the case had there been more points in between. Figure 7-11 shows the effect on FMEP and mechanical efficiency of the engine at 60°C and 90°C oil and coolant set points across engine rpm at full load.

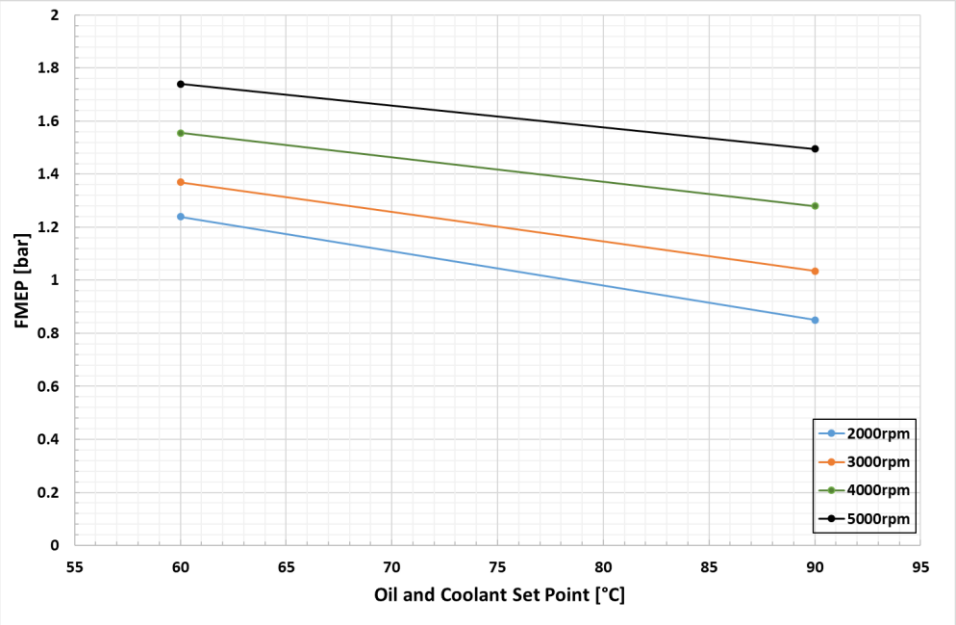

Figure 7-10 Increase in FMEP at WOT with reduction in oil & coolant set points at different engine rpm

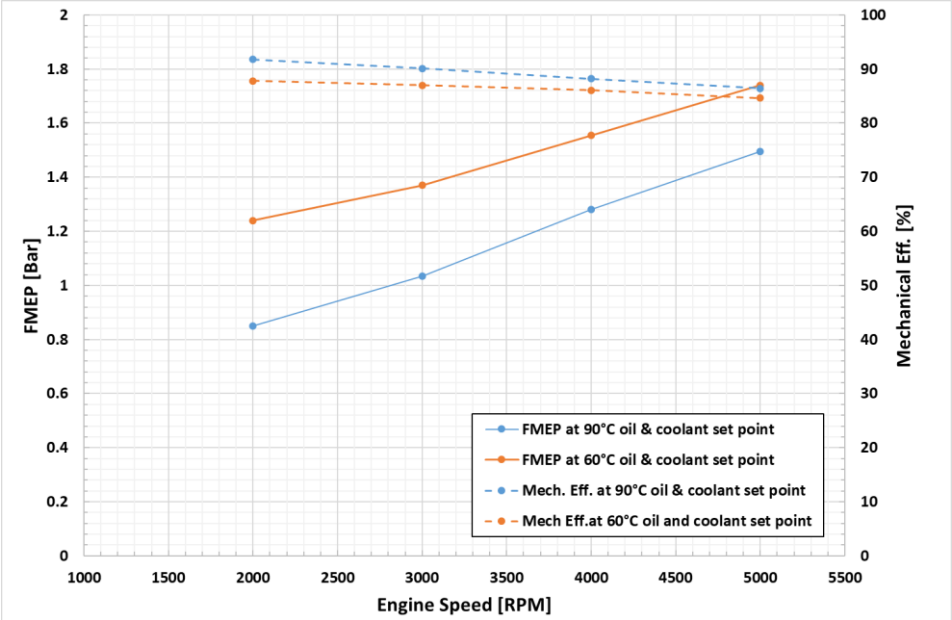

Figure 7-11 Comparison of FMEP & mechanical efficiency at oil and coolant set points of 60° and 90°C across engine rpm, WOT

Figure 7-12 and Figure 7-13 show the BSFC versus engine speed for the two load conditions of 24Nm and full load (WOT).

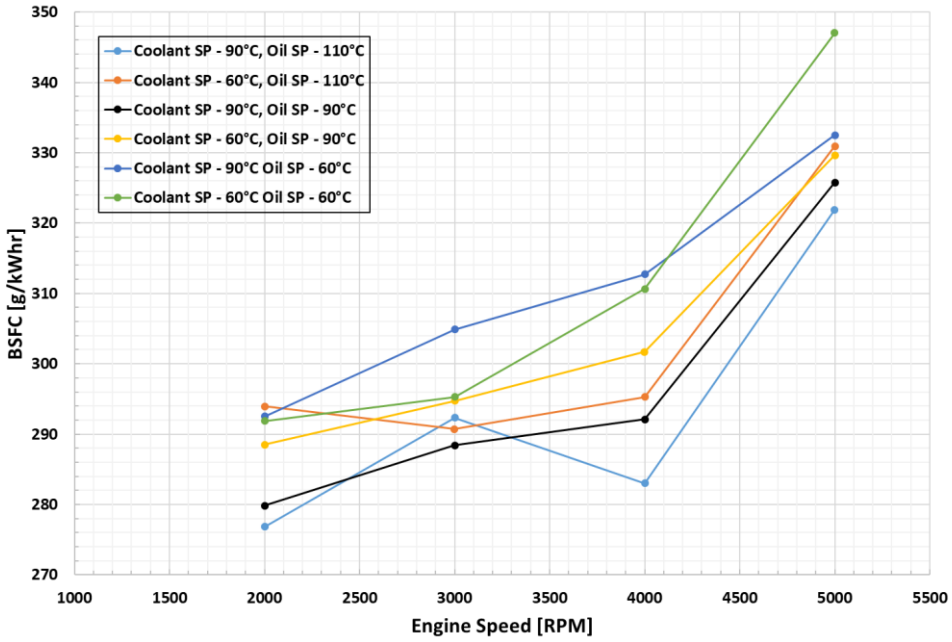

Figure 7-12 BSFC versus engine rpm at varying engine fluid settings at 24Nm torque

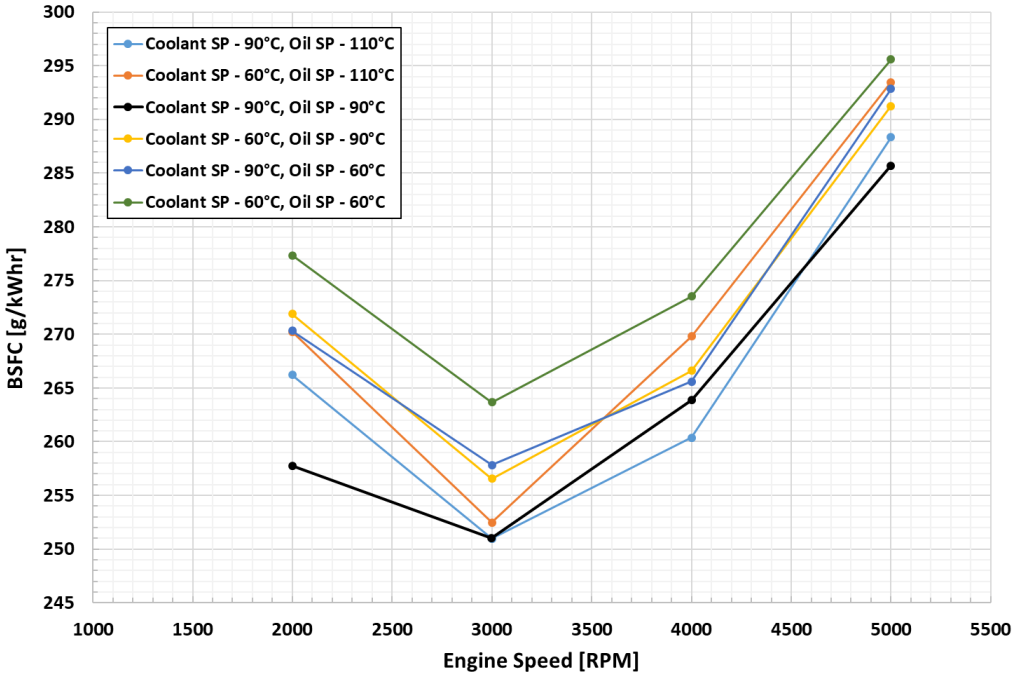

Figure 7-13 BSFC versus engine rpm at varying engine fluid settings at full load (WOT)

Figure 7-13 clearly illustrates that at full load the minimum BSFC is at 3000rpm for various coolant and oil set points. At this engine rpm as the coolant temperature is lowered there is an increase in BSFC. A similar trend is seen at all other engine rpms as well which is expected as brought out earlier in the report.

Comparison of BSFC at WOT for conditions oil and coolant at 90°C versus coolant at 90°C and oil at 110°C merits attention. At 3000rpm increasing the oil temperature set point to 110°C does not affect the BSFC as the oil temperature does not exceed 92.5° and therefore the condition is effectively the same as for the oil temperature set point at 90°C. Likewise at 2000rpm, irrespective of the oil temperature set point of 90°C or 110°C, the oil temperature recorded is 86.3°C and 87.3°C (for coolant set point of 90°C in both cases) and therefore the difference in BSFC observed could not be explained.

At higher rpm of 4000 marginal decrease in BSFC is seen with increase in oil temperature from 90°C to 110°C, which then increases at 5000rpm. This could be attributed to the fact that as the oil gallery temperature set point is increased it also affects the oil sump temperature. At 4000rpm the oil sump temperature at the oil gallery set point of 110°C is higher by 9°C as compared to 90°C set point. As a result, the oil viscosity decreases which reduces the coefficient of friction, see Figure 7-1, and results in lower friction losses. However, at 5000rpm, the oil sump temperature is higher by 17°C, which while further lowering the oil viscosity could push the lubrication regime into the mixed regime resulting in increase in the coefficient of friction.

A similar trend at a load condition of 24Nm is not as clear. This could be attributed to fact that as the engine has a cable operated throttle rather than electronic throttle control (ETC), it was not possible to be at exactly 24Nm load condition at all the concerned test points. This would have affected the calculation of BSFC and hence the comparison would not be for exactly similar load conditions.

It is evident from Figure 7-13 that the engine performance is optimal at oil and coolant set points of 90°C. Running the engine at lower coolant temperatures increases the BSFC. When the coolant and oil set points are decreased to 60°C, at 2000rpm, the BSFC increases from 257.74g/kWh to 277.33g/kWh (increase of 7.6%). Likewise, at 5000rpm the BSFC increases from 285.67g/kWh to 295.59g/kWh (increase of 3.47%). When the coolant and oil set points are increased to 90°C and 110°C respectively, at 5000rpm the BSFC increases from 285.67g/kWh to 288.35g/kWh (increase of 0.93%). However, at 4000rpm, the BSFC decreases from 263.85g/kWh to 260.38g/kWh (decrease of 1.31%).

Based on the above findings, if the BSFC is compared at the oil and coolant set points of 90°C versus 60°C, the BSFC plot clearly brings out the increase in BSFC with reducing temperature, see Figure 7-14, which is an excerpt from Figure 7-13 above. The engine BSFC increased by an average of less than 5% by reducing the oil and coolant temperature set point from 90°C to 60°C at full load across the operating regime.

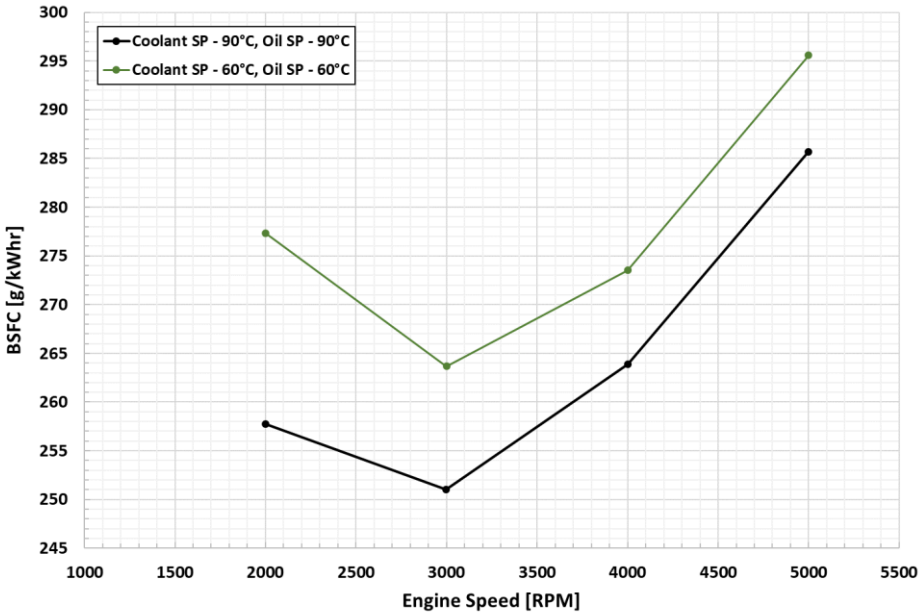

Figure 7-14 Comparison of BSFC at WOT with oil/coolant set point at 90°C versus 60°C. Minimum BSFC seen at 3000rpm

7.6 Conclusion

The conflicting requirements of running the engine at a high temperature (~90°C) and the generator to run as cold as possible (~50°C) has consequences on vehicle system integration such as the need to use separate coolant loops, radiators, pumps etc. Employing a common cooling loop can reduce parasitic loads and simplify vehicle integration but requires operating the engine and/or the generator under sub-optimum thermal conditions. Since the eventual aim was to run the engine and the generator in a single loop, it was important to determine how the engine performance deteriorated with drop in oil and coolant temperature.

An exhaustive thermal survey of the production engine was undertaken to quantify the effect of oil and coolant temperature on engine BSFC.

The engine BSFC increased by an average of less than 5% by reducing the oil and coolant temperature set point from 90°C to 60°C at full load across the operating regime.

The work presented in this chapter formed part of technical paper titled 'Thermal Management of a Low-Cost Range Extender for Electric Vehicles' which was presented at the 6th Hybrid and Electric Vehicles Conference (HEVC 2016) in November 2016. Paper reference is 10.1049/cp.2016.0976.

CHAPTER - 8
APU Commissioning and Performance

This chapter presents the integration of engine with the interior permanent magnet machine. Baseline ESFC testing of the APU was carried out under optimal thermal conditions for the engine and electrical machine with separate coolant circuits. Subsequently the performance of the APU was compared under varying thermal conditions and combining the engine and generator coolant circuit.

8.1 Introduction

This chapter presents the integration of engine with the prototype interior permanent magnet machine (IPM) developed by Ashwoods Automotive Ltd. Initially baseline ESFC testing of the APU was carried out under optimal thermal conditions for the engine and electrical machine with separate coolant circuits. Subsequently, exhaustive experimental analysis was undertaken on the APU to determine whether it was possible to combine the ICE, generator and power electronics in a single coolant circuit to accrue the benefits of reduced parasitic losses and simpler vehicle integration whilst maintaining satisfactory performance. The target best ESFC aimed at was <270g/kWh, and the rated ESFC was 290-320g/kWh. Performance of the APU was quantified by varying thermal conditions and combining the engine and generator coolant circuit.

8.2 Specification of Prototype Motor / Generator Unit

A bespoke IPM machine with integrated inverter was developed by Ashwoods Electric Motors in consultation with TMETC for the purpose of this research, see Figure 8-1.

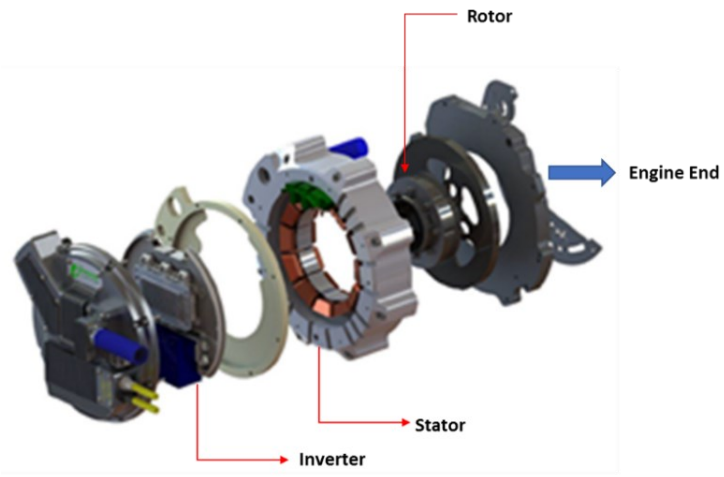

Figure 8-1 IPM machine with integrated inverter developed by Ashwoods Automotive Ltd [110]

This motor/generator (M/G) unit was mounted directly onto the engine crank palm. With such an arrangement the need for extra generator bearings and a compliant coupling between the engine and generator is removed, facilitating a compact APU [50]. The main specifications of the prototype motor/generator (M/G) are given in Table 8-1 below.

Table 8-1 Specifications of the bespoke M/G and inverter [110]

Parameter	Value	Unit
DC voltage	350 ~ 450	V
Peak inverter DC current	100	A
Operating speed	4000-5000	rpm
Cranking torque	80	Nm
Generator/inverter η	>90	%
Continuous power	25	kW

Simulation results versus measured results at the OEM test bed indicated that the generator/inverter efficiency under ideal coolant temperature conditions was of the order of 95% at 4000rpm, see Figure 8-2.

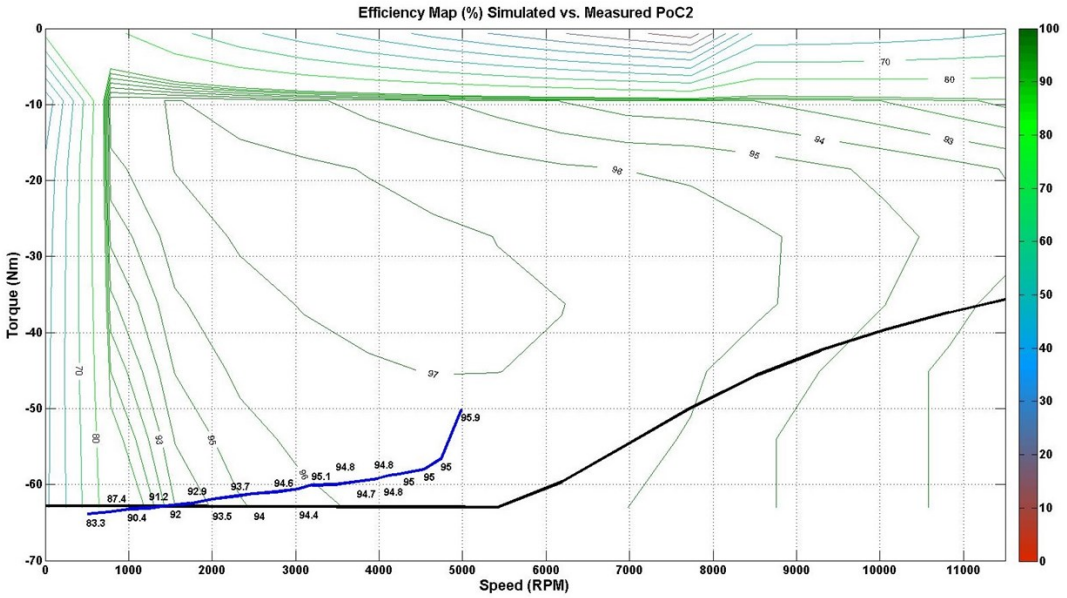

Figure 8-2 Comparison of generating torque efficiency between simulated and measured results on the OEM Ashwoods test bed. Generator/inverter efficiency under ideal coolant temperature conditions was of the order of 95% at 4000rpm

After coupling of the engine with the M/G and inverter unit the total dry weight of the APU was measured to be 81.5kg as against an initial target of 80kg.

8.3 APU test bed configuration

The test bed set up for testing of the APU was similar to that described in Section 3.4. However, the dynamometer was no longer required, and the engine output was absorbed by the generator. The output of the generator was fed to a bi-directional DC power supply. This DC power supply was also used to supply power to the motor for starting of the engine. The test cell set up with the APU is shown in Figure 8-3.

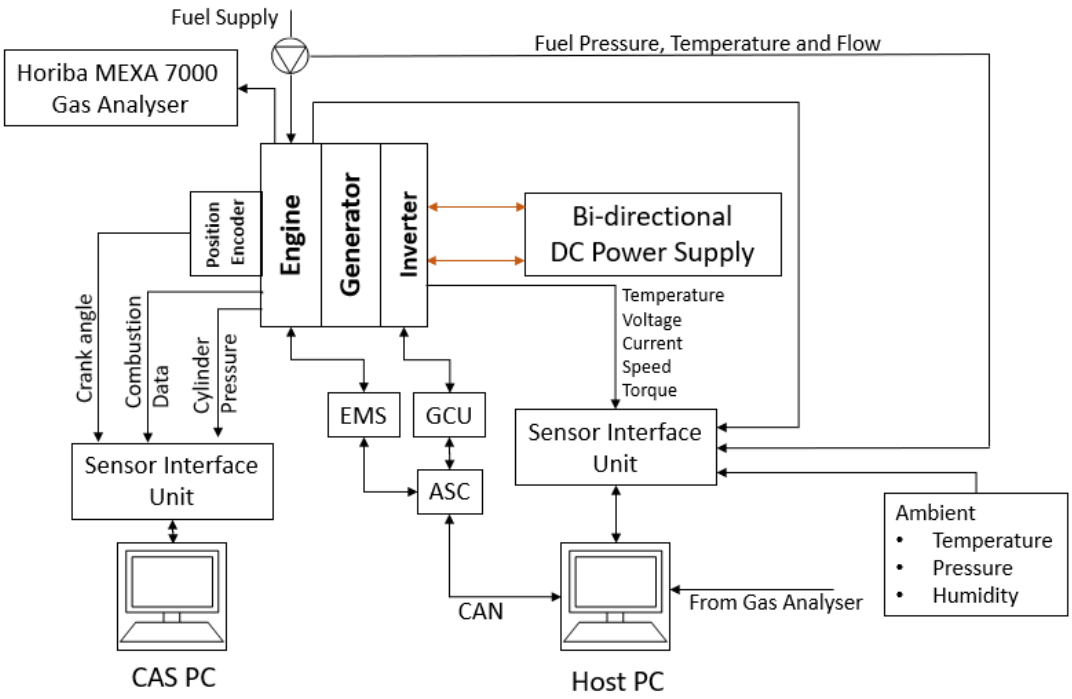

Figure 8-3 Experimental set up for testing of APU

8.4 Benchmarking of APU Thermal Performance

One of the key requirements of an APU is to provide maximum electrical power while minimising fuel consumption. To do so, it is important that the engine and the

generator are operated at their maximum efficiency in addition to optimising the complete system to reduce any parasitic losses in the auxiliary systems. One of the ways to reduce parasitic losses is to combine the engine and generator cooling circuit. This also simplifies vehicle integration by avoiding duplication of cooling circuit components.

The system efficiency is one of the key parameters for an APU since it decides the maximum possible electric power that can be delivered with a given amount of fuel, i.e. the fuel economy. The operating temperature plays an important role on both engine and motor/generator efficiency. However, they have conflicting requirements to achieve their own optimal efficiency.

The positive effect of higher coolant operating temperatures on an engine's fuel economy and emissions is well documented and has been discussed at length in Sections 2.11 and 7.5. The base engine was designed to run with coolant at about 93°C. At this coolant temperature the combustion chamber wall temperature aided fuel vaporisation providing more complete combustion and reducing emissions.

Secondly the oil used to lubricate the engine had a lower viscosity at this temperature so less friction was encountered, consequently reducing parasitic losses and potentially minimising wear and tear of engine components [105]. Drop in coolant temperature set point from 90°C to 60°C resulted in an increase in BSFC across the engine operating range from 2000 to 5000rpm as has been demonstrated at Section 7.5.

On the other hand, the performance of the motor/generator and the power electronics is limited by their peak working temperatures. Low coolant temperature is preferred for better efficiency as opposed to the ICE [51, 52]. Therefore, when designing the combined coolant loop for the APU, a compromise had to be made between adopting a high temperature coolant for the electrical system that is close as

to the production engine set point or reducing the engine operating temperature to improve motor efficiency.

The initial performance characterisation of the APU was carried out using two independent coolant loops as shown at Figure 8-4. This enabled the engine outlet coolant temperature and generator inlet coolant temperature to be controlled independent of each other.

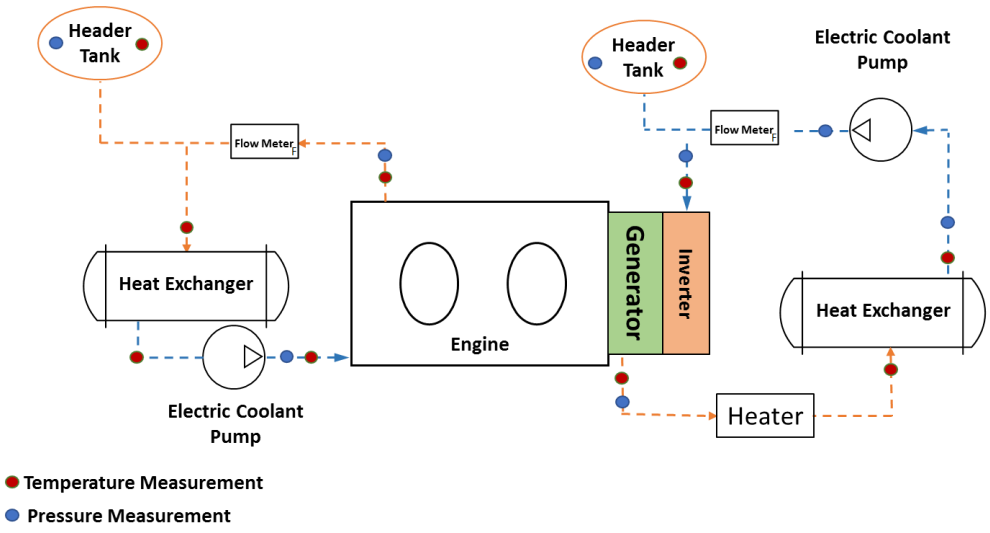

Figure 8-4 Independent coolant loops for engine and generator [110]

The engine's oil gallery temperature was controlled independent to the system coolant circuits as shown in Figure 8-5. Having independent control on the coolant and oil circuits provided greater flexibility while designing the DOE for the thermal performance of the APU.

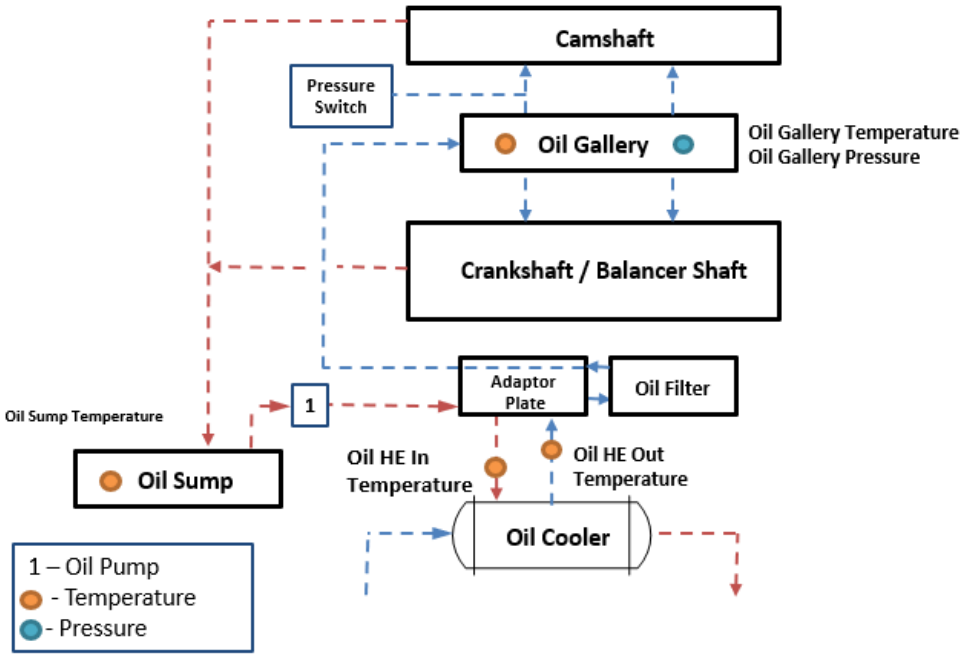

Figure 8-5 Engine oil circuit

The coolant inlet temperature to the generator was set to 35°C. The engine outlet coolant and the oil gallery temperatures were set to 90°C. The EWP on the engine coolant circuit was calibrated to match the erstwhile mechanical pump flow rate, while in the generator coolant circuit it was initially set to 25 litres per minute (LPM) across all speeds. This was done because being a prototype generator its thermal response was not definitively known. The effect of change in coolant flow rate on generator temperatures was not studied at this time.

Testing was undertaken to generate the ESFC map of the APU and the results are shown in Figure 8-6. The APU generated a peak power of 22.78kW at 5100rpm. The full load power curve has been superimposed on the map. A best ESFC of 260g/kWh was measured at 2500rpm, and the ESFC remained below 270g/kWh across 2000 to 3500 rpm at full load.

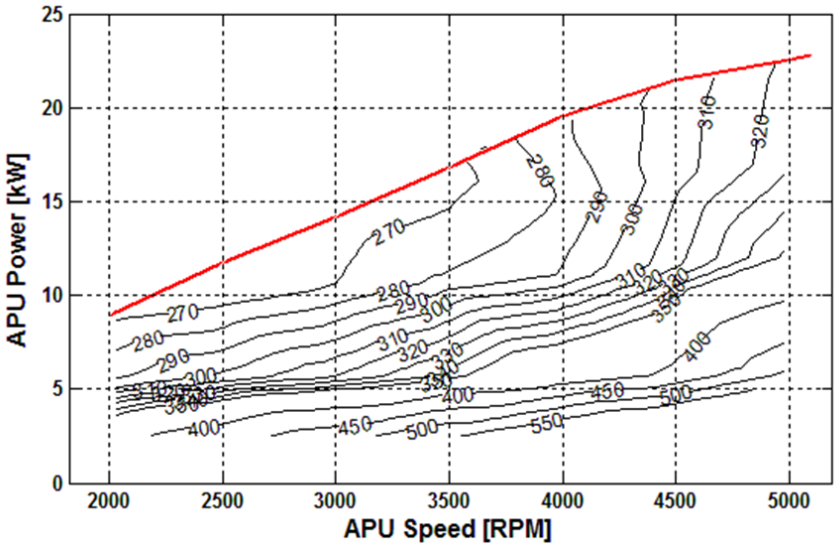

Figure 8-6 ESFC map, generator coolant inlet set point 35°C, engine oil and coolant set point 90°C. A best ESFC of 260g/kWh was measured at 2500rpm, and the ESFC remained below 270g/kWh across 2000 to 3500 rpm at full load [110]

A comparison was done to check the increase in SFC of the APU vis-à-vis the optimised engine in Section 6.7. Figure 8-7 shows the increase in SFC of the APU in comparison to the engine. At WOT conditions there is a drop of APU power by an average of 4.11% and an increase in SFC by 3.63%.

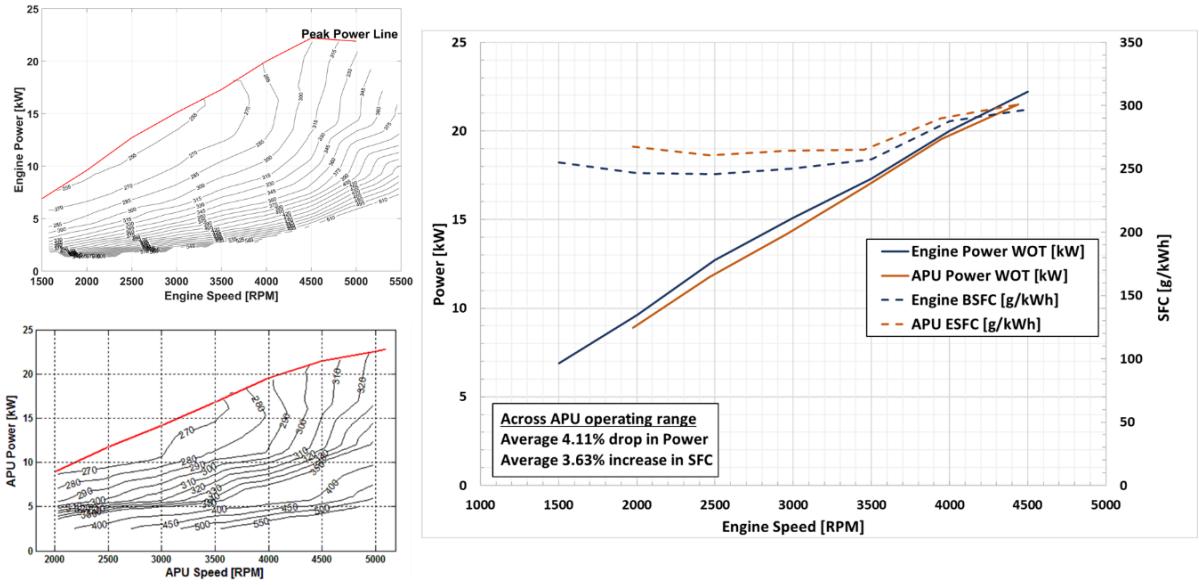

Figure 8-7 Comparison of engine versus APU specific fuel consumption. The SFC maps based on power are shown and the comparison highlighted for WOT

The results at Figure 8-7 compare favourably with simulation/measured results as shown in Figure 8-2. Under ideal thermal conditions the generator has an efficiency of the order of 93% to 95% across 2000-4500rpm. After coupling the engine to the generator, we see a similar drop in APU power and SFC.

The ESFC map at Figure 8-6 was under optimum thermal conditions both for the engine (~90°C) and the generator (~35°C). It became the benchmark to compare the subsequent effects of changing coolant temperatures in the engine and generator coolant circuits with the final aim to integrate the cooling circuits. The ESFC map did not take the power requirements to drive the EWPs for the two independent circuits into consideration.

The power drawn by the engine EWP is shown at Figure 8-8. Since the engine EWP replicates the performance of the erstwhile engine gear driven mechanical pump, the EWP power drawn increases with the engine speed, irrespective of the load. The power drawn by the generator EWP was a constant of 57.88 watts across the entire operating regime to deliver a constant flow rate of 25 LPM.

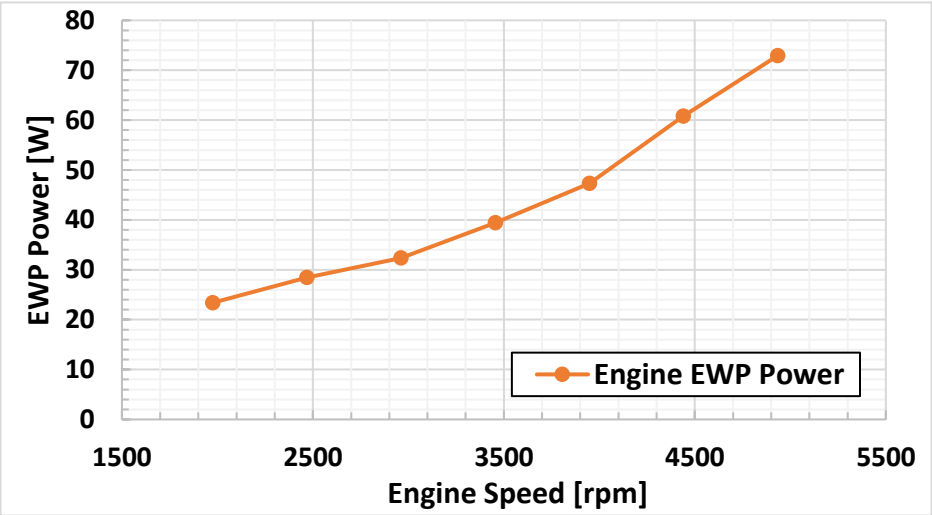

Figure 8-8 Engine EWP power (watts) drawn with respect to APU speed. Power drawn by the EWP is a function of engine speed only and independent of engine load

8.5 APU Performance with varying Coolant & Oil Temperatures

The next stage in the experimental analysis was to determine the effect of generator coolant inlet temperature, engine outlet coolant temperature and oil gallery temperature on the continuous power performance of the generator, while remaining within the temperature limits for the generator. During the initial phase of testing, the temperature limits set for safe operation of the M/G, inverter and power electronics (IGBT), as set by the OEM are at Table 8-2.

Table 8-2 M/G, inverter and IGBT temperature limits provided by the OEM Ashwoods Motors

	Warning	Inverter Trip	Remarks
Motor Temperature	135°C	150°C	Motor de-rates between 140°C to 150°C
IGBT Temperature	110°C	140°C	
Inverter Temperature	95°C	100°C	

This testing was divided into two stages. Initially having two independent coolant circuits for the engine and the M/G unit with the final aim of combining the two coolant circuits.

8.5.1 Independent Coolant Circuits

Initially the engine oil and coolant temperature set points were kept constant at their optimum value of 90°C during the first set of tests, while varying only the generator inlet coolant temperature. The aim was to study the generator continuous performance variation with change in generator inlet coolant temperature. It was expected that as the generator inlet coolant temperature was increased, there would be a drop in its continuous power output.

Subsequently in the second set of tests, the effect of simultaneously varying the generator inlet coolant temperature, engine outlet coolant temperature and the oil gallery temperature set point was tested at maximum power.

For both sets of tests above, the flow rate in the engine coolant loop was matched to the flow with the erstwhile mechanical pump, while the flow rate in the generator coolant circuit was retained at 25 LPM across all speeds.

During the first set of tests, at generator inlet coolant set point of 80°C at 4000rpm maximum power, it was observed that the inverter temperature warning limit of 95°C, was being crossed, see Figure 8-9.

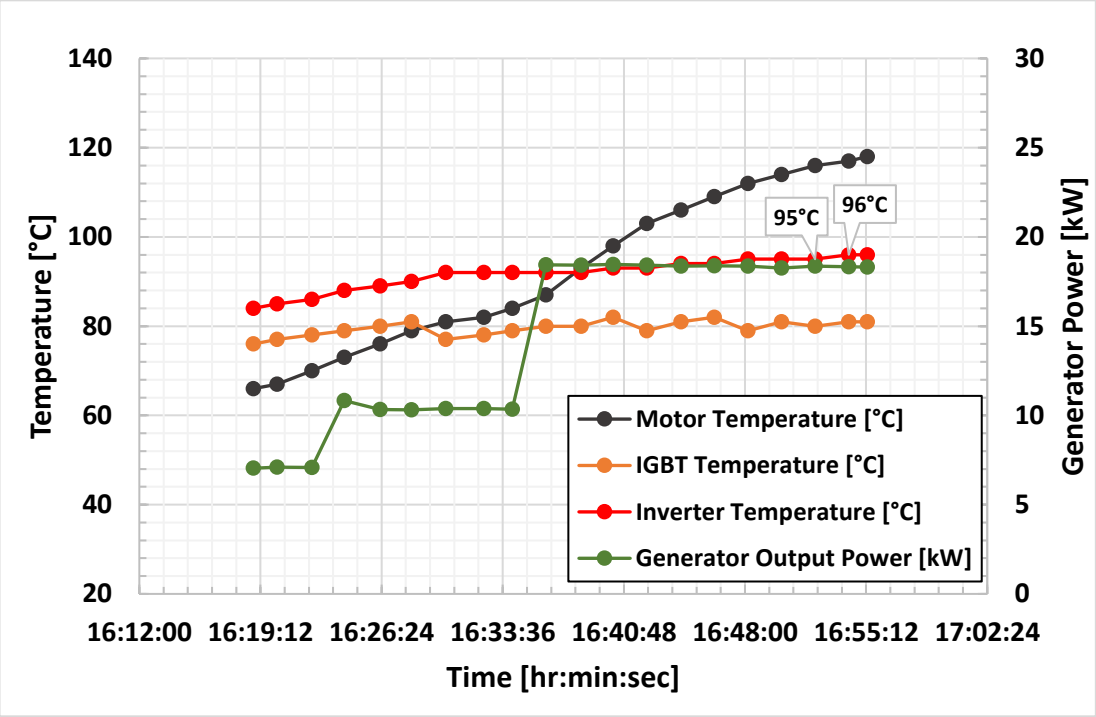

Figure 8-9 Inverter temperature (red line) warning limit of 95°C being crossed at maximum generator power output. APU speed 4000rpm, generator coolant inlet set point 80°C, engine coolant outlet and oil gallery set point 90°C

Accordingly post discussions with the OEM, Ashwoods Motors, the M/G, inverter and IGBT temperature limits were revised and are shown at Table 8-3. The rationale behind the change in temperature limits was since during testing it was observed that the IGBT temperature closely followed the generator inlet coolant temperature set point. Therefore, its warning and invertor trip temperature limits were lowered as it was not foreseen to operate the generator at a coolant inlet temperature greater than 90°C. The motor warning temperature was raised to 140°C as its temperature was well within the safe working temperature.

Table 8-3 Revised motor/generator, inverter and IGBT temperature limits provided by the OEM Ashwoods Motors

	Warning	Inverter Trip	Remarks
Motor Temperature	140°C ↑	150°C	Motor de-rates between 140°C to 150°C.
IGBT Temperature	105°C ↓	115°C ↓	Limits lowered.
Inverter Temperature	100°C ↑	105°C ↑	Limits raised.

Testing was repeated with the revised M/G temperature limits. It was observed that at the generator inlet coolant temperature set at 80°C, at 4000 and 4500rpm, the inverter still reached the warning temperature limit of 100°C and hence the APU power request had to be reduced. The power request was reduced till the inverter temperature dropped to just below 100°C at which it was considered safe for continuous operation of the generator. Figure 8-10 shows the cutback in power request from maximum power down to 18kW to reduce the inverter temperature below the warning limit at 4500rpm.

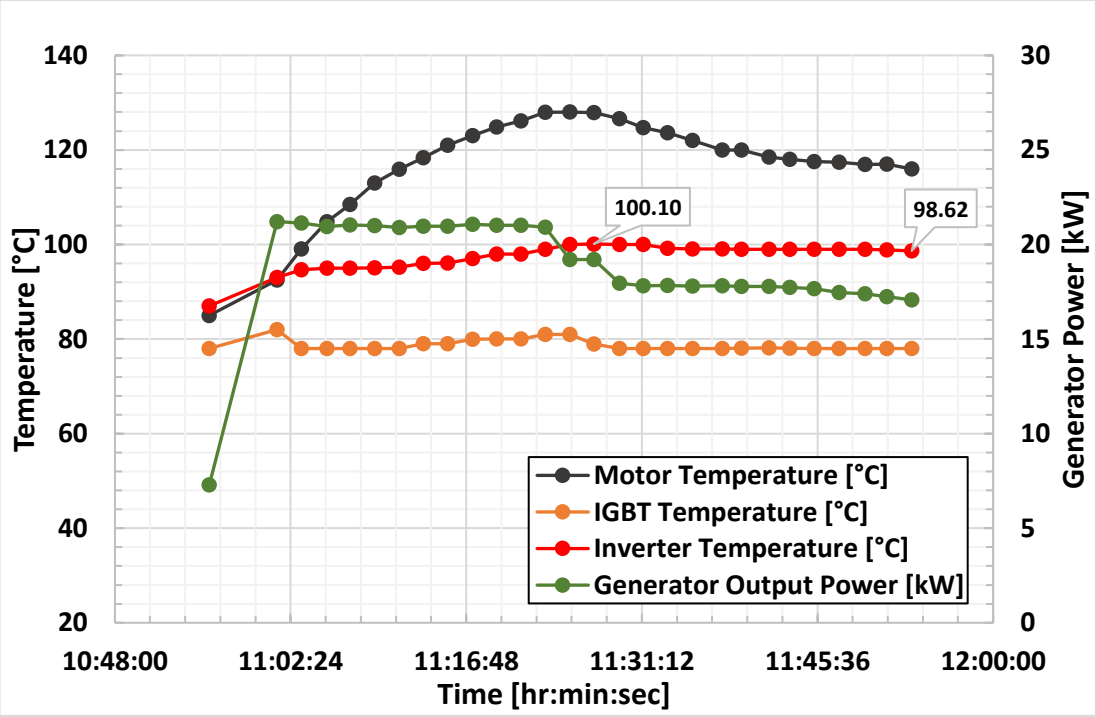

Figure 8-10 Inverter temperature (red line) warning limit of 100°C being crossed at maximum generator power output. APU power demand reduced to 18kW to stay within inverter safe operating temperature limit. APU speed 4500rpm, generator coolant inlet set point 80°C, engine coolant outlet and oil gallery set point 90°C

Based on the revised temperature limits and continuous APU performance, the results of the first set of tests wherein the engine oil and coolant temperature set points were kept constant at their optimum value of 90°C while varying only the generator inlet coolant temperature, are tabulated at Table 8-4 below.

Table 8-4 Generator maximum continuous power and ESFC performance varying only generator inlet coolant set point. Figures in red indicate requirement to cut back on APU power demand to stay within temperature limits specified for the inverter by the OEM Ashwoods Motors [110]

	4000rpm		**4500rpm**		**5100rpm**	
Generator inlet temperature °C (with engine coolant outlet and oil gallery SP 90°C)	Maximum Continuous Power [kW]	ESFC [g/kWh]	Maximum Continuous Power [kW]	ESFC [g/kWh]	Maximum Continuous Power [kW]	ESFC [g/kWh]
60	18.7	304	20.7	305	21.8	329
70	18.4	307	20.7	311	21.9	329.5
80	**17.6**	**287**	**17.9**	**310**	22.5	325.9
90	<2 kW (Inverter tempr 102°C)	680	1.5 (Inverter tempr 100°C)	969	1.5 (Inverter tempr 100°C)	951

Although there was a requirement to cutback power demand at 4000rpm and 4500rpm, at 5100rpm, the generator and the inverter temperatures were maintained within limit at full load. This could be attributed to the fact that although the power output increased at 5100rpm, the mean engine torque at this speed was actually lower than 4000rpm and 4500rpm. This led to lower Joule losses in the motor, which is the dominant part of the total loss, therefore less heat is generated.

Subsequently in the second set of tests, the effect of varying the generator inlet temperature, engine coolant outlet temperature and the oil gallery temperature set point was tested at maximum power. Results of the second set of tests are tabulated at Table 8-5.

Table 8-5 Generator maximum continuous power performance and ESFC while varying generator and engine coolant and oil temperature set points. Figures in red indicate requirement to cut back on power to stay within temperature limits specified for the inverter [110]

	4000rpm		**4500rpm**		**5100rpm**	
Engine coolant, oil gallery and generator coolant temperature [°C]	Maximum Continuous Power [kW]	ESFC [g/kWh]	Maximum Continuous Power [kW]	ESFC [g/kWh]	Maximum Continuous Power [kW]	ESFC [g/kWh]
70	18.9	294.7	20.69	313	21.5	333
80	**18.0**	**291**	20.7	314	21.5	331
90	<2 kW (Inverter tempr 102°C)	680	1.5 (Inverter tempr 100°C)	969	1.5 (Inverter tempr 100°C)	951

The maximum power in red indicates that the power had to be cut back to keep within the inverter warning temperature limits. Here again at 4000rpm the inverter temperature reached its 100°C limit and power had to be reduced to 18kW. In the 4500rpm test case, the inverter temperature remained within its 100°C limit and hence the APU power increased from 17.9kW to 20.7kW despite the drop in engine and oil gallery temperature from 90°C to 80°C. Further analysis of the test data indicated that, due to the inverter being operated extremely close to its limiting temperature, the cell ambient temperature variation of ±2°C was affecting APU peak performance [110].

The detailed tables with M/G, inverter and IGBT temperatures during the two set of tests are placed at Appendix B and Appendix C respectively.

The inverter over-temperature condition was caused due to the limited cooling available to the prototype inverter board. Subsequent design modifications by the OEM to the cooling configuration allowed better internal air flow to the inverter as well as a change in the potting compound with better thermal conductivity improved the cooling.

Further, the internal cooling fan of the M/G unit was replaced with an improved design which was more effective. As a result, post these modifications, the issue of inverter over-temperature was no longer experienced. Figure 8-11 shows the old and the new internal cooling fan. The fan on the left is the old design while the fan on the right is the improved design.

Figure 8-11 M/G unit internal cooling fan. The fan on the left is the old design while the fan on the right is the improved design, courtesy Ashwoods Motors

Based on the results obtained it was evident that a generator coolant inlet temperature of 80°C and engine coolant outlet and oil gallery temperature of 80°C could be used for further testing without any adverse effect on the APU. At these temperatures set points, both the engine and generator were performing satisfactorily without substantial requirement to cut back on power to stay within the temperature limits of the inverter.

Accordingly, a testing was carried out to generate an EFSC map at generator coolant inlet temperature of 80°C and engine coolant outlet and oil gallery temperature of 80°C. The same is placed at Figure 8-12.

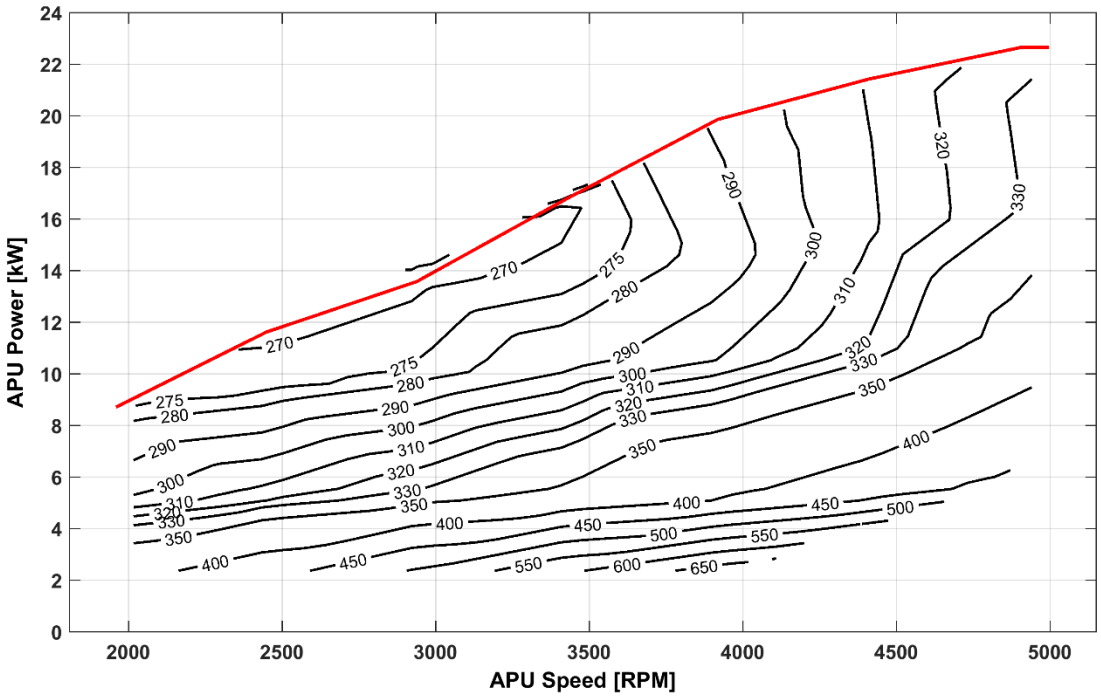

Figure 8-12 ESFC map, separate coolant loops for engine and generator. Generator coolant inlet, engine coolant outlet and oil gallery temperature set point of 80°C

The next step in the integration process was to match the generator coolant circuit flowrates to the engine coolant circuit flow rates across all speeds. This was necessary since in the subsequent simple combined circuit, the flowrate would be similar to that of the engine EWP. Accordingly, the generator EWP duty map was re-calibrated to match the flowrates in the two circuits. The same is shown in Figure 8-13.

The full load power curve testing of the APU was carried out with the matched flowrates in the independent circuits and the performance was found to be satisfactory. However, at this stage the maximum power continuous performance testing was not carried out. It was planned to undertake this once the coolant circuits were combined.

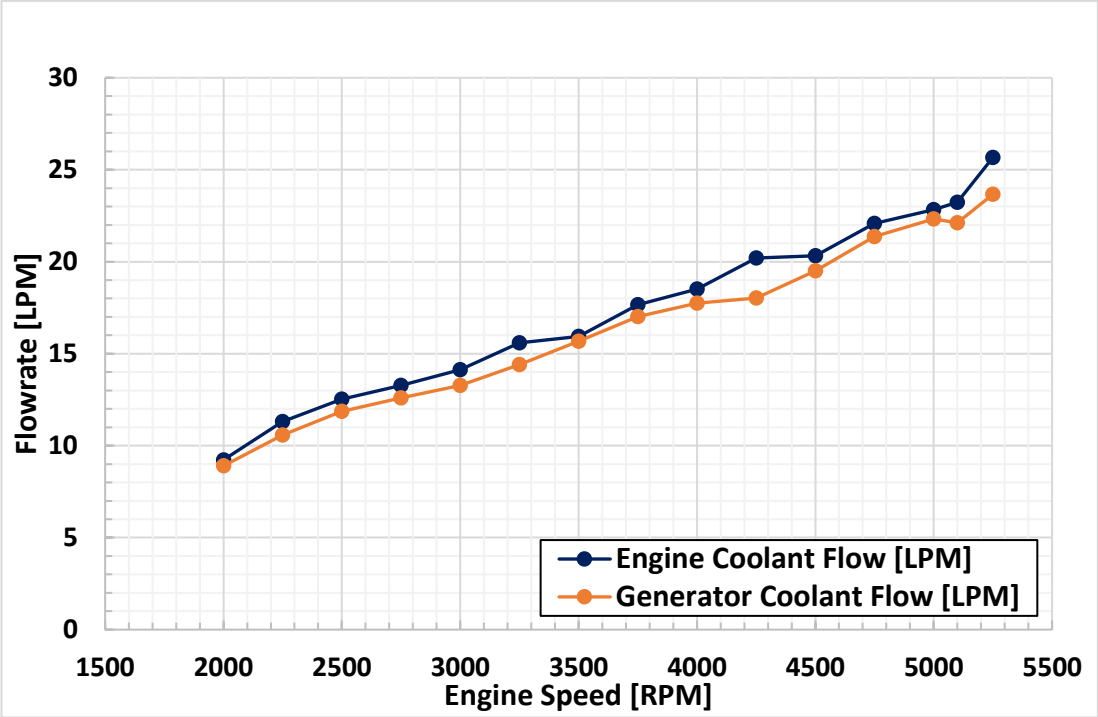

Figure 8-13 Matched engine and generator coolant circuits flowrates

The next step in the integration process was to move to a single coolant loop for the engine and the generator.

8.5.2 Single Coolant Circuit for Engine and Generator

The two coolant circuits were combined as a single circuit as shown in Figure 8-14. The coolant flow was matched to the flow values in the independent engine coolant flow circuit. It was observed that this resulted in coolant flow fluctuation at various engine rpm.

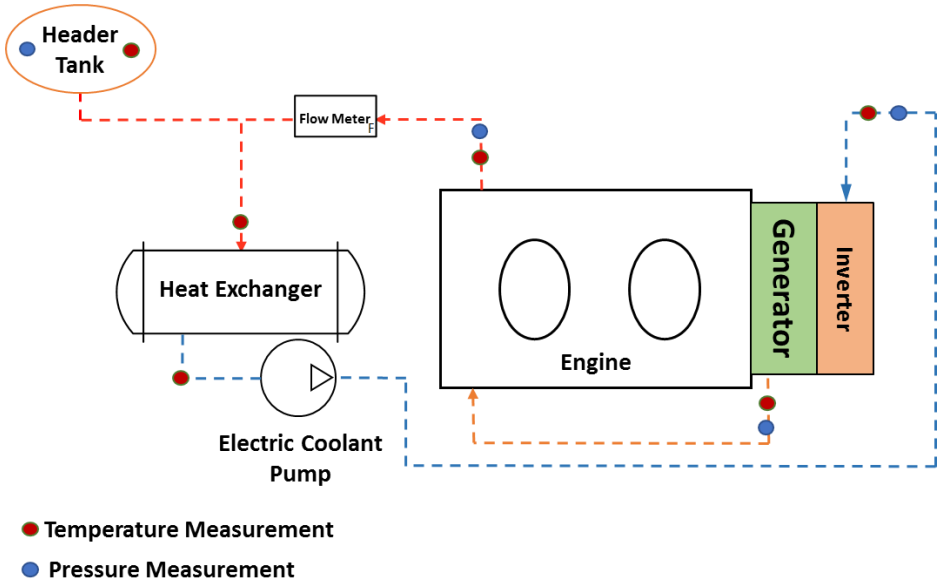

Figure 8-14 Combined engine and generator coolant circuit. The header tank connection is at the inlet of the heat exchanger

To obviate this issue, the header tank connection was relocated to the inlet of the EWP, see Figure 8-15. It was opined that this would reduce the suction pressure at the inlet of the pump. Further, the combined circuit was also pressurised to 0.4 bar to replicate the pressure of a closed coolant circuit of a road vehicle.

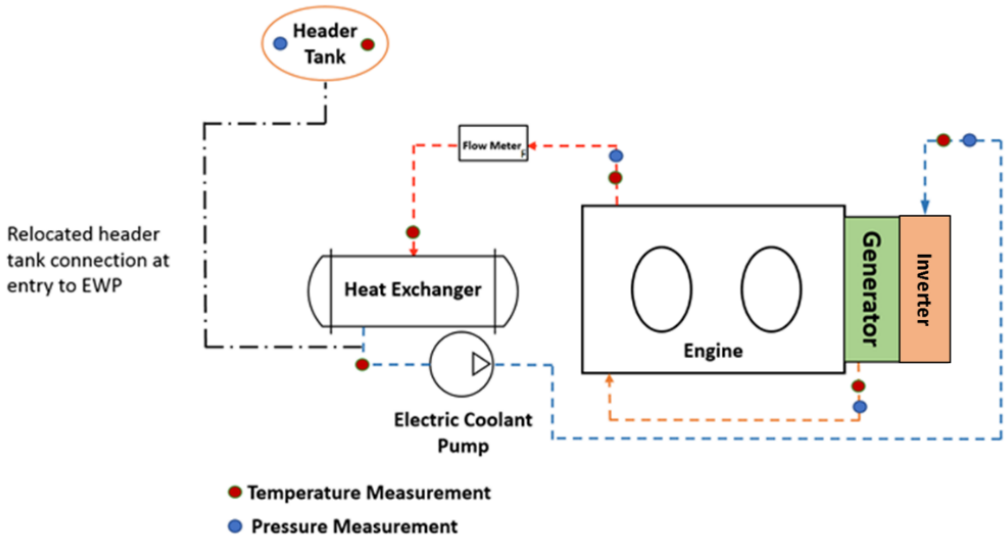

Figure 8-15 Combined engine and generator coolant circuit. Header tank connection relocated at entry to the EWP [110]

The power drawn by the EWP is shown in Figure 8-16. It was observed that the EWP draws less power in the single circuit as compared to the EWP for the engine coolant circuit in the independent circuit. This was attributed to the relocation of the header tank connection of the inlet of the EWP which reduced the suction pressure at the inlet of the pump and consequently reduced the power drawn [110].

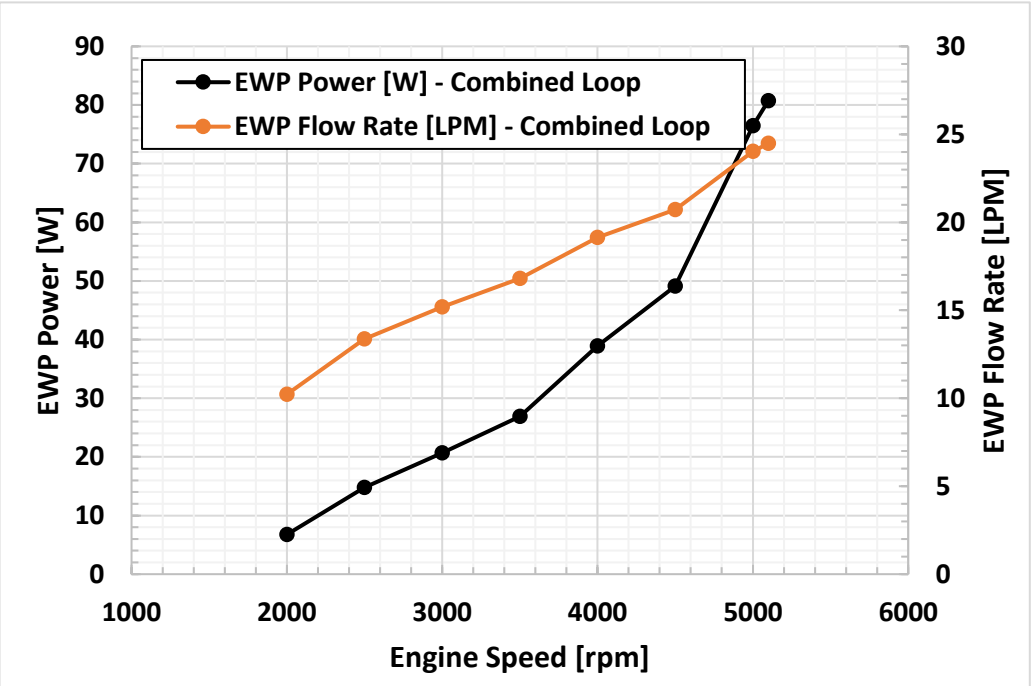

Figure 8-16 EWP power (W) and flow rate (LPM) with respect to APU speed – combined coolant circuit post relocation of coolant header tank [110]

In the single coolant loop, the generator inlet coolant temperature set point of 80°C was potentially high enough to cause the engine outlet coolant temperature to rise to 90°C viz. the engine production manual set point. Under these conditions, the engine was only marginally running below sub-optimal because the oil gallery set point had been lowered from 90°C to 80°C, which would increase the oil viscosity and result in slightly higher frictional losses.

Continuous performance testing was carried out with the combined circuit. It was observed that subsequent to the modifications in the inverter cooling design, the inverter critical temperatures were no longer exceeded. However, motor critical temperatures were reached at 4000 and 4500rpm. Coolant flows were increased to 25 LPM subsequently from their values of 18 LPM and 22 LPM respectively, however the increased flow did not reduce the motor temperatures [110].

Table 8-6 below summarises the maximum continuous power and ESFC in the combined coolant circuit with generator inlet coolant and engine oil gallery set point at 80°C.

Table 8-6 Maximum continuous power in a combined coolant circuit with generator inlet and oil gallery set point at 80°C. Figures in red indicate requirement to cut back power to stay within the motor temperature limits

APU speed [rpm]	Maximum continuous power [kW]	ESFC [g/kWh]
2000	8.62	273
2500	11.33	271
3000	13.77	271
3500	16.37	268
4000	**18.73**	292
4500	**19.97**	310
5100	21.81	333

There was a need to cut back the power at 4000rpm and 4500rpm to keep the motor temperature within limits. The ESFC map of the APU in a combined coolant loop with generator inlet coolant temperature at 80°C with power limitations at 4000rpm and 4500rpm is shown in Figure 8-17 below.

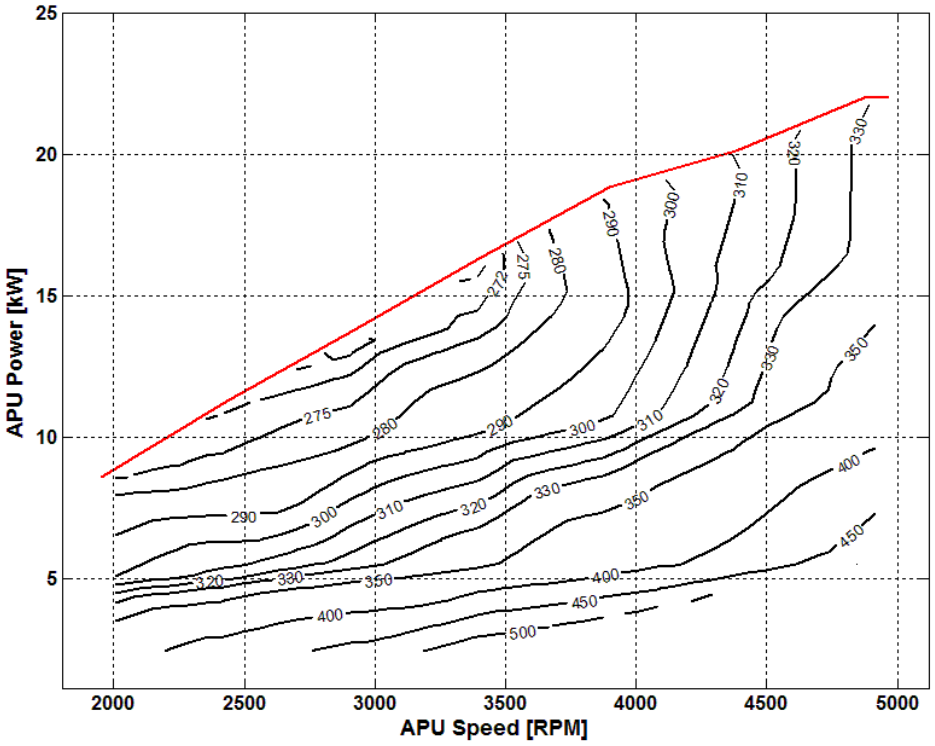

Figure 8-17 APU ESFC map, generator inlet coolant set point 80°C, engine oil gallery set point 80°C, combined coolant circuit with power cut back at 4000rpm and 4500 rpm [110]

8.6 Analysis of Experimental Results

On comparing the maximum power continuous performance data of the APU in Table 8-5 and Table 8-6, it is observed that the performance of the APU with separate and combined coolant loops is comparable with the generator inlet coolant temperature and oil gallery temperature set point at 80°C. The differences observed are well within measurement accuracy and test-to-test variability. Therefore, by combining the coolant loops, with coolant flows matched to the erstwhile mechanical engine coolant pump, we were able to get similar performance and efficiency from the APU while greatly simplifying the cooling circuit and reducing parasitic loads of the EWP.

Based on the experimental results, on comparing the two ESFC maps at full load across 2000rpm to 5100rpm in Figure 8-6 and Figure 8-17, there was a drop in APU

power by an average of 4% with an increase of ESFC by circa of 2%, see Figure 8-18, at operation of the APU at 80°C set points of generator inlet coolant and oil gallery temperature. This can be attributed primarily to the higher operating temperature of the generator with the increase in the generator inlet coolant temperature set point from 35°C to 80°C. Although the engine efficiency also reduced with drop in coolant and oil temperature, however in the combined circuit the engine outlet coolant temperature continues to reach around 88°C. The oil gallery temperature has been reduced by 10°C to 80°C which would marginally increase the frictional losses because of increase in oil viscosity.

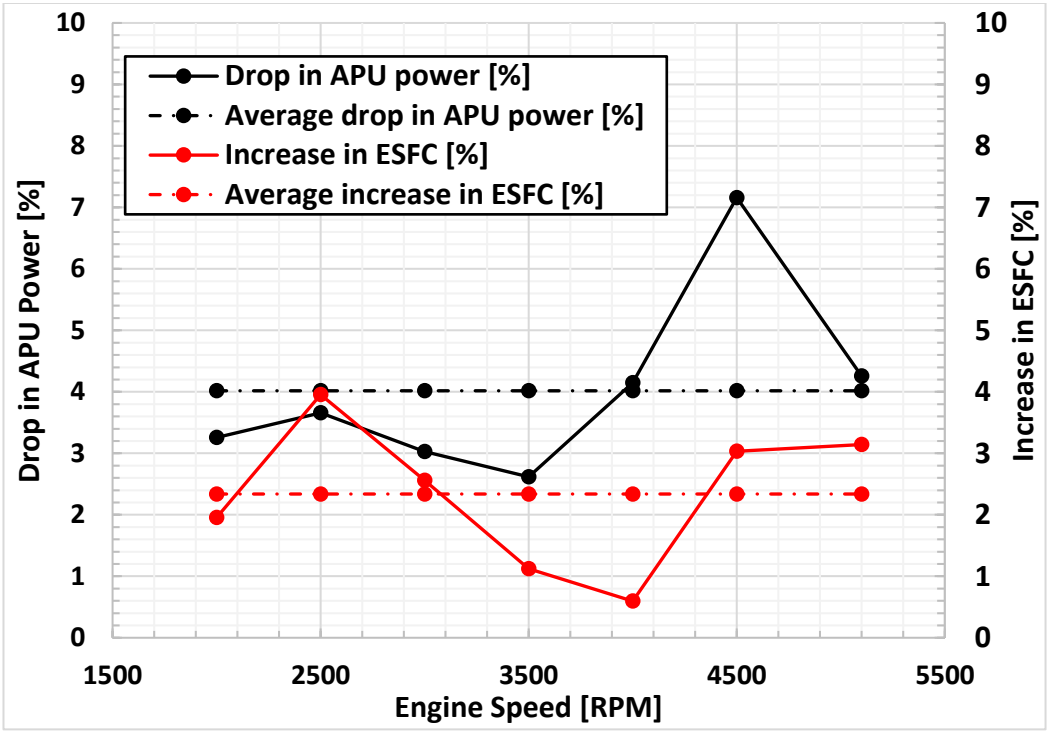

Figure 8-18 Change in APU power and ESFC at generator inlet coolant temperature and engine gallery temperature set point at 80°C vis-à-vis generator inlet coolant temperature at 35°C and engine oil gallery temperature set point at 90°C

Comparing the optimised engine power and BSFC at Figure 6-12 with the APU power and ESFC (combined coolant circuit @ 80°C and oil gallery temperature setpoint at 80°C) at Figure 8-17, indicates average generator efficiency of the order of 91% based on power and 93% based on SFC, see Figure 8-19.

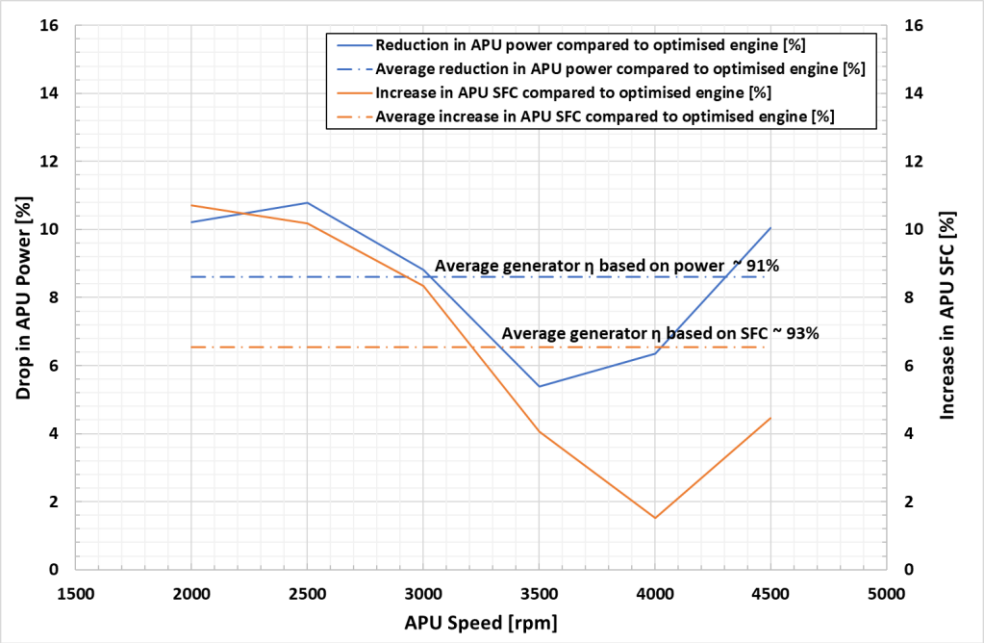

Figure 8-19 Change in APU power and SFC at generator inlet coolant temperature and engine gallery temperature set point at 80°C vis-à-vis optimised engine with engine coolant outlet temperature set point at 90°C and engine oil gallery temperature set point at 90°C

Although there is an increase in ESFC by combining the coolant loops, there is a sizeable saving in parasitic losses as regards the EWP. Over 50% saving in parasitic loads is achieved in the combined circuit at 4500rpm, with even greater savings at lower speeds as shown in Figure 8-20.

This is attributed to two reasons. Firstly, in the independent generator coolant circuit the flow had been set to a maximum of 25 LPM across all engine speeds. This resulted in a large draw of EWP power. However, once the circuits were combined, because of the reduced flows (matched to the independent engine coolant circuit), the EWP power has reduced.

Secondly re-positioning of the header tank to the inlet of the EWP also improved the flow in the combined coolant circuit and hence resulted in reduced EWP power.

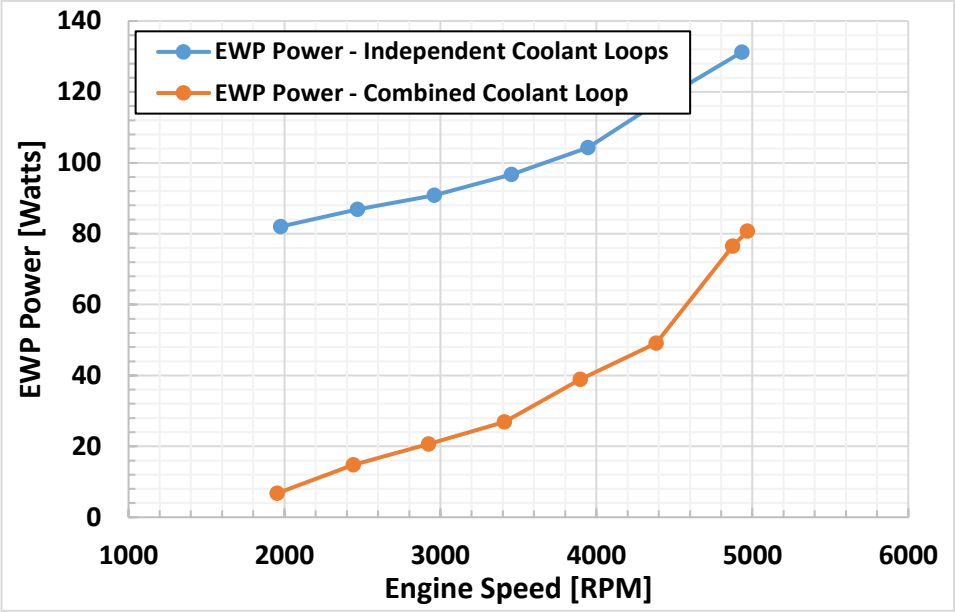

Figure 8-20 Comparison of EWP power in separate and combined coolant loops

Figure 8-21 shows the impact of including EWP power consumed on APU ESFC. It shows the very marginal increase in ESFC after including the EWP power.

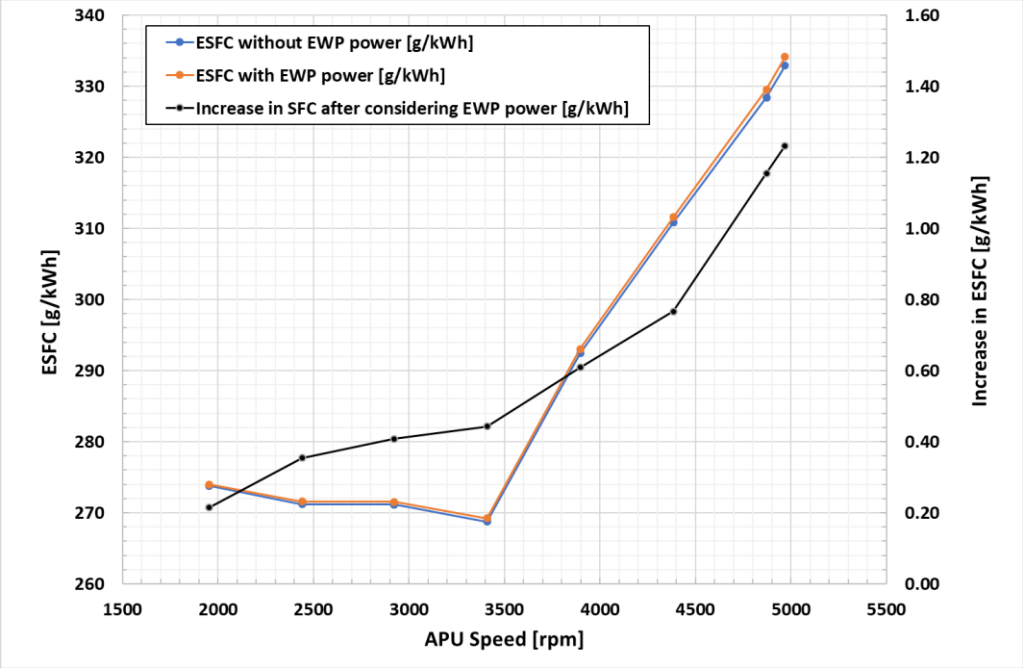

Figure 8-21 Impact of including EWP power consumed on APU ESFC. There is a very marginal increase in ESFC after including the EWP power. Since the EWP power is a function of APU speed only, its impact on ESFC increases with increase in APU speed (black line).

Since the EWP power is a function of APU speed only, its impact on ESFC increases with increase in APU speed. Detailed calculations of the impact of EWP power on the APU ESFC are shown in Appendix D.

8.7 Conclusion

This chapter has discussed the commissioning of the APU subsequent to the engine optimisation and then the development of a thermal management system for using a single coolant loop for the APU. After coupling of the engine with the M/G and inverter unit the total dry weight of the APU was measured to be 81.5kg as against an initial target of 80kg.

The target best ESFC of <270g/kWh was exceeded under optimal temperature conditions with separate coolant circuits for the engine and generator, with peak power of 22.78kW at 5100rpm. Best ESFC of 260g/kWh was measured at 2500rpm, and the ESFC remained below 270g/kWh across 2000rpm to 3500rpm at full load. These exceed the bespoke Mahle APU best ESFC of 283g/kWh. From 4000rpm to 4500rpm the ESFC was between 285g/kWh to 305g/kWh which was also within the target ESFC and are comparable to the Mahle ESFC of 292g/kWh. The specific performance of the APU at peak power was 270W/kg which was within the target of 250 to 313W/kg.

The experimental analysis also demonstrated that it was possible to operate the APU in a combined coolant loop, to meet the conflicting requirement of running the engine at a high temperature and the generator as cold as possible, with marginal drop in power and increase in ESFC. In the combined loop, with a coolant temperature of 80°C at the generator inlet, there was a drop in APU power of an average of 4% and an ESFC penalty of circa 2% at full load across the operating regime. However, the combined loop provides greater flexibility of package installation and simplifies vehicle integration, with reduction in parasitic losses. It also reduces the overall package cost which was one of the objectives of this research. With subsequent

improvement in bespoke generator internal cooling design, cutback of power at 4000–4500rpm could be avoided which would improve APU power and ESFC in this range.

As shown in the experimental analysis, the electric coolant pump output was matched to that of the erstwhile mechanical engine driven coolant pump. The flow rates in such a strategy are designed to cope with peak heat rejection rate at high power conditions, and consequently at other conditions such as city driving or slow cruising, the system is less efficient i.e. wasteful pumping work and negative impact on oil and combustion temperatures. Also, it was seen that the generator is less sensitive to change in coolant flow rates which gives an opportunity to change the flow rates without affecting the generator performance.

As the operating limits on the engine structure revolves around the maximum metal temperature in certain key locations, it is more desirable to regulate the flow rate to ensure that such metal temperature remains within limit, rather than the coolant temperature [86]. By regulating the flow rate such that metal temperatures are always at an optimum level even at low power conditions, savings can be made in fuel consumption and lower emissions. Therefore, further experimental work could be planned to optimise the flow rates in the APU coolant circuit based on metal temperatures to further reduce EWP parasitic power and improve ESFC.

The work presented in this chapter formed part of technical paper titled ‘Thermal Management of a Low-Cost Range Extender for Electric Vehicles’ which was presented at the 6th Hybrid and Electric Vehicles Conference (HEVC 2016) in November 2016. Paper reference is 10.1049/cp.2016.0976.

CHAPTER - 9
APU Performance over NEDC

This is a brief chapter which discusses the performance of the APU over the New European Drive Cycle (NEDC). It demonstrates that the APU was successfully able to produce the necessary power output as demanded by the vehicle supervisory controller (VSC) based on a representative vehicle model developed by TMETC.

9.1 Introduction

In this chapter, the performance of the APU was seen over a New European Drive Cycle (NEDC). The NEDC is discussed and then establishes that the APU was successfully able to produce the necessary power output as demanded by the Vehicle Supervisory Controller, based on a representative vehicle model prepared by TMETC.

9.2 Drive Cycle

A drive cycle is a fixed schedule of vehicle operation which allows an emission test to be conducted under reproducible conditions. Drive cycles are usually defined in terms of vehicle speed and gear selection as a function of time. It is important to note that drive cycles may be used for a variety of purposes other than emissions measurement, such as testing engines or drive train durability. Depending on the character of speed and engine load changes, cycles can be broadly divided into the following: -

(a) Steady state cycle

(b) Transient cycle

A steady state cycle is a sequence of constant engine speed and load conditions. Such cycles are mainly used for testing of heavy-duty diesel engines. In transient cycles, the vehicle speed and engine load are changing continuously. These are used for testing of light-duty vehicle [57]. There are various drives cycles which are used all over the world such as NEDC, Artemis, FTP etc, however for purpose of this research the performance of the APU was tested against the NEDC since this is the cycle used for type approval of light-duty vehicle models in the European Union. Brief discussion on the various drive cycles that have been mentioned in the thesis is covered in the succeeding paragraphs.

9.3 Artemis Drive Cycle

The Assessment and Reliability of Transport Emission Models and Inventory Systems (Artemis) drive cycle project was undertaken to collect data on the actual driving of European cars and to derive representative real-world driving cycles to ensure the compatibility and integration of all the resulting emission data in the European systems of emission inventory [111]. With 77 passenger cars used under actual driving conditions, taking into account the diversity of driving conditions and behaviours, led to the identification of 12 classes obtained by automatic clustering of speed profiles recorded on-board vehicles. Urban, rural-road and motorway cycles were developed, see Figure 9-1. The Motorway cycle has two variants with maximum speeds of 130 and 150 km/h. The set of the Artemis real-world and reference drive cycles is widely used in the frame of European projects [111].

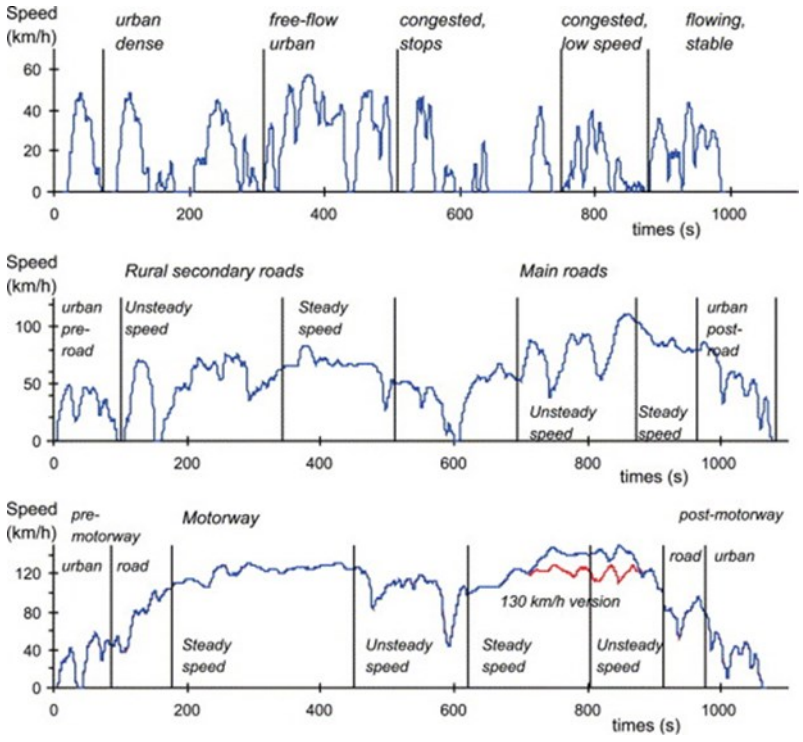

Figure 9-1 Artemis urban, rural-road and motorway driving cycles [111]

9.4 Hyzem Drive Cycle

The hybrid technology approaching efficient zero emission mobility (HYZEM) drive cycle is a test cycle developed for evaluating hybrid vehicles. It is an unofficial European transient drive cycle that involves many speed changes representing the constant speed changes typical of on-road driving [57]. The APU operating strategies by Rogge et al [55] discussed in Section 2.7 were simulated on this cycle.

9.5 New European Drive Cycle (NEDC)

The NEDC is a highly stylised drive cycle which is used for type approval of light-duty vehicle models in the European Union. It has periods of constant acceleration, deceleration and speed [57]. The NEDC is made up of two parts, the urban cycle (part 1) and the extra urban cycle (part 2), see Figure 9-2. The urban cycle is made up of 4 repeats of the elementary urban cycle, each lasting 195 seconds and part two lasts for 400 seconds making the total cycle time of 1180 seconds covering a theoretical distance of 11023 meters.

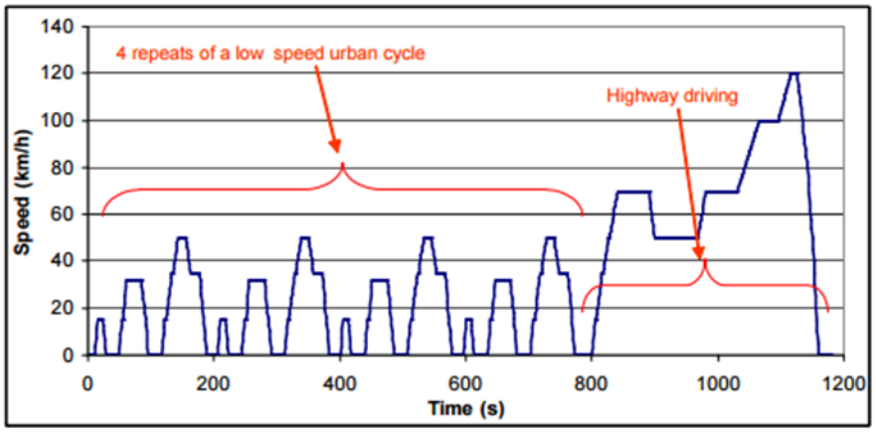

Figure 9-2 NEDC drive cycle is a highly stylised drive cycle which is used for type approval of light-duty vehicle models in the European Union [57]

Since the NEDC bears little resemblance to real world driving conditions, the worldwide harmonised light vehicles test procedure (WLTP) has been developed and a new cycle, the worldwide harmonised light-duty driving cycle (WLTC) has replaced the NEDC in Europe with effect from September 2017 [112]. The new procedure covers a greater range of vehicle and engine speeds, engine load, gear changes and ambient temperatures.

9.6 Energy Demand from APU to complete NEDC

The electrical power output of the RE for this study was defined by considering the average electrical load drawn from the high voltage bus during extended range (or charge sustaining operation) for 3 vehicle applications. This load was the sum of tractive power (suitably corrected for drive system losses) together with ancillary load requirements, see Section 3.2.

In a conventional vehicle, operation of the engine at peak efficiency is not possible for sustained periods because the engine is normally sized to meet peak vehicle power requirements. The engine therefore operates at low load, speed and efficiency under most typical driving conditions.

As discussed earlier, see 2.6 in a charge sustaining mode, the APU only supplies the average power and not the instantaneous power requested from the driveline, thus allowing it to choose its operating points. This flexibility to operate the engine at its efficient operating points or in a high-efficiency operating region allows it to have a very good fuel economy performance in charge sustaining mode. The total range of the REEV can be enhanced by employing energy management strategies that enable the efficient use of fuel energy when the APU is turned on considering NVH, emissions and durability constraints.

In order to minimise the fuel energy in the charge sustaining mode, TMETC examined various energy management strategies [113, 114] with the following objectives:-

(a) Minimise fuel consumption in charge sustaining mode when the APU is ON. This implies that over a drive cycle the energy used for propelling the vehicle is only from the APU and the battery is only used as a temporary energy buffer which allows to reduce fuel consumption.

(b) Sustain the battery charge over different types of driving trips.

(c) Reduce the noise output of the APU when in operation to below the vehicle noise.

However, TMETC did not include emission requirements while optimising the energy management strategy. Based on the energy management strategy, the following operating points were selected for the APU over the NEDC cycle, see Table 9-1. The selected operating points superimposed on the APU ESFC map are shown at Figure 9-3.

Table 9-1 APU operating points selected to complete the NEDC. Operating points were chosen to minimise fuel consumption, sustain HV battery state of charge over the drive cycle and reduce APU noise to below vehicle noise

APU speed [rpm]	**APU power [kW]**
1500	3
1500	3.5
2108	6
2918	12
3322	15
3322	15.5
3525	16.5

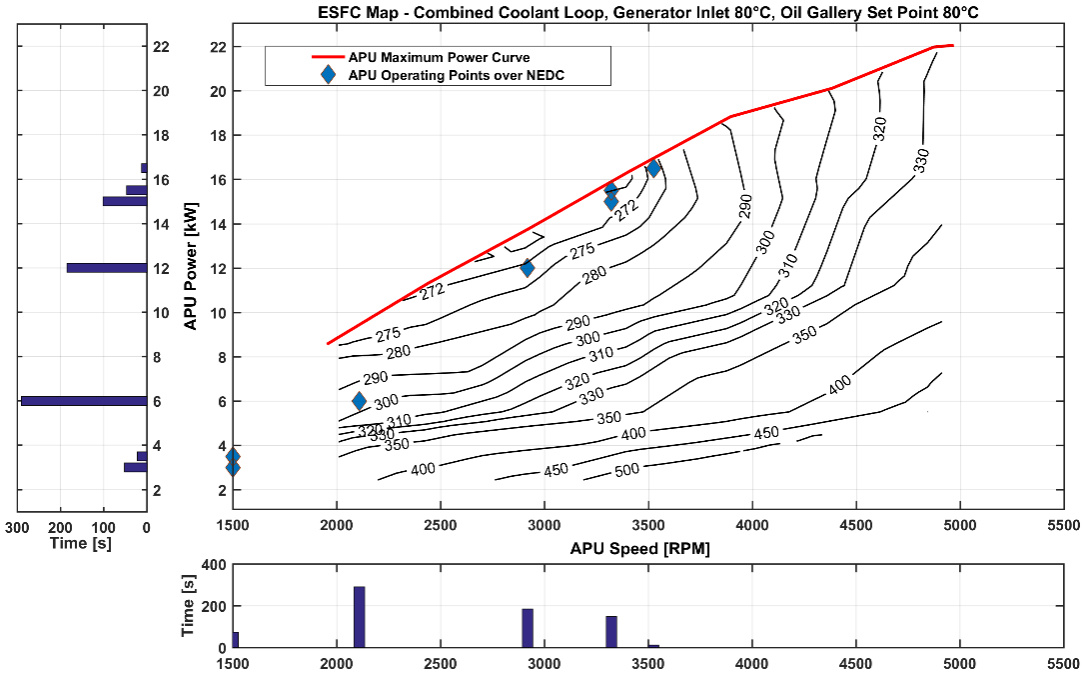

Figure 9-3 APU ESFC map with operating points during NEDC superimposed. Operating points chosen are essentially at best ESFC to minimise fuel consumption over the NEDC

TMETC worked out that the APU must produce 1.76kWh to complete the NEDC. This was based on many factors such as vehicle mass, aerodynamics, motor and generator efficiency, tyre friction, battery efficiency etc. TMETC had the above data for their representative vehicle which was then used in their vehicle model. The throttle was then controlled over the NEDC and 1.76kWh was the energy dissipated over the cycle [115]. Based on 1.76kWh energy required, the VSC demanded 1.87kWh over the NEDC, see Figure 9-4. The reason for the extra demand was to cater for the delay in generation of power from the time of demand. This additional demand could be subsequently fine-tuned during the calibration process if required.

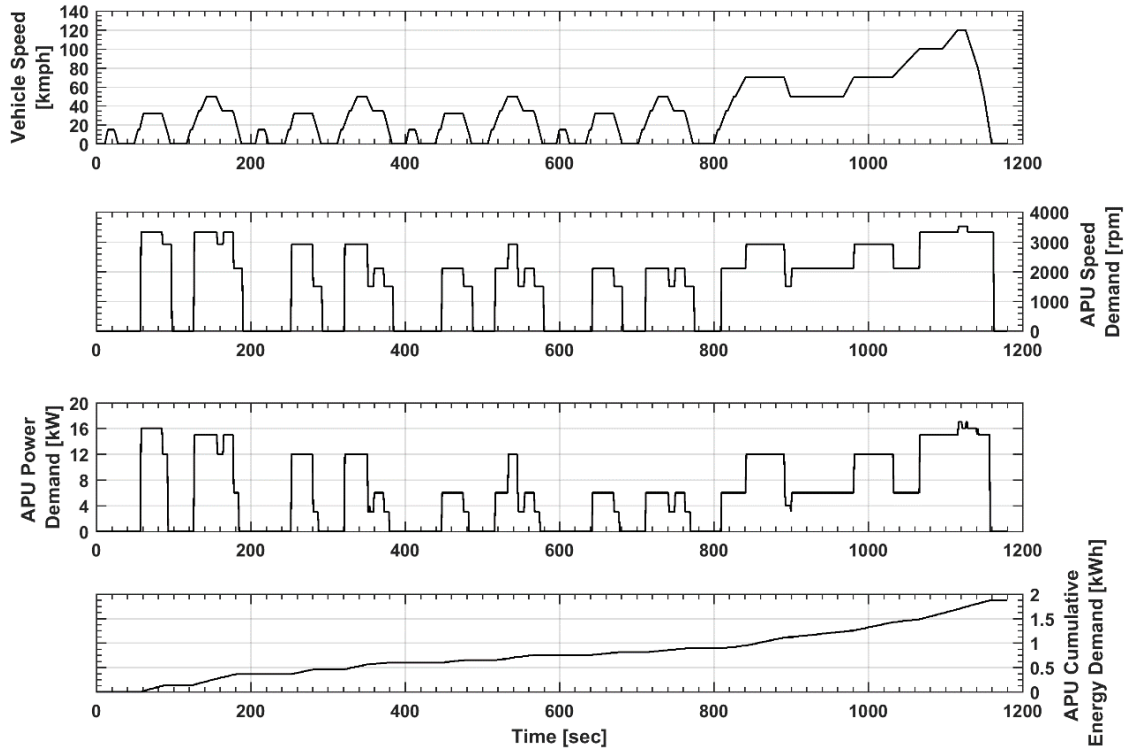

Figure 9-4 APU speed, power and cumulative energy demand to complete NEDC

9.7 APU Performance over NEDC

The test cell set up has already been discussed in the previous chapter, see Figure 8-3. The test cell temperature was controlled to 25±2°C. The generator inlet coolant temperature and engine oil gallery temperature were controlled to 80±2°C. The performance of the APU over the NEDC is shown in Figure 9-5 and Figure 9-6.

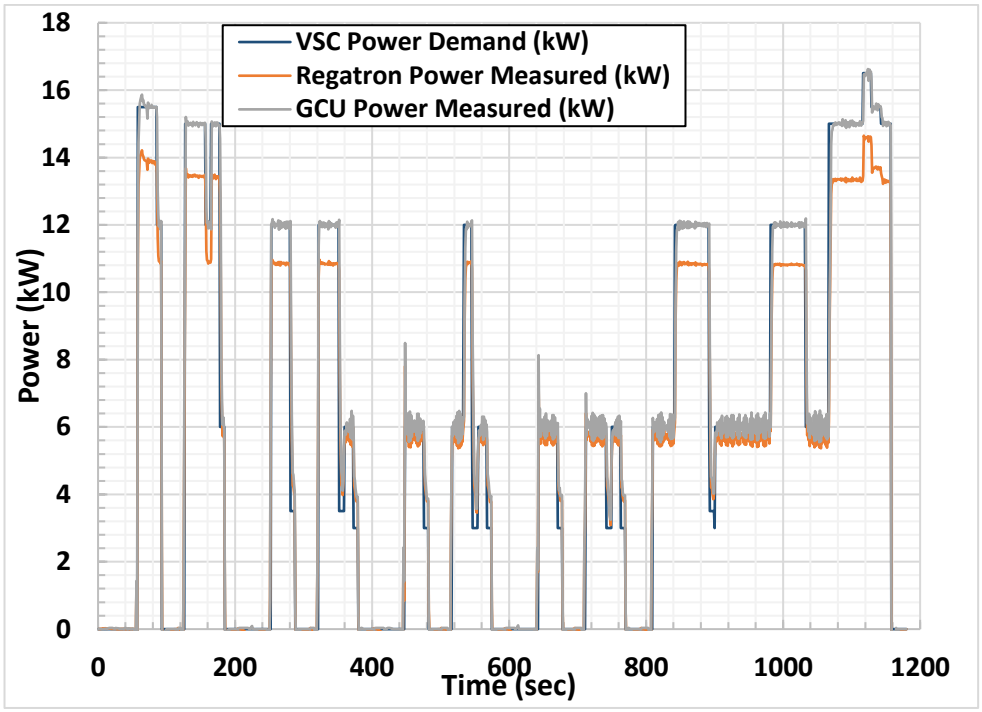

Figure 9-5 Power demand and output of APU over NEDC.

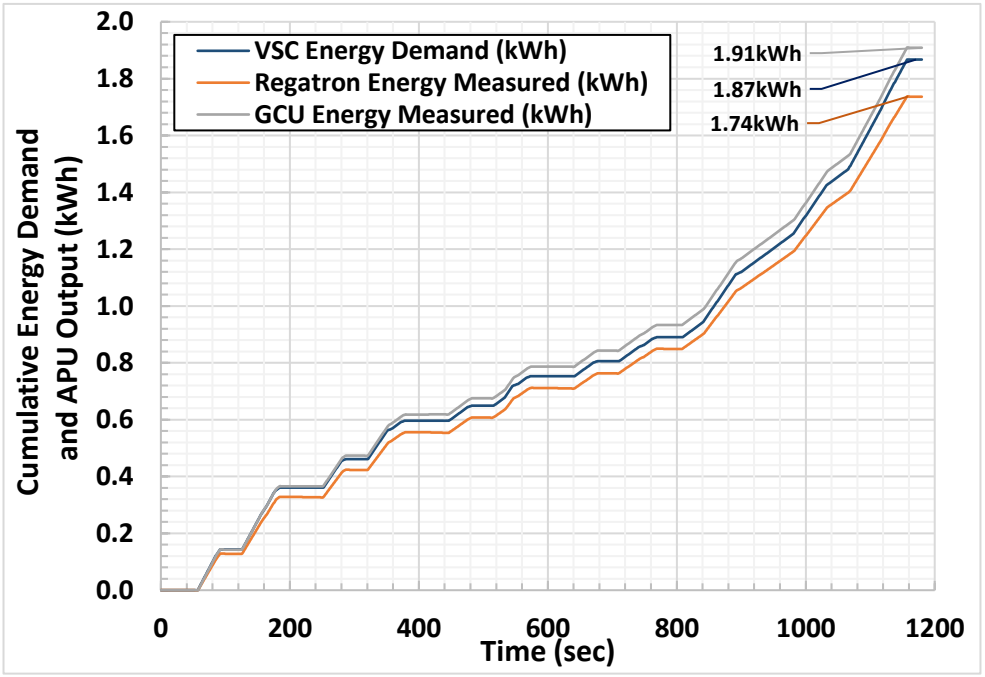

Figure 9-6 Cumulative energy demand and APU output. Based on 1.76kWh energy required, the VSC demanded 1.87kWh over the NEDC

Based on the VSC demand the APU was satisfactorily able to cope with the demand as measured by the GCU. On the VSC cumulative energy demand of

1.87kWh, the APU produced 1.91kWh which was within 3% and was considered acceptable [115].

The Regatron bi-directional DC power supply measured 1.74kWh over the NEDC. The difference between the GCU measured energy and Regatron measured energy could not be ascertained at the test cell level and was communicated to Ashwoods. However, no clarification was received from Ashwoods and to progress with further work, it was decided to use the GCU measurement. This was justifiable since the APU output was being controlled based on the GCU measurement and not the Regatron unit.

During the test the APU required 0.716 litres of gasoline to complete the NEDC. This compared favourably against the 25kW APU with a bespoke engine developed for the Manza REEV which consumed 0.78 litres during the NEDC [113].

9.8 Conclusion

The performance of the APU was tested over the NEDC, which was designed to minimise fuel consumption based on an energy management strategy taking into consideration fuel consumption, battery SOC and minimise NVH. However, the choice of the APU operating points during the NEDC did not take into consideration the emissions map for minimising emissions.

Based on the results obtained, the APU could successfully produce the necessary power as demanded by the VSC for a representative vehicle model. There remained the need to further improve the calibration of the GCU with respect to power measurement, however that was not possible within the project time framework and was left to Ashwoods to resolve in case the APU was going to market.

During the test the APU consumed 0.716 litres of gasoline to complete the NEDC. This compared favourably against the 25kW APU with a bespoke engine developed for the Manza REEV which consumed 0.78 litres during NEDC.

CHAPTER - 10
Emissions Performance

This chapter discusses the experimental results of the emissions performance of the conventional three-way catalyst of the APU over the NEDC. Based on the performance, strategies to improve catalyst light off and steady state emissions were explored. The analysis concluded that the existing catalyst was unsuitable for range extender application.

10.1 Introduction

Three-way catalysts (TWC) are essential for automotive-exhaust purification for gasoline engines. This chapter discusses the performance of the TWC similar in size and precious metal loading of the original vehicle TWC for treatment of the exhaust of the APU over the NEDC. The emissions from the APU were measured over the NEDC based on the APU power demand as per the drive cycle discussed in Chapter 9. Since the emission levels were exceeding the EU6 legislative limits, attempts were made to improve the emission performance by experimental analysis of various light off strategies and improving air-fuel ratio control. Based on the results, it was evident that the existing TWC was not suitable for APU application and would require to be redesigned. There also exists the opportunity to look at other technologies such as electrically heated catalyst which would come at an additional cost.

10.2 Pollutant Formation in SI Engines

An exothermic reaction releases energy as heat during the combustion of fuels with oxygen from the air, which contains 21% by volume O_2, <1% by volume noble gases and nitrogen N_2. Theoretically the only components formed from the complete combustion of hydrocarbons under ideal conditions or excess air are carbon dioxide and water. Pollutants form primarily from the interruption of the combustion reaction chain due to short residence time in the combustion chamber. An equilibrium state therefore no longer exists. Further inhomogeneities in the mixture due to different air/fuel ratios, combustion wall effects and contaminants and additives in the fuel also lead to formation of undesirable by-products [94].

The exhaust of SI engines contains oxides of nitrogen (nitric oxide, NO and nitrogen dioxide, NO_2, which are collectively known as NO_x), carbon monoxide (CO) and organic compounds which are unburnt or partially burnt hydrocarbons (HC)plus other e.g. N_2O. The formation and destruction reactions of CO, organic compounds

and particulates are closely coupled with the primary fuel combustion process. For NO_x, the formation and destruction reactions are not directly part of the fuel combustion process, however their formation takes place in an environment created by the combustion process [94, 99]. Pollutant formation in a cylinder of a SI engine is shown at Figure 10-1.

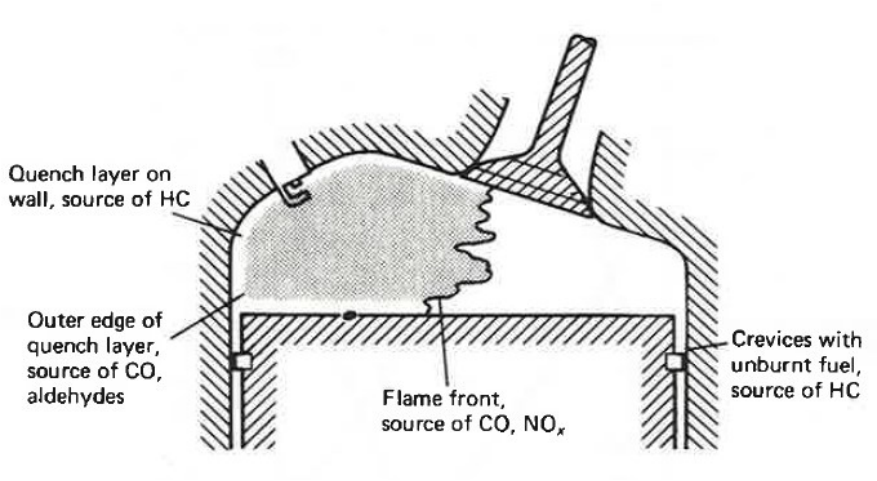

Figure 10-1 Source of THC, CO and NOx emissions in a spark ignition engine [104]

Nitric oxide (NO) formation occurs throughout the high-temperature burnt gases behind the flame by chemical reactions involving oxygen and nitrogen in air, which do not attain chemical equilibrium. The processes are described by the expanded Zeldovich mechanism (1946), see equation below [94].

$$\begin{aligned} O_2 &\Longleftrightarrow 2O \\ O + N_2 &\Longleftrightarrow NO + N \\ N + O_2 &\Longleftrightarrow NO + O \end{aligned} \qquad (11)$$

Formation of NO and other oxides of nitrogen increase very strongly with increasing flame temperature [99, 104]. As the burnt gases cool during the expansion

stroke, the reactions involving NO freeze and the NO concentrations remain far in excess of levels corresponding to equilibrium at exhaust conditions. NO_x formation is also influenced by flame speed. Lower flame speeds with lean mixtures provide a longer time for NO_x to form. Likewise NO_x emissions increase with reduced engine speed [104].

Since NOx formation is very sensitive to the combustion temperature, it has also acted against the pursuit of higher fuel efficiency by increasing engine compression ratios [96].

Carbon monoxide forms during the combustion process. It is intermediate step in the formation of carbon dioxide and is characterised by the equation below

$$CO + H_2O \Longleftrightarrow CO_2 + H_2O \quad (12)$$

With rich fuel-air mixtures, there is insufficient oxygen to fully burn all the carbon in the fuel to CO_2. In such a scenario the CO emissions have a nearly linear relationship with the air/fuel ratio. Also, in high-temperature products, even with lean mixtures, dissociation ensures there are significant CO levels. During the expansion stroke the CO oxidation process freezes as the burnt gas temperature falls.

HC emissions can originate both from the fuel and the lubricants and have several different sources. The increasing cylinder pressure, during compression and combustion forces some of the gas in the cylinder into crevices such as the volume between the piston, rings and cylinder wall, see Figure 10-1. The fuel-air mixture in these crevices does not undergo the primary combustion process as the entrance to these crevices is too narrow for the flame to enter. During the expansion this unburnt gas leaves the crevice and becomes a source of unburnt hydrocarbons. Another source is the partial ignition of the overall combustion chamber volume and the wall deposits

of fuel. Other reasons are residual fuel in the dead spaces such as gaps in the cylinder head seal, valve seats, fire land, spark plugs and squish area. Misfiring, emissions of hydrocarbons from the lubricant, and absorption of fuel molecules in the lubricant film of the cylinder barrel also increase hydrocarbon emissions [94].

10.3 Emission Control by Design Modifications & Calibration

Emissions of CO, NOx and HC vary with different engines and are dependent on factors such as ignition timing, load, speed and in particular fuel/air ratio relative to stoichiometric. Some degree of control over their formation is possible by engine and engine-calibration modification such as spark timing changes, exhaust gas recirculation (EGR) and air-fuel ratio (AFR) changes.

10.3.1 Spark Timing

Spark timing influences peak cylinder pressures and consequently peak unburnt and burnt gas temperatures. Spark retard will result in lower cylinder temperatures but increases the temperature in the exhaust as considerable burning occurs in the expansion stroke. Lower cylinder combustion temperatures will reduce NO_x formation and the higher exhaust temperature will reduce HC by their oxidation in the exhaust port and manifold if excess O_2 is present. However retarding spark from MBT reduces fuel economy, see Section 6.4. Retarded timing may be utilised at engine start up to bring the catalyst to achieve light-off temperature faster, more is covered on this aspect in Appendix D [99, 116, 117].

10.3.2 Exhaust Gas Recirculation (EGR)

Recirculation of cooled exhaust gas back in the engine intake manifold replaces a portion of the fresh charge. This gas mixture can absorb a large amount of heat under dissociation and hence will reduce combustion temperature and as a result NO_x

formation. Figure 10-2 below shows the relation between air-fuel ratio (λ) and the specific heat of exhaust gas at constant pressure. During combustion, CO_2 and H_2O with high heat capacities, increase the specific heat capacity of the exhaust gases to values greater than air. EGR effectively utilises this phenomenon by recirculating a portion of the exhaust gas back into the intake port to act as a heat sink that lowers the combustion temperature [118]. Substantial reduction in NO_x concentrations are achieved with 10 to 25% EGR. However EGR also reduces the combustion rate which makes stable combustion more difficult to achieve [99]. Also, lower combustion temperatures increase the wall quench layer thickness, see Figure 10-1, and consequently the hydrocarbon emissions. It also results in a cooler exhaust and less homogeneous hydrocarbon oxidation [99, 116].

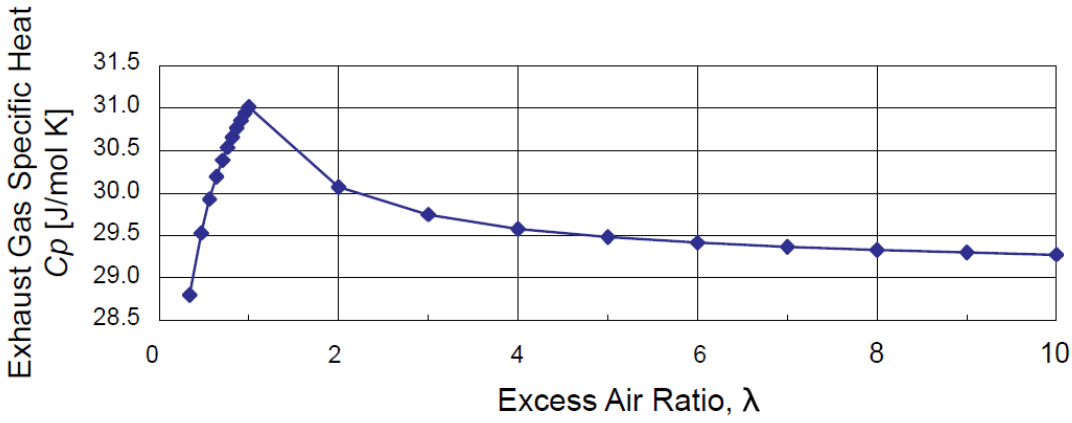

Figure 10-2 Excess air ratio and specific heat of exhaust gas at constant pressure [118]. The exhaust gas specific heat peaks at an excess air ratio of 1

10.3.3 Air Fuel Ratio (AFR)

The air fuel ratio of the mixture in the combustion chamber has the greatest influence on untreated emissions. The emissions of CO and HC are lowest in the slightly lean range of lambda, λ, of 1.05 – 1.1, however untreated NO_x emissions are the highest in this range, see Figure 10-3. When run rich the raw exhaust contains more CO and HC than NO_x. This is due to there not being enough oxygen to burn the fuel

all the way to CO_2. Further the relatively cool-in cylinder temperatures combined with low oxygen availability limits the amount of NO_x formed.

Conversely as the AFR becomes lean, more NO_x is formed. With more oxygen available and the higher in-cylinder temperatures less CO and HC are produced but more NO_x is formed. This trend continues until the engine becomes lean enough that the additional air intake begins the cool the combustion temperature and NO_x production decreases. Quite lean operation i.e. AFR ~20, will reduce both NO_x and CO but in general will produce high HC levels, see Figure 10-3.

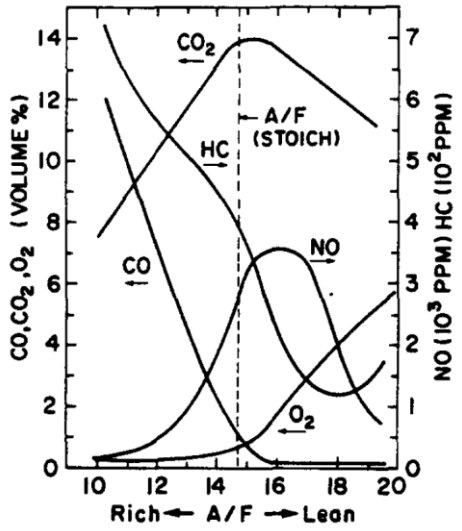

Figure 10-3 The concentration of CO, NO and hydrocarbons emitted by a spark ignition engine as a function of intake AFR [116]

10.4 Exhaust Treatment for Gasoline Engines

Treatment of exhaust gas after it leaves the exhaust ports can be either thermal or catalytic. Homogenous oxidation of hydrocarbons in the exhaust requires temperatures in excess of 600°C and a holding time of ~50ms. Likewise, to homogenously oxidise CO, temperatures in excess of 700°C are required. Since during majority of the time, the exhaust temperatures are in the range of 400-600°C, it is not

high enough for effective oxidation. In addition homogenous oxidation requires that excess oxygen be present at all times [116].

Catalytic oxidation of CO and HC in the exhaust can however effectively be carried out at temperatures as low as 250°C. Further the only satisfactory known method for the removal of NO_x from the exhaust involves catalytic processes. As a result three way catalysts have now become the norm for automotive-exhaust purification [116]. TWCs used in modern vehicles reduce CO and UHC emissions by 90-95% and NO_x by 80-90% when they are fully warmed up [117].

10.5 Catalyst Construction

Present day catalysts used in SI engines consist of an active catalytic material in a specially designed metal casing which directs exhaust gas flow through the catalytic bed. It comprises of three layers – the substrate, washcoat and catalytically active materials. Two design configurations for the construction are commonly used. The first one uses a ceramic honeycomb structure or monolith held in a metal can in the exhaust stream. The second design configuration uses a bed of spherical ceramic plates to provide a large surface area in contact with the flow [99]. Since the original vehicle TWC was a monolith design, it is elaborated further in more detail in the succeeding paragraphs.

The substrate is the framework that supports everything else so that exhaust gases can come in contact with the catalytically active layer. Design targets for ceramic catalyst substrates include high geometric surface area (GSA), large open frontal area (OFA), low thermal mass and heat capacity, high use temperature, low coefficient of thermal expansion, good coatability and washcoat compatibility, strength and oxidation resistance. Substrates with a high cell density and thin walls are suitable for improving the light-off behaviour when the catalyst is heated quickly. A typical monolith has square cross section passageways with inner dimensions of ~1mm

separated by thin, 0.15 to 0.3mm, porous walls. The number of passageways per square centimetre varies between about 30 and 60 [99, 119].

The washcoat provides more surface area on which to deposit the catalytically active materials. The substrate overall has fairly little surface area, and washcoating the substrate increase the available surface area dramatically. The washcoat is essentially highly porous inert aluminium oxide (γ-Al_2O_3) and 5 to 15% of the weight of the monolith having a surface area of 100 to 200m^2/g [99, 119].

The catalytically active noble metals are most suitable as catalytic material. A mixture of palladium (Pd) and platinum (Pt) is most common and is distributed as finely as possible on the washcoat to prevent particle-to-particle metal contact. This augments catalytic behaviour which is a function of surface atoms as well as suppresses high temperature sintering of catalytic material [99, 119].

10.6 Catalyst Sizing

As per literature survey, the ceramic monolith volume required is about half of the engine displaced volume. This gives a space velocity through the catalyst converter (volume flow rate of exhaust divided by converter volume) over the normal engine operating range of 5 to 30 per second [99, 116]. Space velocity implies the time it takes for a segment of exhaust gas to pass from the catalyst's inlet face to its outlet face, see equation below: -

$$Space\ Velocity = \frac{Exhaust\ Flow\ (cubic\ feet/hour)}{Catalyst\ Volume\ (cubic\ feet)} \tag{13}$$

The conversion efficiency (CE), see section 10.7, of a catalyst is a function of the space velocity and temperature for a given substrate. Space velocity and CE have an inverse relationship. When sizing a catalyst for an engine, the CE is calculated for a compound based on the raw emissions and the required operating limit. The CE value is then used to determine the space velocity that yields the CE for the temperature of the exhaust gas in the inlet face of the catalyst. Based on the space velocity, equation (13) above is used to calculate the catalyst volume. The ratio of ceramic monolith volume and the engine displaced volume of the catalyst provided by TMETC was 1.15 [120].

10.7 Catalyst Conversion Efficiency (CE)

As per Heywood [99], the conversion efficiency of a catalyst is the ratio of the rate of mass removal in the catalyst of the particular constituent of interest to the mass flow rate of that constituent into the catalyst. For example, for HC:

$$\eta_{cat} = \frac{\dot{m}_{HC,in} - \dot{m}_{HC,out}}{\dot{m}_{HC,in}} \tag{14}$$

10.8 Conversion Efficiency and AFR Relationship

An engine which is operated at or very close to the stoichiometric AFR enables both NO_x reduction (chemically) and CO and HC oxidation in a single catalyst bed. The exhaust composition is brought to a near-equilibrium state i.e. a composition of CO_2, N_2 and H_2O under these conditions. For a catalyst to be efficient a very tight control of the AFR around stoichiometric is necessary, see Figure 10-4. There is a narrow window, termed window width, of around 0.1 AFR (0.007 in equivalence ratio

terms) near stoichiometric in which high conversion efficiencies for all three pollutants are achieved [99, 116].

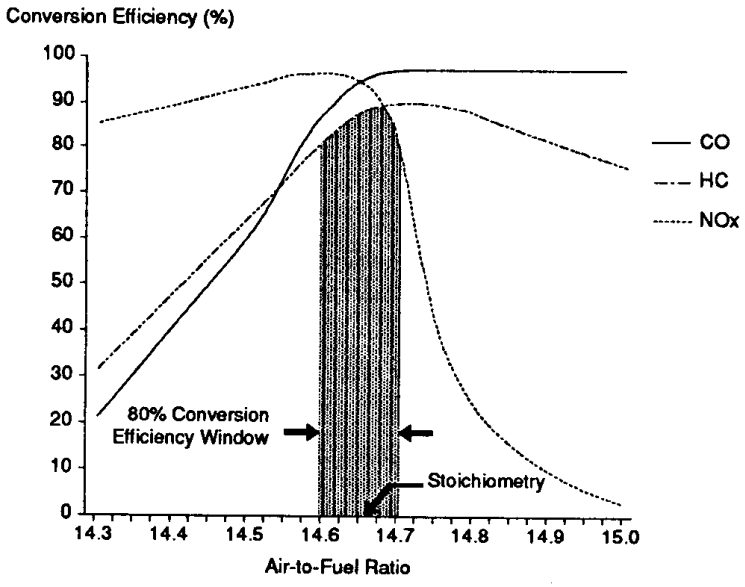

Figure 10-4 Typical TWC efficiency as a function of exhaust gas AFR. A narrow window of 0.1AFR near stoichiometric exists in which high conversion efficiencies for all 3 pollutants are achieved [121]

To achieve such a tight control over AFR, closed loop control using an oxygen sensor is introduced in the exhaust, which provides feedback to the fuel system based on whether the engine is operating lean or rich.

Heywood [99] and Kaidantzis et al [121] provide a cogent explanation on the operation of the oxygen sensor and that under moderate AFR modulation very high CO, HC and NO_x conversion efficiencies can be traded for conversion window width. The effect of AFR modulation depends on the frequency and the amplitude of the modulation. Frequencies above 1 Hz are reported to be most effective and the 80% conversion window can with modulation frequencies greater that 1 Hz be broadened to about 0.8 AFR. The modulation frequency should be as high as possible since the catalyst is a distributed system and the AFR oscillations are therefore averaged at higher frequencies.

10.9 Catalyst Light Off

TWCs do not operate effectively at temperatures below the range of 250-340°C. It is therefore absolutely essential to bring the catalyst to a temperature, termed light-off temperature, where at least 50% conversion of the emissions can occur as soon as possible [94, 116, 117]. The response of the catalyst has two distinct stages. In the first stage the catalyst heats up due to the presence of the high temperature exhaust gases but without any significant chemical reaction. After a relatively short span of time, the temperature in the interior of the catalyst becomes sufficiently high for significant reaction to occur, which generates heat faster than can be swept away by the gas stream. The temperature and reaction rate increase dramatically at this point and the catalyst lights-off. The catalyst then rapidly gets divided into a region upstream of this light-off position where the catalyst temperatures are low and the reaction rates are small. The narrow transition between these regions is called the light-off front. The second stage of the response is characterised by a relatively slow movement of the light-off front towards the catalyst inlet. Once the light-off front reaches the inlet face of the catalyst, it is then fully operational [122]. Experimental results show that catalyst light-off temperature is of the order of 300°C, based on the catalyst brick temperature at a distance of 25mm from the front face of the catalyst [123, 124]. Basshuysen et al [94] and Chan [117] provides a comprehensive summary on the various strategies for rapid catalyst light-off using different heat sources. These vary from improving the catalyst design to reduce heat capacity, moving from an underfloor catalyst to a close coupled catalyst and varying the air gap wall of the exhaust pipe for improved heat preservation. Other methods include exhaust gas ignition, secondary air injection, afterburner and burner-assisted catalyst methods to supply additional thermal energy to the exhaust to aid faster catalyst light-off. Electrically heated catalyst [59] and microwave dielectric techniques [125] have also been studied.

10.10 Exhaust Gas Legislation for EU6

The acceptable limits for principal emission components in g/km as per EU4 and EU6 norms for spark ignition engines are shown in Table 10-1 below.

Table 10-1 Limit values of THC, CO and NOx pollutants – EU 4 & EU6 legislation [126, 127]

Emissions Standards	**THC**	**CO**	**NOx**
	g/km	g/km	g/km
EU 4	0.1	1.0	0.08
EU 6	0.1	1.0	0.06

As mentioned in Section 10.1, the emissions were to be measured against the NEDC cycle EU6 limit. Accordingly considering the NEDC cycle total distance of 11.007 km, the cumulative emissions in grams over the NEDC are shown in Table 10-2 below.

Table 10-2 EU6 limit values of THC, CO and NOx pollutants over NEDC cycle

THC	**CO**	**NOx**
g	g	g
1.1	11.01	0.66

10.11 EU6 Testing Norms for Electric Vehicles

In accordance with Regulation No. 83 [128] of the Economic Commission for Europe of the United Nations (UNECE) there is a requirement to perform two tests for an electric vehicle without an operating mode switch. The first test is to be carried out with a fully charged electrical energy storage device. If the electrical range of the vehicle is greater than the distance of the driving cycle, emissions will not be present in this test.

The second test is to be carried out with the electrical energy storage device in a minimum state of charge. In this scenario, the range extender starts immediately at the beginning of the test cycle and depending on the operating strategy must at least provide an energy amount to hold the charge state of the battery.

The above tests must be carried out twice. First with a starting temperature between 20°C and 30°C with the emission limits in accordance with Table 10-1 and Table 10-2 above. The vehicle has to be kept in a room in which the temperature remains relatively constant between 20°C and 30°C and has to be undertaken for at least 6 hours and until the engine oil and coolant temperature are within ±2°C of the temperature of the room. The second is with a starting temperature of -7°C. In this cold started test, the emission limits are 15 times higher than the regular EU6 legislation. Investigations on vehicles show that the adherence to these higher limits is not difficult [126] and hence have not been considered further in this research.

10.12 Test Cell Set for Catalyst Testing

The specifications of the close coupled catalyst were decided by TMETC and was manufactured by BTB Exhausts [129, 130]. TMETC had ordered a standard brick size (commercially off the shelf) from BTB exhaust for keeping the cost of the catalyst low and specified the Platinum group metals (PGMs) loading as per the Nano car BS4 catalyst [131].

The rationale for using a BS4 specification catalyst was that the EU6 emissions were not actually much lower, essentially NOx limit being reduced from 80mg/km to 60mg/km, rest of the limits remaining the same, refer Table 10-2. Further, since for a RE application the freedom existed to operate the engine at a few fixed load/speed points it was felt that raw emissions would be easier to control. Some of the specifications of the catalyst which were made available by TMETC are in Table 10-3 below.

Table 10-3 Specifications of bespoke closed coupled catalyst [129, 130]

Parameter	Value	Remarks
Brick size	86mm * 93mm	
Cell density	600 cpsi	
Foil thickness	3 mil (0.0762mm)	

Parameter	Value	Remarks
Platinum group metals (PGMs) loading	30g/cft	Platinum: Palladium: Rhodium ratio: 0: 26: 4
Maximum allowable catalyst mid-brick temperature	1360°C	Monolith softening temperature

Figure 10-5 shows the schematic of the test bed and the instrumentation used for the emissions measurement and catalyst light off experimental analysis. The arrangement was essentially same as has been discussed at Section 8.3. However, some aspects and modifications specific to emissions measurement are elucidated in the succeeding paragraphs.

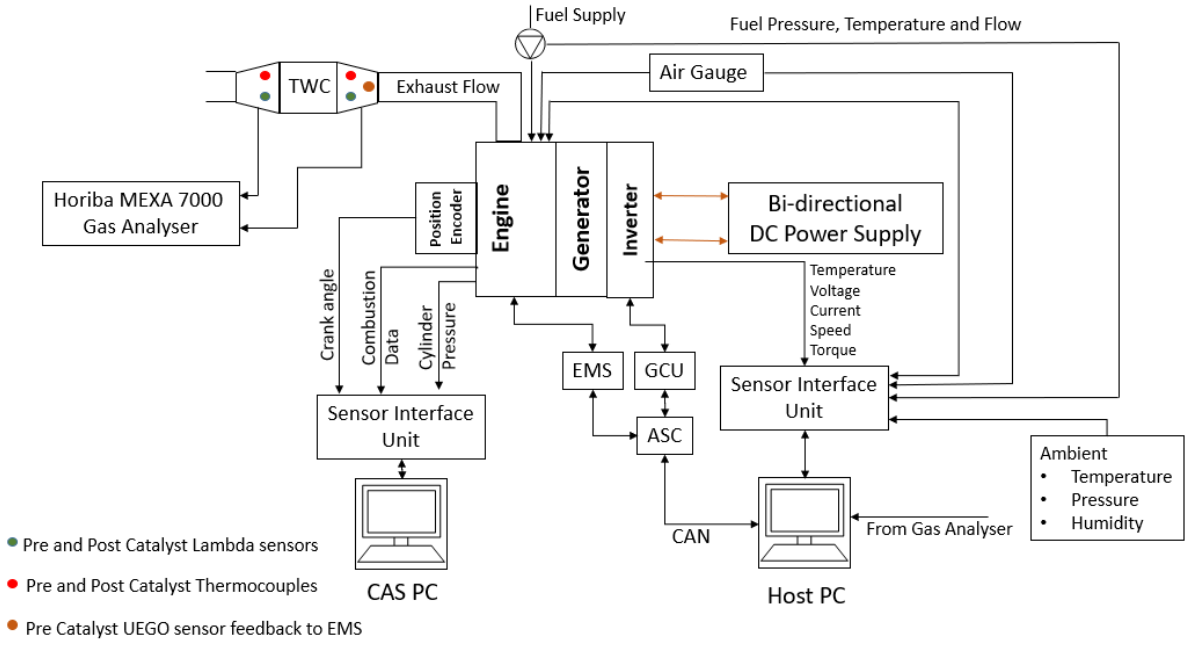

Figure 10-5 Schematic arrangement of the test cell set up at University of Bath

The exhaust gas AFR was measured using two Labcell lambda sensor, NTK 6ma which were installed pre and post the TWC. These also provided the value of lambda before and after the TWC and were recorded continuously on the Host PC, see Figure 10-6.

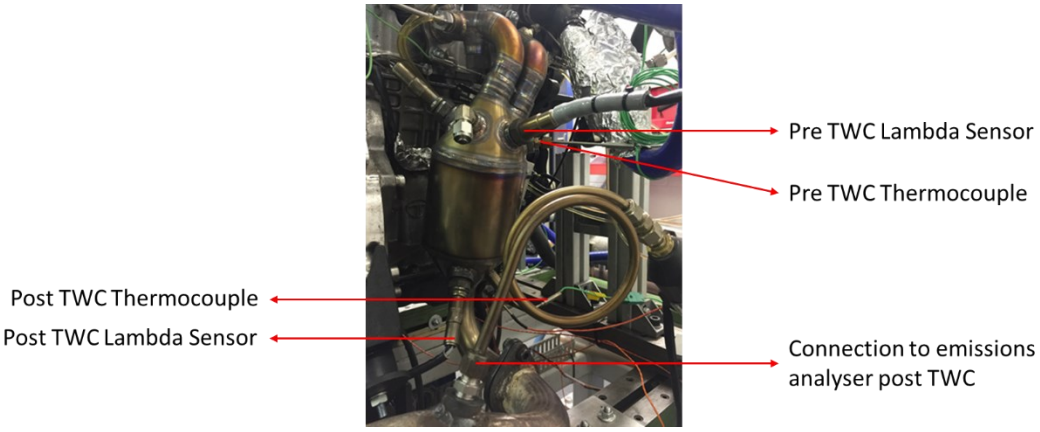

Figure 10-6 Instrumented three-way catalyst. Additional instrumentation included pre and post TWC thermocouples and lambda sensors as well as connection to the heated line for emissions measurement

Intake air was measured by a Labcell Meriam flow meter type 50MC2-2F (laminar flow element) equipped with a differential pressure transducer. The mass flow rate was then calculated from the volume flow rate based on ambient temperature and pressure. Fuel flow rates were measured using a micro motion Coriolis flow meter.

The exhaust gas temperatures, both pre-catalyst and post-catalyst were measured using type-K thermocouples, see Figure 10-6. The exhaust emissions were measured by the Horiba Mexa 7000 gas analyser and recorded on the host PC.

10.13 Catalyst Ageing

The performance of a new catalyst changes with usage and light–off temperatures can increase by 50°C as the catalyst ages [124]. As a result, the emissions measured downstream of a new TWC would be lower than that using a used catalyst. For a conventional vehicle, the performance of the catalyst should be satisfactory after 50,000 vehicle miles [116, 124]. Reasons for catalyst ageing include exposure to elevated temperatures of the order of 900°C and above which can result in precious metal sintering and substrate material sintering. Presence of catalyst poisons such as

lead, phosphorous and sulphur which can be present in gasoline or motor oil also degrade the catalyst performance [116].

A typical catalyst ageing is carried out in an oven at a temperature of 980°C in an atmosphere comprising 2% O_2, 10% H_2O with the remainder being N_2 for a duration of 4hrs [132]. Since it was not possible to age the catalyst under these conditions, the catalyst provided was run-in by operating the APU at 3000rpm, 6kW for 6hrs in consultation with TMETC to achieve stability in conversion efficiency.

On completion of the catalyst running-in, the APU was started from cold and emissions measured post catalyst. Figure 10-7 shows the cumulative NOx emissions after a cold start post TWC. Two separate tests measuring post-TWC NOx emissions indicated stability in catalyst performance.

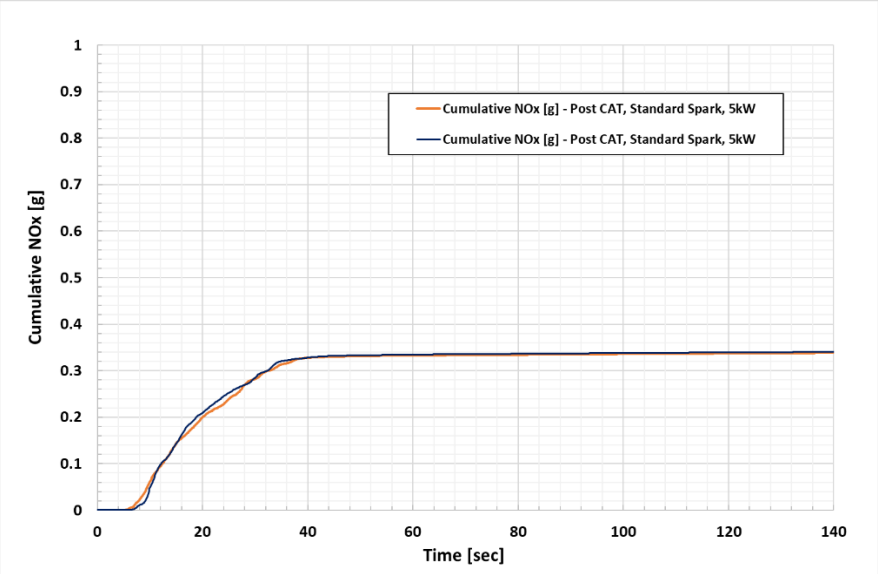

Figure 10-7 Cumulative NOx emissions post TWC after cold start of APU, two independent tests show stability in performance of the TWC after running-in to achieve stability in conversion efficiency

10.14 Emission measurement over NEDC

After running-in of the TWC, catalyst performance over the NEDC from cold was carried out to determine the efficiency of the close coupled catalyst provided by TMETC. The catalyst is considered to be lit-off when the pre-cat exhaust temperature reached 350°C, as discussed in Section 10.9.

The APU was operated on the NEDC and APU power and speed demand was varied as per the cycle discussed in chapter 9, see Figure 10-8.

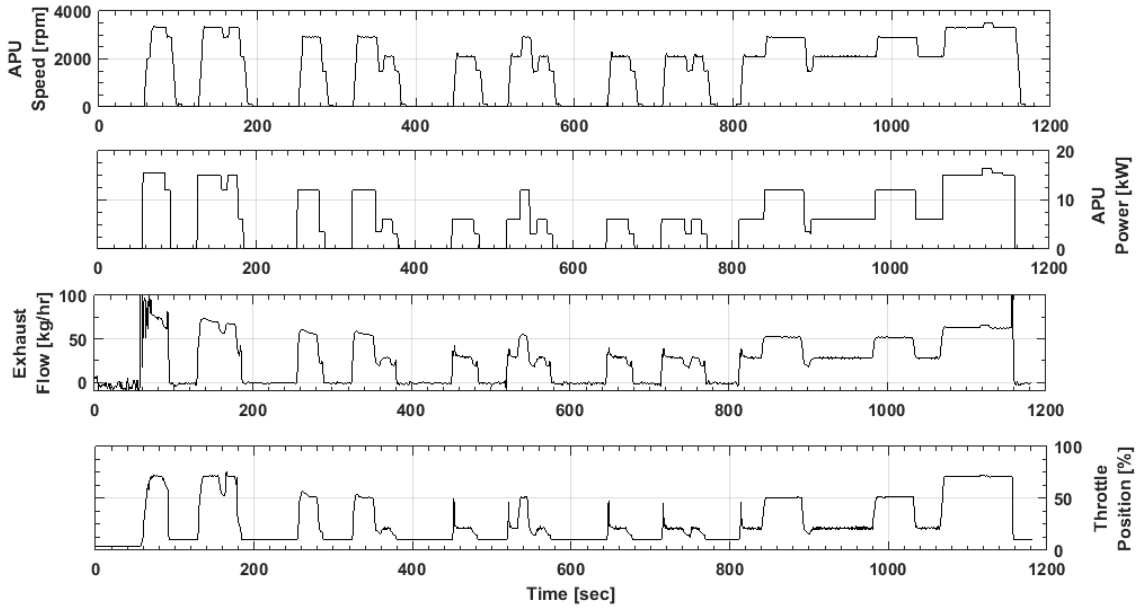

Figure 10-8 APU speed, power, engine throttle position and exhaust mass flow over NEDC

The cumulative emissions of NOx, THC and CO observed over the NEDC are at Figure 10-9. It is observed that NOx emissions show a rise prior to the catalyst light-off, then plateau off. However, there is a steep rise in emissions toward the end of the drive cycle when the APU speed is over 3000rpm and power demand is of the order of 15kW.

As regards THC emissions were concerned, see Figure 10-9, it was observed that the emissions rose steeply prior to catalyst light off, quickly exceeding the EU6 limits, and then plateau off. It was clear that while the conversion efficiency of the TWC with respect to THC was high over the drive cycle, there was a need to have a catalyst light off strategy to reduce THC emissions.

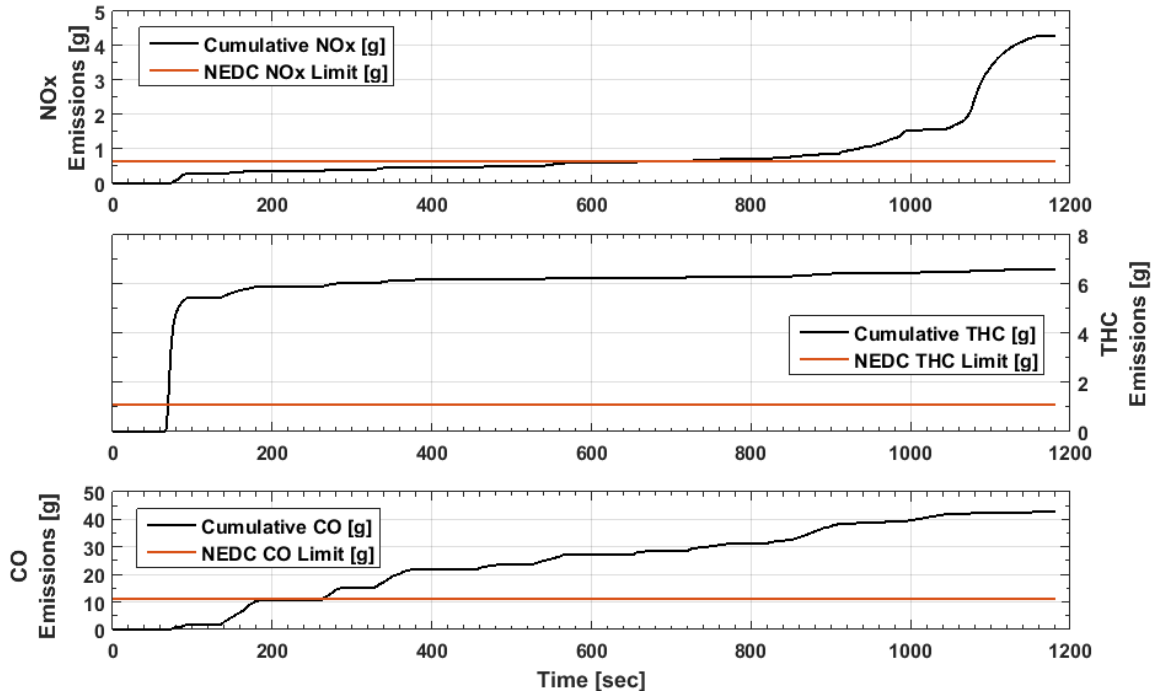

Figure 10-9 Cumulative NOx, THC and CO emissions measured over the NEDC which substantially exceed the NEDC legislative limits

As regards CO emissions, see Figure 10-9, little conversion appeared to be taking place over the NEDC. While the CO emissions during catalyst light-off do not exceed NEDC limits, as was seen with THC emissions, the cumulative emissions exceeded the EU6 emission limits as little conversion appears to occur in the catalyst over the drive cycle

Based on the results obtained, to improve the performance of the current TWC two strategies were explored to improve catalyst conversion. One was to reduce engine out emissions and second to speed up catalyst light-off.

10.15 Faster TWC Light-off

From the preceding section it was evident that there was a need to reduce THC emissions during start-up from cold if the present catalyst was to be considered suitable for the APU. Based on literature review, two strategies considered to be easily implementable without any additional hardware, with a calibration level access engine EMS was implementation of ignition timing retard and higher power demand at engine start [117].

Since the engine was to be used in a RE application, it offered the flexibility to start the engine at load and speeds higher than the conventional idle speed. Accordingly, the ignition retard was carried out at 2000rpm, 5kW power demand. Likewise, the power demand at engine start was also varied at 2000rpm.

The two ignition retard strategies were 10° and 20° retard relative to the normal timing. As regards power demand, it was varied between 4kW and 6kW to see the effect of catalyst light-off. Results of the experimental analysis that was undertaken are presented in Appendix E. Experimental analysis showed that while the light-off emissions decreased with spark timing retard and increasing power demand, the improved light-off was still not enough to meet cumulative EU6 legislative limits.

10.16 Additional control strategy to improve AFR control

Section 10.3.3 covers the influence of AFR on emission formation. Air fuel ratio has the greatest influence on untreated emissions. Further for a catalyst to be efficient a very tight control of the AFR around stoichiometric is necessary. The engine AFR with respect to APU speed and power demand were analysed, see Figure 10-10 and it was found that the AFR was showing large variation even during low frequency/amplitude throttle changes.

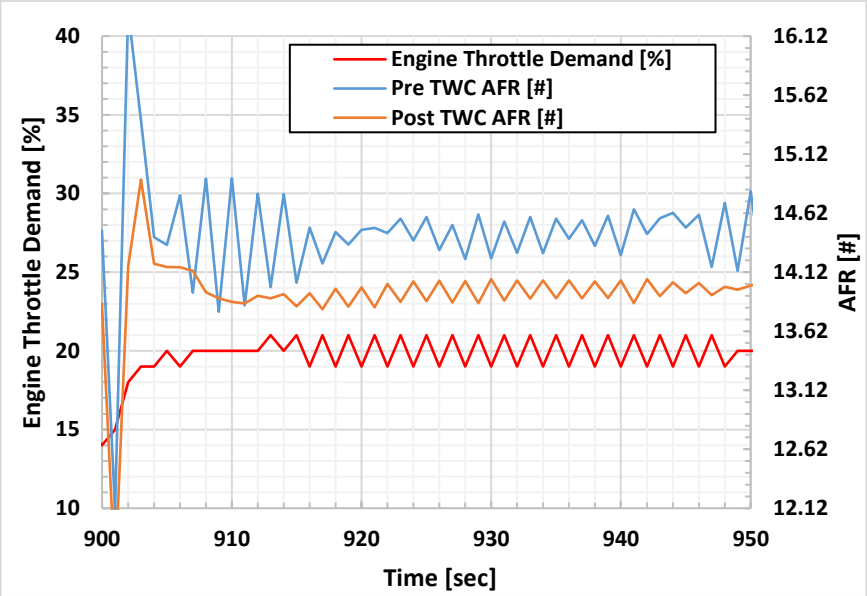

Figure 10-10 Air fuel ratio shows large variation to low frequency / amplitude throttle changes

Figure 10-11 shows the variation in pre TWC lambda vis-à-vis the engine lambda demand for minor throttle demand changes.

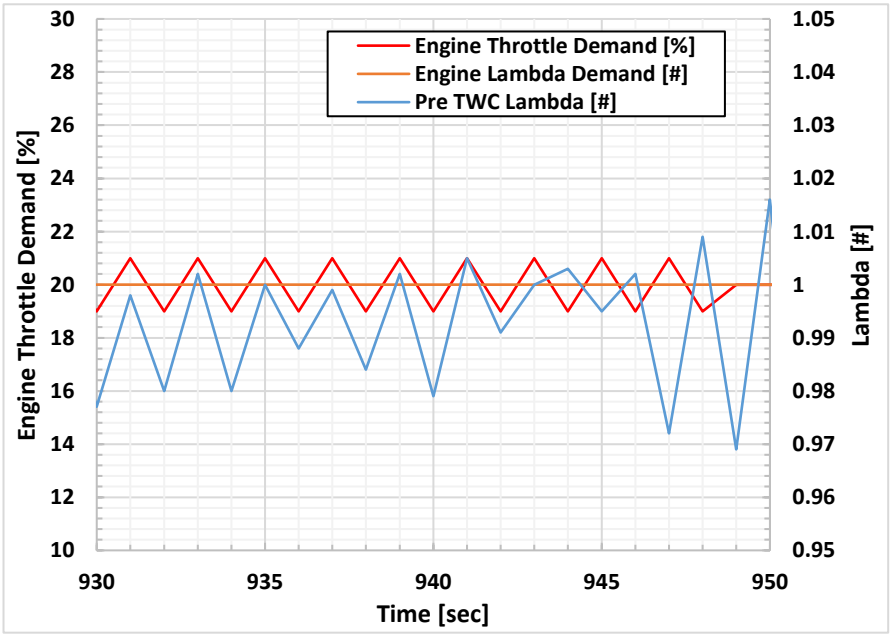

Figure 10-11 Variation in pre TWC lambda with minor changes in engine throttle, despite lambda demand remaining constant at 1

Though not part of this research, collaborative work was undertaken with University of Bristol to see the effect of a new AFR control structure for gasoline engines. Subsequent to the implementation of the new control strategy there was considerable improvement in the oscillations observed earlier, see Figure 10-12 below.

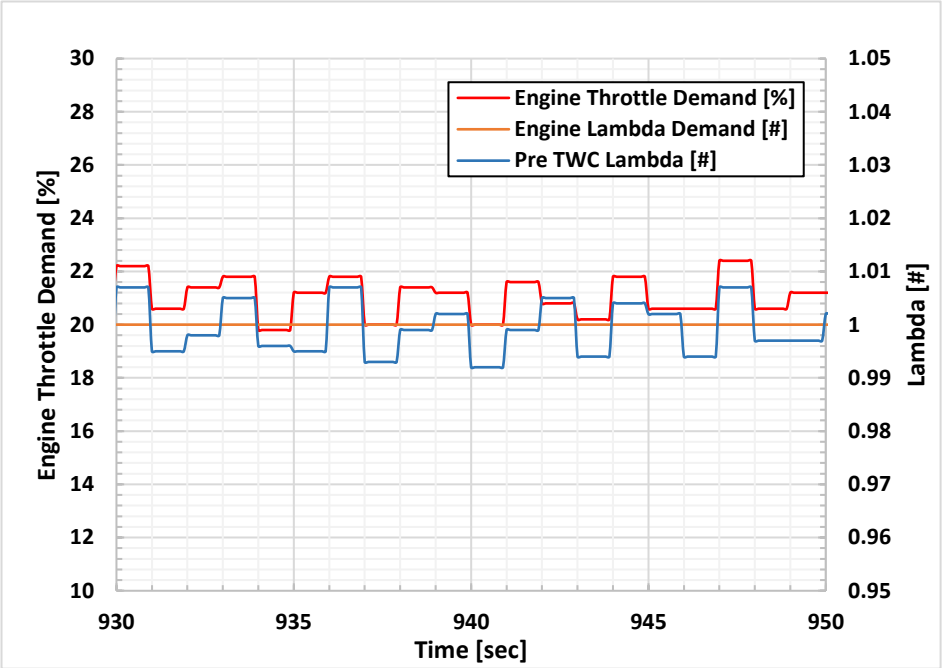

Figure 10-12 Improved lambda control after introduction of a dynamic estimator (reference TCST-2019-0325 – IEEE paper under preparation)

However, despite the improved AFR control, while there was a drop in the cumulative emissions, the NEDC limits continued to be exceeded for all three pollutants.

10.17 Analysis of TWC Performance

Since the purpose of the APU is to run at the more efficient engine regime, i.e. low BSFC, this was translating into operation at high emissions regions. Figure 10-13 shows that regions of low ESFC are also regions where the NOx emissions are the highest. Test results also showed that NOx breakthrough was a problem during steady

state as was evident during the highway driving phase of the NEDC, Figure 10-9. On the other hand, THC was more important during catalyst light-off phase. Similar behaviour was also expected with respect to CO, however test results showed little conversion over the NEDC.

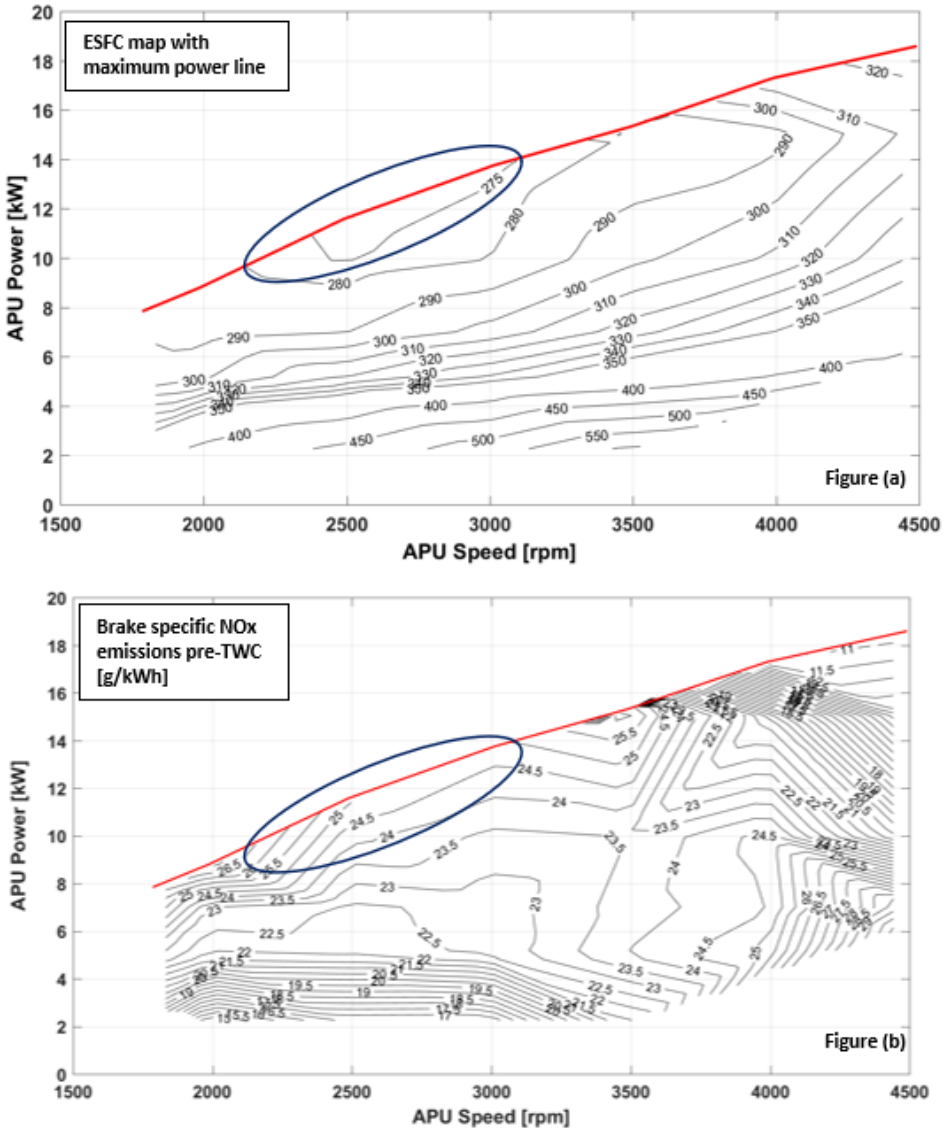

Figure 10-13 Regions of high ESFC (lower CO2 emissions), see figure (a) coincides with high NOx levels, see figure (b)

Based on the testing results, it was evident that the existing catalyst was not designed for high speed/load conditions. In order to meet requirements of operation at

optimum ESFC while keeping the CO, HC and NOx emissions within legislation limits, the existing TWC would require to be changed.

Aleksandrova et al had carried out considerable research in the design of a TWC for RE application and had reached similar conclusions. They have then examined the influence of several factors such as catalyst length and diameter, cell density, precious metal loading on engine emissions. They concluded that while precious metal loading had the most effect on NOx conversion, a combination of measures would be required to improve NOx conversion to meet legislative requirements. Modification of catalyst design parameters alone would not be enough for required NOx reduction and engine calibration (ignition timing retard or cooled EGR) would be also be required. Alternatively, the APU operating strategy would require to be reviewed to operate at lower speed/part load at the expense of higher fuel consumption [50, 133, 134].

As regards cold start emissions, Mercedes for their C-class hybrid had employed an electrically heated catalyst as early as 1998 to improve cold start emissions [59]. This would greatly solve the poor THC and CO emissions during engine start. Electrically heated catalyst technologies such as EMICAT® are now available which are conventional catalysts with an additional heating disc which provide for faster light-off during cold start phases [125]. However, these solutions come at a technical and financial cost which need to be taken into consideration.

10.18 Conclusion

The performance of a TWC similar in size and precious metal loading of the original vehicle TWC was analysed for treatment of the exhaust over the NEDC. Analysis showed that the conventional catalyst was unsuitable for high speed / high load operations which are the essential operating points of the APU from a power requirement standpoint. Further there is a requirement for a satisfactory catalyst light-

off strategy. Two strategies namely spark timing retard and higher power/speed engine start were examined to improve catalyst light-off. While an improvement was seen, it was not sufficient to meet EU6 NEDC legislation. To reduce steady state emissions, work was undertaken to improve AFR control, with limited success.

It was concluded that the original vehicle TWC was unsuitable for RE application and would require a multi-pronged strategy to meet legislative requirements. These would include factors such as catalyst length and diameter, cell density and precious metal loading. Further, satisfactory performance would need engine calibration to employ ignition retard or EGR. Electrically heated catalyst technologies such as EMICAT® are now available which would greatly improve cold start emissions but come at an additional cost. These were outside the scope of this research.

CHAPTER - 11
Conclusion and Further Work

This chapter concludes this research work and highlights the key findings and results. Research limitations and future work opportunities of this research are discussed.

11.1 Conclusion

This objective of this research was to carry out experimental analysis to support the development of an industry first low-cost auxiliary power unit for electric vehicles. A very low cost highly optimised production automotive engine was selected with an aim to optimise it in critical speed/load ranges for range extender application. The engine modifications included changes which were possible in normal production process to accrue the cost savings over development of a bespoke engine. Finally, during the integration process with the motor/generator and inverter unit, it was aimed to combine them in a single coolant loop to reduce parasitic losses as well as reduce overall package volume and weight without significant drop in overall system efficiency. Since the range extender was intended for replacing a portion of the high voltage battery, it was important to accrue the maximum benefit by keeping the overall package weight of the range extender to the minimum possible. This was the novelty of this research since the literature review revealed that though researchers have written about potential cost savings on combining of coolant circuits, there was no evidence that it had been implemented.

The modifications to the production engine included introduction of a new EMS, electronic throttle, bespoke manifolds, spark advance, AFR calibration and introduction of an EWP. Post modifications the BSFC was comparable with that of the production engine over the APU operating regime with reduction in overall package volume. A best BSFC of 245g/kWh was achieved at 2500rpm at WOT.

This compared favourably against the Lotus and MAHLE bespoke RE engines that have a BSFC of the order of 241g/kWh. Further, while this was a reasonably modest level of performance for a naturally aspirated gasoline engine compared to modern passenger car performance levels but considering the cost and packaging targets as well as being a 2-cylinder engine with two valves per cylinder, it was a satisfactory result.

Since one of the main objectives of the research was to run the APU in a single coolant loop, a thermal survey was carried out on the base engine to quantify the reduction in performance at lower oil and coolant temperatures. The engine BSFC increased by an average of less than 5% by reducing the oil and coolant temperature set point from 90°C to 60°C at full load across the operating regime.

On commissioning of the APU, the total dry weight of the APU was measured to be 81.5kg as against an initial target of 80kg. Experimental analysis showed the target best ESFC of <270g/kWh was exceeded under optimal temperature conditions of the engine, M/G and inverter unit in separate coolant circuits for the engine and generator, The APU produced a peak power of 22.78kW at 5100rpm. Best ESFC of 260g/kWh was measured at 2500rpm, and the ESFC remained below 270g/kWh across 2000 to 3500rpm at full load.

These exceeded the bespoke Mahle APU best ESFC of 283g/kWh. From 4000rpm to 4500rpm the ESFC was between 285g/kWh to 305g/kWh which was also within the target ESFC and were comparable to the Mahle ESFC of 292g/kWh. The specific performance of the APU at peak power was 270W/kg which was within the target of 250 to 313W/kg.

On combining the engine and M/G unit in a single coolant loop with oil and coolant temperature set points at 80°C there was a drop in APU power by an average of 4% with an increase of ESFC by circa of 2%. This could be attributed primarily to the higher operating temperature of the generator with the increase in the generator inlet coolant temperature set point from 35°C to 80°C. Although the engine efficiency also reduced with drop in coolant and oil temperature, however in the combined circuit the engine outlet coolant temperature continued to reach around 88°C. The oil gallery temperature was reduced by 10°C to 80°C which marginally increased the frictional losses because of increase in oil viscosity.

However, the combined loop provides greater flexibility of package installation and simplifies vehicle integration, with reduction in parasitic losses. It also reduces the overall package cost which was one of the objectives of this research. With subsequent improvement in bespoke generator internal cooling design, cutback of power at 4000–4500rpm could also be avoided which would improve APU power and ESFC in this range. This demonstrated that a balance can be achieved by trading engine efficiency for overall system efficiency and simplicity.

The performance of the APU was tested over the NEDC and it was demonstrated that the APU could successfully produce the necessary power as demanded by the VSC for a representative vehicle model. The APU consumed 0.716 litres of gasoline to complete the NEDC. This compared favourably against the 25kW APU with a bespoke engine developed for the Manza REEV which consumed 0.78 litres during NEDC.

As regards emission control to meet EU6 legislation, based on experimental analysis over the NEDC, it was shown that the original vehicle TWC was unsuitable for RE application. At the end of the drive cycle the emissions of THC, CO and NOx were 6.62g/km, 42.72g/km and 4.29g/km respectively, far exceeding the EU6 limits. Despite attempting strategies like ignition retard, higher power demand at engine start as well as improved AFR control, though some improvement was observed, it was not enough to meet EU 6 legislation.

A multi-pronged strategy would be required to meet legislative requirements. These would include factors such as catalyst length and diameter, cell density and precious metal loading. Further, satisfactory performance would need engine calibration efforts to employ techniques like ignition retard for faster catalyst light off.

11.2 Research Limitations

During this research study, certain unforeseen restrictions/factors emerged that led to some weaknesses and limitations that need to be highlighted.

Firstly, as mentioned in Chapter 3, the ambient cell temperature was manually controlled to 25±2°C by a switching on/off a set of exhaust fans. While all efforts were made to stay within the temperature limits, there were instances when the cell temperature exceeded the limits during testing. These excursions would have affected the results to a certain extent. Automated control of test cell temperature could not be implemented because of the expenditure involved and test cell downtime which could not be afforded in the project timeframe.

Another limitation during the experimental analysis being the development of the bespoke inlet manifold. While most testing / calibration was done with a 150mm runner length, however the final bespoke manifold that was introduced during the commissioning of the APU had runners of length 248mm. As per TMETC they were eventually governed by packaging criteria while trying to adhere as closely as possible to the experimental results. This reasoning was considered satisfactory as the aim of this collaborative project was to eventually introduce a low cost APU in the commercial market.

Likewise, during the APU testing, as defects / failures occurred in the prototype motor/generator unit and the inverter unit, Ashwoods Ltd would provide an improved version and not necessarily the changes in design / firmware /software were shared with the University research team. These changes would have also impacted the test results and it was not always possible to quantify the differences in test results.

11.3 Future Work

Presently the engine cooling strategy is based on controlling engine outlet temperature within a specified value. It is more desirable to control the engine cooling system based on the metal temperature rather than the coolant temperature. With knowledge of the limits on the temperature of the metal temperature, experimental work could be undertaken to optimise coolant flow rates to reduce the EWP parasitic power and improve overall efficiency. The additional instrumentation to the base engine would involve additional cost and would need to be factored in.

A study could also be undertaken on the thermal management of the overall APU package. Future work could include quantification of the heat dissipated by the oil, coolant and by cooling air. This would facilitate sizing of radiators for vehicle application.

The production engine was developed for Indian conditions and accordingly oil 15W-40 was selected. Since the research work has been undertaken with the APU being operated in European climatic conditions, a tribology study and experimental work could be undertaken to see the effect of various oils.

Currently new car registrations are based on the Tank to Wheel (TTW) assessment of CO_2. The Automotive Council roadmap has indicated that in the 2025-2030 timeframe the use of Well to Wheel is likely to appear. They have also indicated that over a longer timeframe they would consider the implications of Life Cycle Analysis (LCA) on energy and CO_2 consumption. This would include the energy and CO_2 consumption during manufacturing and disposal. Such an approach of looking at CO_2 assessment for compliance/taxation based on cradle to grave could pose a challenge to electrification of vehicles because of the high levels of embedded CO_2 in battery manufacture.

Keeping the above in mind, despite dropping battery prices, it is opined that a low cost APU designed to operate at distinct point(s) allowing optimisation of design to maximise efficiency would lend itself favourably to reducing battery size, since as mentioned in Chapter 2, 80km EV range enables electric driving in and around most major cities. The APU can be utilised outside of the cities / zero-tailpipe zones to provide propulsive power and slowly charge the battery, increasing battery life and efficiency. It also overcomes the driver's range anxiety. The additional range comes at a significantly lower penalty to a BEV, both in terms of mass and cost.

While the research briefly touched upon the APU usage strategy, with the advent of Geofenced operation and eHorizon technology, the driver would be able to drive in EV mode in certain areas (e.g. major cities, ZEVs, schools etc) and use the APU to charge the battery while on the motorway. For example, if a driver is traveling from London to Edinburgh via Birmingham, the battery provides all power for propulsion in the Geofenced city areas of London, Birmingham and Edinburgh producing zero tailpipe emissions. Once the vehicle is outside the Geofenced zone, the APU could provide all the propulsive power plus power to trickle charge the traction battery since high engine efficiency produces low tailpipe emissions.

To summarise, the introduction of an APU in a BEV maintains the BEV's performance/driveability and at the same time reduces reliance on charging infrastructure growth. It facilitates a lower cost and mass production system through battery size reduction. While this research has focused on a gasoline engine as prime mover for the APU, various energy generation technology opportunities could emerge through the decoupling of operating envelopes. The total cost of ownership could further improve if fuel prices reduce as supply exceeds demand. It also improves both the low temperature and high temperature operating capability of the electric vehicle.

References

1. Dunkan Kay, Nik Hill, and Newman, D., *Powering Ahead - The future of low-carbon cars and fuels*. 2013.

2. Agarwal, A., Lewis, A., Akehurst, S., Brace, C., et al., "Development of a Low Cost Production Automotive Engine for Range Extender Application for Electric Vehicles," presented at, 2016, doi: 10.4271/2016-01-1055, (http://dx.doi.org/10.4271/2016-01-1055).

3. Turner, J., Blake, D., Moore, J., Burke, P., et al., "The Lotus Range Extender Engine," *SAE Int. J. Engines,* 3(2): 318-351, 2010, doi:10.4271/2010-01-2208.

4. Bassett, M., "Range Extenders," *Engineering & Technology Reference*, 2014, doi:10.1049/etr.2014.0039.

5. Mattarelli, E., Rinaldini, C.A., Cantore, G., and Agostinelli, E., "Comparison between 2 and 4-Stroke Engines for a 30 kW Range Extender," *SAE Int. J. Alt. Power.,* 4(1): 67-87, 2014, doi:10.4271/2014-32-0114.

6. Kirkpatrick, G., *LowCAP – Target Specification Document*. 2014, LowCAP Consortium.

7. Bassett, M., Hall, J., OudeNijeweme, D., Darkes, D., et al., "The Development of a Dedicated Range Extender Engine," presented at, 2012, doi: 10.4271/2012-01-1002, (http://dx.doi.org/10.4271/2012-01-1002).

8. "SAE Surface Vehicle Information Report J1715," 2014.

9. Ribeiro, B., Brito, F., and Martins, J., "A Survey on Electric/Hybrid Vehicles," presented at, 2010, doi: 10.4271/2010-01-0856, (http://dx.doi.org/10.4271/2010-01-0856).

10. Mock, P. and Yang, Z., *Driving Electrification-A Global Comparison of Fiscal Incentive Policy for Electric Vehicles*. 2014, The International Council on Clean Transportation.

11. Arbib, J. and Seba, T., *Rethinking Transortation 2020-2030*. 2017, RethinkX.

12. *Jaguar I-Pace range, battery & charging*. 2019 [cited 2019 27 July 2019]; Available from: https://www.drivingelectric.com/jaguar/i-pace/410/jaguar-i-pace-range-battery-charging.

13. France-Presse, A. *Germany to give €1bn subsidy to boost electric car sales*. 2016 [cited 2016 07 May 2016]; Available from: http://www.theguardian.com/world/2016/apr/28/germany-subsidy-boost-electric-car-sales.

14. *On a charge*, in *The Economist*. 2016, The Economist.

15. *Electric cars set to get road priority in clean air zones*. 2016 [cited 2016 15 Oct 2016]; Available from: http://www.bbc.co.uk/news/uk-37654584.

16. *Charging Ahead*, in *The Economist*. 2016, The Economist: Shanghai.

17. *Wireless electric car charging gets cash boost*. 2019 [cited 2019 17 August 2019]; Available from: https://www.bbc.co.uk/news/business-48913028.

18. *Ultra Low Emission Zone*. 2019 [cited 2019 22 July 2019]; Available from: https://tfl.gov.uk/modes/driving/ultra-low-emission-zone.

19. *Car firms to build electric charge network*. 2016 [cited 2016 09 Feb 2017]; Available from: http://www.bbc.co.uk/news/technology-38147478.

20. *Charge of the battery brigade - An infrastructure for charging electric vehicles takes shape*, in *The Economist*. 2017, The Economist.

21. Tajima, T., Noguchi, W., and Aruga, T., "Study of a Dynamic Charging System for Achievement of Unlimited Cruising Range in EV," presented at, 2015, doi: 10.4271/2015-01-1686, (http://dx.doi.org/10.4271/2015-01-1686).

22. Gerrard, B. *2018 Was A Huge Year For Electric Vehicles (In Charts)*. 2019 [cited 2019 17 August 2019]; Available from: https://medium.com/@braydeng/2018-was-a-huge-year-for-electric-vehicles-in-charts-b6aad055bdff.

23. *Global sales for electric vehicles to reach 2.8 million*. 2019 [cited 2019 22 July 2019]; Available from: https://www.smart-energy.com/industry-sectors/electric-vehicles/evs-frost-sullivan-sales-2019/.

24. *Electric cars are set to arrive far more speedily than anticipated*, in *The Economist*. 2017, www.economist.com.

25. Ribau, J., Silva, C., Brito, F.P., and Martins, J., "Analysis of four-stroke, Wankel, and microturbine based range extenders for electric vehicles," *Energy Conversion and Management,* 58: 120-133, 2012, doi:http://dx.doi.org/10.1016/j.enconman.2012.01.011.

26. *RON 95 Reference fuel certificate of analysis*. 2014, Petrochem Carless.

27. Sandy Thomas, C.E., "How green are electric vehicles?," *International Journal of Hydrogen Energy,* (37): 10, 2012, doi:10.1016/j.ijhydene.2011.12.118.

28. *A plug for the battery*. The Economist 2016 27 Jan 2016; 16 Jan 2016:[Available from: http://www.economist.com/news/leaders/21688394-virtual-reality-and-artificial-intelligence-are-not-only-technologies-get-excited-about?frsc=dg%7Cc.

29. *An increasingly precious metal*. The Economist 2016 16 Jan 2016; Available from: http://www.economist.com/news/business/21688386-amid-surge-demand-rechargeable-batteries-companies-are-scrambling-supplies?frsc=dg%7Cc.

30. *The death of the internal combustion engine*, in *The Economist*. 2017, The Economist.

31. West, K., *Carmakers' electric dreams depend on supplies of rare minerals*, in *The Guardian*. 2017, The Guardian.

32. *What if China corners the cobalt market?*, in *The Economist*. 2018, The Economist.

33. Birch, S. *Nissan Europe and partners form battery R&D venture*. 2016 [cited 2016 29 Feb 2016]; Available from: http://articles.sae.org/14604/.

34. Cobb, J. *Chevy Bolt Production Confirmed For 2016*. 2015 [cited 2016 03 June 2016]; Available from: http://www.hybridcars.com/chevy-bolt-production-confirmed-for-2016/.

35. Cole, J. *GM: Chevrolet Bolt Arrives In 2016, $145/kWh Cell Cost, Volt Margin Improves $3,500*. 2015 [cited 2016 03 June 2016]; Available from: http://insideevs.com/gm-chevrolet-bolt-for-2016-145kwh-cell-cost-volt-margin-improves-3500/#comments.

36. Jain, S., *Emerging Trends in Battery Technology*, in *Auto Tech Review*. 2017, www.autotechreview.com: New Delhi. p. 3.

37. Hofstetter, D., *Demystifying Electric Vehicles, From Market Adoption to Distributed Storage*. 2011.

38. *Better Place: what went wrong for the electric car startup?*, in *The Guardian*. 2013, The Garadian.

39. Evans, R. *Deploying Electric Vehicles in Fleets*. [cited 2016 03 March 2016]; Available from: http://evfleetworld.co.uk/news/2014/Sep/Deploying-Electric-Vehicles-in-Fleets/0438016255.

40. Garrick, D. *Car2Go switching electric cars to gas*. 2016 [cited 2016 21 March 2015]; Available from: http://www.sandiegouniontribune.com/news/2016/mar/16/car-share-car2go-fleet-gas-electric/?#article-copy.

41. Duhon, A.N., Sevel, K.S., Tarnowsky, S.A., and Savagian, P.J., "Chevrolet Volt Electric Utilization," *SAE Int. J. Alt. Power.,* 4(2): 269-276, 2015, doi:10.4271/2015-01-1164.

42. *Extreme Temperatures Affect Electric Vehicle Driving Range, AAA Says*. [cited 2016 10 March 2016]; Available from: http://newsroom.aaa.com/2014/03/extreme-temperatures-affect-electric-vehicle-driving-range-aaa-says/.

43. Zhang, S.S., Xu, K., and Jow, T.R., "The low temperature performance of Li-ion batteries," *Journal of Power Sources,* 115(1): 137-140, 2003, doi:10.1016/S0378-7753(02)00618-3.

44. Grebe, U.D. and Nitz, L.T., *Voltec - The Propulsion System for Chevrolet Volt and Opel Ampera*, in *MTZ Worldwide*. 2011.

45. Klippenstein, M. *Nissan Leaf, Chevy Volt Range Loss In Winter: New Data From Canada*. 2013 02 March 2016]; Available from:

http://www.greencarreports.com/news/1089160_nissan-leaf-chevy-volt-range-loss-in-winter-new-data-from-canada.

46. Weissler, P. *Leaf incorporates features to prevent range anxiety*. 2011 [cited 2016 02 March 2016]; Available from: http://articles.sae.org/9212/.

47. Voelcker, J., *Nissan Tests New Heat-Resistant Battery For Leaf Electric Car*. 2013, Green Car Reports.

48. Thorn, K. *Range Extender Concepts*. 2012 [cited 2016 11 March 2016]; Available from: https://www.fh-zwickau.de/fileadmin/ugroups/ftz/Konferenzen/Ami_Kongress_2012/Thorn_VCC_Range_Extender_Presentation_Leipzig_2012_final.pdf.

49. Fraidl, G.K., Beste, F., Kapus, P.E., Korman, M., et al., "Challenges and Solutions for Range Extenders - From Concept Considerations to Practical Experiences," presented at, 2011, doi: 10.4271/2011-37-0019, (http://dx.doi.org/10.4271/2011-37-0019).

50. Powell, N., Little, M., Reeve, J., Baxter, J., et al., *Auxiliary power units for range extended electric vehicles*, in *Sustainable Vehicle Technologies: Driving the green agenda*. 2012, Woodhead Publishing: Cambridge. p. 225-236.

51. Christian Hubmann, F.B., Hubert Friedl, Wolfgang Schöffmann, "Single Cylinder 25kW Range Extender as Alternative to a Rotary Engine Maintaining High Compactness and NVH Performance," *SAE International*, 2013, doi:2013-32-9132.

52. Fischer, R., Fraidl, G., Hubmann, C., KAPUS, P., et al., "Range Extender Module. Enabler for Electric Mobility," *ATZ AUTOTECHNOLOGY,* VOL 9: 7, 2009.

53. Pischinger, M., Tomazic, D., Wittek, K., Esch, H.-J., et al., "A Low NVH Range-Extender Application with a Small V-2 Engine - Based on a New Vibration Compensation System," presented at, 2012, doi: 10.4271/2012-32-0081, (http://dx.doi.org/10.4271/2012-32-0081).

54. Bassett, M., Fraser, N., Brooks, T., Taylor, G., et al., "A Study of Fuel Converter Requirements for an Extended-Range Electric Vehicle," *SAE Int. J. Engines,* 3(1): 631-654, 2010, doi:10.4271/2010-01-0832.

55. Rogge, M., Lehner, and Sauer, D., *Operating Strategies for a Range Extender Used in Battery Electric Vehicles*. 2013. 1-5.

56. Bhiwapurkar, N. and Ganti, V., *Comparison of On-Board Charging Strategies for Range-Extender Hybrid Vehicles with Lead-Acid Batteries*. 2013. 1-5.

57. TJ Barlow, S.L., IS McCrae, PG Boulter, *A reference book of driving cycles for use in the measurement of road vehicle emissions*. 2009, TRL Limited.

58. Tulpule, P., Marano, V., and Rizzoni, G., *Effects of different PHEV control strategies on vehicle performance*. 2009. p. 3950-3955.

59. Abthoff, J., Antony, P., Krämer, M., and Seiler, J., "The Mercedes-Benz C-Class Series Hybrid," presented at, 1998, doi: 10.4271/981123, (http://dx.doi.org/10.4271/981123).

60. Mattarelli, E., Rinaldini, C.A., and Cantore, G., "CFD optimization of a 2-stroke range extender engine," *International Journal of Automotive Technology,* 16(3): 351-369, 2015, doi:10.1007/s12239-015-0037-y.

61. Bassett, M., Thatcher, I., Bisordi, A., Hall, J., et al., "Design of a Dedicated Range Extender Engine," presented at, 2011, doi: 10.4271/2011-01-0862, (http://dx.doi.org/10.4271/2011-01-0862).

62. Atzwanger, M., Hubmann, C., Schoeffmann, W., Kometter, B., et al., "Two-Cylinder Gasoline Engine Concept for Highly Integrated Range Extender and Hybrid Powertrain Applications," 2010-32-0130, 2010, doi: 10.4271/2010-32-0130, (http://dx.doi.org/10.4271/2010-32-0130).

63. Boretti, A., "Electric vehicles with small batteries and high‐efficiency on‐board electricity production," *Energy Storage,* 1, 2019, doi:10.1002/est2.75.

64. *Mazda Rotary Engine to Return as EV Range-Extender*. 2018 [cited 2019 14/09/2019]; Available from: https://www.mazda-press.com/eu/news/2018/mazda-rotary-engine-to-return-as-ev-range-extender-/.

65. Longee, H., "The Capstone MicroTurbineä as a Hybrid Vehicle Energy Source," presented at, 1998, doi: 10.4271/981187, (http://dx.doi.org/10.4271/981187).

66. Mackay, R., "Gas Turbine Generator Sets for Hybrid Vehicles," presented at, 1992, doi: 10.4271/920441, (http://dx.doi.org/10.4271/920441).

67. Mackay, R. and Kesseli, J., "High Efficiency Vehicular Gas Turbines," presented at, 2005, doi: 10.4271/2005-01-3461, (http://dx.doi.org/10.4271/2005-01-3461).

68. Mackay, R., "Practical Vehicular Gas Turbines," presented at, 2001, doi: 10.4271/2001-01-2541, (http://dx.doi.org/10.4271/2001-01-2541).

69. *Jaguar Introduces C-X75 Gas Micro-turbine Extended Range Electric Vehicle Concept*. 2010 02 March 2016]; Available from: http://www.greencarcongress.com/2010/09/cx75-20100930.html.

70. Holloway, H., *Plug and Play*, in *Autocar*. 2015, Autocar. p. 4.

71. *Wrightspeed unveils new turbine range extender for medium- and heavy-duty electric powertrains; 30% more efficient than current microturbine generators*. 2015; Available from: http://www.greencarcongress.com/2015/05/wrightspeed.html.

72. Pollard, T. *Techrules tries to rewrite the rules: new TREV supercar revealed*. 2016 [cited 2016 24 Apr 16]; Available from: http://www.carmagazine.co.uk/car-news/motor-shows-events/geneva/2016/techrules-tries-to-rewrites-the-rules-the-new-trev-supercar/#.Vx0ioAiB4_c.email.

73. *An Independent Report on the Future of the Automotive Industry in the UK*. 06 May 2009, New Automotive Industry Growth Team (NAIGT): UK.

74. Warburton, A., Mossop, D., Burslem, B., Rama, P., et al., "Development of an Evaporatively Cooled Hydrogen Fuel Cell System and its Vehicle Application," presented at, 2013, doi: 10.4271/2013-01-0475, (http://dx.doi.org/10.4271/2013-01-0475).

75. Chubbock, S. and Clague, R., "Comparative Analysis of Internal Combustion Engine and Fuel Cell Range Extender," *SAE Int. J. Alt. Power.,* 5(1): 175-182, 2016, doi:10.4271/2016-01-1188.

76. Phillips, T. *BMW i3 range extender*. 2013 [cited 2016 09 March 2013]; Available from: http://www.autoexpress.co.uk/bmw/i3/66751/bmw-i3-range-extender.

77. *MetroCab*. [cited 2016 09 March 2016]; Available from: http://www.newmetrocab.com.

78. Trego, L. *Compact range extender*. 2012 [cited 2016 09 March 2016]; Available from: http://articles.sae.org/10675/.

79. *EP Tender*. [cited 2016 09 March 2016]; Available from: http://www.eptender.com/.

80. Mildenhall, O. *Mazda 2 EV gets new rotary range extender engine*. 2013 [cited 2016 10 March 2016]; Available from: http://www.autoexpress.co.uk/mazda/2/84660/mazda-2-ev-gets-new-rotary-range-extender-engine.

81. *2011 Volt*. [cited 20`6 07 May 2016]; Available from: http://web.archive.org/web/20110223173940/http://www.chevrolet.com/volt/features-specs/.

82. Stacey Stewart, Brian Gross, and Weldon, P. *Polaris Range EXtender Technology (REX)*. 2011 [cited 2016 11 March 2016]; Available from: http://www.dtic.mil/ndia/2011power/Session23_12836Stewart.pdf.

83. *On the way to electric vehicles boosted range extender*. [cited 2016 11 March 2016]; Available from: http://www.getrag.com/media/products/extendeddrive/2ret300/Broschuere_Range_Extender_EN_052010.pdf.

84. Krause, W. and Spies, K.H., "Dynamic Control of the Coolant Temperature for a Reduction of Fuel Consumption and Hydrocarbon Emission," presented at, 1996, doi: 10.4271/960271, (http://dx.doi.org/10.4271/960271).

85. Willumeit, H.P., Steinberg, P., HÖTting, H., Scheibner, B., et al., "New temperature control criteria for more efficient gasoline engines," presented at, 1984, doi: 10.4271/841292, (http://dx.doi.org/10.4271/841292).

86. Pang, H.H. and Brace, C.J., "Review of engine cooling technologies for modern engines," *Proceedings of the Institution of Mechanical Engineers, Part*

D: Journal of Automobile Engineering, 218(11): 1209-1215, 2004, doi:10.1243/0954407042580110.

87. *Technical training W20 Engine*. 2103, BMW Group.

88. *The Chevrolet Volt Cooling/Heating Systems Explained*. 2010 [cited 2019 27 July 2019]; Available from: https://gm-volt.com/2010/12/09/the-chevrolet-volt-coolingheating-systems-explained/.

89. Brace, C.J., Burnham-Slipper, H., Wijetunge, R.S., Vaughan, N.D., et al., "Integrated Cooling Systems for Passenger Vehicles," presented at, 2001, doi: 10.4271/2001-01-1248, (http://dx.doi.org/10.4271/2001-01-1248).

90. Staunton, R.H., Hsu, J.S., and Starke, M.R., *Barriers to the Application of High-Temperature Coolants in Hybrid Electric Vehicles*, E. Ee Usdoe - Office Of Energy and E. Renewable, Editors. 2006, Oak Ridge National Laboratory, Power Electronics and Electric Machinery Research Facility.

91. Bassett, M., Hall, J., Kennedy, G., Cains, T., et al., "The Development of a Range Extender Electric Vehicle Demonstrator," presented at, 2013, doi: 10.4271/2013-01-1469, (http://dx.doi.org/10.4271/2013-01-1469).

92. Morris, A.S. and Langari, R., *Measurement and Instrumentation : Theory and Application*. 2012.

93. Chappell, E.C., *Improving the precision of vehicle fuel economy testing on a chassis dynamometer*, in *Department of Mechanical Engineering*. 2015, University of Bath: UK.

94. Basshuysen, R.V. and Schaefer, F., *Internal Combustion Engine Handbook*. 2nd ed. 2016: SAE International.

95. Standardisation, I.O.f., "ISO 1585 - Road vehicles - Engine test Code - Net power," 1992.

96. Martyr, A. and Plint, M., *Engine Testing*. 2012: Butterworth Heinemann. 601.

97. Chappell, E., Brace, C., and Ritchie, C., "The control of chassis dynamometer fuel consumption testing noise factors and the use of response modelling for validation of test repeatability," *Proceedings of the Institution of Mechanical*

Engineers, Part D: Journal of Automobile Engineering, 227(6): 853-865, 2013, doi:10.1177/0954407012469557.

98. Heisler, H., *Advanced Engine Technology* 1995: Butterworth-Heinemann

99. Heywood, J.B., *Internal combustion engine fundamentals*. 1988, London: London : McGraw-Hill.

100. Engelman, H., "Design of a Tuned Intake Manifold," *ASME*: 8, 1973.

101. Tabaczynski, R.J., "Effects of Inlet and Exhaust System Design on Engine Performance," presented at, 1982, doi: 10.4271/821577, (http://dx.doi.org/10.4271/821577).

102. Vorum, P., "Short Pipe Manifold design for Four-Stroke Engine," *American Society of Mechanical Engineers*, 1976, doi:76-WA/DGP-4.

103. Gandhi, Y., *LowCAP Intake and Exhaust Manifold Design Study*. 2014, Tata Motors European Technical Centre: UK.

104. Stone, R., *Introduction to internal combustion engines*. 4th ed. 2012, Basingstoke: Basingstoke : Palgrave Macmillan.

105. *nano e-Workshop Manual*. Tata Motors. p. 857.

106. McGeehan, J.A., "A Literature Review of the Effects of Piston and Ring Friction and Lubricating Oil Viscosity on Fuel Economy," presented at, 1978, doi: 10.4271/780673, (http://dx.doi.org/10.4271/780673).

107. Rosenberg, R.C., "General Friction Considerations for Engine Design," presented at, 1982, doi: 10.4271/821576, (http://dx.doi.org/10.4271/821576).

108. Zaidi Mohd. RIPIN, H.G.-B., Mohd. Zulkifly ABDULLAH, "Frictional Analysis of a Small Two-Stroke Utility Engine via Tear-Down Testing," *SAE*, 2007.

109. Viscopedia. *Engine Oil*. [cited 2016 09/04/2016]; Available from: http://www.viscopedia.com/viscosity-tables/substances/engine-oil/#c1330.

110. Agarwal, A., Rodrigues, L., Liu, D., Lewis, A., et al., "Thermal Management of a Low Cost Range Extender for Electric Vehicles," presented at 6th Hybrid and Electric Vehicles Conference (HEVC 2016), London, UK, 2-3 Nov. 2016, 2016, doi: 10.1049/cp.2016.0976, (https://digital-library.theiet.org/content/conferences/10.1049/cp.2016.0976).

111. André, M., "The ARTEMIS European driving cycles for measuring car pollutant emissions," *Science of the Total Environment,* 334: 73-84, 2004, doi:10.1016/j.scitotenv.2004.04.070.

112. Peters, S. *All new emissions testing cycle comes into force*. 2017 [cited 2017 10 September 2017]; Available from: http://www.enginetechnologyinternational.com/news.php?NewsID=87182.

113. Rodrigues, M., King, S., Scott, D., and Wang, D., "Advanced Energy Management Strategies for Range Extended Electric Vehicle," presented at, 2015, doi: 10.4271/2015-26-0121, (https://doi.org/10.4271/2015-26-0121).

114. Rodrigues, M., *Development and optimisation of energy management strategies for Manza REEV*. 2015, Tata Motors Eurpoean Techncal Centre. p. 110.

115. Cecotti, M., *NEDC drive cycle - corrections not needed*, A. Agarwal, Editor. 2016,

116. Kummer, J.T., "Catalysts for automobile emission control," *Progress in Energy and Combustion Science,* 6(2): 177-199, 1980, doi:http://dx.doi.org/10.1016/0360-1285(80)90006-4.

117. Chan, S.H., "A practical approach for rapid catalyst light-off by means of strategic engine control," *Proceedings of the Institution of Mechanical Engineers, Part D: Journal of Automobile Engineering,* 215(4): 545-555, 2001, doi:10.1243/0954407011528149.

118. Adachi, M. and Nakamura, H., *Engine Emissions Measurement Handbook*. 2014: sae.org.

119. Robinson, J.W. *Understanding Catalysts - A Handbook for the User*. [cited 2016 30 August 2016]; Available from: http://www.catalyticcombustion.com/documents/misc/en-us/catalyst101bulletinseries1-19.pdf.

120. Mudd, C., *Pre CAT HC*, A. Agarwal, Editor. 2016,

121. Kaidantzis, P., Rasmussen, P., Jensen, M., Vesterholm, T., et al., "Robust, Self-Calibrating Lambda Feedback for Sl Engines," presented at, 1993, doi: 10.4271/930860, (http://dx.doi.org/10.4271/930860).

122. Please, C.P., Hagan, P.S., and Schwendeman, D.W., "Light-Off Behavior of Catalytic Converters," *SIAM Journal on Applied Mathematics,* 54(1): 72-92, 1994.

123. Craig, A., Warkins, J., Aravelli, K., Moser, D., et al., "Low Cost LEV-III, Tier-III Emission Solutions with Particulate Control using Advanced Catalysts and Substrates," *SAE Int. J. Engines,* 9(2): 1276-1288, 2016, doi:10.4271/2016-01-0925.

124. Hallgren, B.E., *Impact of Retarded Spark Timing on Engine Combustion, Hydrocarbon Emissions, and Fast Catalyst Light-Off*. 2005, Massachusetts Institute of Technology.

125. Klein, B. and Malwald, O., *48 Volt Technology*. 2016.

126. Ebner, A., Winkler, F., Abart, M., Luz, R., et al., "Study of Possible Range Extender Concepts with Respect to Future Emission Limits," presented at, 2010, doi: 10.4271/2010-32-0129, (http://dx.doi.org/10.4271/2010-32-0129).

127. *Delphi Worldwide Emissions Standards Passenger Cars and Light Duty*. 2016 22 July 2016; 104].

128. *Regulation No 83 of the Economic Commission for Europe of the United Nations (UNECE), Revision 4*, U. Nations, Editor. 2011.

129. Kirkpatrick, G., *PO14599 BTB Exhausts*, J. Ellis, Editor. 2016,

130. Mudd, C., *PO14599 BTB Exhausts, technical information request*, J. Ellis, Editor. 2016,

131. Kirkpatrick, G., *LowCAP Catalyst*, A. Agarwal, Editor. 2017,

132. Brück, R., Diewald, R., Hirth, P., and Kaiser, F.-W., "Design Criteria for Metallic Substrates for Catalytic Converters," presented at, 1995, doi: 10.4271/950789, (https://doi.org/10.4271/950789).

133. Aleksandrova, S., Benjamin, S., and Okhuahesogie, F., *Aftertreatment for Range Extended Electric Vehicles*. 2011, Coventry University: United Kingdom. p. 36.

134. Aleksandrova, S. and Benjamin, S., *Using Wave for reducing emissions for REEV application*. 2011, Coventry University: United Kingdom. p. 25.

Appendix A

Test Matrix for Thermal Survey of Base Production Engine

Test #	Engine Speed rpm	Torque Nm	Coolant Outlet °C	Oil Gallery °C
1	2000	10	110	110
2	2000	24Nm	110	110
3	2000	WOT	110	110
4	3000	24Nm	110	110
5	3000	WOT	110	110
6	4000	24Nm	110	110
7	4000	WOT	110	110
8	5000	24Nm	110	110
9	5000	WOT	110	110
10	2000	10	90	110
11	2000	24Nm	90	110
12	2000	WOT	90	110
13	3000	24Nm	90	110
14	3000	WOT	90	110
15	4000	24Nm	90	110
16	4000	WOT	90	110
17	5000	24Nm	90	110
18	5000	WOT	90	110
19	2000	10	60	110
20	2000	24Nm	60	110
21	2000	WOT	60	110
22	3000	24Nm	60	110
23	3000	WOT	60	110
24	4000	24Nm	60	110
25	4000	WOT	60	110
26	5000	24Nm	60	110
27	5000	WOT	60	110
28	2000	10	110	90
29	2000	24Nm	110	90
30	2000	WOT	110	90
31	3000	24Nm	110	90
32	3000	WOT	110	90
33	4000	24Nm	110	90
34	4000	WOT	110	90
35	5000	24Nm	110	90

Test #	Engine Speed rpm	Torque Nm	Coolant Outlet °C	Oil Gallery °C
36	5000	WOT	110	90
37	2000	10	90	90
38	2000	24Nm	90	90
39	2000	WOT	90	90
40	3000	24Nm	90	90
41	3000	WOT	90	90
42	4000	24Nm	90	90
43	4000	WOT	90	90
44	5000	24Nm	90	90
45	5000	WOT	90	90
46	2000	10	60	90
47	2000	24Nm	60	90
48	2000	WOT	60	90
49	3000	24Nm	60	90
50	3000	WOT	60	90
51	4000	24Nm	60	90
52	4000	WOT	60	90
53	5000	24Nm	60	90
54	5000	WOT	60	90
55	2000	10	110	60
56	2000	24Nm	110	60
57	2000	WOT	110	60
58	3000	24Nm	110	60
59	3000	WOT	110	60
60	4000	24Nm	110	60
61	4000	WOT	110	60
62	5000	24Nm	110	60
63	5000	WOT	110	60
64	2000	10	90	60
65	2000	24Nm	90	60
66	2000	WOT	90	60
67	3000	24Nm	90	60
68	3000	WOT	90	60
69	4000	24Nm	90	60
70	4000	WOT	90	60
71	5000	24Nm	90	60
72	5000	WOT	90	60
73	2000	10	60	60
74	2000	24Nm	60	60
75	2000	WOT	60	60
76	3000	24Nm	60	60

Test	Engine Speed	Torque	Coolant Outlet	Oil Gallery
#	rpm	Nm	°C	°C
77	3000	WOT	60	60
78	4000	24Nm	60	60
79	4000	WOT	60	60
80	5000	24Nm	60	60
81	5000	WOT	60	60

Appendix B

Maximum Continuous Power with Change in Generator Coolant Inlet Temperature

(Engine Coolant Outlet and Oil Gallery Set Point 90°C)

	4000 RPM					4500 RPM					5100 RPM				
Generator Inlet Tempr	Maximum Continuous Power	ESFC	Motor Tempr	IGBT Tempr	Inverter Tempr	Maximum Continuous Power	ESFC	Motor Tempr	IGBT Tempr	Inverter Tempr	Maximum Continuous Power	ESFC	Motor Tempr	IGBT Tempr	Inverter Tempr
[°C]	[kW]	[g/kWhr]	[°C]	[°C]	[°C]	[kW]	[g/kWhr]	[°C]	[°C]	[°C]	[kW]	[g/kWhr]	[°C]	[°C]	[°C]
60	18.7	304	116	60	80	20.7	305	114	60	79	21.8	329	109	57	78
70	18.4	307	119	72	89	20.7	311	127	71	90	21.9	329.5	117	70	89
80	17.6*	287	129	80	100	17.9*	310	116	78	99	22.5	325.9	127	80	100
90	<2 kW*	680	85	83	102	1.5*	969	83	83	100	1.5*	951	87	83	101

* Indicates that power had to be cutback to keep inverter temperature within limits.

Appendix C

Maximum Continuous Power with Change in Generator Coolant Inlet, Engine Coolant Outlet and Oil Gallery Temperature

	4000 RPM					4500 RPM					5100 RPM				
Coolant Tempr and Oil Gallery Tempr	Maximum Continuous Power	ESFC	Motor Tempr	IGBT Tempr	Inverter Tempr	Maximum Continuous Power	ESFC	Motor Tempr	IGBT Tempr	Inverter Tempr	Maximum Continuous Power	ESFC	Motor Tempr	IGBT Tempr	Inverter Tempr
[°C]	[kW]	[g/kWhr]	[°C]	[°C]	[°C]	[kW]	[g/kWhr]	[°C]	[°C]	[°C]	[kW]	[g/kWhr]	[°C]	[°C]	[°C]
70	18.9	294.7	121	71	89	20.69	313	120	71	89	21.51	333	112	70	88
80	18*	291	125	80	100	20.73	314	134	80	99.6	21.5	331	120	79	97
90	<2 kW*	680	85	83	102	1.5*	969	83	83	100	1.5*	951	87	83	101

* Indicates that power had to be cutback to keep inverter temperature within limits.

Appendix D

Effect of EWP Power on APU ESFC

APU Speed	APU (Generator) Power	Original ESFC (without EWP power considered)	EWP Power	Coriolis (Fuel) Mass Flow	Net Power Output of APU	ESFC (EWP power consumption factored in)	Increase in ESFC after considering EWP Power
rpm	kW	g/kWh	W	g/sec	kW	g/kWh	kW
1956	2.35	379.65	7.04	0.248	2.343	380.79	1.14
1955	5.1	298.83	6.90	0.423	5.093	299.23	0.40
1953	**8.62**	273.78	**6.76**	**0.656**	**8.613**	**273.99**	**0.21**
2442	2.27	428.78	14.21	0.270	2.256	431.48	2.70
2441	5.27	311.37	14.63	0.456	5.255	312.24	0.87
2438	9.39	275.12	14.77	0.718	9.375	275.55	0.43
2441	**11.33**	**271.21**	**14.77**	**0.854**	**11.315**	**271.56**	**0.35**
2926	2.37	466.66	20.84	0.307	2.349	470.80	4.14
2925	5.45	325.97	20.98	0.493	5.429	327.23	1.26
2924	10	278.23	20.98	0.773	9.979	278.81	0.58
2923	13.56	268.27	20.84	1.010	13.539	268.68	0.41
2924	**13.77**	**271.15**	**20.70**	**1.037**	**13.749**	**271.55**	**0.41**
3410	2.34	542.06	26.91	0.352	2.313	548.37	6.31
3412	5.49	345.63	27.19	0.527	5.463	347.35	1.72
3411	10.34	288.53	27.05	0.829	10.313	289.28	0.76
3409	14.11	272.65	27.05	1.069	14.083	273.17	0.52
3410	**16.37**	**268.78**	**26.91**	**1.222**	**16.343**	**269.22**	**0.44**
3897	5.52	379.02	38.50	0.581	5.481	381.68	2.66
3897	10.68	298.95	39.05	0.887	10.641	300.05	1.10
3897	14.64	285.18	38.78	1.160	14.601	285.94	0.76
3897	18.13	289.80	38.92	1.459	18.091	290.42	0.62
3896	**18.73**	**292.45**	**38.92**	**1.522**	**18.691**	**293.05**	**0.61**
4385	5.66	412.33	48.85	0.648	5.611	415.92	3.59
4384	11.12	325.94	49.27	1.007	11.071	327.39	1.45
4384	15.51	314.02	49.13	1.353	15.461	315.02	1.00
4384	19.22	309.02	49.13	1.650	19.171	309.81	0.79
4384	**19.97**	**310.80**	**49.13**	**1.724**	**19.921**	**311.57**	**0.77**
4871	5.76	465.50	76.18	0.745	5.684	471.74	6.24
4872	11.51	360.58	76.73	1.153	11.433	363.00	2.42
4869	16.39	332.38	76.59	1.513	16.313	333.94	1.56
4871	20.31	332.11	76.45	1.874	20.234	333.37	1.25
4873	**21.81**	**328.40**	**76.45**	**1.990**	**21.734**	**329.55**	**1.16**
4968	5.75	478.11	80.32	0.764	5.670	484.88	6.77
4967	11.46	368.36	80.73	1.173	11.379	370.97	2.61
4965	16.58	334.02	81.01	1.538	16.499	335.66	1.64
4969	20.63	337.05	80.73	1.931	20.549	338.37	1.32
4969	**21.89**	**332.89**	**80.73**	**2.024**	**21.809**	**334.12**	**1.23**

Appendix E

This appendix discusses the experimental analysis that was undertaken to improve the light-off performance of the catalyst in an attempt to meet EU 6 emission legislation limits.

E.1 Spark Retard for Faster TWC Light-off

As it was seen in Chapter 10, Section 10.14, that there was a need to reduce THC emissions during start-up from cold if the present catalyst was to be considered suitable for the APU. Based on literature review, a strategy considered to be easily implementable without any additional hardware, with a calibration level access engine EMS was implementation of ignition timing retard.

Since the APU was expected to start at 2000rpm, 5kW, the ignition retard was carried out at 2000rpm, 5kW power demand. Maintaining this higher engine speed would result in higher exhaust gas temperature and higher exhaust mass flowrate, which would increase the total enthalpy of the exhaust gas for heating up the catalyst and hence achieve rapid catalyst light-off.

Two factors had to be borne in mind while retarding ignition timing. Firstly, the amount of spark retard and secondly the amount of time the retarded spark is maintained. Over-retarding ignition timing would result in engine backfiring and high engine-out HC emissions owing to poor combustion efficiency. Holding retarded ignition for a longer time means the TWC and exhaust valves would be exposed to high exhaust gas temperatures for a longer time. Since the heat capacity of a catalyst is very small and much lower than that of exhaust valves, therefore a long holding time of retarded ignition was not considered necessary. Further holding time of retarded spark should be as short as possible to reduce unnecessary fuel consumption due to spark retard.

Figure E-1 illustrates the normal spark timing and the two spark retard timings as measured during experimental tests based on the two strategies employed. The two ignition retard strategies were 10° and 20° retard relative to the normal timing. Negative values of ignition advance means values that are before top dead centre (BTDC). The holding time of retarded ignition lasted for 25sec.

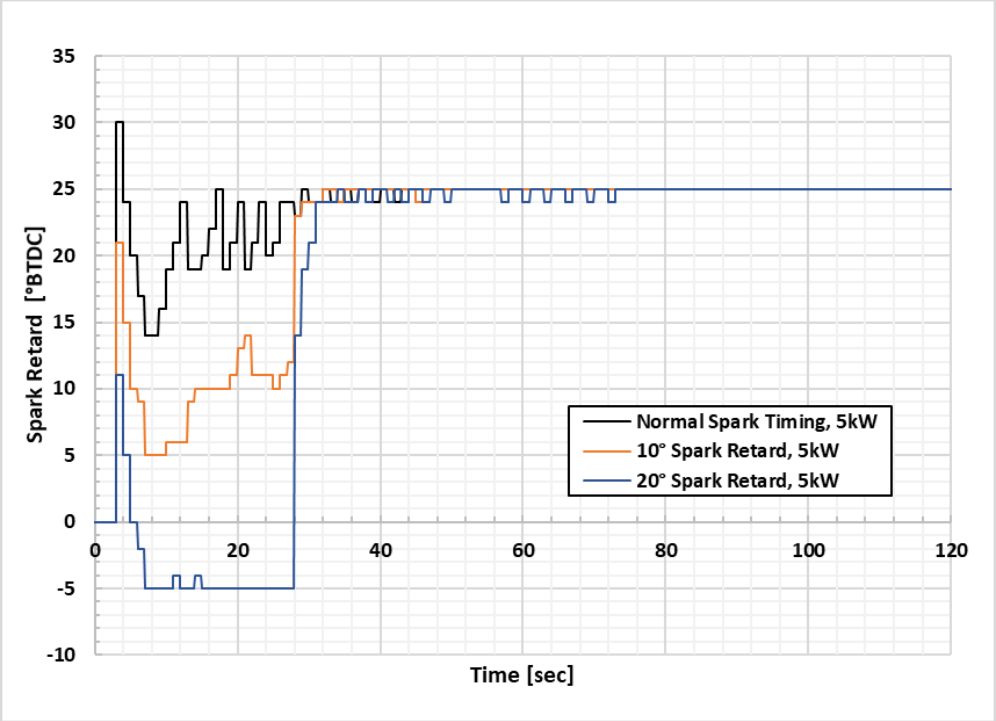

Figure E -1 Ignition time versus time. Normal spark timing and ignition retard of 10° and 20° crank angle relative to normal timing

Figure E-2 shows the exhaust gas temperature as a function of spark timing retard. As expected, higher the value of spark timing retard higher was the exhaust gas temperature. The exhaust gas temperature at the catalyst upstream associated with 20° spark retard was about 250°C higher than that of normal timing. This was because most of the heat released from combustion in the cylinders took place in the expansion stroke and was discharged in the exhaust system. Further retarding of spark timing could result in engine backfiring which would have adverse effects on engine-out emissions.

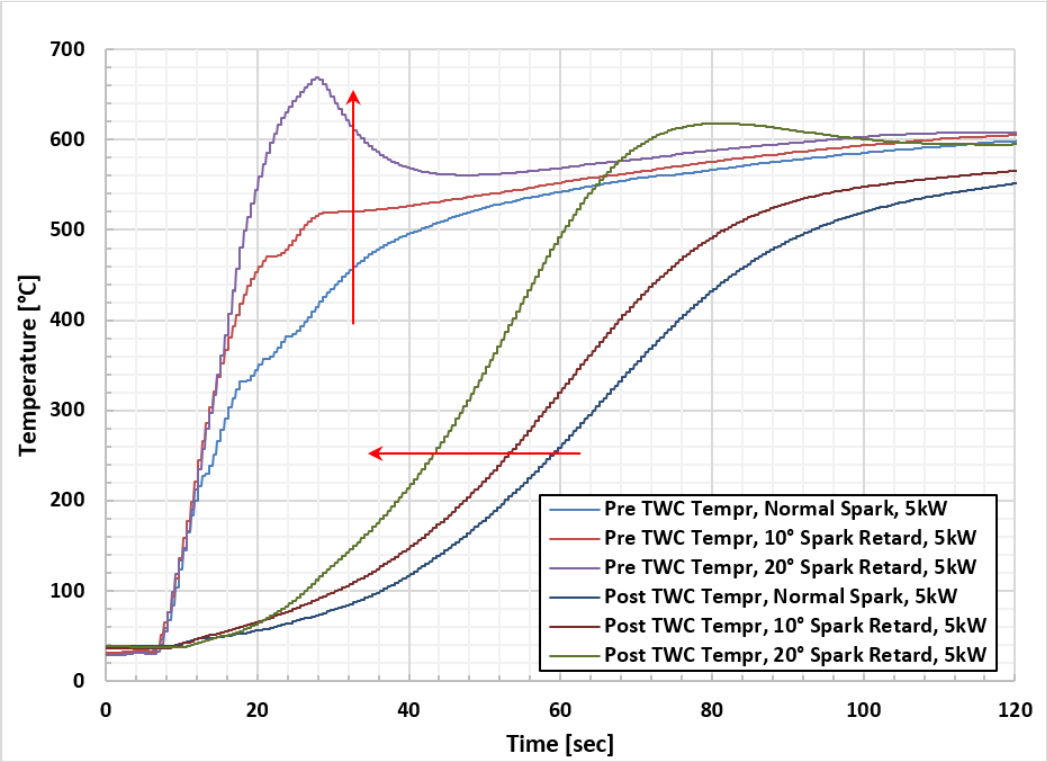

Figure E-2 Exhaust temperature at TWC upstream and downstream under normal spark timing and varying spark timing conditions

The NOx emissions downstream of the TWC with varying spark timing retard were compared with the NOx emissions with normal spark timing, Figure E-3. It was seen that as expected emissions reduced as spark retard was increased from normal to 20°. Further the cumulative post TWC emissions were well below the NEDC NOx limit of 0.66 grams.

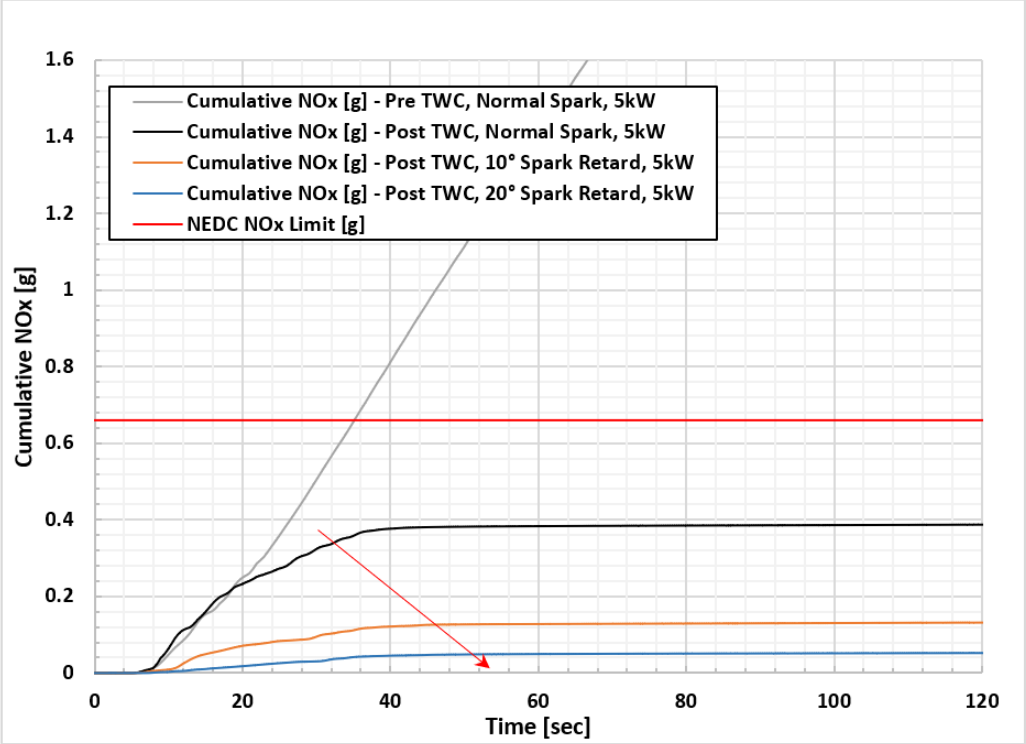

Figure E-3 Comparison of downstream TWC cumulative NOx emissions under varying spark timing vis-à-vis normal spark timing. Emissions reduce as spark retard is increased from normal to 20°. Cumulative post TWC emissions are well below the NEDC NOx limit

The THC emissions downstream of the TWC with varying spark timing retard were compared with the THC emissions with normal spark timing, Figure E-4. It was seen that emissions reduced as spark retard was increased from normal by 20°. However, the THC cumulative post TWC emissions continued to exceed the NEDC THC limit of 1.1 grams.

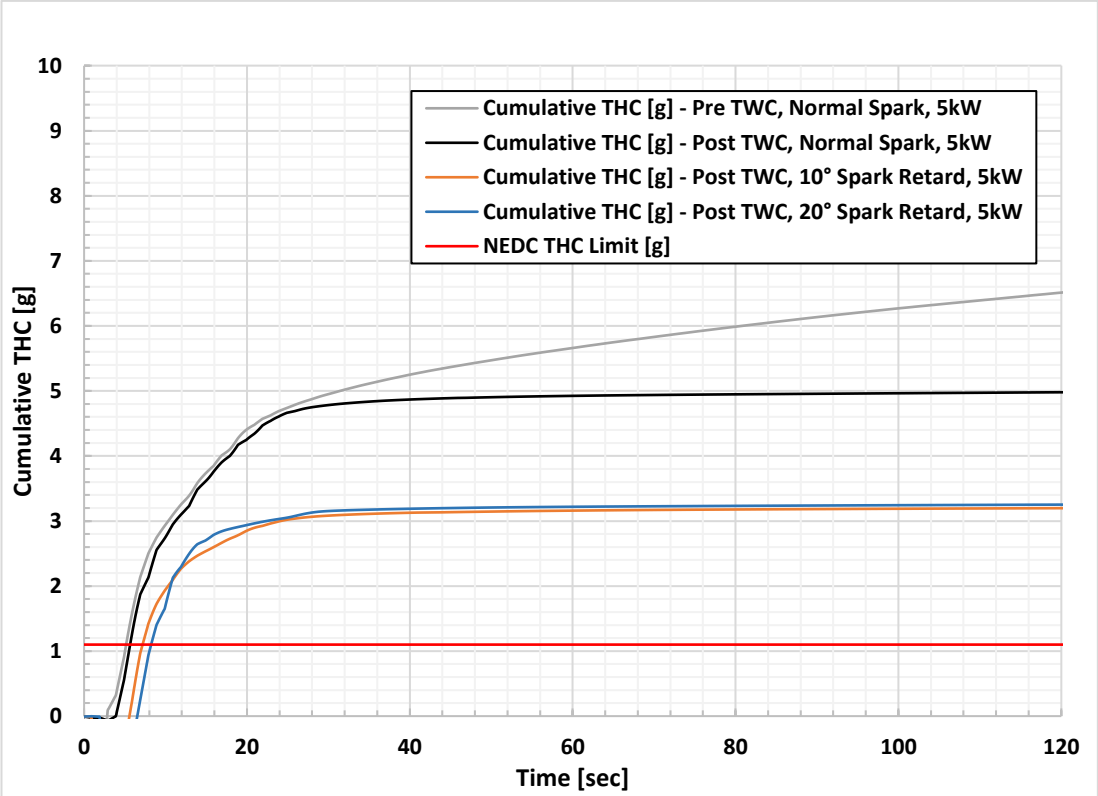

Figure E-4 Comparison of downstream TWC cumulative THC emissions under varying spark timing vis-à-vis normal spark timing. Emissions reduce as spark retard is increased from normal to 20°. Cumulative post TWC emissions are well above the NEDC THC limit

Hence, while the cumulative emissions decreased with spark timing retard, the improved light-off of the catalyst was still not enough to meet EU6 legislative limits.

E.2 Higher Power Demand at Engine Start for Faster Catalyst Light-off

Since the gasoline engine was being used for a RE application, it provided the flexibility to start the engine at varying power demands and engine speeds. Higher power demand would result in higher exhaust gas temperature and higher exhaust mass flow rate, which would heat the catalyst faster. However, too high a power demand at cold start may cause problems of engine wear and high fuel consumption. Since during the NEDC, the engine was being started at 2000rpm, for the purpose of examining the effect of varying power demand on catalyst light-off, the rpm was kept at 2000rpm and the power demand varied from 4kW to 6kW. From Figure E-5, it was observed

that as expected the THC emissions reduce with increasing power demand at engine start. However, the rise in THC emissions prior to catalyst light-off still exceeded the EU6 NEDC limit.

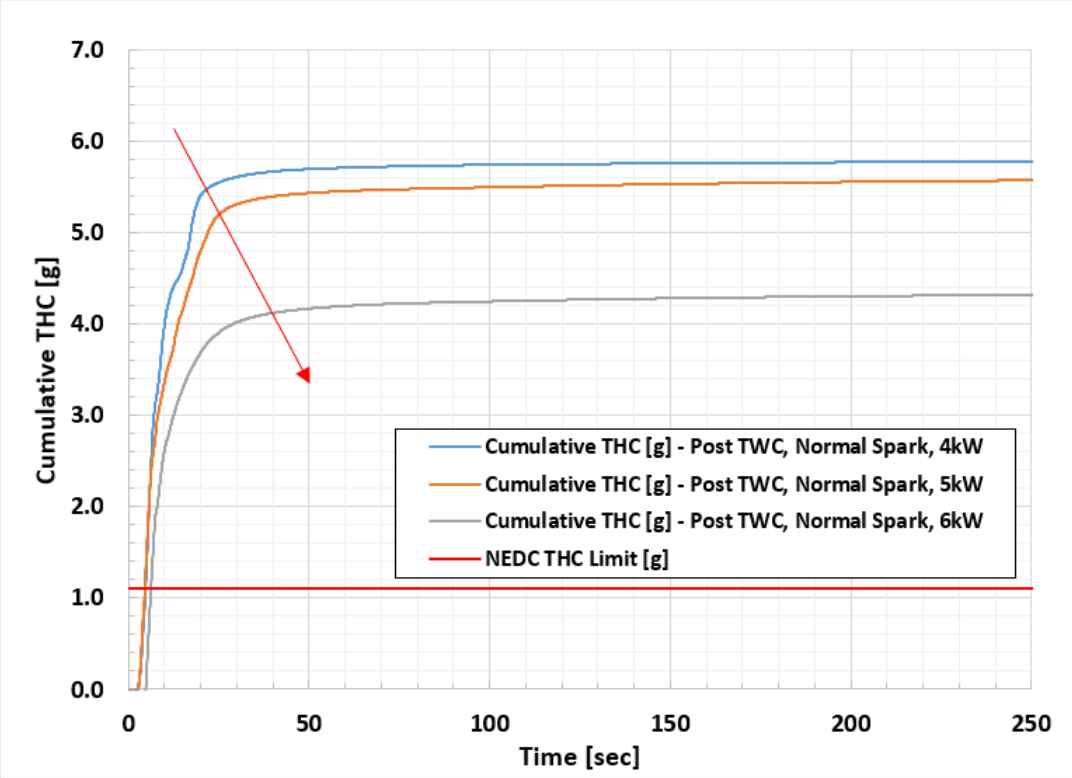

Figure E5 Comparison of downstream TWC cumulative THC emissions under varying spark timing. Cumulative THC emissions reduce as power demand at engine start is increased from 4 to 6kW. However, emissions still exceed NEDC THC limit

Publications

1. ‘***Development of a Low-Cost Production Automotive Engine for Range Extender Application for Electric Vehicles’***

   Ashwini Agarwal, Andrew Lewis, Sam Akehurst, Chris Brace, Yash Gandhi, Gary Kirkpatrick,

   SAE World Congress 2016

   Abstract

Range Extended Electric Vehicles (REEVs) are gaining popularity due to their simplicity, reduced emissions and fuel consumption when compared to parallel or series/parallel hybrid vehicles. The range extender internal combustion engine (ICE) can be optimised to a number of steady state points which offers significant improvement in overall exhaust emissions. One of the key challenges in such vehicles is to reduce the overall powertrain costs, and OEMs providing REEVs such as the BMW i3 have included the range extender as an optional extra due to increasing costs on the overall vehicle price. This paper discusses the development of a low cost Auxiliary Power Unit (APU) of c.25 kW for a range extender application utilising a 624 cc two cylinder automotive gasoline engine. Changes to the base engine are limited to those required for range extender development purposes and include prototype control system, electronic throttle, redesigned manifolds and calibration on European grade fuel. Modifications to the intake/exhaust manifolds were initially modelled using GT-Power and validated by engine tests. These modifications improved the engine torque in the APU planned operating range, and the new control system achieved improved BSFC up to 4000 RPM with European grade fuel. The use of European grade fuel also allowed operation at lambda 1 across a marginally wider portion of the engine operating range to improve fuel economy. Further modifications include replacing the mechanical coolant pump with an electric pump to reduce engine warmup duration and improve fuel economy.

2. '***Thermal Management of a Low-Cost Range Extender for Electric Vehicles'***

Ashwini Agarwal, Leon Rodrigues, Dian Liu, Andrew Lewis, Sam Akehurst, Chris Brace, Gary Kirkpatrick, Llyod Ash

The 6th Hybrid and Electric Vehicle Conference (HEVC), 2016

Abstract

Range extenders are a solution to partly overcome the limitations of current battery technology and are gaining popularity despite their complexity, due to the potential for reduced tailpipe emissions and fuel consumption. The range extender or Auxiliary Power Unit (APU) consists of an on-board fuel convertor that converts fuel such as gasoline into electrical power while the vehicle is in operation. This enables the traction battery storage capacity to be reduced whilst still maintaining an acceptable driving range. One of the key requirements of an APU is to provide maximum electrical power. In order to do so it is important that the engine as well as the generator are operated at their maximum efficiency in addition to optimising the complete system to reduce any parasitic losses in auxiliary systems. The conflicting requirements of running the engine at a high temperature (~90°C) and the generator to run as cold as possible (~50°C) has consequences on vehicle system integration such as the need to use separate coolant loops, radiators, pumps etc. Employing a common cooling loop can reduce parasitic loads and simplify vehicle integration but requires operating the engine and/or the generator under sub-optimum thermal conditions. The paper discusses the development of a thermal management system using a single coolant loop for the APU. The APU was tested on a bespoke rig first using two independent cooling loops to characterise the APU performance. The benefits of employing a single coolant loop are then weighed against the compromise in performance observed as a result of operating the engine and/or generator under

suboptimum thermal conditions in a single loop. In the single coolant loop, there is a drop in APU power of around 4% and an ESFC penalty of circa 2% at full load across the operating regime. However, there is a sizeable saving in parasitic losses, simplified package installation with reduction in overall package cost.

3. '***Air-Fuel Ratio Control of Spark Ignition Engines with Unknown Dynamics Estimator: Theory and Experiments'***

Jing Na, Member IEEE, Anthony Siming Chen, Yingbo Huang, Ashwini Agarwal, Andrew Lewis, Guido Herrmann, Senior Member IEEE, Richard Burke and Chris Brace

IEEE Transactions on Control Systems Technology, reference TCST-2019-0325

Abstract

This paper addresses the emission reduction of spark ignition engines by proposing a new control to regulate the air-fuel-ratio (AFR) around the ideal value. After revisiting the engine dynamics, the AFR regulation is represented as a tracking control of the injected fuel amount. This allows to take the fuel film dynamics into consideration and simplifies the control synthesis. The lumped unknown engine dynamics in the new formulation are online estimated by suggesting a new effective unknown dynamics estimator. The estimated variable is then superimposed into a commercially configured, well-calibrated gain scheduling like PID control to achieve better AFR response. The salient feature of this proposed control scheme lies in its simplicity and the less required measurements, i.e. only the air mass flow rate, the pressure and temperature in the intake manifold, and the measured AFR value are used. Practical experiments on a Tata Motors Limited 2-cylinder gasoline engine are carried out under realistic driving cycles. Comparative results show that the proposed control can achieve an improved AFR control response and reduced emissions.